National Library
of Canada

Bibliothèque nationale
du Canada

Canadian Theses Service

Service des thèses canadiennes

Ottawa, Canada
K1A 0N4

NOTICE

The quality of this microform is heavily dependent upon the quality of the original thesis submitted for microfilming. Every effort has been made to ensure the highest quality of reproduction possible.

If pages are missing, contact the university which granted the degree.

Some pages may have indistinct print especially if the original pages were typed with a poor typewriter ribbon or if the university sent us an inferior photocopy.

Previously copyrighted materials (journal articles, published tests, etc.) are not filmed.

Reproduction in full or in part of this microform is governed by the Canadian Copyright Act, R.S.C. 1970, c. C-30.

AVIS

La qualité de cette microforme dépend grandement de la qualité de la thèse soumise au microfilmage. Nous avons tout fait pour assurer une qualité supérieure de reproduction.

S'il manque des pages, veuillez communiquer avec l'université qui a conféré le grade.

La qualité d'impression de certaines pages peut laisser à désirer, surtout si les pages originales ont été dactylographiées à l'aide d'un ruban usé ou si l'université nous a fait parvenir une photocopie de qualité inférieure.

Les documents qui font déjà l'objet d'un droit d'auteur (articles de revue, tests publiés, etc.) ne sont pas microfilmés.

La reproduction, même partielle, de cette microforme est soumise à la Loi canadienne sur le droit d'auteur, SRC 1970, c. C-30.

NL-339 (r. 88/04)

Canada

THE UNIVERSITY OF ALBERTA

DEFORMATION OF DAMS ON SHEARED FOUNDATIONS

by

JULIO AUGUSTO DE ALENCAR JUNIOR

©

A THESIS
SUBMITTED TO THE FACULTY OF GRADUATE STUDIES AND RESEARCH
IN PARTIAL FULFILMENT OF THE REQUIREMENTS FOR THE DEGREE
OF DOCTOR OF PHILOSOPHY

DEPARTMENT OF CIVIL ENGINEERING

EDMONTON, ALBERTA
FALL 1988

Permission has been granted to the National Library of Canada to microfilm this thesis and to lend or sell copies of the film.

The author (copyright owner) has reserved other publication rights, and neither the thesis nor extensive extracts from it may be printed or otherwise reproduced without his/her written permission.

L'autorisation a été accordée à la Bibliothèque nationale du Canada de microfilmer cette thèse et de prêter ou de vendre des exemplaires du film.

L'auteur (titulaire du droit d'auteur) se réserve les autres droits de publication; ni la thèse ni de longs extraits de celle-ci ne doivent être imprimés ou autrement reproduits sans son autorisation écrite.

ISBN 0-315-45480-6

THE UNIVERSITY OF ALBERTA

RELEASE FORM

NAME OF AUTHOR JULIO AUGUSTO DE ALENCAR JUNIOR

TITLE OF THESIS DEFORMATION OF DAMS ON SHEARED FOUNDATIONS

DEGREE FOR WHICH THESIS WAS PRESENTED DOCTOR OF PHILOSOPHY

YEAR THIS DEGREE GRANTED FALL 1988

Permission is hereby granted to THE UNIVERSITY OF ALBERTA LIBRARY to reproduce single copies of this thesis and to lend or sell such copies for private, scholarly or scientific research purposes only.

The author reserves other publication rights, and neither the thesis nor extensive extracts from it may be printed or otherwise reproduced without the author's written permission.

(SIGNED) ....

PERMANENT ADDRESS:

AV. BRAZ DE AGUIAR, 458 APT. 301
BELEM - PARA - BRAZIL .....
66.000 ....

DATED .... JUNE 14th, 1988

THE UNIVERSITY OF ALBERTA

FACULTY OF GRADUATE STUDIES AND RESEARCH

The undersigned certify that they have read, and recommend to the Faculty of Graduate Studies and Research, for acceptance, a thesis entitled *Deformation of Dams on Sheared Foundations* submitted by Julio Augusto de Alencar Junior in partial fulfilment of the requirements for the degree of Doctor of Philosophy.

Dr. N.R. Morgenstern
Supervisor

Dave Chan
Dr. D. Chan

J. D. Scott
Dr. J.D. Scott

Dr. P.M. Byrne

W.H. Griffin
Prof. W.H. Griffin

Date June 2nd, 1988

To my wife Myrian and my son Pedro

Abstract

The main objectives of the thesis are to develop a methodology for incorporating measured pore pressures into the finite element analysis using an effective stress approach and to study the mechanism of deformability of foundations in cases where an earth dam is constructed on a site containing a horizontal weak seam.

A finite element program capable of performing non-linear analysis is used. A relatively inexpensive and flexible procedure is presented for interpolating pore pressure values at the integration points within an element based on piezometric measurements. The interpolated pore pressure distribution is incorporated into the analysis as a work equivalent load vector which is then applied to the system to obtain an equilibrium state.

This procedure is tested in idealized cases and is used for the back analysis of a case history where construction of a section of a tailings dam is simulated numerically over a period of eight years. The foundation of this dam experienced horizontal displacements of over 25cm along a 2m thick horizontally pre sheared layer of weak material located approximately 20m below the ground surface.

The effective stress analysis using the pore pressures measured in field proved to be much more efficient than the total stress analysis and the results obtained are in very good agreement with field observations.

Numerical difficulties during the back analysis due to tensile stresses led to the use of a cracking model in substitution for the no-tension model originally formulated in the finite element program. Comparative analysis of the two models is presented.

The mechanism of deformation of dam foundations containing a horizontal weak seam is computed in terms of effective stresses. The pore pressures are calculated based on pore pressure ratio, ru, and incorporated into the analysis as described above.

A parametric study using non-linear finite element analysis is also performed by varying the position of the weak seam and the stiffness of the upper foundation layer. Tentative correlations between Factors of Safety calculated by limit equilibrium analysis and lateral movements in the foundation are presented.

The results from the finite element analyses are compared to field observations from two other dams constructed on sites condition similar to the one studied and were found to able to explain the levels of foundation displacements observed in such cases.

Acknowledgments

I thank God for giving me this opportunity and I pray that I will be able to honor such a responsability.

The development of this thesis would not have been possible without the continuous love and support of my family, especially my wife Myrian, whose courage, strength and understanding have so often helped me during the difficult periods in these past four years, and my two year old son Pedro who has taught both Myrian and I so many beautiful and important things.

I am deeply grateful to Dr. N.R.Morgenstern for his continuous support, guidance and enthusiasm during these years of research. His ideas, surpervision and orientation were fundamental for the development of this work.

I wish to thank Dr. D. chan for his support and orientation since the beginning of this work. His discussions and suggestions were invaluable for the accomplishment of this research. I also thank Dr. Chan for his work on reviewing the thesis.

This research would not have been possible without the financial support provided by the Brazilian Government, through the "Coordenacao de Aperfeicoamento de Pessoal de Nivel Superior"(C.A.P.E.S.).

The support offered by Syncrude Canada Ltd., specially by Mr. Gerry Handford, allowing access to the records relative to the construction of the tailings dyke is gratefuly acknowledged.

My thanks also to Prof. W.H. Griffin for his comments relative to the interpolation technique.

The love and support of my parents Julio and Terezinha and my brothers and sister have always been an essential source of strength at all stages of my life. To them I am deeply grateful.

I owe special thanks to my Aunt Alice Alencar and to Manuel Aragao Filho for their help, which, contributed significantly for my coming to Canada.

I am grateful to my parents-in-law Francisco and Raquel for their continuous support during these years.

I also wish to thank Dr. Sergio Fountoura for suggesting and supporting the idea of pursuing my Ph.D. degree at the University of Alberta.

I thank all the new friends we met in Canada for making our living here the most enjoyable, in particular Andre Assis, Angela Kupper, Antonio Carlos,Arsenio Negro, Flavio Kuwajima,Heinrich Heinz, Jose Brandt, Jose Napoleao, Mauro Santos, Milton de Matos, Paulo Branco, Paulo Gomes, Sergio and their families.

Table of Contents

Chapter Page

1. Introduction 1

    1.1 Back-analysis - Choice between total and effective stress analysis 1

    1.2 Weak seams in foundations of dams 3

    1.3 Purpose of the research 9

    1.4 Organization of the thesis and scope of each Chapter 10

2. Incorporation of Measured Pore Pressures into the Finite element Analysis 14

    2.1 Introduction 14

    2.2 Pore Pressure Interpolation 16

        2.2.1 Incorporation of Additional Information ...22

        2.2.2 Influence of the number of piezometers 25

        2.2.3 Influence of the value of m and selection of the weighting function 26

            2.2.3.1 Influence of m for a specific weight function 26

            2.2.3.2 Influence of the selection of the weight function exponent for a specific m 27

        2.2.4 Consideration of Material Parameters 28

        2.2.5 Examples of Application 29

            2.2.5.1 Flow through dam foundation 29

            2.2.5.2 Pore pressures generated during an earth fill construction 32

    2.3 Introduction of pore pressure as known quantity in the finite element analysis 37

        2.3.1 Example of application 39

    2.4 Conclusion 40

3. Cracking Model 74

3.1 Introduction 74

3.2 Cracking model as a no tension model in plane strain 75

3.2.1 Crack formation and incremental stiffness for cracks oriented in one direction 75

3.2.2 Formation of cracks oriented in two directions 80

3.2.3 Closing of cracks 80

3.3 Eigenanalysis of cracked stiffness matrices 83

3.4 Comparison between the cracking model and Zienkiewiczs stress transfer procedure 86

3.5 Example of application 90

3.6 Conclusion 94

4. Finite Element Analysis of Syncrude Tailings Dyke ..118

4.1 Introduction 118

4.2 Geology of the Site and Soil Stratigraphy 120

4.3 Material properties based on laboratory tests ..121

4.4 Dyke Construction 123

4.5 Monitoring Program and Performace of the Dam ...124

4.5.1 Slope Indicators 124

4.5.2 Sliding micrometers 125

4.5.3 Piezometers 126

4.6 Finite Element Analysis 127

4.6.1 Linear Elastic Analysis 128

4.6.1.1 Analysis LE-1 129

4.6.1.2 Analysis LE-2 130

4.6.1.3 Analysis LE-3 130

4.6.1.4 Analysis LE-4 130

4.6.1.5 Analysis LE-5 131

4.6.2 Non-linear Finite Element Analysis 132

4.6.2.1 Material Modelling 136

4.6.3 Total Stress Analysis 138

4.6.3.1 Analysis NLT-1 139

4.6.3.2 Analysis NLT-2 140

4.6.3.3 Analysis NLT-3 140

4.6.3.4 Analysis NLT-4 141

4.6.3.5 Analysis NLT-5 142

4.6.3.6 Analysis NLT-6 142

4.6.3.7 Analysis NLT-7 143

4.6.3.8 Total Stress Analysis - Conclusion 145

4.6.4 Effective Stress Analysis 147

4.6.4.1 Pore Pressures 148

4.6.4.2 Analysis NLE-1 150

4.6.4.3 Analysis NLE-2 150

4.6.4.4 Analysis NLE-3 151

4.6.4.5 Analysis NLE-4 151

4.6.4.6 Analysis NLE-5 152

4.6.4.7 Effective stress analysis - conclusion 158

5. Parametric Analysis 199

5.1 Introduction 199

5.2 Geometry 202

5.3 Embankment and Foundation Materials 202

5.3.1 Numerical modelling,deformability and strength parameters 203

5.3.1.1 Layer 1: Till 203

5.3.1.2 Layer 2: Slickensided clay seam ..207

5.3.1.3 Layer 3: Bedrock 208

5.3.1.4 Embankment material: compacted till 208

5.4 Pore pressures 209

5.5 Limit equilibrium analysis 210

5.6 Finite element analysis 211

5.7 Presentation and Interpretation of the results .213

5.7.1 Lateral displacements 213

5.7.1.1 Foundation displacements 213

5.7.1.2 Correlation between Factor of Safety and Foundation displacement.......................216

5.7.1.3 Horizontal displacement within the embankment 218

5.7.2 Shear strains 221

5.7.3 Mobilization of shear strength 222

5.8 Case Histories presenting similar deformation mechanism 225

5.8.1 Syncrude Tailings Dyke 226

5.8.2 Nipawin dam 226

5.8.3 Comparisson of some aspects of Syncrude and Nipawin dams 227

5.8.4 Simplified uniaxial compression analysis .228

5.9 Conclusion 231

6. CONCLUSIONS 278

6.1 Conclusions 278

6.2 Suggestions for further research 282

Bibliography 284

Appendix I - Extension of the cracking model to allow for shear stress on the plane of the crack 288

Appendix II - Analyses terminated before reaching 1985 in the finite element analyses of Syncrudes tailings dyke, presented in chapter 4 293

List of Tables

Table Page

2.1 Influence of **m** and **exp** on weight λ 42

2.2 Influence of **m** and **exp** on the number of iterations 43

2.3 Material parameters for fill construction 44

3.1 Material parameters used for the idealized excavation 96

4.1 Piezometer tip elevations and total head 160

4.2 Piezometer tip elevations and pore pressures 162

4.3 Summary of the material parameters used in the linear elastic analyses 164

4.4 Summary of the material parameters used in the non-linear total stress analyses 165

4.5 Summary of the material parameters used in the non-linear finite element analyses NL7 in terms of total stresses 166

4.6 Summary of the material parameters used in the non-linear effective stress analyses 167

5.1 Strength parameters for till 234

5.2 Deformability parameters for till 235

5.3 Initial modulus at the center of the foundation till 236

5.4 Clayey seams characteristics 237

Table Page

5.5 Compacted till characteristics 238

5.6 Material parameters used in the parameteric analysis 239

A1 Summary of the material parameters used in the finite elemen analysis in terms of total stresses terminated prior to 1985 294

List of Figures

Figure Page

2.1 Pore pressure evaluation method 45

2.2 Pore pressure interpolation 46

2.3 Weight function 47

2.4 Weight function 48

2.5 Flowchart of the interpolation procedure 49

2.6 Incorporation of additional information - stratigraphy 50

2.7 Piezometric readings and interpolation positions 51

2.8 Results obtained by the use of fictitious piezometers 52

2.9 Incorporation of additional information using a reference distribution 53

2.10 Comparison between interpolated values 54

2.11 Significance of the number and position of the piezometers 55

2.12 Significance of the distance between the piezometers 55

2.13 Influence of **m** and **exp** on the results of the interpolation 56

2.14 Foundation stratigraphy 57

2.15 Piezometers and positions of interpolation 58

2.16 Comparison between results of the interpolation and the finite element analysis - elev. 31m 59

2.17 Comparison between the results of the interpolation and the finite element analysis - elev. 22m 60

2.18 Comparison between results of the interpolation and the finite element analysis - elev. 31m 61

Figure Page

2.19 Comparison between the results of the interpolation and the finite element analysis - elev. 22m 62

2.20 Earth fill construction - stratigraphy 63

2.21 Finite element mesh 64

2.22 Piezometers location 65

2.23 Pore pressures calculated by the finite element analysis 66

2.24 Reference distribution and initial guess with depth 67

2.25 Reference distribution and initial guess with the horizontal axis 68

2.26 Comparison between pore pressures calculated by the finite element analysis and by interpolation - section AA 69

2.27 Comparison between pore pressures calculated by the finite element analysis and by interpolation - section BB 70

2.28 Comparison between pore pressures calculated by the finite element analysis and by interpolation - section CC 71

2.29 Comparison between pore pressures calculated by the finite element analysis and by interpolation - section DD 72

2.30 Horizontal displacements along section AA and BB 73

3.1 Cracks oriented in one direction 97

3.2 Schematic stress-strain relationship before and after cracking 98

3.3 Cracks oriented in two directions 99

3.4 Crack opening and closing at an integration point 100

3.5 Closure of cracks at an integration point 101

3.6 Uniaxial loading analyses 102

Figure Page

3.7 Eigenvectors for the vertically cracked element 103

3.8 Eigenvectors for the horizontally cracked element 104

3.9 Schematic representation of the cracked elements 105

3.10 Problem analyzed by the use of the cracking model and the use of Zienkiewicz no tension technique 106

3.11 Displacement error with the number of iterations 107

3.12 Step 1 - Vertical and horizontal stresses along section AA' 108

3.13 Step 1 - Vertical and horizontal stresses along section BB' 109

3.14 Step 2 - Vertical and horizontal stresses along section AA' 110

3.15 Step 3 - Vertical and horizontal stresses along section AA' 111

3.16 Step 4 - Vertical and horizontal stresses along section AA' 112

3.17 Excavation analysis - stratigraphy 113

3.18 Finite element mesh 114

3.19 Schematic representation of the cracks formed in case B 115

3.20 Effective minor principal stress at integ. points closest to the center line of the excavation 116

3.21 Schematic representation of the cracks formed in case C 117

4.1 Stratigraphy of Cell 23, Section 53 168

4.2 Construction stages from 1979 to 1986 169

4.3 Plan view of the slope indicator locations 170

4.4 Slope indicator positions - cross section 171

Figure Page

4.5 Measured horizontal displacements until 1986 172

4.6 Plan view of the piezometers positions 173

4.7 Piezometers positions - cross section 174

4.8 Phreatic surfaces at each year of construction and average total head at elevation 290m measured in 1986 175

4.9 Average pore pressures measured by PN852307 and PN852311 in 1985 176

4.10 Finite element idealization of the Dyke and foundation 177

4.11 Soil stratigraphy used in the finite element analysis 178

4.12 Horizontal displacements at SI842332(Berm 319) position for single and multiple steps - linear elastic analysis 179

4.13 Horizontal displacements at SI842332(Berm 319) position for different elastic modulus for PGS and PGC materials 180

4.14 Horizontal displacements at SI842332(Berm 319) position for different elastic modulus for KCA material 181

4.15 Comparison between measured and calculated horizontal displacements at SI842332(Berm 319) position for reduced modulus for KCW material - linear elastic analysis 182

4.16 Comparison between measured and calculated horizontal displacements at SI842334(Crest) position - non-linear total stress analysis 183

4.17 Comparison between measured and calculated horizontal displacements at SI842332(Berm 319) position - non-linear total stress analysis 184

4.18 Comparison between measured and calculated horizontal displacements at SI842334(Crest) position - non-linear total stress analysis 185

Figure Page

4.19 Comparison between measured and calculated horizontal displacements at SI842332(Berm 319) position - non-linear total stress analysis 186

4.20 Comparison between measured and calculated horizontal displacements at SI842334(Crest) position - non-linear total stress analysis 187

4.21 Comparison between measured and calculated horizontal displacements at SI842332(Berm 319) position - non-linear total stress analysis 188

4.22 Comparison between measured and calculated horizontal displacements with time at SI842332(Berm319) position (elevation 290m) - non-linear total stress analysis 189

4.23 Comparison between measured and interpolated pore pressures at PN852307 position 190

4.24 Comparison between measured and interpolated pore pressures at PN852311 position 191

4.25 Comparison between measured and calculated horizontal displacements at SI842334(Crest) position - non-linear effective stress analysis 192

4.26 Comparison between measured and calculated horizontal displacements at SI842332(Berm 319) position - non-linear effective stress analysis 193

4.27 Comparison between measured and calculated horizontal displacements at SI842337(Toe) position - non-linear effective stress analysis 194

4.28 Comparison between measured and calculated horizontal displacements with time at SI842332(berm 319) and SI842337(toe) positions at elevation close to Kca/Kcw contact - non-linear effective stress analysis 195

Figure Page

4.29 Calculated horizontal displacements along KCA/KCW contact - non-linear effective stress analysis 196

4.30 Contours of maximum shear strains - 1986 197

4.31 Schematic representation of the cracks - 1986 198

5.1 Foundation containing horizontal weak seam 240

5.2 Weak seam daylights downstream of the dam 240

5.3 Stratigraphy used in the parametric analysis 241

5.4 Stress-strain curve for the till with various stiffnesses 242

5.5 Variation of the initial modulus of the foundation till with depth 243

5.6 Piezometric level for the foundation after the completion of the dam 244

5.7 Variation of the Factor of Safety with the position of the weak seam 245

5.8 Critical failure surfaces -$(h_1/H)=0.75$ 246

5.9 Critical failure surfaces - $(h_1/H)=0.5$ 246

5.10 Critical failure surfaces - $(h_1/H)=0.25$ 246

5.11 Finite element mesh - $(h_1/H)=0.75$ 247

5.12 Finite element mesh - $(h_1/H)=0.50$ 248

5.13 Finite element mesh - $(h_1/H)=0.25$ 249

5.14 Variation of horizontal displacements with the foundation stiffness - $(h_1/0.75)$ 250

5.15 Variation of horizontal displacements with the foundation stiffness - $(h_1/0.50)$ 251

5.16 Variation of horizontal displacements with the foundation stiffness - $(h_1/0.25)$ 252

Figure Page

5.17 Comparison between horizontal displacements in cases with different depth ratios and different foundation stiffnesses 253

5.18 Variation of the horizontal displacements along clayshale/till contact with depth ratio 254

5.19 Variation of the horizontal displacements along clayshale/till contact with depth ratio 255

5.20 Influence of the embankment stiffness on the horizontal displacements 256

5.21 Dimensionless factor Π versus depth ratio 257

5.22 Effect of the ratio ru of the embankment on the horizontal displacements ($(h_1/H)=0.75$ - $K_{till}=7000$) 258

5.23 Maximum shear strain($(h_1/H)=0.75$ - $K_{till}=7000$) 259

5.24 Maximum shear strain($(h_1/H)=0.75$ - $K_{till}=3500$) 260

5.25 Maximum shear strain($(h_1/H)=0.75$ - $K_{till}=700$) 261

5.26 Maximum shear strain($(h_1/H)=0.50$ - $K_{till}=7000$) 262

5.27 Maximum shear strain($(h_1/H)=0.50$ - $K_{till}=3500$) 263

5.28 Maximum shear strain($(h_1/H)=0.50$ - $K_{till}=700$) 264

5.29 Maximum shear strain($(h_1/H)=0.25$ - $K_{till}=7000$) 265

5.30 Maximum shear strain($(h_1/H)=0.25$ - $K_{till}=3500$) 266

5.31 Zone of yielding initiation 267

5.32 Mobilized shear strength($(h_1/H)=0.75$ - $K_{till}=7000$) 268

5.33 Mobilized shear strength($(h_1/H)=0.75$ - $K_{till}=3500$) 269

Figure Page

5.34 Mobilized shear strength($(h_1/H)=0.75$ - $K_{till}=700$) 270

5.35 Mobilized shear strength($(h_1/H)=0.50$ - $K_{till}=7000$) 271

5.36 Mobilized shear strength($(h_1/H)=0.50$ - $K_{till}=3500$) 272

5.37 Mobilized shear strength($(h_1/H)=0.50$ - $K_{till}=700$) 273

5.38 Mobilized shear strength($(h_1/H)=0.25$ - $K_{till}=7000$) 274

5.39 Mobilized shear strength($(h_1/H)=0.25$ - $K_{till}=3500$) 275

5.40 Schematic stratigraphy and horizontal displacements - Nipawin dam 276

5.41 Schematic representation of the problem in an unidimensional situation 277

A.1 Rough cracks oriented in one direction 292

A.2 Mohr circle for cracked material 292

1. Introduction

The thesis involves the use of finite element analysis in terms of effective stresses for the back-analysis of problems in which pore pressures are measured in the field and for the study of the deformation mechanism of foundations of earth dams constructed on sites containing a geologically pre-defined weak layer along which displacements occur.

1.1 Back-analysis - Choice between total and effective stress analysis

Despite the fact that the behaviour of soils and rocks are fundamentally controlled by effective stresses,in practical applications of the finite element method, in many cases in which pore pressures are important, the analyses are performed in terms of total stresses. This choice is usually said to be made to avoid the complexities involved in effective stress analyses. That is, to avoid the problems involved in the prediction of pore pressures based on theoretical models.

Non-linear finite element analysis in terms of total stresses requires a smaller number of parameters and is in general less expensive than an analysis in terms of effective stress. However, in problems where pore pressure effects are important total stress analysis presents serious difficulties for the selection of the appropriate values for the parameters involved as well as for the interpretation of the results.

Some of these difficulties are that engineering experience with respect to strength parameters is built almost entirely in terms of effective stresses,except for the cases of saturated materials loaded under undrained conditions. Strength parameters in terms of total stresses are very sensitive to the stress path. In general the use of a unique value for each material is not realistic.

Even though the total stress analysis does not consider pore pressures in an explicit way, the effect of pore pressures has to be implicitly reflected in the parameters selected. For example, the existence of positive pore pressures requires the selection of lower shear strength parameters. In fact, the value of the parameters should ideally vary for different pore pressure levels.

In many cases the selection of parameters for total stress analysis cannot rely on laboratory or field tests and the interpretation of the results obtained is obscured by the over-simplification of the problem.

Any analysis in terms of effective stresses requires explicit consideration of the pore pressures. But this does not mean that these pressures need to be predicted. In many situations pore pressures are measured in the field. This is true specially in large projects, in which the monitoring of pore pressures has become relatively commom practice. These measured pore pressures have not so far been directly used as known quantities in finite element analyses.

The present work proposes a procedure for directly incorporating the measure pore pressures into the finite element analysis as known quantities at each load stage so that the complexities and increase in costs associated with their prediction may be eliminated and the theoretical and practical drawbacks of the analysis in terms of total stresses may be avoided by performing the analysis in terms of effective stresses.

One difficulty for the use of measured pore pressures in the finite element analysis is that the measurements are specific at the piezometer tips, while the finite element analysis requires their values to be specified over the entire domain (at each integration point or node depending on the kind of element being used). This problem is resolved in the research to be reported here.

1.2 Weak seams in foundations of dams

The geological evolution of certain regions generates planes of discontinuity or relatively thin layers of weak material within stronger strata. In the present work these planes or layers will be referred to by the general term "weak seam".

These seams are mainly encountered in sedimentary and metamorphic enviroments. The layered structure of such environments is directly responsible for their formation. In both bedded and foliated deposits relatively stronger layers may be interlayered with weaker layers, with which localized shear strains are in general associated.

It is often observed during site investigations that in these deposits the weaker material has been subjected to a shearing process in the past.

Various phenomena have been identified as possible causes of the pre-shearing of the weaker material. Some of these are the occurrence of landslides, valley rebound, glacial drag, non uniform swelling and folding due to tectonic activities.

A number of works has been published dealing with the presence of seams at a particular site, but only few of them have treated the problem in a more general manner. Casinader(1980) presents a discussion on the engineering significance and material properties of the weak seams occuring in rock formations associated with dam foundations. This matter has also been discussed by Deere(1973).

Casinader, *op. cit.*, points out that "It is the shear strength of the seams that is their most significant property affecting the design of all types of dams".

The geological stratigraphy in western Canada is generally composed of upper units of pleistocene sediments and glacial tills underlaid by cretaceous sedimentary soft bedrock which consists mainly of interbedded shales, clay-shales, siltstones and sandstones. Coal and thin bentonite seams are often found within this lower formation.

The bedding orientation is in general approximately horizontal. A varying number of sheared planes or slickensides oriented parallel to the bedding have frequently been observed within the clay shale and at the contact of the this layer with the other materials. These may have been originated by straining of the material due to valley rebound, as discussed by Matheson(1972), and glacial action.

Although in these cases the compressibility of the weak layer may also be an important parameter for the assessment of the foundation behaviour, the statement made by Casinader is still true. That is, in these cases also, the shear strength of the weak layer is in general the most important property for design.

According to Matheson(1972) in cases where shearing is restricted to bedding planes or clay shale-sandstone interfaces both field studies and theory indicate that residual shear strength condition is developed at very small displacements in the direction parallel to the bedding. Other works with similar conclusions have been referred to by Morgenstern *et al.* (1977).

Stability evaluation and assessment of lateral deformation of the foundation material are of major concern for the successful accomplishment of projects constructed on deposits possessing horizontal or sub horizontal weak seams.

Dams constructed on deposits possessing these features have often required preventive or corrective work to minimize movements in the foundation. Some examples of this are the cases of Muda dam (see Taylor and James, 1967);Dughganga dam(see Deshmukh *et al.*, 1982); Gardiner dam(see Morgenstern and Simmons, 1982); Syncrude's tailings dyke(see Handford, 1985); Nipawin dam(see Matheson *et al.*, 1987).

At the sites of Muda dam, constructed in Malaysia, and Dughganga dam, constructed in India, the foundation consisted of quartizite containing sub horizontal beds of mudstones at numerous levels, many of which were shaly and weathered. In the first case high tensile cable anchorage was used to improve stability conditions along the weak seams and in the latter shear keys were adopted.

Gardiner dam, Syncrude tailings dyke and Nipawin dam were constructed in western Canada. Their foundation profile is typical of this region. They consist basically of pleistocene units underlain by cretaceous bedrock as mentioned above. All three sites present clay shale lying approximately horizontal and possessing sheared planes due to prior straining.

In the cases of Gardiner dam and the Syncrude tailings dyke the downstream slope in certain sections had to be substantially flattened and in the case of Nipawin dam drains were constructed throughout the foundation to reduce the pore pressure level which existed within the overlying deposits.

Despite the fact that limit equilibrium methods do not involve deformability parameters, in design practice the lateral deformations are often controlled empirically by the definition of a minimum acceptable Factor of Safety calculated by limit equilibrium analysis based on the assumption that the higher the Factor of Safety the lower the deformation level expected.

For a realistic assessement of the stress distribution in the foundation and the corresponding displacement field of this class of problem it is necessary to use a numerical approach. However, only a very limited number of published work can be found dealing with the finite element analysis of the behaviour of dam foundations during construction in a general way for cases involving the presence of horizontal or sub horizontal weak seams.

The analyses which have been presented in the literature so far are generally performed in terms of total stresses. The great majority of them is related to concrete dams and focus on the numerical simulation of a specific case, in which the geometry and material parameters are fixed, e.g. Mueller *et al.*(1977), Souza Lima *et al.*(1982), or the geometry is fixed but the parameters are varied in search for a combination that best reproduces field measurements, e.g. Morgenstern and Simmons(1982). Sharma *et al.*(1986) presented the analysis of the influence of the position of a horizontal weak seam on the lateral displacements of the foundation during the construction of a 100m high concrete dam.

Even though earth dams are in many cases constructed on sites containing horizontal or sub horizontal weak seams the understanding of the influence of these geological features on the deformation level of the foundation still lacks a systematic study. The present work attempts to obtain a clearer identification and understanding of the mechanisms of deformation involved in this kind of problem.

The process chosen to achieve this involves the back analysis of a case history in which pore pressures and displacements were measured and a parametric analysis in which some of the controlling parameters are varied within a certain range.

The majority of the finite element analysis dealing with deformability of dams and their foundations are performed in terms of total stresses. In cases where pore pressures are important this may be a significant drawback as discussed in section 1.1. Therefore, the analysis in this research were carried out in terms of effective stresses. The pore pressures were considered as known quantities at all stages and directly incorporated into the finite element analysis.

1.3 Purpose of the research

The basic objectives of the thesis are:

- To suggest a procedure for incorporating measured pore pressures into the finite element analysis using an effective stress approach in cases where pore pressure is important to the behaviour of the structure.
- To perform the back analysis of a case history where construction of a section of a tailings dam is numerically simulated over a period of eight years.The monitoring of the foundation behaviour of this dam showed high pore pressure levels and horizontal displacements of over 25cm along a 2m thick horizontally pre-sheared layer of weak material located approximately 20m below the ground surface.
- To study in a systematic way the mechanism of deformability of the foundation material in cases where an earth dam is contructed on a site containing a relatively thin horizontal weak layer positioned between two stronger layers using finite element analyses in terms of effective stresses.

1.4 Organization of the thesis and scope of each Chapter

In order to achieve the goals mentioned above the following steps were necessary:

i) To select a finite element program capable of performing non-linear analysis

ii) To program an interpolation procedure for interpolating pore pressure values at the integration point positions within each finite element based on the piezometric measuments and any other additional information that may be relevant to the generation of an interpolated pore pressure distribution that satisfies the physical constraints of the problem.

iii) To incorporate the pore pressure distribution obtained by interpolation into the finite element program selected as known quantities and test the procedure.

iv) To perform the back-analysis of the tailings dam using both the total stress approach and effective stress approach using the measured pore pressures and compare the results obtained in each analysis with field observations.

v) To perform a parametric study using the finite element analysis in terms of effective stresses to investigate the controlling parameters involved in the deformation of the foundation during the contruction of an earth dam on a site containing a relatively thin horizontal weak layer and compare the results obtained with field observations published about real cases.

The finite element program chosen was the program "Soil Analysis by Finite Element" (S.A.F.E.) developed by Chan(1986). This program uses isoparametric elements with six and eight nodes. It is capable of performing one, two and three dimensional linear and non-linear elastic analysis as well as elastic-plastic analysis involving various yield criteria. The analysis can be performed in terms of total and effective stresses. In this last case the pore pressures are calculated by the use of the pore pressure parameters **A** and **B** (Skempton,1954).

During the execution of the effective stress back-analysis mentioned in item iv serious numerical convergence problems were encountered at certain stages of the loading process due to the generation of tensile stresses at some integration points. The solution of this problem required the investigation and programming of an alternative procedure for handling tensile stresses other than the stress transfer method suggested by Zienkiewicz *et al.*(1968), originally existent in the program. The procedure adopted was the one proposed by Chen and Suzuki(1980) for modelling cracking in concrete.

Since the load transfer technique previously available is used in a large number of the computer programs used in geotechnical engineering it was decided to compare critically the two techniques and dedicate a whole chapter to the discussion of some aspects of the cracking model adopted and the results of the comparisons made.

The scope of each Chapter is:

- Chapter II: This Chapter presents the interpolation procedure referred to in item ii and the way the interpolated pore pressure distribution was incorporated in the finite element analysis(item iii). Results of tests performed on idealized cases are also presented.
- Chapter III: The cracking model mentioned above is briefly described. An eigenvalue analysis of an element stiffness matrix possessing cracks in two orientations is presented. Comparison is made between the cracking model and the stress tansfer method suggested by Zienkiewicz *et al.,op. cit.*. Example of the use of the cracking model is given in an idealized case.
- Chapter IV: Description of the tailings dam referred to in item iv and some geological and geotechnical information about the foundation materials are briefly presented. The monitoring program is summarized. The stages involved in performing the back analysis as well as the results obtained are presented and discussed. Comparisons are shown between calculated and measured displacements values.
- Chapter V: The geometry , material models and parameters used in the parametric study referred to in item v are presented. Limit equilibrium analysis and finite element analysis in terms of effective stresses are performed. The results obtained are presented and discussed. Comparison

between these finite element results and field observations published on two dams constructed on similar sites are made.

- Chapter VI: Final conclusions and suggestions for further research are presented

2. Incorporation of Measured Pore Pressures into the Finite element Analysis

2.1 Introduction

Proper consideration of pore pressures is essential for the understanding and modelling of soil or rock behaviour. Despite this, finite element analyses involving cases where pore pressures are significant are in general performed in terms of total stresses to avoid the complexities related to explicit consideration of pore pressures.

As shown schematically in fig.2.1, the pore pressure values may be calculated based on theoretical or empirical methods, or may be obtained by observation. The present work concerns the incorporation of observed pore pressure values into an effective stress finite element analysis.

Field measurements are in general the most reliable information that can be obtained with respect to the stress or strain level of materials involved in any geotechnical work. One of the major difficulties in interpreting and using these data in the analysis of the problem is that they are very localized, i.e. they refer to very small zones relative to the volume of material affected.

In the case of pore pressures, the value measured by a piezometer is specific only at the tip. Readings at different positions may yield completely different values depending on many factors. In general, the incorporation of such measurements into any kind of analysis requires the knowledge of values in locations that most of the times do not coincide with a piezometer tip, and,therefore,need to interpolated based on the measured values.

A practical method facilitating such interpolation should have the following characteristics:

a. It should be simple and relatively inexpensive, since, it is very frequent that the quantity or quality of the available data does not justify a high degree of complexity or cost.

b. It should be physically intuitive and flexible enough to allow engineering judgement to be exercised and to make possible the use of any additional knowledge that may be available about the problem beyond that reflected by the piezometric observations.

Knowledge of the local geology, initial water pressure conditions and type of structure to be constructed may yield important information about the pore pressure distribution in addition to the piezometer measurements, and, in fact, are often essential to the proper interpretation of these measurements.

In many cases the pore pressure levels at certain regions may be estimated without the need for measurements. The general pattern of the pore pressure distribution may be anticipated based on the type of structure and initial water conditions. This information should be accommodated by the interpolation procedure.

In this chapter an interpolation procedure which satisfies conditions a and b is described and tested for idealized cases. The incorporation of pore pressures as known quantities into finite element analysis in terms of effective stresses is then discussed, as a way of maximizing the use of field measurements in the analysis, avoiding the increase in costs and complexity involved in the use of theoretical models for pore pressure prediction or the oversimplification frequently imposed by analysis in terms of total stresses.

2.2 Pore Pressure Interpolation

The problem is shown schematically in fig. 2.2. It consists of estimating the values of pore pressure at points x'_1 to x'_q, based on measurements made at positions x_1 to x_p

The procedure involves basically 3 steps:

a. An initial assumption (or initial guess) is made for the pore pressure distribution. In the case of a finite element analysis, this means that an initial set of values are assigned for each integration point (or node) of the mesh.

b. The error of this initial assumption with respect to the measured pore pressure value is calculated at each piezometer location.

c.The assumed distribution is then corrected as a function of these calculated errors through an iterative process until a certain tolerance is reached, i.e. until a measure of the errors becomes smaller than a specified value. The closer the initial guess assumed in stage a is to the real distribution, the less a correction is needed.

In stage a, the initial guess distribution may be arbitrarily given by the user or the program may generate it through a weighed average interpolation:

$$Ux'_i = \lambda_{i1} UPx_1 + \ldots\ldots + \lambda_{im} UPx_m \qquad [2.1]$$

- Ux'_i is the pore pressure value at position x'_i to be calculated by interpolation.
- UPx_1 to UPx_m are the measured pore pressure values at points x_1 to x_m (data points). The number m of points is specified by the user. The maximum m value is equal to the total number of measured points. The closest m data points relative to point x'_i are selected for the interpolation at that position.
- λ_{i1} is the weight given to the measurement at position x_1 in relation to position x'_i.

$$\lambda_{i1} = \frac{W_{i1}}{\sum_{j=1}^{m} W_{ij}} , \qquad [2.2]$$

$$\sum_{j=1}^{m} \lambda_{ij} = 1$$

- W_{i1} is a function of the distance between points i and 1. The smaller the distance between the two points the higher the value of W_{i1} and the higher the weight λ_{i1}. As the distance approachs zero, λ_{i1} approaches unity.

The function **W** is selected by the user. The presently available ones are shown in figs. 2.3 and 2.4. Similar weighting functions can be found in Sampson(1978).

In stage **b** , it is necessary to estimate at each piezometer location the value of the distribution being corrected. Since the piezometer positions rarely coincide with the position of an integration point (or node), an interpolation is required.

The interpolation is done by a weighed average technique similar to the one described above. In this stage, however, equations 2.1 and 2.2 are expressed as:

$$Ux_i = \lambda_{i1}Ux'_1 + \ldots\ldots + \lambda_{im}Ux'_m \qquad [2.3]$$

- Ux_i is the pore pressure value at position x_i to be calculated by interpolation. The position x_i corresponds to a piezometer location.
- Ux'_1 to Ux'_m are the pore pressure values at points x'_1 to x'_m, which, in this stage correspond to integration point (or node) positions. The number **m** of points is specified by the user. The closest **m** points relative to point x_i are selected

for the interpolation at that position.

- λ_{i1} is the weight given to the pore pressure at position x'_1 in relation to position x_i.

$$\lambda_{i1} = \frac{W_{i1}}{\sum_{j=1}^{m} W_{ij}} \qquad [2.4]$$

$$\sum_{j=1}^{m} \lambda_{ij} = 1$$

After the pore pressure distribution being corrected is interpolated at each piezometer location, the values are compared with the field data. For a certain iteration t such a comparison is made by:

$$^{t}F_i^{piz} = \frac{UPx_i}{^{t}Ux_i} \qquad [2.5]$$

- $^{t}F_i^{piz}$ is the correction factor (or error) at position of piezometer i at iteration t
- UPx_i is the measured pore pressure value at position i
- $^{t}Ux_i$ is the interpolated value at location of piezometer i based on the interpolated pore pressure distribution at iteration t.

The correction of the assumed distribution (step c), i.e. the correction of the pore pressure values at each node or integration point, is done by a weighed average of the correction factors calculated by the equation above for each piezometer position. The weighting function is the same one selected in step b. Again, only a limited number of calculated correction factors is used in the correction of the pore pressure value of each node or integration point. This number is the same as specified by the user in step b and they are also selected according to their distance to the point being corrected:

$$ {}^{t+1}F_i^{ip} = \sum_{j=1}^{m} \lambda_{ij} \; {}^{t}F_j^{piz} \qquad [2.6] $$

$$ {}^{t+1}Ux_i = {}^{t}Ux_i \; {}^{t+1}F_i^{ip} \qquad [2.7] $$

- ${}^{t+1}F_i^{ip}$ is the correction factor for integration point (or node) i at iteration t + 1.
- ${}^{t+1}Ux_i$ is the pore pressure value at position of integration point i at iteration t+1.

$$ \lambda_{i1} = \frac{W_{i1}}{\sum_{j=1}^{m} W_{ij}} \qquad [2.8] $$

$$ \sum_{j=1}^{m} \lambda_{ij} = 1 $$

Steps b and c are repeated until the norm of the errors is less than a specified tolerance:

$$ {}^{t+1}E = \sqrt{\frac{\sum_{j=1}^{npiz} \left[{}^{t+1}F_j^{piz} - {}^{t}F_j^{piz} \right]^2}{\sum_{j=1}^{npiz} \left[{}^{t}F_j^{piz} \right]^2}} \qquad [2.9] $$

- ${}^{t+1}E$ is the norm of the errors (or correction factors)
- npiz is the total number of piezometers.

A flowchart of the interpolation procedure described is presented in fig.2.5

This process is physically intuitive. It is generally expected that the difference between the real and assumed distribution (i.e. the error) at a certain point should be similar to the difference in the neighborhood of that point. As the distance between the point being corrected and the position where an specific error was calculated increases the lower is the likelihood that the error at those two points should be related.

The rate of decrease of the influence of a calculated error with the distance is dictated by the weighting function selected(see fig. 2.3 or fig. 2.4).

Since the interpolation procedure is relatively fast and inexpensive, the selection of the weighting function and the number of points to be used in the interpolation process (constant **m**) is left to the user in order to allow him to reach a combination that best approximates the field measurements and is in accordance with the physical constraints of the problem.

2.2.1 Incorporation of Additional Information

Adittional information may be incorporated into the interpolation procedure by :

a. Specifying fictitious piezometer measurements

b. Assuming a certain pore pressure distribution as reference and use as piezometer measurements the difference between the measured values and the reference distribution and as initial guess the difference between the initial guess and the reference distribution. In the regions where no corrections are needed, the initial guess coincides with the reference distribution.

After the corrections have been made, the corrected distribution is added to the reference distribution.

To illustrate the two methods, consider the simple one dimensional problem shown in fig.2.6. A 4m thick clay layer exists between two layers of sand. The initial piezometric distribution is hydrostatic.

Some time after the application of an external load, the measurements of three piezometers installed in the clay layer are as shown in fig.2.7. Suppose it is necessary to interpolate the pore pressures to the depths indicated in the same figure.

Under these circumstances it is expected that the pore pressure values in the sand layer would have returned to the initial condition. Such information will be first incorporated into the problem by the specification of fictitious piezometers (item a)

In this case the fictitious piezometers are assumed to exist at the elevations 1,2,3,7,8,9 and 10m (see fig.2.7). The pore pressure values at such fictitious piezometers correspond to the initial condition. A total of 10 piezometers are now considered to exist.

The initial guess for the distribution was that it was hydrostatic in the sandy materials and constant along the clay layer.

The initial guess for the pore pressure distribution, the corrected values obtained by interpolation and the constants used are presented in fig. 2.8.

The same information about the pore pressure distribution in the sand layers will now be introduced as described in item b *op. cit.*.

The reference distribution is assumed to be hydrostatic. The initial guess for the pore pressure values are the same as used before (see fig.2.9b). The difference between the piezometers readings and the reference distribution and the difference between the initial guess and the reference distribution are shown in fig. 2.9c. Note that now no fictitious piezometer is considered to exist.

The values presented in fig.2.9c are then used for the interpolation and the results are added to the reference distribution. The results obtained are compared to the values calculated by the use of fictitious piezometers in fig.2.10. A slight difference is noted.

In this simple one dimensional problem involving only a few points it may seem simpler and less confusing to use fictitious piezometers to incoporate the additional information, but when dealing with larger two dimensional problems like a finite element analysis involving a large number of piezometers and points to be interpolated the other procedure may be less confusing since it avoids mixing up real and fictitious piezometers.

The generation of the reference distribution and initial guess as well as the necessary subtractions can be made in general quite easily with the use a simple program for individual cases.

It is evident that the more information is available about the real distribution through piezometer readings or geological observation, the more realistic will be the interpolated pore pressure surface.

2.2.2 Influence of the number of piezometers

The number of piezometers alone does not say whether there are or are not sufficient piezometers for the interpolation to generate a pore pressure distribution close to the real distribution. It depends essentially on how completely the piezometer readings reflect the pore pressure distribution characteristics.

To illustrate this point it is useful again to make use of a simple one dimensional example. Fig.2.11 shows a pore pressure distribution which is constant along the horizontal axis at a certain elevation except for a specific sector where for some reason (a drain installed for example) the pore pressures were forced to assume lower values. In this case independently of the number of piezometers installed in zones **A** and **C**, if no piezometer is placed in zone **B** the reduction of pore pressure in that zone will not be shown in the interpolated distribution.

The interpolation procedure being discussed makes no consideration about the distances between piezometers, it uses only the distance between the point where the interpolation is to be made and each piezometer. The effect of this is shown in fig. 2.12. In both cases **a** and **b** the weight of each piezometer on the interpolation at point **o** is 0.25.

This seems reasonable for case a.In case b it is very likely that piezometers P_3 and P_4 would have approximately the same value and it would seem more reasonable that the sum of their weights on the interpolation at point o should reach 1/3, leaving 2/3 to be divided equally by the other two piezometers.

In practice this is not very significant since in general there is no necessity for installing or considering piezometers excessively close to each other in cases where their readings are approximately the same.

2.2.3 Influence of the value of m and selection of the weighting function

The degree of influence of the number of data points to be used in the interpolation at a specific position (m) depends on the weighting function selected. In order to observe the effect of each one separately some simple examples were analysed in which one of them is held constant while the other was varied.

2.2.3.1 Influence of m for a specific weight function

Consider the problem shown in fig 2.13. In this case it is intended to interpolate values at positions A and B based on measured values at points P_1, P_2, P_3 and P_4. Since only 2 points are considered for interpolation (A and B) only one iteration was performed,i.e the tolerance was set equal to unity. The weight function used is shown in fig. 2.3 with **exp**=1.

As a first case it was assumed that the value of **m** was 2, i.e. two piezometers were used for interpolation at point **A** and two piezometers for interpolation at point **B**. The results obtained are presented in fig.2.13. The values at **A** and **B** are 7.5 and 5.0 ,respectively. If the **m** is chosen to be 4 the result at point **A** is 7.02 and at point **B** is 5.66(see fig.2.13).

The weights for each piezometer in each case are presented in tab. 2.1. It is noted that the weights vary depending on the number of piezometers used for the interpolation. This variation causes the difference in values obtained.

2.2.3.2 Influence of the selection of the weight function exponent for a specific m

Consider the same problem shown in fig. 2.13 with **m**=4 and the weight function shown in fig.2.3 with **exp**=1. The results for this case have been calculated above and are presented in fig. 2.13. If **exp** is changed to 3 the values obtained for points **A** and **B** are 7.45 and 5.095, respectively. These values are close to the ones obtained for the case where **exp**=1 and **m**=2 , presented before.

The weights for each piezometer in each case are shown in tab.2.1. It is noted that the increase of **exp** implies a greater reduction of the weight function with distance. Therefore, the data points which are closer to the position where interpolation is to be performed have their influence increased while the others have theirs reduced.

In general, cases of problem involving high pore pressure gradients tend to require smaller **m** values or larger **exp** values.

2.2.4 Consideration of Material Parameters

It is noted that the interpolation procedure described above does not involve physical parameters of the materials.

It is known that the variation of the pore pressure distribution is very much influenced by the permeability of the material. This might be considered by reducing the influence of piezometers installed in certain materials over points positioned in materials of very different permeability and vice-versa.

Such a reduction would need to be in the form of a function relating a measure of the difference in permeability to the weight reduction factor.

The problem is that such a function would be arbitrary and would not necessarily imply better accuracy of the results.

Instead of adopting this kind of procedure, the program was made flexible enough to accommodate variations in pore pressure by allowing the user to choose the type and rate of decrease of the weight function, the number of data points to be used for interpolation at each position and by allowing the incorporation of boundary conditions as discussed above.

It has also been coded to consider extreme pore pressure gradients which may occur, for example, in regions close to the contact of two layers of very different permeability, by allowing the user to eliminate the interference of specified piezometers over specified regions and vice-versa independent of their proximity.

2.2.5 Examples of Application

As examples of the use of the scheme described, two idealized cases are presented below. In the first example the pore pressure distribution to be interpolated has a smooth variation. In the second example it contains an abrupt variation at a certain region.

2.2.5.1 Flow through dam foundation

The geometry and soil profile used in this initial example are shown in fig.2.14. An impermeable 10m dam is constructed on a 4m thick layer with coefficient of permeability K = 0.01m/s. Underneath, there is a 1m layer with k=1.0m/s, underlain by a 30m stratum with k=0.00005m/s, limited by an impermeable boundary.

The height of the reservoir is 8m and on the downstream side the water level is at the surface. La Place's equation was solved using the finite element method with rectangular 4 nodes elements and the pore pressure values for steady state conditions were calculated at the node positions. These calculated pore pressures were considered the real, or field, pressures.

It was, then, assumed that 44 piezometer tips were installed as shown in fig. 2.15 and the pore pressures measured at each tip location. Each location coincided with a node position in the finite element mesh.The piezometers measurements were the same as the finite element solution at those positions.

The problem was then, knowing the pore pressures at the piezometer tip positions (which were equal to the finite element solution at these points) it was necessary to interpolate the pore pressures at the positions indicated in fig. 2.15.

For the initial guess, the pore pressure distribution was considered to be hydrostatic over the entire region with the water surface coinciding with the top of the reservoir, i.e. 8m above the ground surface.

Such a distribution is clearly unrealistic since no head loss is considered.

The initial guess was then corrected by the interpolation scheme. Both weighting functions presented in figs. 2.3 and 2.4 were used. The exponent **exp** and the number of piezometers involved in the correction of each point (constant **m**) were varied. Tab.2.2 presents the values used.

Figs. 2.16 to 2.19 show the initial guess values, the corrected values and the results from the finite element analysis along two elevations (31m and 22m).

The values calculated by the use of the weight function shown in fig. 2.4 are presented in figs.2.16 and 2.17. It is noted that for **exp**=1, as the constant **m** increased from 4 to 10 the interpolated values got farther from the finite element result. No significant difference was observed between **exp**=2 and **exp**=4 for the same value of **m**. The best results were obtained with **exp**=2(or 4) and **m**=4.

Figs.2.18 and 2.19 present the values calculated by the use of the weighing function shown in fig. 2.3. The same trends commented above are observed. No significant difference was observed between **exp**=2 and **exp**=4 for **m**=4 For **exp**=1 as **m** increased the interpolated values got farther from the finite element results. The best results were obtained with **exp**=2(or 4) and **m**=4.

The values calculated by the use of the weighting function showed in fig.2.3 were a little closer to the finite element results than those calculated by the use of the other weighting function.

Tab.2.2 shows the number of iterations necessary to reach an error of smaller than 0.1%. It is noted that as **m** increases or **exp** decreases the number of iterations increases.

2.2.5.2 Pore pressures generated during an earth fill construction

The geometry of the problem in this example is shown in fig.2.20. A 4.5 meters high earth fill is constructed on a site composed of an upper layer of sandy material with thickness of 11.25m. Underlying it there is a 1m thick clayey soil which rests on a very stiff bedrock. The pore pressure distribution was originally under hydrostatic condition with the water level at the ground surface.

The construction of the fill was numerically simulated by non-linear finite element analysis in terms of effective stresses, as presented by Chan(1986). The pore pressures calculated at this stage by the use of pore pressure parameters **A** and **B** (Skempton,1954) were considered as the "real" field pore pressures.Piezometers were assumed to be installed at positions which coincided with integration point positions. The pore pressure calculated at that integration point was considered as the measured value.

The problem was then, knowing the pore pressure values at certain integration point positions it was necessary to interpolate values at the other integration point locations.

The finite element mesh used is shown in fig.2.21. It is composed of 268 isoparametric elements and 847 nodes. Gaussian integration of 3x3 and 2x2 points were used for the quadrilateral and triangular elements respectively.

The upper foundation layer was considered to behave according to a hyperbolic stress-strain relationship (see Duncan and Chang,1970). The clayey material was modelled as linear elastic-perfect plastic material. The bedrock and the fill material were assumed to be linear elastic.

Tab.2.3 presents the values of the material parameters used in the analysis. It is noted that the pore pressure parameters used for the clay material are higher than the values used for the upper layer and for the bedrock.

The *in situ* stress field was generated by a linear elastic switch-on-gravity procedure. The parameters used in this stage are shown in tab.2.3. The fill was then placed in five load stages of 0.90 meters.

The assumed piezometers are indicated in fig.2.22, which shows only the upper part of the finite element mesh. Each piezometer position coincided with the integration point at the center of the element.

The calculated pore pressures along sections **AA**, BB and CC (see fig. 2.22) are shown in fig.2.23 . It is noted that in this case the distribution displays an abrupt variation at the contact of the clayey soil with the other materials in the region underneath the fill. This variation is due to the higher values of pore pressure parameters used for the clayey material(see tab.2.3).

The boundary conditions for the interpolation were imposed by the use of a reference distribution (see item 2.2.1). The reference distribution coincided with the pore pressure distribution before the fill construction,i.e. hydrostatic with the water level at the ground surface.

It is reasonable to assume that below elevation 70m and beyond the distance of 299m from the center of the fill the pore pressures would remain unaltered by its construction. Even if this is not exactly true, it should not have a very significant effect on the analysis.

The initial guess distribution was assumed to vary linearly with depth. Fig.2.24 shows the reference and initial guess distributions along section **AA**. At the original ground surface the initial guess corresponds to a 4.5m high column of water and increases linearly with depth. Below the 70m elevation it was made to coincide with the reference surface so that no correction would be made in that region.

Fig. 2.25 shows the initial guess and reference distributions along section **DD** (see fig.2.22). It is noted that beyond 299m from the center line the initial guess coincides with the reference surface. Therefore the pore pressure values in that region will remain as defined originally.

The initial guess values and the piezometer values were then subtracted from the reference distribution and this difference was used for the interpolation. After the corrections the resulting values were added to the reference surface.

The weighting function shown in fig.2.3 was used. Values of constant **m** equal to 4, 3 and 2 were used. Values of exponent **exp** equal to 2, 3 and 5 were tried.

No matter what combination was used the abrupt change in pore pressures showed in fig.2.23 would be smoothed in the interpolated distribution.

This smoothing happened because the distance between the piezometers was very small and the correction of the pore pressure values at integration points close to the contact between the layers (i.e. region of highest gradient) were being significantly influenced by piezometers positioned within both materials.

The pore pressure parameters of the clayey soil are very different from those of the other materials. This difference causes the abrupt variation in pore pressures. Therefore it was decided that the piezometers within the clayey material should not influence the interpolation of points within other materials and that the interpolation of points within the clayey layer should not be influenced by piezometers positioned in other layers.

The results obtained were then in much better agreement with the finite element results than initially. Figs. 2.26 to 2.29 show the values for the initial guess, the interpolated pore pressures and the finite element results at the integration points along 4 different sections(see fig.2.22). Note that none of the sections coincide with a piezometer position.

It is observed that by eliminating the interference between the different materials the abrupt variation in the pore pressures was successfully approximated.

2.3 Introduction of pore pressure as known quantity in the finite element analysis

The incremental finite element displacement formulation may be expressed by(see Bathe-1982):

$$\sum_{e=1}^{nel} \left(\int_{ve} [B_e]^t \, \{\Delta\sigma_e\} \, dv_e = \{\Delta P_e\} \right) \qquad [2.10]$$

where,

- the subscript **e** denotes elemental quantities and nel the total number of elements.

$[\ ]^t$ is the transpose of matrix $[\ ]$

$[B]$ = strain-displacement matrix

$\{\Delta\sigma\}$ = increment of total stress vector

$\{\Delta\sigma\}^t = \langle \Delta\sigma_{xx}, \Delta\sigma_{yy}, \Delta\sigma_{xy}, \Delta\sigma_{zz} \rangle$

$\{\Delta P\}$ = increment of external applied load vector

$\int_{ve}$ = integration over the volume of the element

the increment of total stress vector may be expressed as:

$$\{\Delta\sigma\} = \{\Delta\sigma'\} + \{m\}\Delta u \qquad [2.11]$$

where,

$\{\Delta\sigma'\}$ = increment of effective stress vector

$\{\Delta\sigma'\}^t = \langle \Delta\sigma'_{xx}, \Delta\sigma'_{yy}, \Delta\tau'_{xy}, \Delta\sigma'_{zz} \rangle$

$\{m\}^t = \langle 1, 1, 0, 1 \rangle$

Δu = pore pressure increment

equation 2.10 may be rewritten as:

$$\sum_{e=1}^{nel} \left(\int_{ve} ([B_e]^t(\{\Delta\sigma'_e\} + \{m\}\ \Delta u_e))\ dv_{ve} = \{\Delta P_e\} \right) \qquad [2.12]$$

where,

$\int_{ve} [B_e]^t\ \{m\}\ \Delta u_e\ dv_{ve}$ represents the work equivalent load vector of the pore pressure increment.

considering,

$$\{\Delta R_e\} = \{\Delta P_e\} - \int_{ve} [B_e]^t\ \{m\}\ \Delta u_e\ dv_{ve} \qquad [2.13]$$

equation 2.12 may, then, be rewritten as:

$$\sum_{e=1}^{nel} \left(\int_{ve} [B_e]^t\ \{\Delta\sigma'_e\}\ dv_e = \{\Delta R_e\} \right) \qquad [2.14]$$

Introducing the incremental constitutive relationship of the material in terms of effective stresses by the matrix $[C']$:

$$\{\Delta\sigma'_e\} = [C']\ \{\Delta\epsilon_e\}$$

considering,

$$\{\Delta\epsilon_e\} = [B_e]\ \{\Delta\delta_e\}$$

where $\{\Delta\delta_e\}$ is the increment of nodal displacement vector. Equation 2.14 may be rewritten as:

$$\sum_{e=1}^{nel} \left(\int_{ve} [B_e]^t \, [C'] \, [B_e] \, dv_e \, \{\Delta\delta_e\} = \{\Delta R_e\} \right)$$

that is,

$$\sum_{e=1}^{nel} \left([K'_e] \, \{\Delta\delta_e\} = \{\Delta R_e\} \right) \qquad [2.15]$$

where $[K'_e]$ is the element stiffness matrix in terms of effective stress:

$$[K'_e] = \int_{ve} [B_e]^t \, [C'] \, [B_e] \, dv_e$$

The technique described above has been used in various works, e.g. Christian(1968), Byrne(1976), Zienkiewicz and Humpheson(1977).

2.3.1 Example of application

The numerical simulation of the construction of the earth fill described in item 2.2.5.2 was repeated. But this time the pore pressures calculated by the previous finite element analysis were considered to be known and were incorporated into the analysis. The material parameters used were the same as shown in tab.2.3, except for the pore pressure parameters.

The difference in displacements between the two analysis was less than 0.1%. Even lower differences were observed in stresses.

The analysis was repeated once more. The pore pressure distribution obtained by interpolation that best approximated the pore pressures calculated by the finite element analysis, discussed in item 2.2.5.2, was incorporated into the analysis as known quantities.

The differences in relation to the original analysis were around 7% in terms of displacement.Smaller differences were observed in terms of stresses. Fig. 2.30 shows the displacements calculated by the use of the interpolated pore pressures in comparison with the original values along vertical sections **AA** and **BB**.

2.4 Conclusion

The interpolation procedure described was found to be relatively inexpensive and flexible enough to allow the incorporation of additional information other than the piezometer measurements. Engineering judgment can be exercised and boundary conditions can be imposed with the purpose of satisfying the physical constraints of each individual case.

The examples of application presented included smooth and abrupt pore pressure variations. In both cases the distribution obtained by interpolation was in good agreement with the values calculated by the finite element analysis, which was considered to be the "real" distribution.

The number of equilibrium iterations necessary for the analysis in which the pore pressures were incorporated as known quantities was lower than the number necessary for the analysis in which the pore pressures were calculated by the use of pore pressure parameters **A** and **B**.

The methodology presented for the interpolation of piezometer measurements and incorporation of the interpolated values into the finite element analysis may be very useful for back analysis purposes in cases where pore pressures are measured in field.

It may also be useful for prediction if reasonable assumptions about the pore pressure distribution can be made. Various possible distributions can be considered and their effects on the behaviour of the structure can be analysed.

	EXP=1		EXP=3
	m=2	m=4	m=4
λ_{1A}	0.5000	0.4028	0.49545
λ_{2A}	0.5000	0.4038	0.49545
λ_{3A}	0.0000	0.1346	0.00903
λ_{4A}	0.0000	0.0577	0.00007
λ_{1B}	0.0000	0.1316	0.00611
λ_{2B}	0.5000	0.3947	0.49683
λ_{3B}	0.5000	0.3947	0.49683
λ_{4B}	0.0000	0.0789	0.00023

λ_{1A} - weight of influence of piezometer i on the interploation at position **A**.

Tab.2.1 - Influence of **m** and **exp** on weight λ

weight function	m	exp	number of iter.
a	4	2	11
a	4	4	9
a	4	1	13
b	4	2	13
b	4	4	11
b	4	1	17
b	10	1	22

a - ref. to weight function shown in fig.2.3
b - ref. to weight function shown in fig.2.4

Tab.2.2 - influence of m and exp on the number of iterations.

	mat	γ Kn/m^3	E (Mpa)	μ	K	n	c (Kpa)	ϕ (Deg)	rf	A	B
switch on gravity	1	22	325	0.45							
	2	20	50	0.45							
	3	22	2000	0.45							
fill construction	1	22		0.40	3500	0.2	10	37	0.9	0.2	0.2
	2	20	50	0.40			0	25		0.3	0.4
	3	22	2000	0.30						0.1	0.2
	4	20	15	0.40							

Tab.2.3 - Material parameters for fill construction

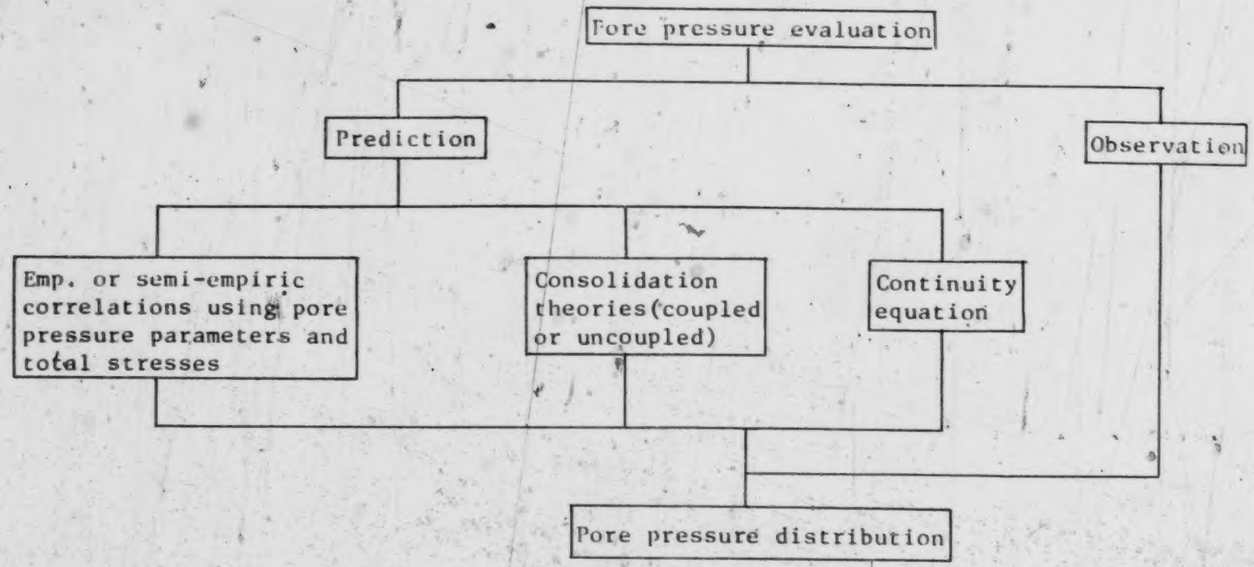
Pore pressure evaluation
Prediction
Observation
Emp. or semi-empiric correlations using pore pressure parameters and total stresses
Consolidation theories(coupled or uncoupled)
Continuity equation
Pore pressure distribution

Fig. 2.1: Pore pressure evaluation methods

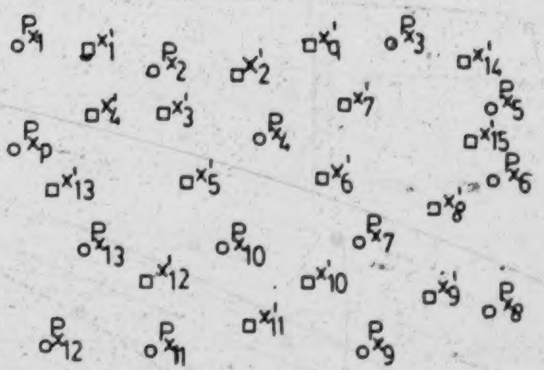
x_1^P
x'_1
x_2^P
x'_2
x'_q
x_3^P
x'_{14}
x'_4
x'_3
x'_7
x_5^P
x_p^P
x_4^P
x'_{15}
x'_{13}
x'_5
x'_6
x'_8
x_6^P
x_{13}^P
x_{10}^P
x_7^P
x'_{12}
x'_{10}
x'_9
x_8^P
x_{12}^P
x_{11}^P
x'_{11}
x_9^P

$\circ x_p^P$ Piezometer place at position x_p

$\square x'_q$ Position where interpolation is to be performed

Figure 2.2: Pore pressure interpolation

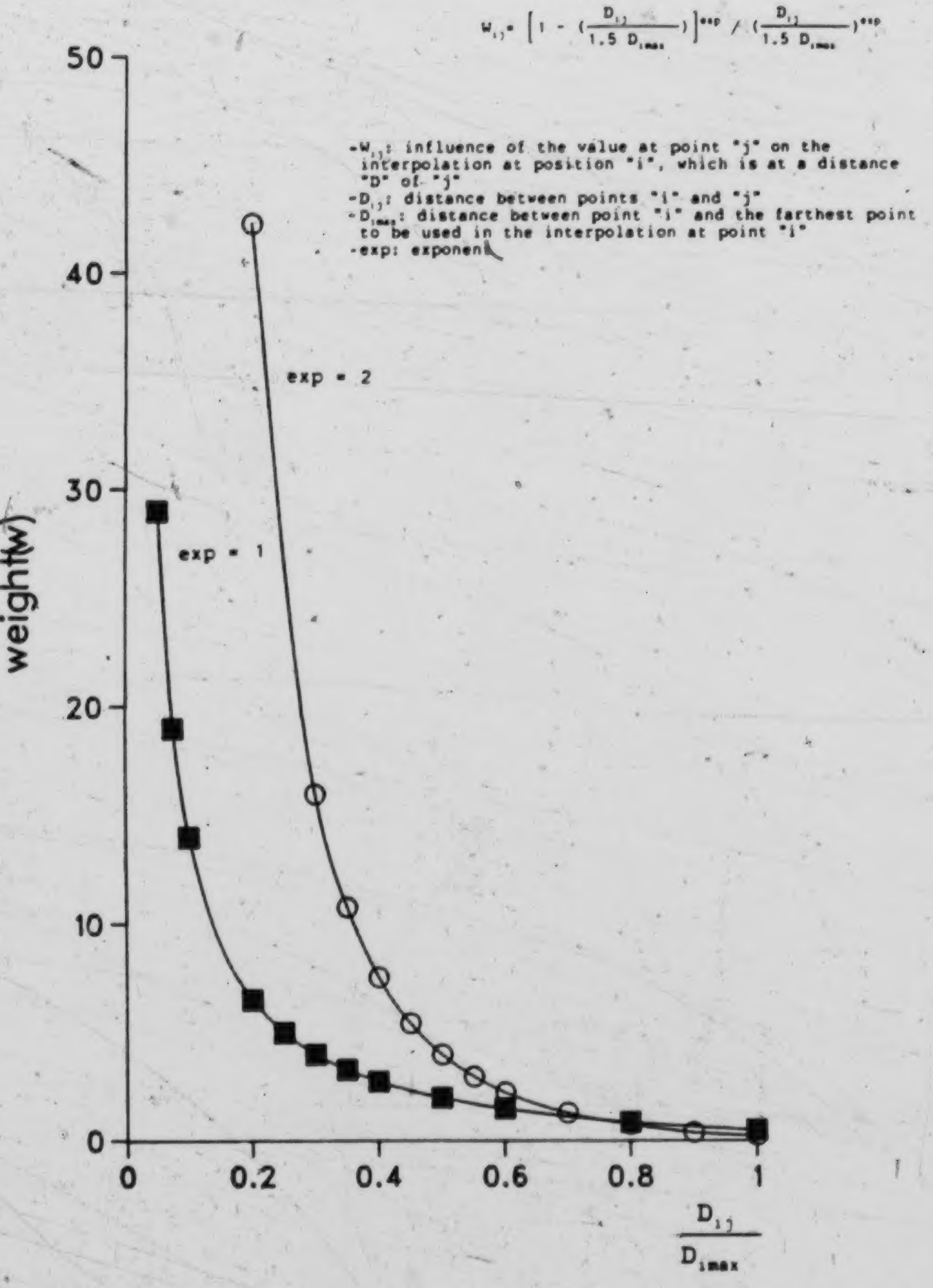

$$W_{ij} = \left[1 - \left(\frac{D_{ij}}{1.5\ D_{imax}}\right)\right]^{exp} / \left(\frac{D_{ij}}{1.5\ D_{imax}}\right)^{exp}$$

-W_{ij}: influence of the value at point "j" on the interpolation at position "i", which is at a distance "D" of "j"

-D_{ij}: distance between points "i" and "j"

-D_{imax}: distance between point "i" and the farthest point to be used in the interpolation at point "i"

-exp: exponent

Figure 2.3: weight function

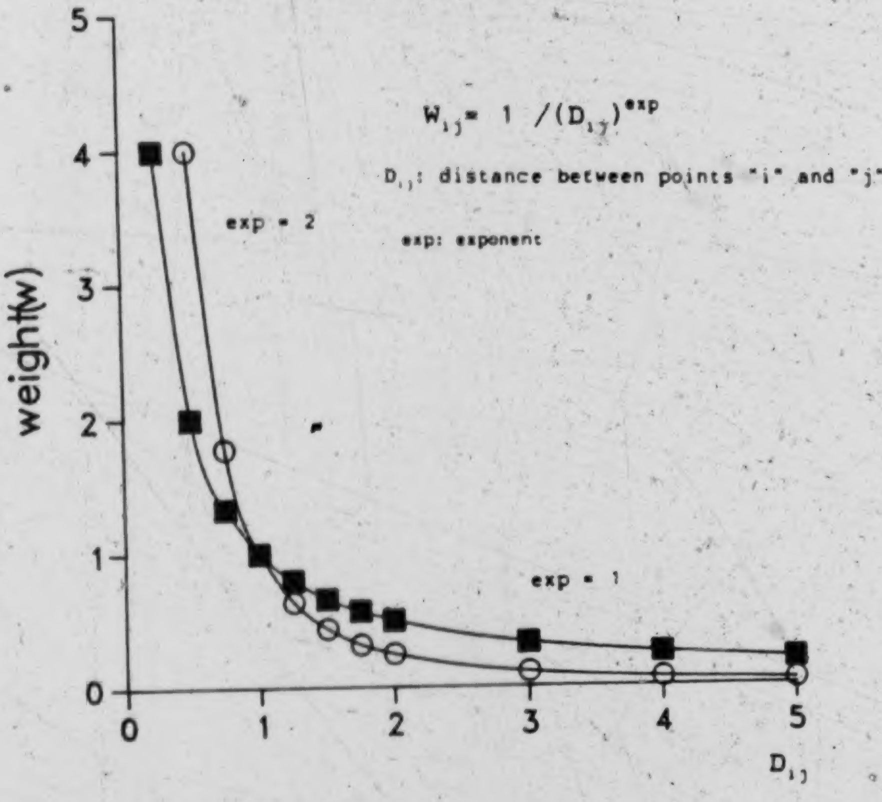

Figure 2.4: weight function

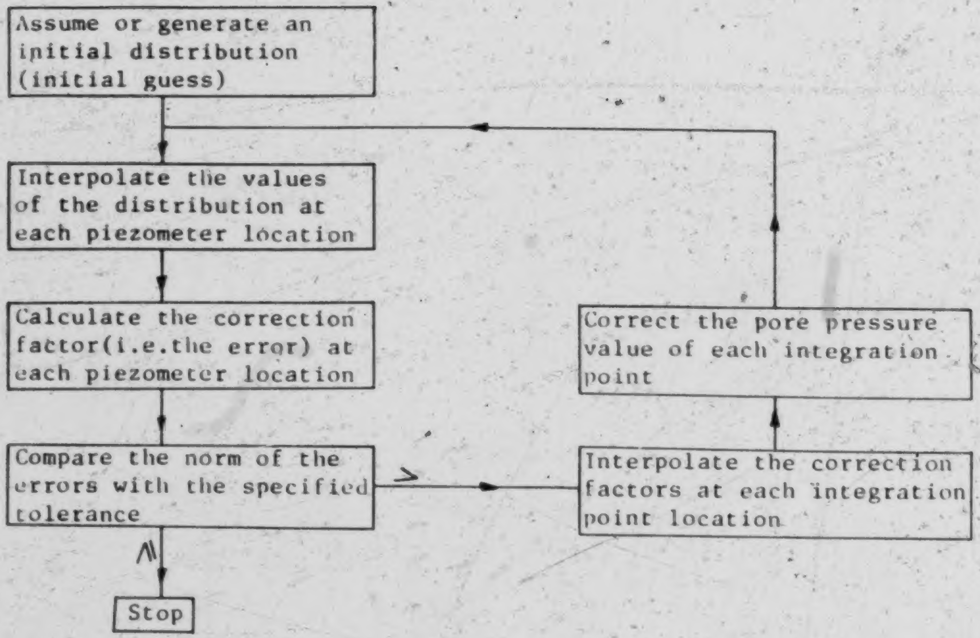
Assume or generate an initial distribution (initial guess)
Interpolate the values of the distribution at each piezometer location
Calculate the correction factor(i.e.the error) at each piezometer location
Compare the norm of the errors with the specified tolerance
>
≤
Stop
Interpolate the correction factors at each integration point location
Correct the pore pressure value of each integration point

Fig. 2.5: Flowchart of the interpolation procedure

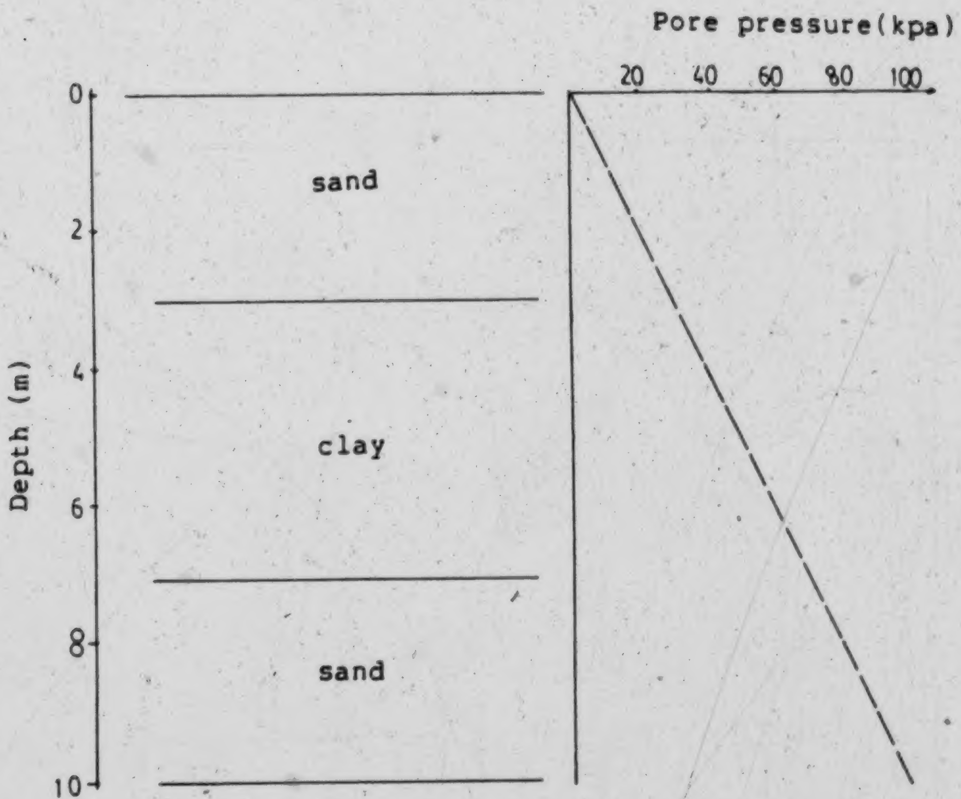
Pore pressure(kpa)
20
40
60
80
100
0
2
4
6
8
10
Depth (m)
sand
clay
sand

Figure 2.6: Incorporation of additional information - statigraphy

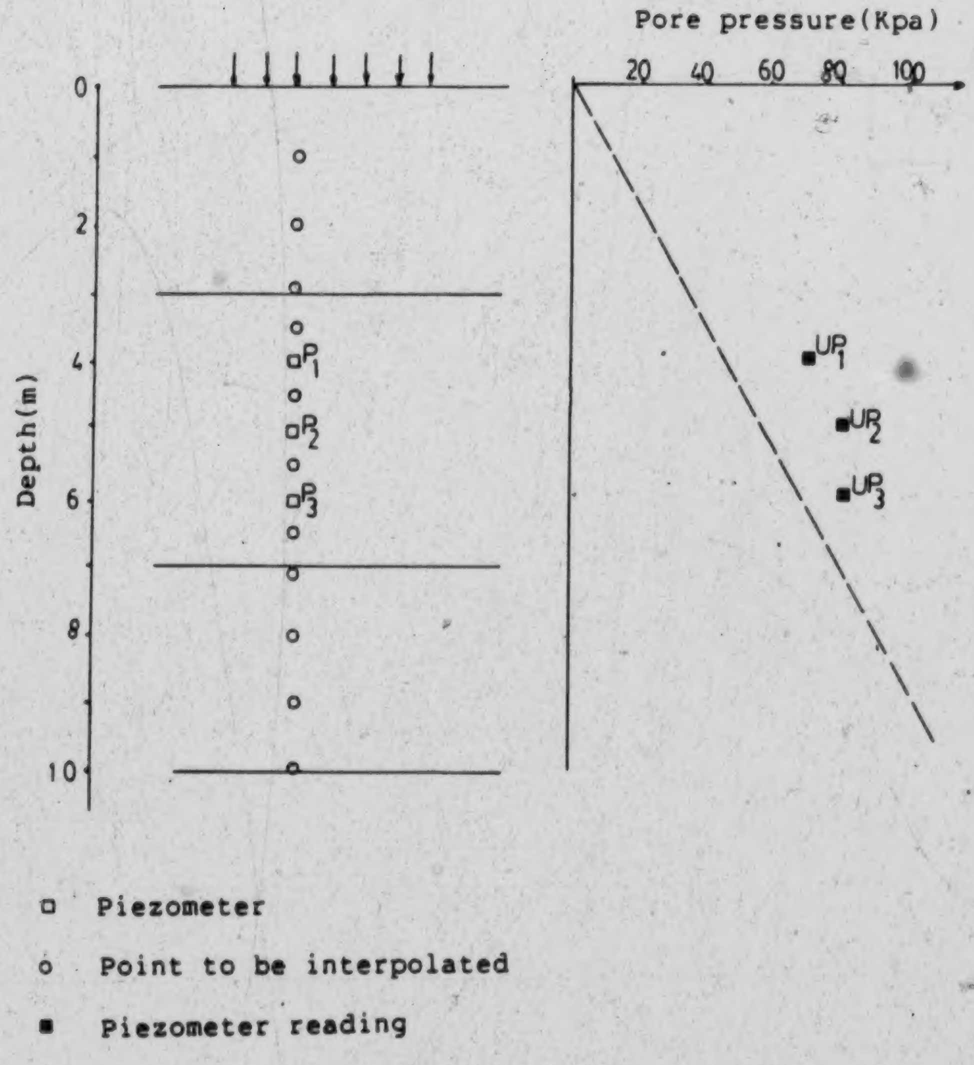

Figure 2.7: Piezometric readings and interpolation positions

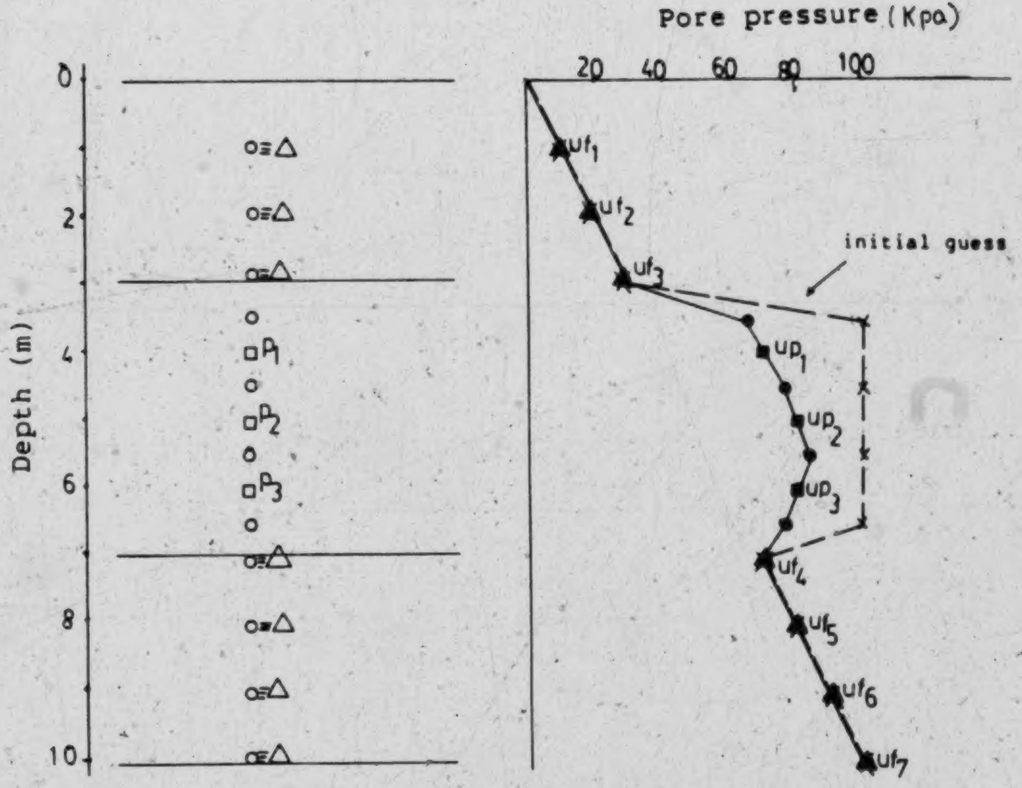

□-real piezometers
o-point to be interpolated
Δ-fictitious piezometers
▲-uf_i: pore pressure of fictitious piez. at position 'i'
■-up_j: pore pressure of real piezometer at positrion 'j'
o≡Δ point to be interpolated coinciding with fictitious piez.
-weight function used is shown in fig 2.3
-constant m = 3 and constant exp = 2
●-values obtained by interpolation

Figure 2.8: Results obtained by the use of fictitious piezometers

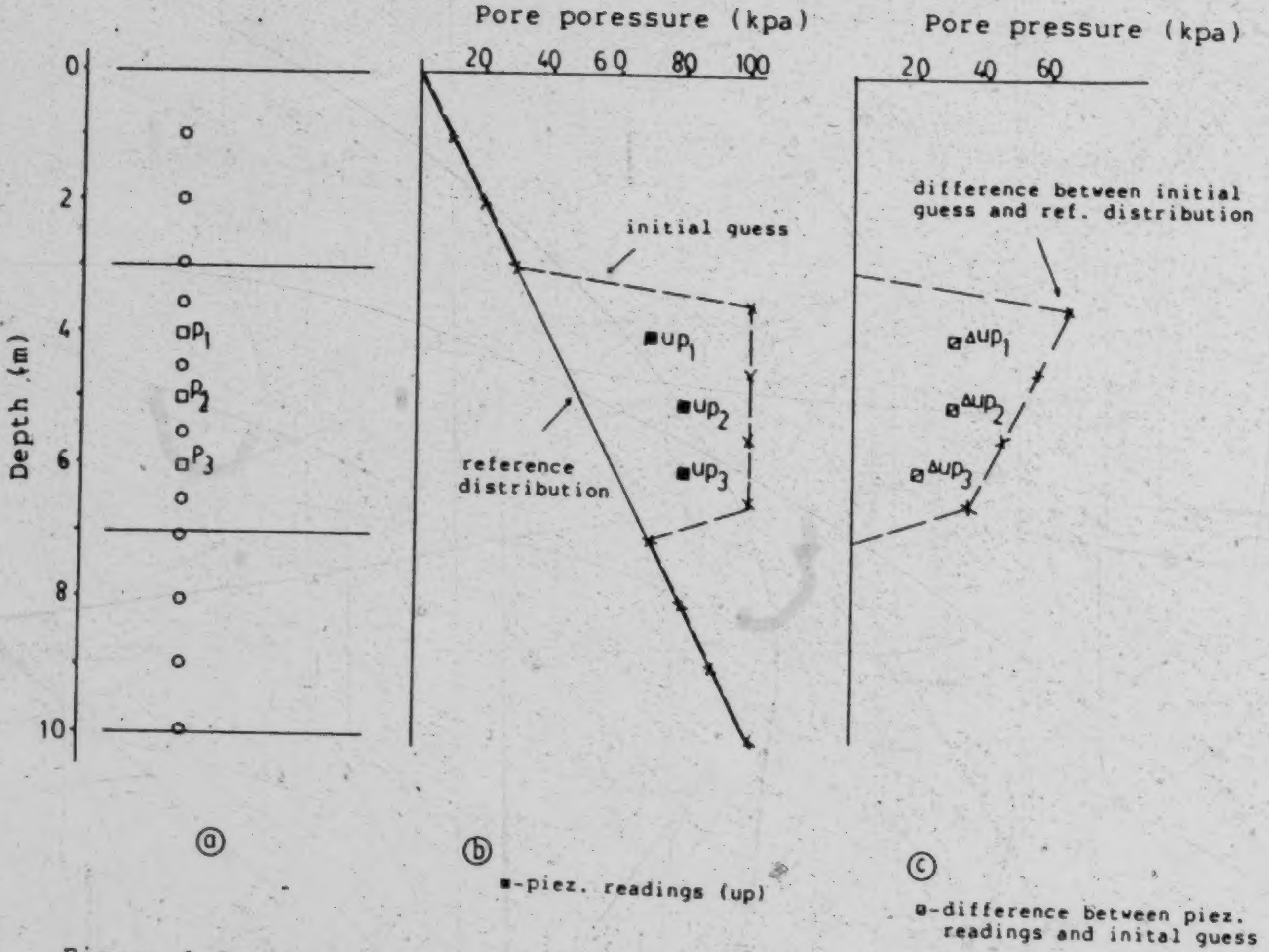

Figure 2.9: Incorporation of additional information using a reference distribution

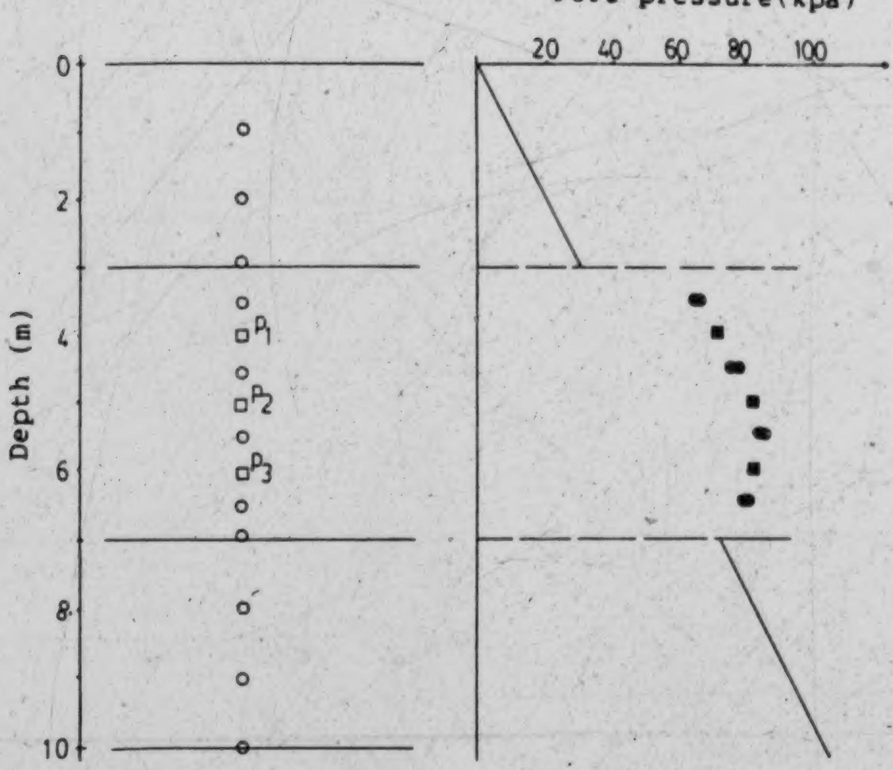

■-piezometer reading
●-interpolated values (boundary conditions imposed by use of fictitious piezometers)
●-interpolated values (boundary conditions imposed by use of a reference distribution)

Figure 2.10: Comparison between interpolated values

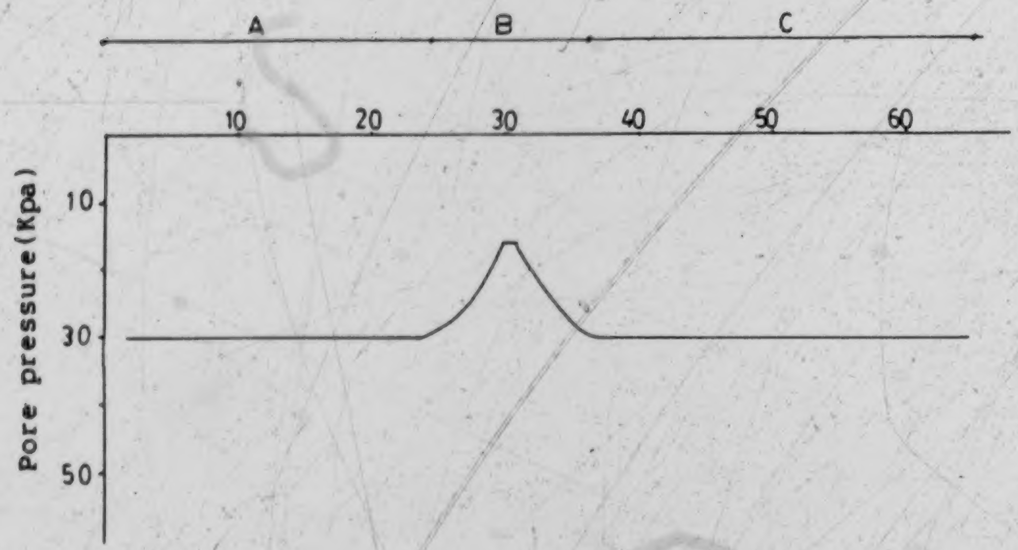

Figure 2.11: Significance of the number and position of the piezometers

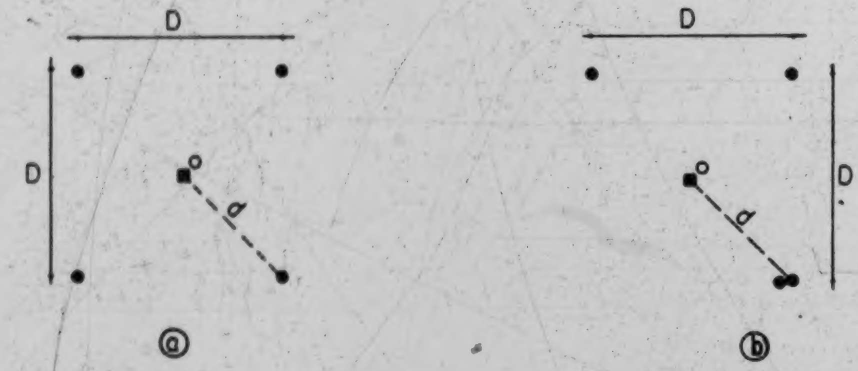

Figure 2.12: Significance of the distance between the piezometers

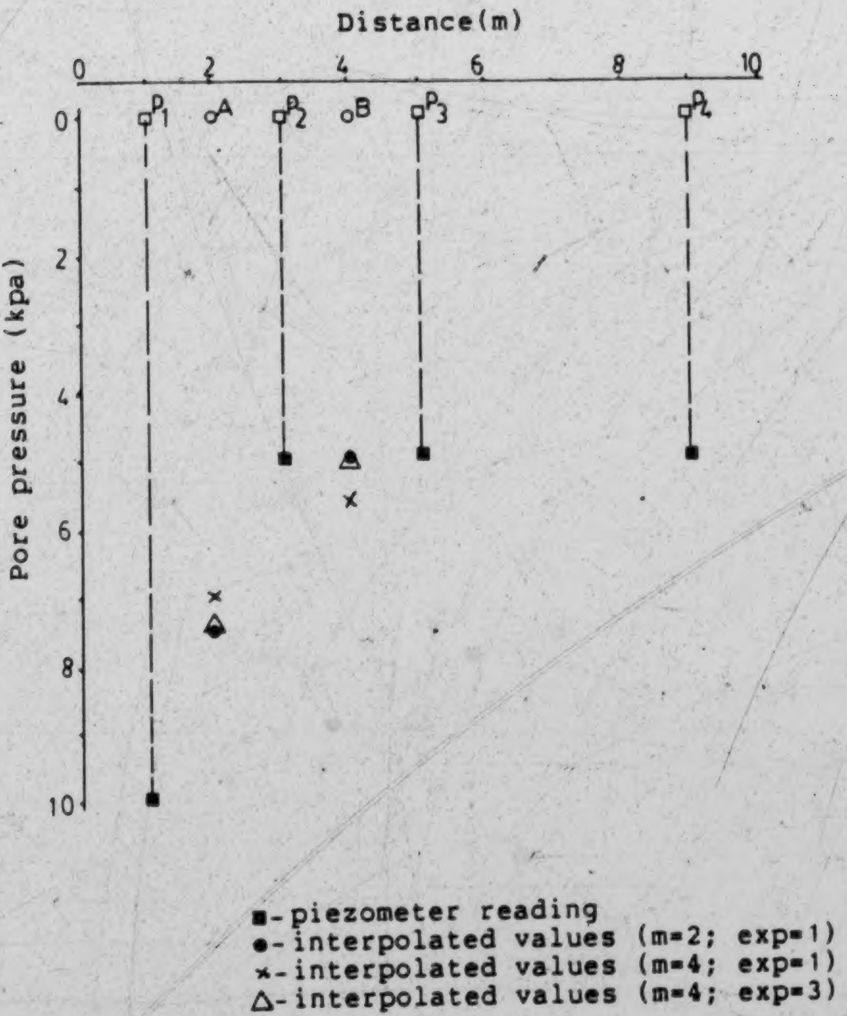

Figure 2.13: Influence of m and exp on the results of the interpolation

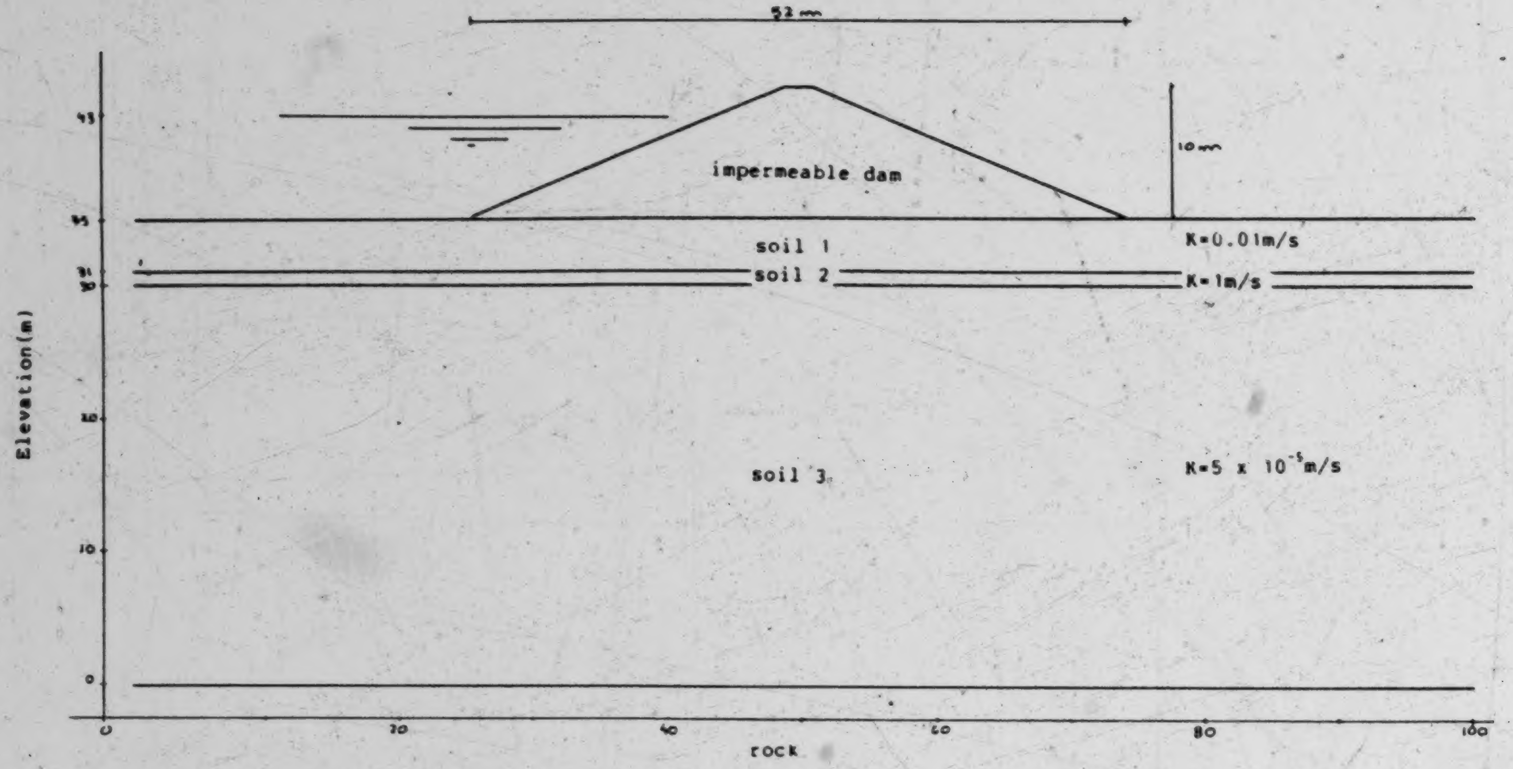
52 m
10 m
impermeable dam
soil 1
K=0.01m/s
soil 2
K=1m/s
soil 3
K=5 x 10^{-5}m/s
rock
Elevation(m)
45
35
31
30
20
10
0
0
20
40
60
80
100

Figure 2.14: Foundation stratigraphy

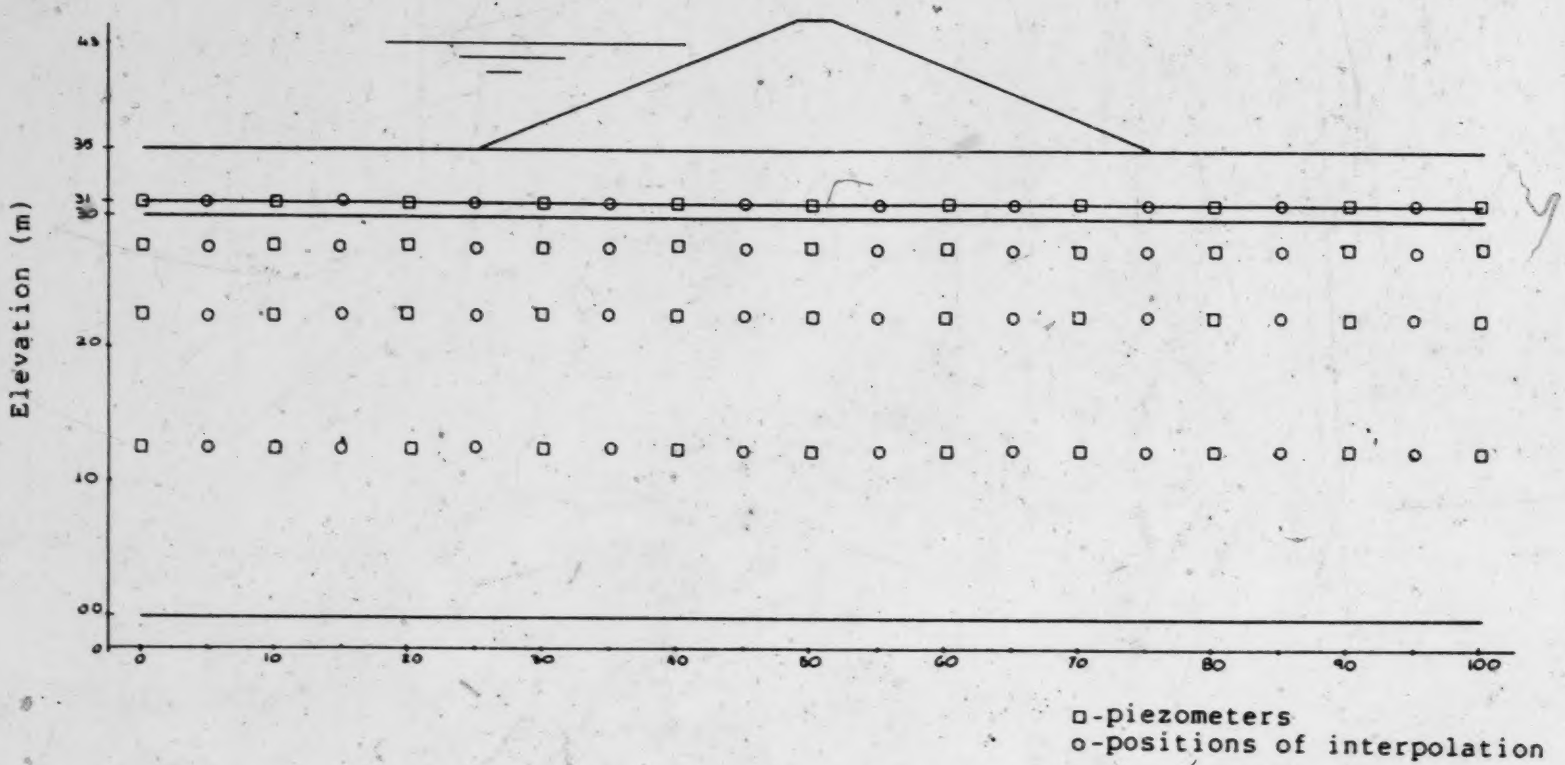
Elevation (m)
45
35
31
30
20
10
00
0
0
10
20
30
40
50
60
70
80
90
100
□-piezometers
o-positions of interpolation

Figure 2.15: Piezometers and positions of interpolation

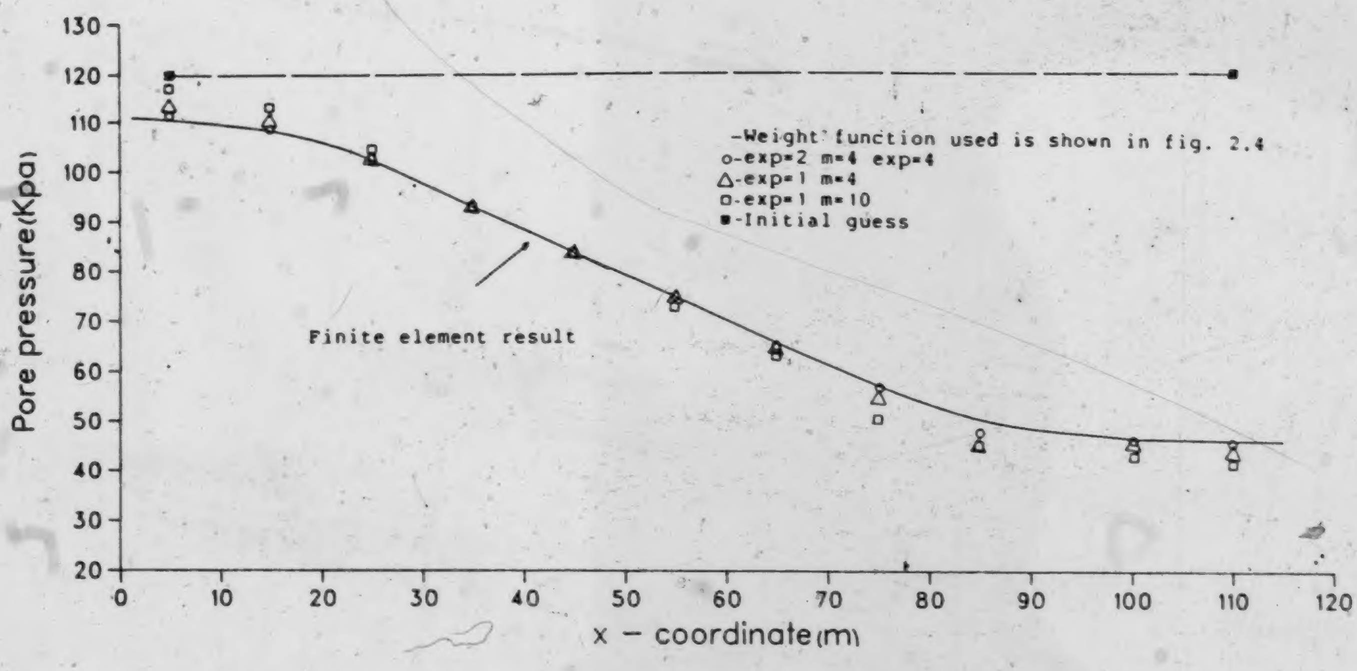

Figure 2.16: comparison between results of interpolation and finite element analysis - elevation=31m

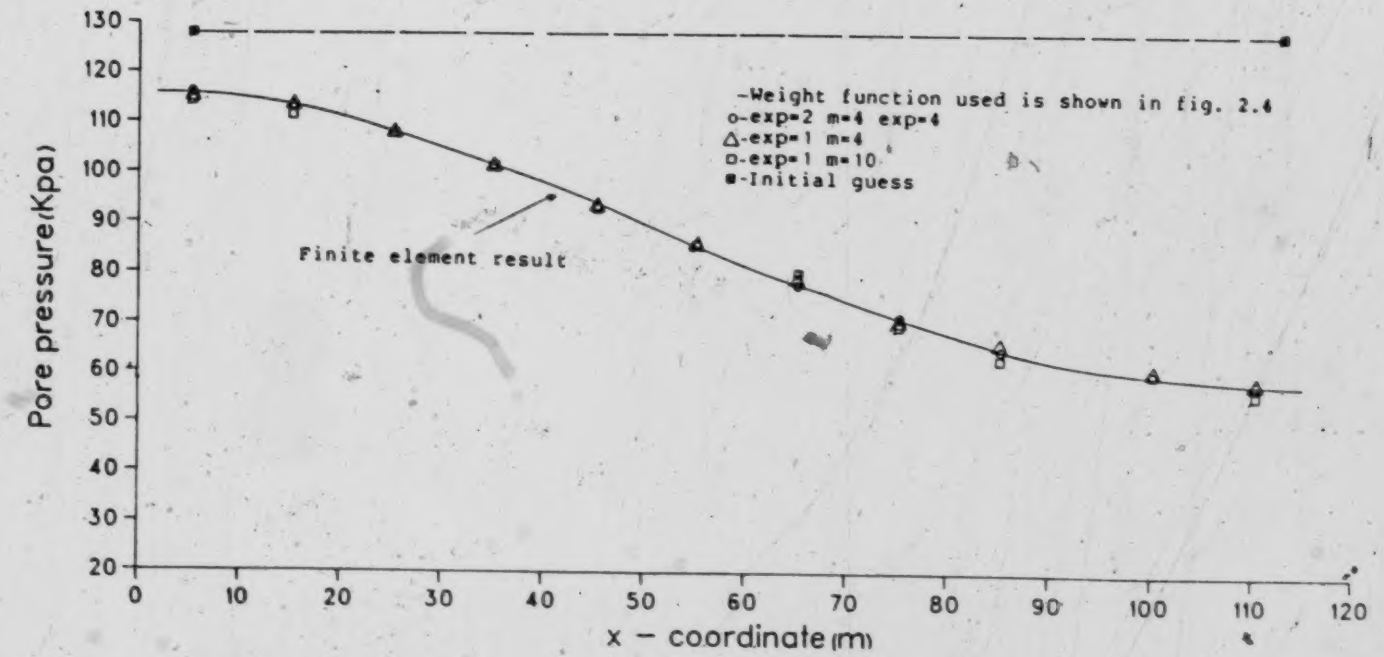

Figure 2.17: comparison between results of interpolation and finite element analysis - elevation=22m

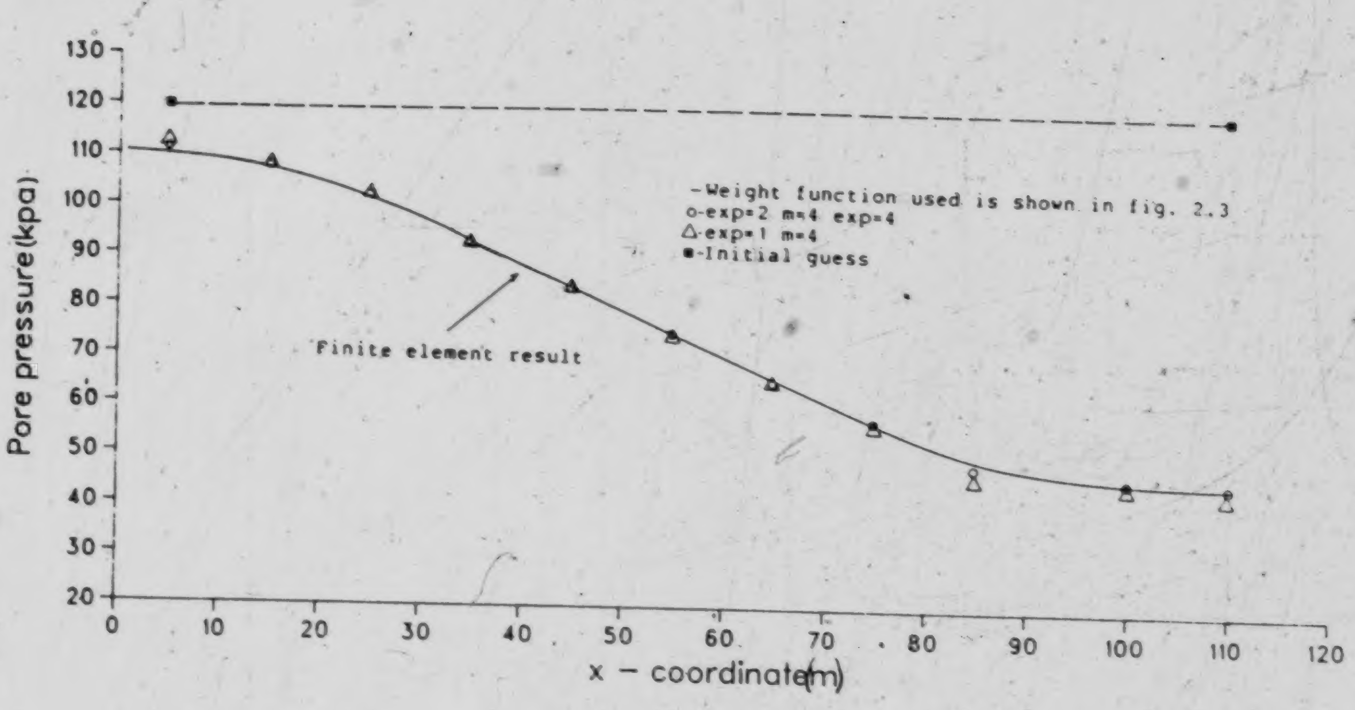

Figure 2.18: comparison between results of interpolation and finite element analysis - elevation=31m

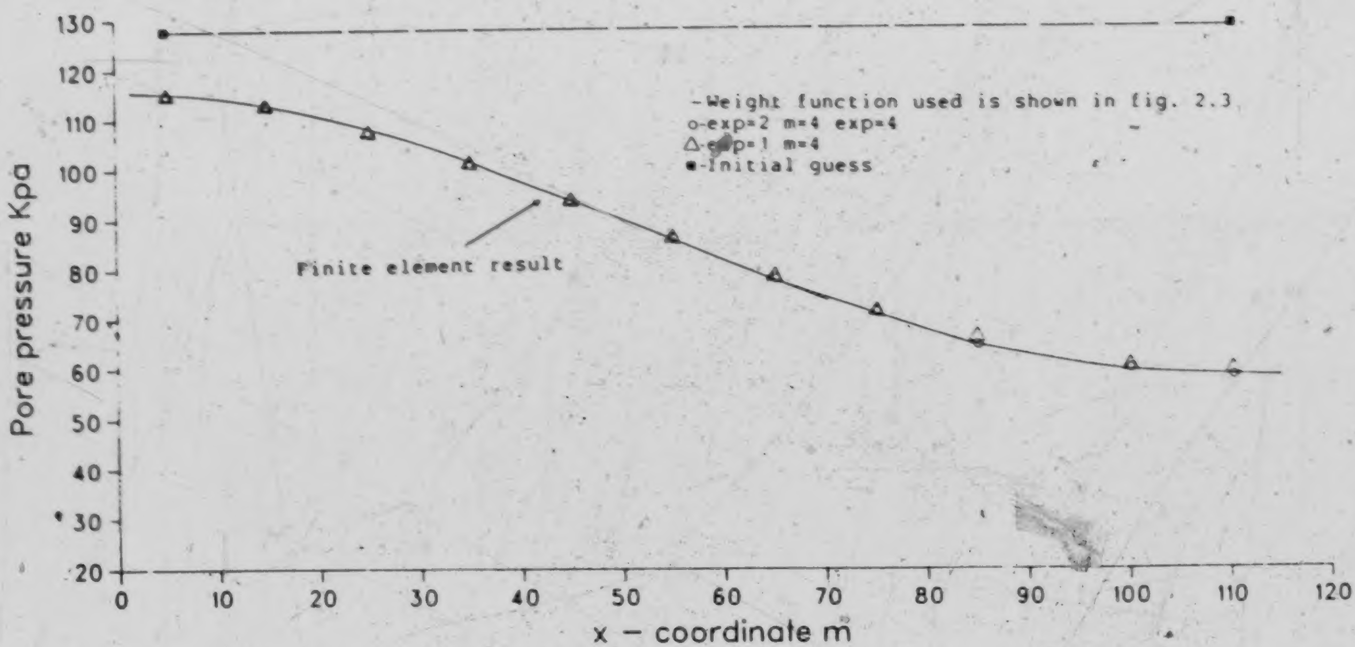

Figure 2.19: comparison between results of interpolation and finite element analysis - elevation=22 m

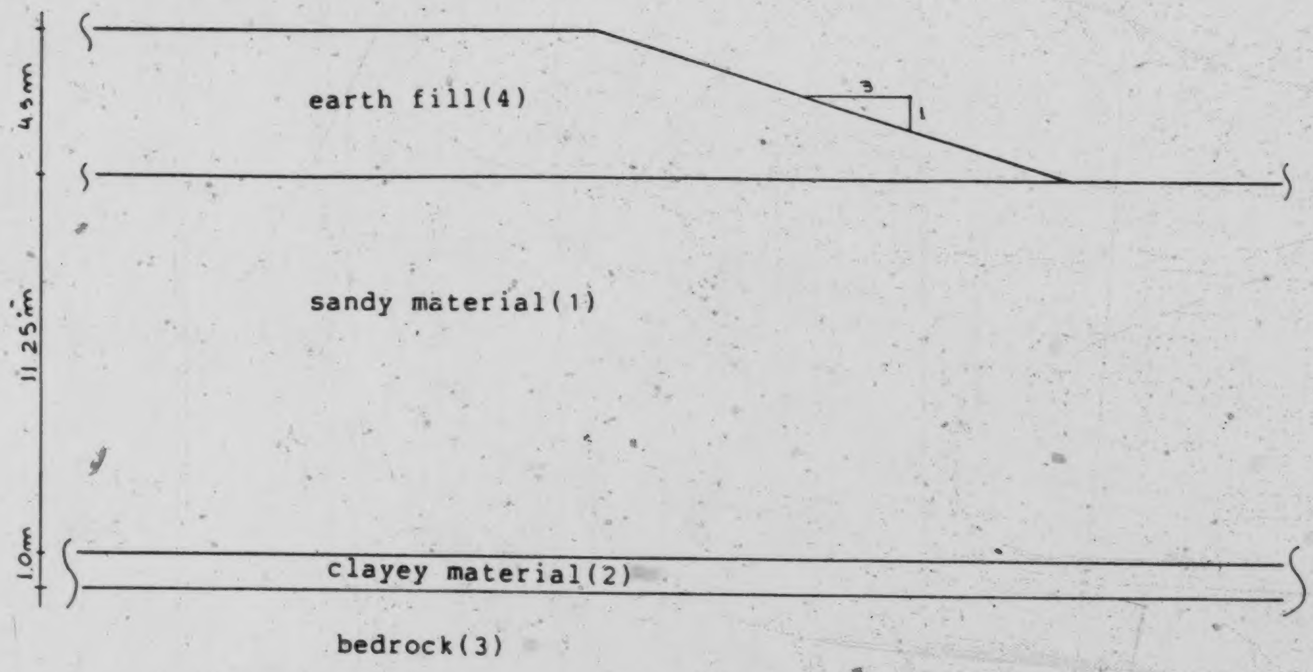
4.5m
11.25m
1.0m
earth fill(4)
3
1
sandy material(1)
clayey material(2)
bedrock(3)

Figure 2.20: Earth fill construction - foundation stratigraphy

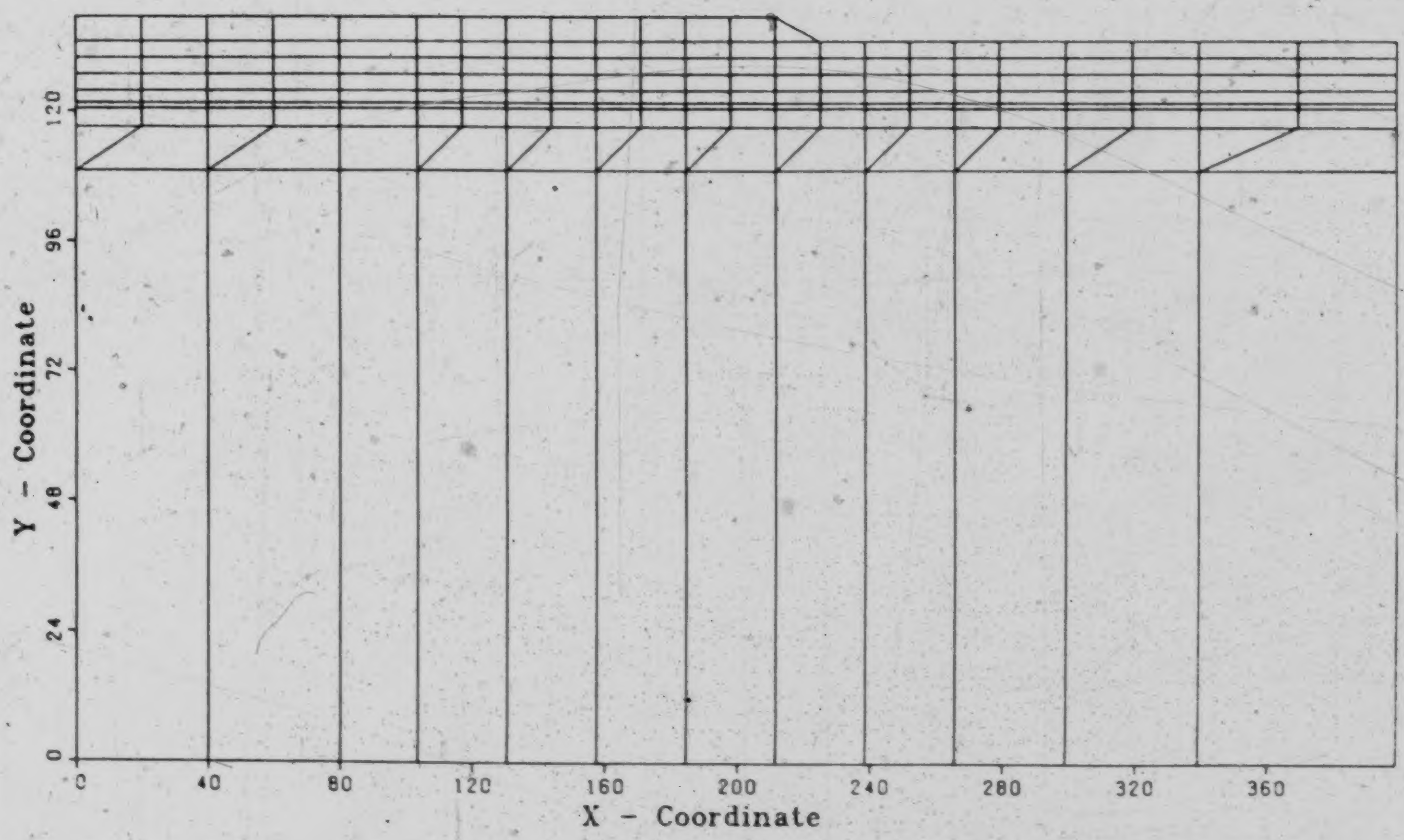
0
24
48
72
96
120
Y - Coordinate
0
40
80
120
160
200
240
280
320
360
X - Coordinate

Figure 2.21: Finite element mesh

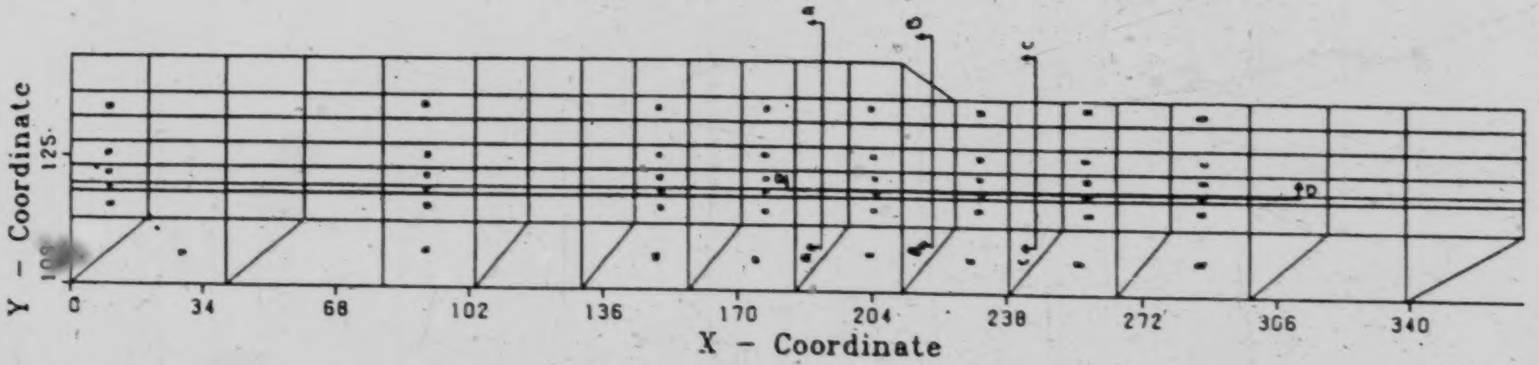
a
b
c
d
Y - Coordinate
125
109
0
34
68
102
136
170
204
238
272
306
340
X - Coordinate

■-Piezometer tips (located at the center of the
element in which they are indicated)
-Total of 48 tips

Figure 2.22: Piezometers location

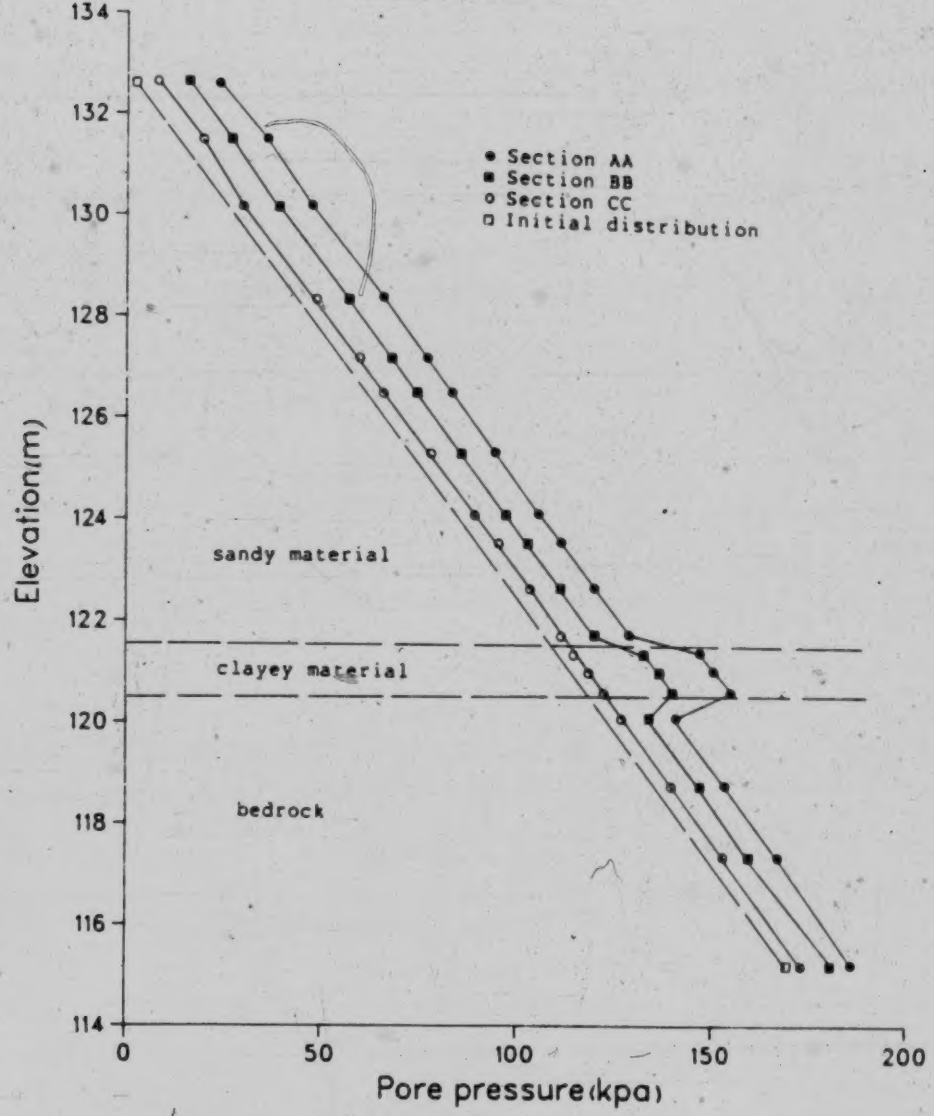

Figure 2.23: Pore pressures calculated by the finite element analysis

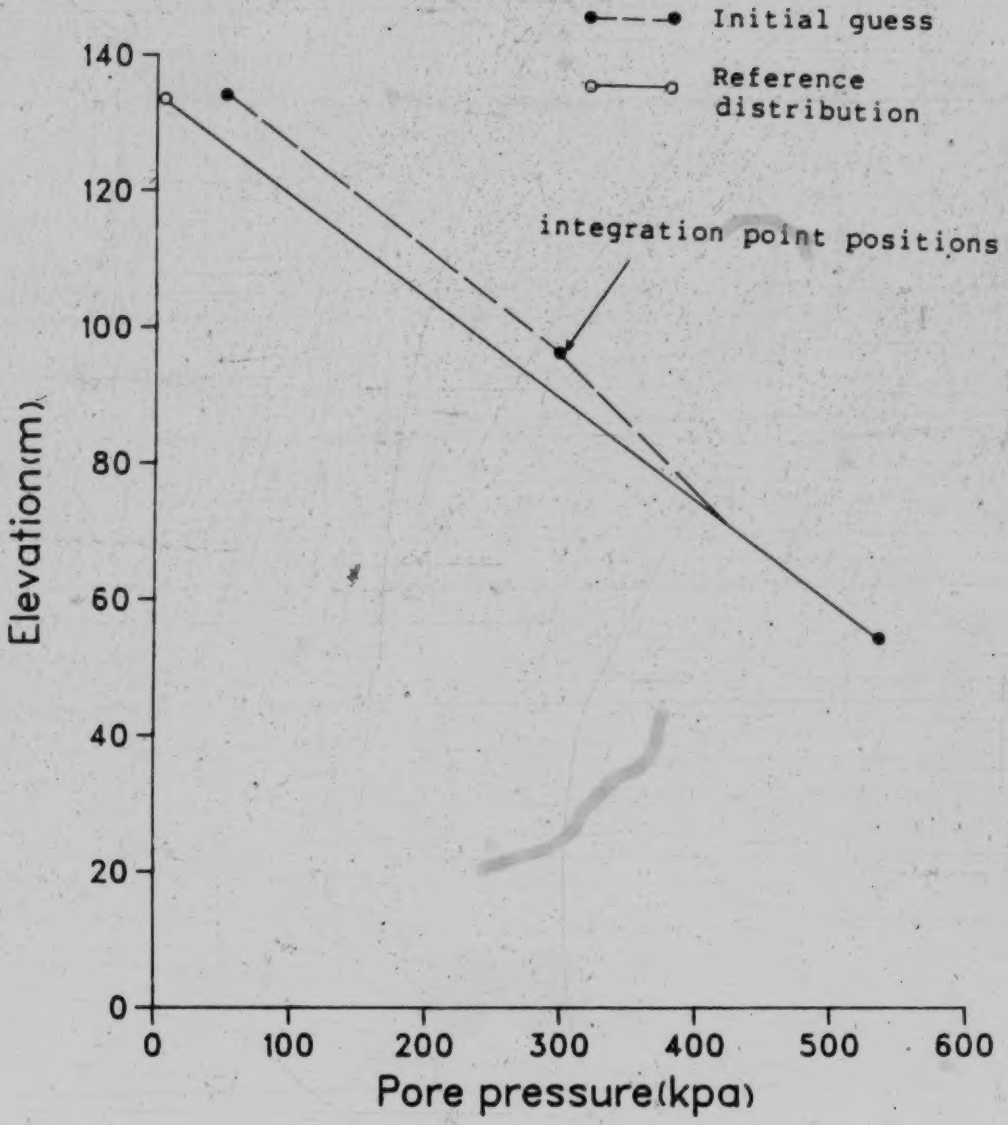

Figure 2.24: Reference distribution and initial guess with depth

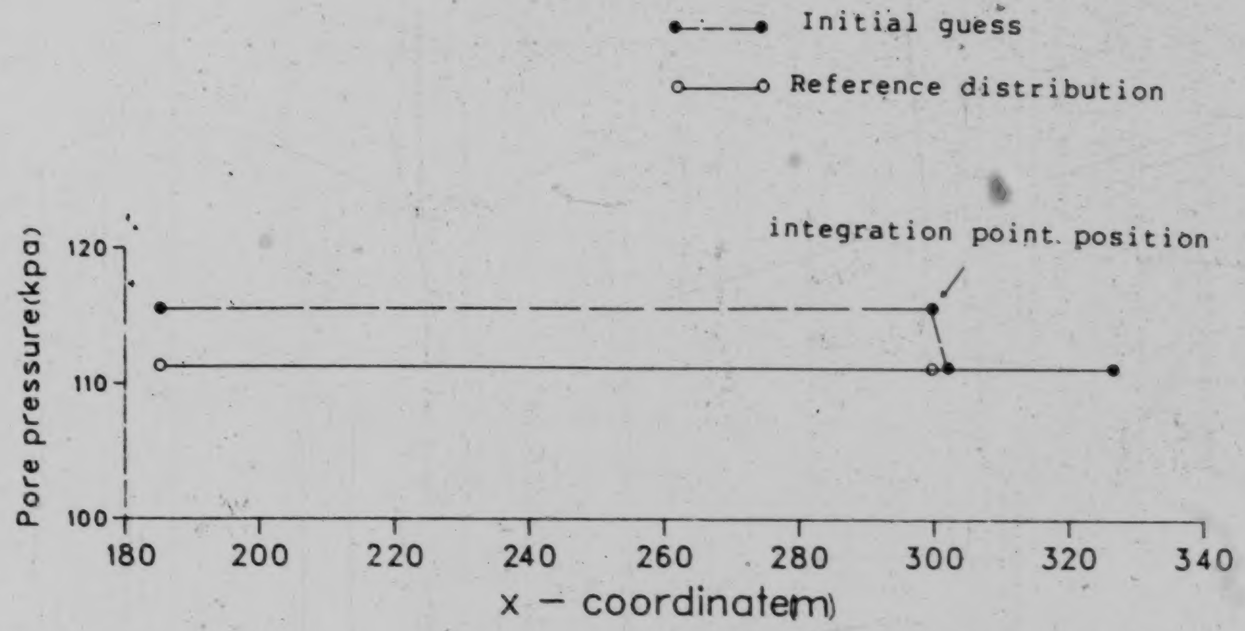

Figure 2.25: Reference distribution and initial guess with horizontal axis

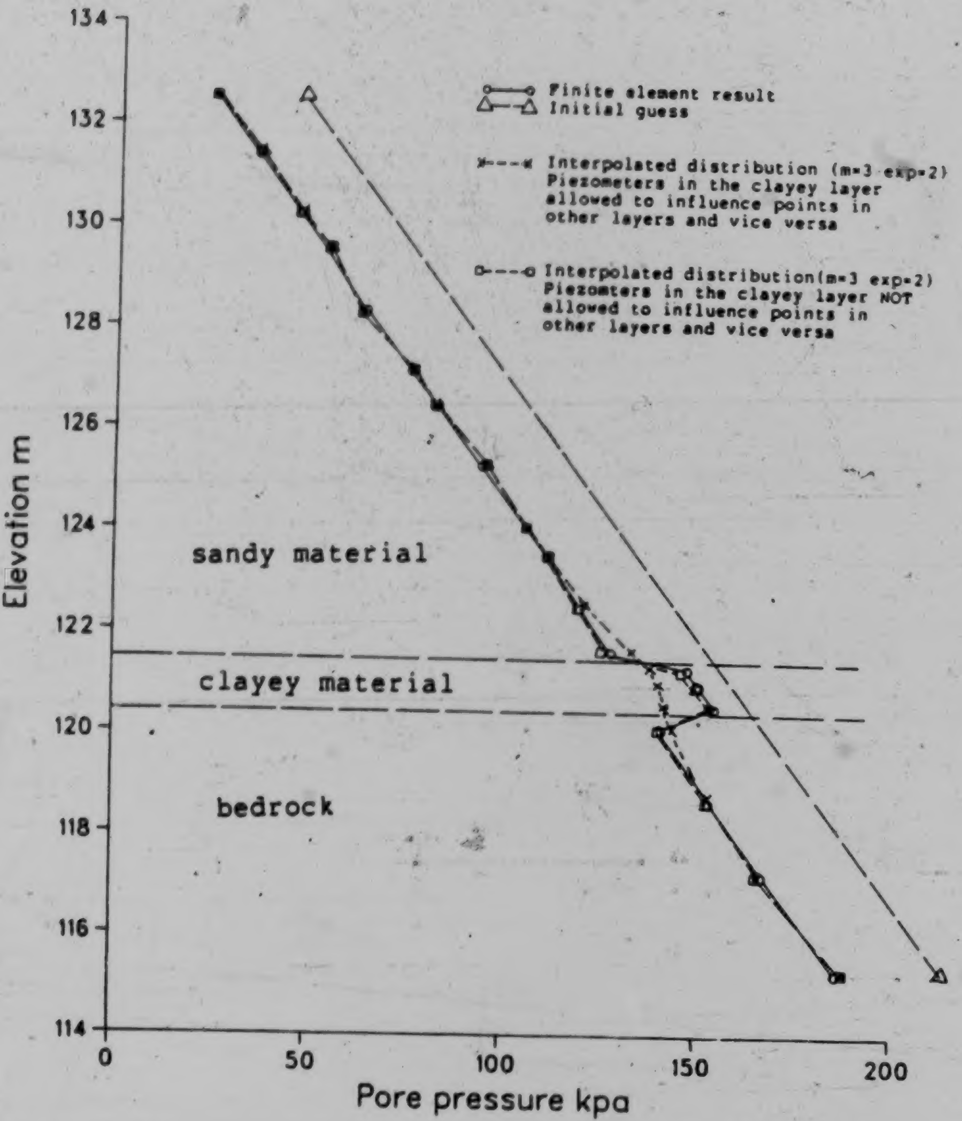

Figure 2.26: Comparison between pore pressures calculated by the finite element analysis and by interpolation- section AA

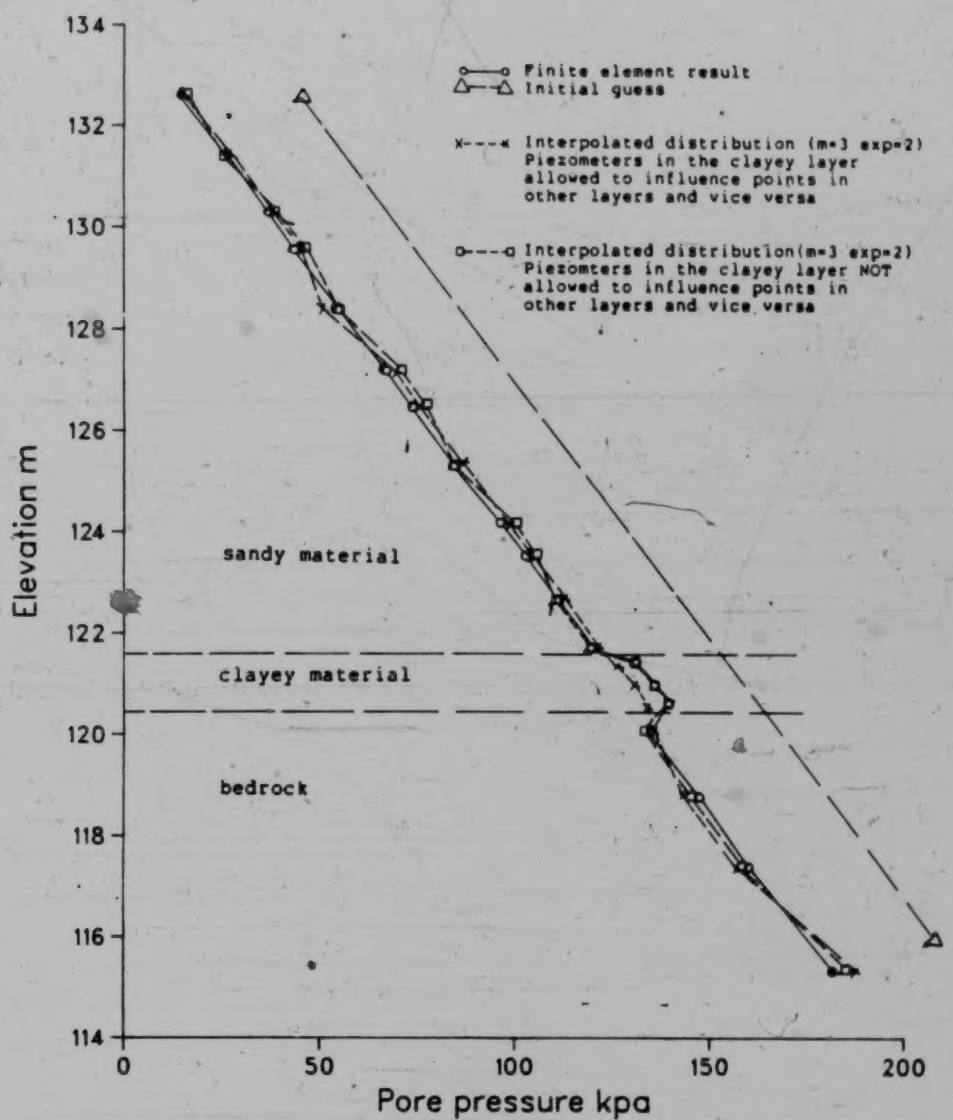

Figure 2.27: Comparison between pore pressures calculated by the finite element analysis and by interpolation- section BB

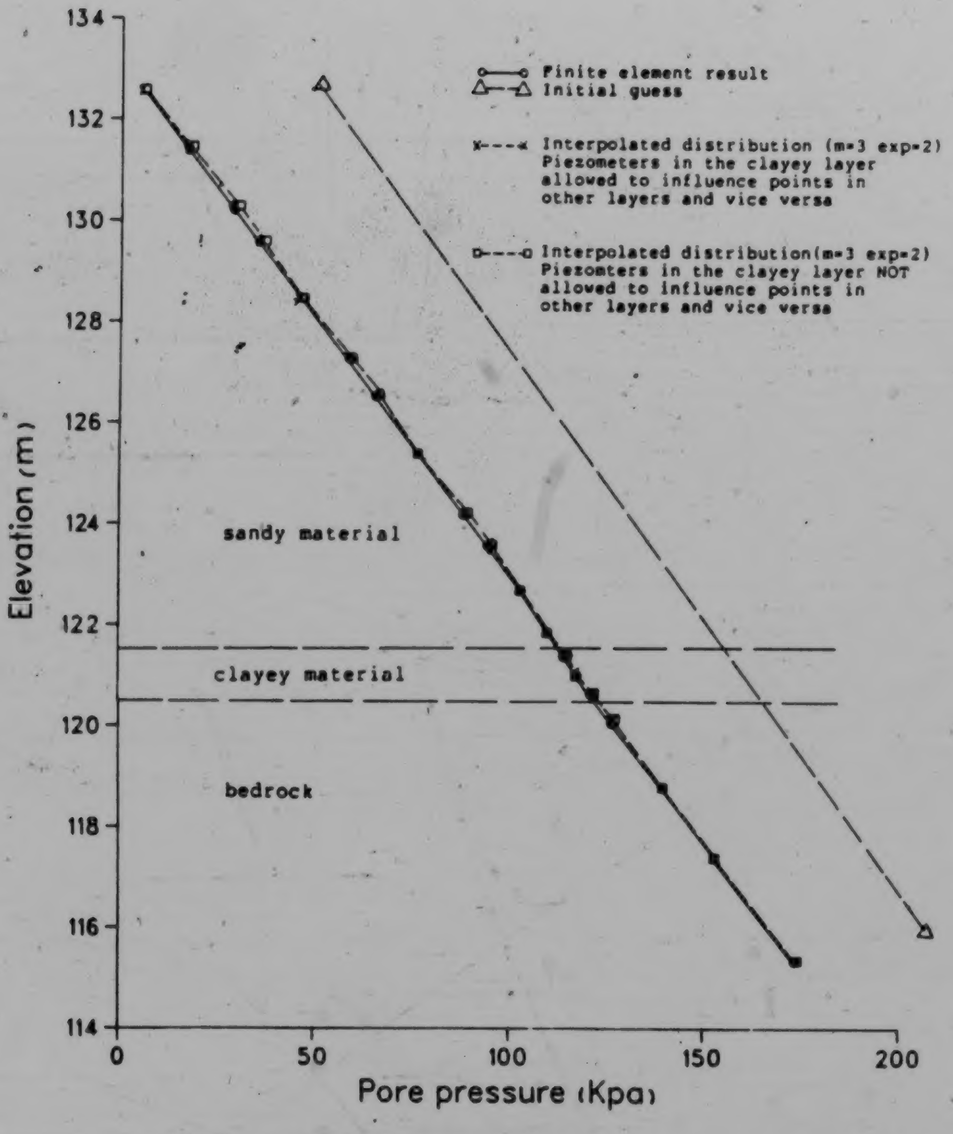

Figure 2.2[illegible]: Comparison between pore pressures calculated by the finite element analysis and by interpolation- section CC

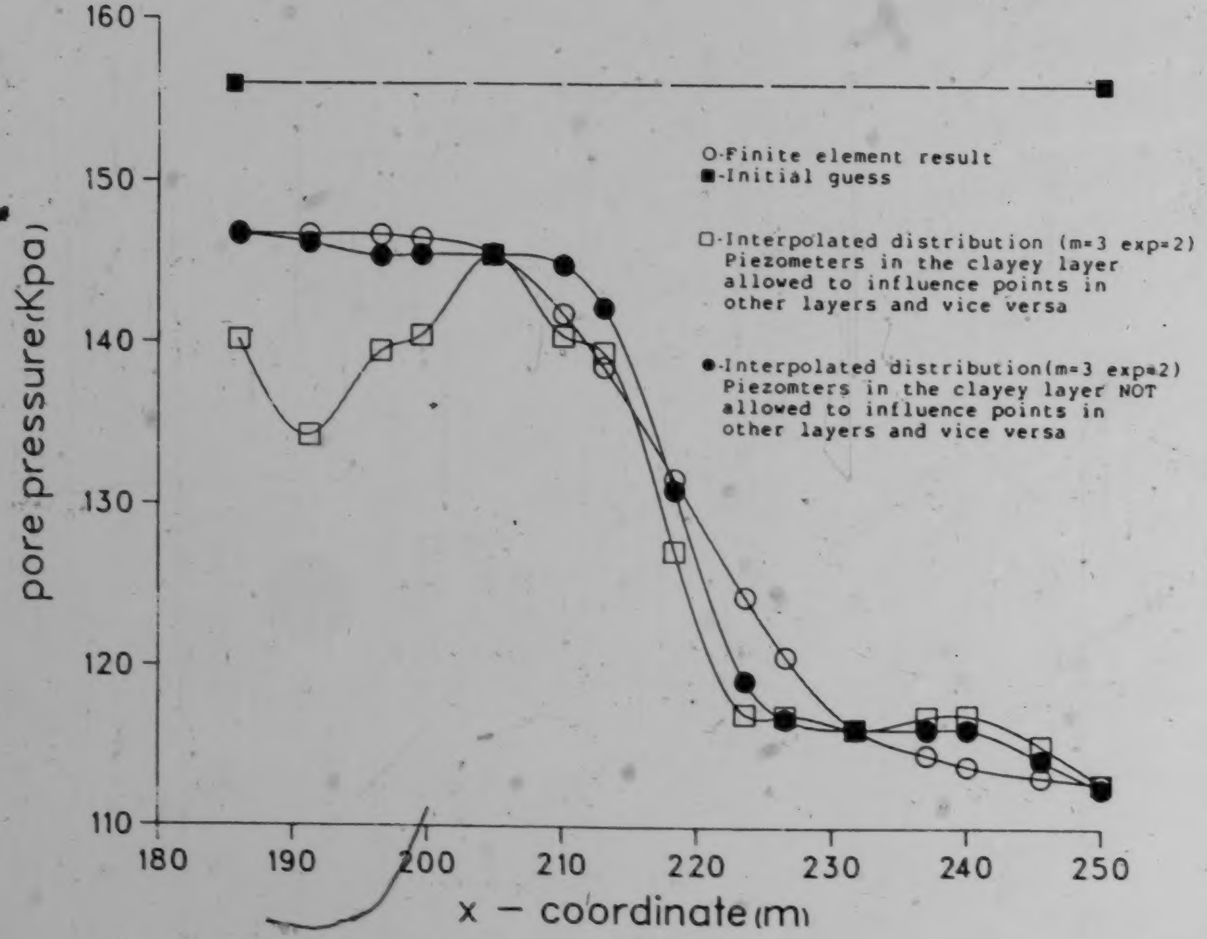

Figure 2.29: Comparison between pore pressures calculated by the finite element analysis and by interpolation- section DD

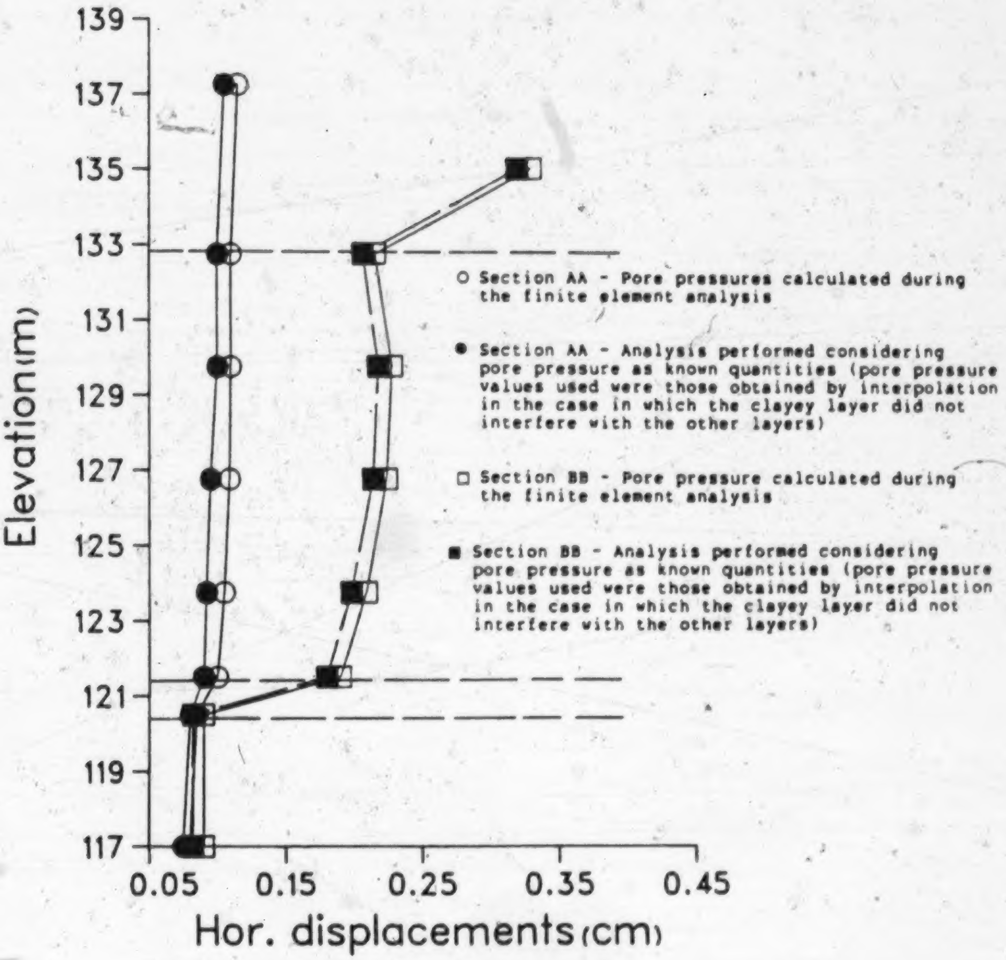

Figure 2.30: Horizontal displacements along sections AA and BB

3. Cracking Model

3.1 Introduction

Soils and most rocks have low tensile strength and are often considered incapable of sustaining any tensile stress. In a large number of finite element computational schemes used in geotechnical engineering, this is modelled by means of an iterative stress transfer method suggested by Zienkiewicz *et al.* (1968).

By the procedure usually adopted, the elastically calculated tensile stresses in excess of the tensile strength are eliminated and no anisotropy is introduced in the stiffness of the region in tension (i.e. in the stiffness of the element where tension occurred).In general the material in this region remains with its original isotropic elastic parameters. The equilibrium configuration is then searched iteratively,even in case of the linear elastic model, by successive application of the work equivalent unbalanced load vector. This procedure has poor convergence characteristics in practice, since, at each iteration,the regions where tension tends to develop attract and release additional tensile stresses in a process of continuous loading of the surrounding elements.

In this chapter an alternative procedure based on the constitutive relationship for fractured concrete presented by Chen and Suzuki(1980) is described. This scheme accounts for opening and closing of fissures and is,in general, numerically more stable than the one mentioned above. For simplicity, the model is presented in plane strain, but it can, of course, be extended to a three dimensional situation.

The results of an eigen-analysis performed on two cracked element stiffness matrices with cracks in horizontal and vertical orientations are discussed as a way of more clearly understanding the physical meaning of the model and checking its numerical implementation.

Differences between Zienkiewicz's procedure and the cracking model are illustrated by solving an idealized problem using both techniques and by comparing the results. The use of the cracking model as an indicator of hydraulic fracture potential is shown by the finite element simulation of a 3m deep excavation.

3.2 Cracking model as a no tension model in plane strain

3.2.1 Crack formation and incremental stiffness for cracks oriented in one direction

According to this model, a crack is assumed to form in the plane perpendicular to a principal stress direction whenever it exceeds the tensile strength of the material, as shown in fig.3.1.

At the instant the crack is formed, the normal stress perpendicular to the crack plane is released (shear stress is zero since it is a principal plane), but the normal stress in the direction parallel to the crack orientation remains unchanged. Stresses acting on planes of intermediate orientation experience varying degree of release in order to maintain equilibrium, as shown schematically by segment AB of fig.3.2. In matrix formulation this stress release is expressed by:

In the principal stress coordinates O-X'Y'(see fig.3.1)

$$\{\Delta\sigma'\} = \{\sigma'\}_A - \{\sigma'\}_B \qquad [3.1]$$

in which

$\{\Delta\sigma'\}$ = stress release due to cracking expressed in the coordinate system O-X'Y'

$\{\Delta\sigma'\}^t = \langle\Delta\sigma_x', \Delta\sigma_y', \Delta\tau_{xy}'\rangle$

$\{\sigma'\}_A$ = stress vector in the coordinate system O-X'Y' just before cracking

$\{\sigma'\}_A^t = \langle\sigma_x', \sigma_y', \tau_{xy}'\rangle$

$\{\sigma'\}_B$ = stress vector in the coordinate system O-X'Y' just after cracking

$\{\sigma'\}_B^t = \langle \sigma_x', 0, 0 \rangle$

It is noted that the normal stress oriented perpendicular to the plane of the crack (σ_x') remains unchanged. That is, σ_x' at point **A** in fig. 3.2 is the same as at point **B**.

Derivation of the following relations can be found on Chen and Suzuki(1980).By using transformation of coordinates it can be shown that, since σ_y' and τ_{xy}' are vanished after the crack is formed, in the global coordinate system O-XY(see fig.3.1), equation 3.1 is expressed as:

$$\{\Delta\sigma\} = \{\sigma\}_A - \{B\theta\}\ \sigma_x' \qquad [3.2]$$

in which

$\{\Delta\sigma\}$ = stress release due to cracking expressed in the coordinate system O-XY

$\{\Delta\sigma\}^t = \langle \Delta\sigma_x, \Delta\sigma_y, \Delta\tau_{xy} \rangle$

$\{\sigma\}_A$ = stress vector in the coordinate system O-XY just before cracking

$\{\sigma\}_A^t = \langle\sigma_x, \sigma_y, \tau_{xy}\rangle$

$\{B\theta\}^t = \langle\cos^2\theta, \sin^2\theta, \sin\theta\cos\theta\rangle$

In the global coordinate system O-XY, $\sigma_x{}'$ may be expressed as:

$$\sigma_x{}' = \{b\theta\} \{\sigma\}_A$$

in which
$\{b\theta\}^t = \langle\cos^2\theta, \sin^2\theta, 2\sin\theta\cos\theta\rangle$

Therefore, equation 3.2 may be rewritten as:

$$\{\Delta\sigma\} = \{\sigma\}_A - (\{B\theta\} \{b\theta\}^t) \{\sigma\}_A \qquad [3.3]$$

Equation 3.3 expresses the stress release vector due to cracking as a function of the stress vector just before cracking and the crack orientation.

Assuming the behaviour of the cracked material to be linear elastic, the incremental stress-strain relationship for a cracked material (segment BC on figure 3.2) is given by:

$$\{\delta\sigma\} = \frac{E}{(1-\mu^2)}\{B\theta\}\{B\theta\}^t\{\delta\epsilon\} \qquad [3.4]$$

in which,

$\{\delta\sigma\}$ = stress vector increment for a cracked material in the coordinate system O-XY

$\{\delta\sigma\}^t = \langle\delta\sigma_x, \delta\sigma_y, \delta\tau_{xy}\rangle$

$\{\delta\epsilon\}$ = strain vector increment in the coordinate system O-XY

$\{\delta\epsilon\}^t = \langle\delta\epsilon_x, \delta\epsilon_y, \delta\gamma_{xy}\rangle$

E = Young's modulus for a non-cracked material

μ = Poisson's ration for a non-cracked material

Equation 3.4 may be expressed as:

$$\{\delta\sigma\} = [C_c]\{\delta\epsilon\} \qquad [3.5]$$

in which

$[C_c]$ = constitutive matrix for a cracked material

$$[C_c] = \frac{E}{(1-\mu^2)}\{B\theta\}\{B\theta\}^t$$

This formulation introduces an anisotropy in the stiffness matrix making the normal and shear stiffness across the crack plane to be zero and increasingly stiffer as the orientation considered changes from perpendicular to parallel to the plane of crack.

3.2.2 Formation of cracks oriented in two directions

In this case, see fig.3.3, the stresses in all directions are completely released and the stiffness matrix at that particular integration point is assumed to be close to zero,i.e., it becomes unable to sustain stresses in any direction.

3.2.3 Closing of cracks

The strain normal to the crack plane just prior to the crack formation is used as reference for verification if the crack remains active(i.e. open) or has closed at each integration point. As an illustration, consider the case presented schematically in fig.3.4. Fig 3.4a shows the orientation of a certain plane β along which a crack will be formed at time t + 1.

The normal strain ϵ_t is, then, the reference strain for considering the crack open or closed(see fig.3.4b). If it is now considered that a subsequent straining ϵ_{t+2} occurs, in the case of fig.3.4c the crack remains open, while in the case of fig.3.4d it closes.

In this last situation,for the calculation of stresses, the stiffness is formulated considering the existence of a crack for the fraction of the strain increment $(\epsilon_{t+1}-\epsilon_{t+2})$ relative to a strain level greater or equal ϵ_t, indicated as strain increment fraction A in fig.3.4d. From then on, i.e., for the strain increment fraction indicated as (B-A), the stiffness matrix is formulated as non-cracked, which results in stiffness increase.

This procedure is not very stable since the displacements corresponding to the entire strain increment $\epsilon_{t+2}-\epsilon_{t+1}$ are calculated using a stiffness matrix which considers the existence of a crack, therefore, overestimating the fraction of the strain increment relative to a non-cracked material. This overestimation of strains tends to generate excessively high stresses at that point, since, for the calculation of the stress increment associated with the non-cracked fraction of the strain increment (B-A) in fig 3.4d the stiffness matrix is increased, as the crack is closed.

In case of the closure of two cracks at the same integration point, decision needs to be made on which crack is considered to close first, since this influences the value of stress to be calculated. In the present implementation this decision is taken based on the crack width.

As an illustration, consider that at a certain integration point two cracks are open as shown schematically in fig.3.5a. An increment of confining stress causes both cracks to close. In this example the increment of strain is devided into 3 distinct stages: stage 1, where both cracks are open, and no increment of stresses occur(see fig.3.5a);

stage 2, where only the crack with narrower width has closed(see fig.3.5b) and stage 3 in which both cracks have closed(see fig.3.5c). Stages 2 and 3 have different stiffnesses.

When substantial closing of cracks may occur, the load increment should be reduced in order to improve convergence characteristics. If all cracks are closed, the material behaves as non-cracked, or solid, at that point. The process of crack formation described above may, then, be restarted with cracks in any orientation.

Considering fig.3.1 the normal strain across a crack is given by:

$$\epsilon_n = \{B(\theta+\frac{\pi}{2})\}^t \{\epsilon\} \qquad [3.6]$$

in which

ϵ_n = strain normal to the plane of the crack

$\{\epsilon\}$ = strain vector in the coordinate system O-XY

$\{\epsilon\}^t = \langle \epsilon_x, \epsilon_y, \gamma_{xy} \rangle$

$\{B(\theta+\frac{\pi}{2})\}^t = \langle \cos^2(\theta+\frac{\pi}{2}), \sin^2(\theta+\frac{\pi}{2}), \sin(\theta+\frac{\pi}{2}) \cos^2(\theta+\frac{\pi}{2}) \rangle$

Procedure for extension of the cracking model to allow for shear stresses along the plane of crack is indicated in the appendix I.

3.3 Eigenanalysis of cracked stiffness matrices

One way of investigating the stiffness characteristics of an element is by determining the eigenvalues of the stiffness matrix, that is:

$$[K]\ \{\phi\}_i = \lambda_i\ \{\phi\}_i \qquad [3.7]$$

[K] is the element stiffness matrix

$\{\phi\}_i$ is the eigenvector associated to the eigenvalue λ_i

If it is considered in a finite element problem:

$$[K]\ \{\phi\}_i = \{R\}_i \qquad [3.8]$$

that the nodal loads $\{R\}_i$ on a certain element are proportional to the nodal displacements $\{u\}_i$ through a factor λ_i, the problem becomes:

$$[K]\ \{u\}_i = \lambda_i\ \{u\}_i \qquad [3.9]$$

which, as mentioned above, is an eigenproblem where the eigenvectors $\{u\}_i$ represent modes of displacements associated with the eigenvalue λ_i.

The physical meaning of the eigenvalues in this kind of problem can be understood by making:

$$\{u\}_i^t \, [K] \, \{u\}_i = \lambda_i \, \{u\}_i^t \, \{u\}_i \qquad [3.10]$$

If each eigenvector is normalized so that:

$$\{u\}_i^t \, \{u\}_i = 1$$

Equation 3.10 may be rewritten as:

$$\lambda_i = \{u\}_i^t \, [K] \, \{u\}_i = \{u\}_i^t \, \{R\}_i = 2U_i \qquad [3.11]$$

U_i = element strain energy

Thus, each eigenvalue λ_i of [K] is twice the element strain energy U_i when the normalized nodal displacement vector $\{u\}_i$ is imposed. More extensive discussion on the use of eigenanalysis associated with the finite element method can be found on Bathe(1982).

Eigenanalysis were performed on the cracked element in the two problems shown in fig.3.6. In the case shown in fig.3.6a the orientation of the cracks is vertical while in the other case the cracks are horizontal. The zero and non-zero eigenvalues, i.e. the zero and non-zero energy modes, and associated normalized eigenvectors for each situation are presented in figs.3.7 and 3.8. The stiffness matrix in both cases was integrated exactly.

According to the model described before, the stiffness in the direction perpendicular to the crack orientation is zero. All integration points in element two of each problem analysed have cracked along the same orientation (vertical or horizontal), which means physically that the element is slabbed vertically in case a and horizontally in case b, as shown in figs.3.9.

It is seen in fig.3.7 that the only non-zero eigenvalues are associated with vertical deformation along a certain vertical section of the element. It can be observed that independently of the horizontal deformation, as long as there is no vertical deformation along a specific vertical section, the associated strain energy, i.e. eigenvalue, is zero. Similar observations can be made in case of fig.3.8, where the non zero eigenvalues are associated with the displacement modes presenting horizontal deformation along a certain horizontal section of the element. Therefore, the eigenanalysis shows, indeed, that the elements are behaving according to the model presented before.

3.4 Comparison between the cracking model and Zienkiewicz's stress transfer procedure

In both of theses procedures, it is generally assumed that once the minimum principal stress exceeds the tensile strength of the material(which in soils is usually considered approximately zero) there is a stress release, which generates an unbalanced system. The unbalanced stresses are then transformed into a work equivalent load vector which is applied to the structure. That is, both techniques use the stress transfer concept.

The fundamental difference between the two methods is that in the no tension procedure suggested by Zienkiewicz *et al*. the stiffness at the integration point where the tensile stress occurs is maintained isotropic while in the cracking model the stiffness in the direction of the tensile stress is reduced to zero, i.e. an anisotropy is introduced.

These different considerations have a significant influence on the numerical convergence characteristic of the solution. In the first case(isotropy is maintained) the application of the work equivalent unbalanced load vector is likely to give rise to additional tensile stress which will again need to be released. In the second case (cracking model) the application of the unbalanced load vector does not generate stress normal to the plane of crack since the stiffness in that direction was set to zero.

In order to illustrate this point a problem has been solved using both methods so that results can be compared. The problem is shown in fig.3.10. Element 5 has a tensile strength of 0.0001kpa, while all the other elements have tensile strength of 1000Kpa. The material is linear elastic with E=1500Kpa and μ=0.00. A vertical extensional traction of 5Kpa(i.e. +5Kpa)is applied simultaneously to the application of a lateral compressive traction of 5Kpa(i.e. -5Kpa). This generates vertical tensile stresses in the system.

Using Zienkiewicz's no tension procedure, 13 iterations were necessary to reach the prescribed tolerance of 0.1% for the convergence error.In the case of the cracking model 3 iterations were necessary. The convergence error at each iteration is shown in fig.3.11. Despite this very different behaviour in terms of convergence, the final results in terms of stresses and strains indicate no significant difference. This is illustrated by fig.3.12 and fig.3.13, which show σ_x and σ_y along sections **AA'** and **BB'** (see fig. 3.12), respectively.

If some tensile strength is considered, Zienkiewicz's procedure eliminates the tensile stresses in excess of that strength and maintains the minor principal stress equal to σ_t. In the case of the cracking model, when σ_t is exceeded the minor principal principal stress is reduced to zero, and maintained at that value as long as the crack is open.

The consideration of existence of a crack with a certain width has other implications. If subsequently to the opening of a crack, the external forces are changed in such a way that they tend to induce a compressive stress state across the crack, this does not mean that stresses immidiately build up on that plane, since the crack needs to be closed to sustain any load again. In the case of Zienkiewicz's procedure, as the stiffness in the direction of the tensile stress has not been set to zero, stresses build up as soon as a compressive state is induced.

This is observed if additional external vertical traction is applied to the problem shown in fig.3.10, but this time directed downward. The second and third load steps are then applied as -3Kpa and -2Kpa in the vertical direction, as shown in fig.3.10.

When the cracking model is used, the application of -3Kpa is not sufficient to close the crack, therefore, no vertical stresses are generated in the central element. The same does not happen in the case of the other procedure. The stress distributions are, therefore, quite different in each case, as shown in fig 3.14.

When the increment of -2Kpa is applied, in the case of the cracking model, the cracks are closed and the vertical stress is very close to zero in all elements. Since the resultant vertical external load is now zero and the material is linear elastic, no residual vertical stresses remain(see fig 3.15).The horizontal stress returns to -5Kpa in all elements. When the other procedure is used a completely different and non uniform stress state results, and even though the material is linear elastic, the zero vertical stress state is not obtained. This is due to the fact that, as soon as the external vertical traction is reversed the central element is in a loading state while the others are unloading.

If an additional increment of -2Kpa is applied vertically, the vertical stresses assume an uniform distribution of the same value when the cracking model is used, since all cracks have been closed, while non uniform distribution persists when Zienkiewicz's method is used(see fig.3.16).

Another important aspect that must be commented is that the cracking model,as described above, implies that as long as the crack is open, the plane of the crack is necessarily a plane of principal stress, since the shear stress along that plane is zero. As the orientation of the crack is fixed, so are the directions of the principal stresses.Before a rotation of principal stresses is allowed, the crack must first be closed. This does not happen with the other procedure.

3.5 Example of application

The problem to be presented will be used to discuss how the cracking model may be useful in indicating the potential for hydraulic fracturing and its limitations in modelling such a phenomenon.

Consider a 3m excavation executed as shown in fig.3.17. For simplicity, the two existing layers are linear elastic. The material parameters used for both layers are shown in table 3.1.

No pore pressure exists in the upper layer. Three different pore pressure conditions are considered for the bottom layer:

a. Material is under artesian pressure with pore pressure at the top of the layer coresponding to a water height of 2m, as indicated in fig. 3.17.

b. Material is under artesian pressure with pore pressure at the top of the layer coresponding to a water height of 4.3m

c. The artesian pressure in this case corresponds to a water height of 5.10m

Hydraulic fracture occurs in situations where the pore pressures cause the soil a complete loss of shear strength along one or more planes. In the present simulation,in which only linear elasticity is used, this corresponds to a level where a zero effective stress condition is reached and the total stress is equal to the pore pressure.

In case a the pore pressure level is not sufficient to cause hydraulic fracturing. In cases b and c hydraulic fracture is expected to occur at the top region of the bottom layer.

At some distance from the corner of the excavation, the plane of zero effective stress is expected to be approximately horizontal, since the minor principal stress orientation should be approximately vertical.

The finite element analysis of the excavation has been divided in two stages. In the first stage, "switch-on-gravity" technique with simultaneous application of surface traction on the excavation borders (see fig. 3.18) and pore pressure values at the integration points are applied to the system to create an initial stress field.

In the second stage, surface traction of same magnitude but opposite sign as applied in the first stage is imposed in order to create a stress free surface along the excavation. For simplicity, no variation of pore pressure is assumed to occur due to the excavation.

The results obtained showed no cracks occuring in case a. In case b, the uppermost integration points (elevation 23.89m) of the bottom layer presented approximately horizontal cracks generated by hydraulic fracturing of the material. The cracks are indicated schematically in fig. 3.19. Below that elevation,no cracks occurred since at lower integration points the minor principal effective stresses are greater than zero. Fig. 3.20 shows the minimum principal effective stress with depth for the integration points which are closest to the center of the excavation.

Even though cracks were formed, the effect of hydraulic fracture in this case was not modelled. Since only the uppermost integration points of the elements at the top of the bottom layer positioned below the excavation presented cracks, the overall stiffness of those elements in the vertical direction was not reduced to zero because the other integration points still maintained the original stiffness.

It was possible, therefore, to reach numerical convergence since equilibrium could be preserved. In reality this should not happen. Hydraulic fracture in such a case would disrupt completely the bottom of the excavation.

In case c all integration points of the elements at the top of the bottom layer positioned below the bottom of the excavation presented approximately horizontal cracks(see fig.3.21). The pore pressure level was intentionally selected to be slightly greater than the weight of the material above the lowest integration points of those elements .

Under these conditions the stiffness of such elements in the vertical direction was reduced to zero and the expected effect of hydraulic fracture was modelled. That is, equilibrium could not be achieved and no numerical convergence was obtained.

The use of such a model may be useful in analysing the potential for hydraulic fracture. The direction of the cracks allow the judgement of how significant they may be for the specific problem. If the finite element mesh is sufficiently discretized in the regions where hydraulic fracture is likely to occur, the modelling of at least some of its effects may be attempted.

It must be kept in mind that the effect of hydraulic fracture is not only the loss of stiffness, but involves other problems, like flow concentration increasing the seepage forces in particular directions. The successful numerical modelling of such a complex phenomenon and its various consequences would require more than the use of a cracking model.

This example provides a very good insite into the effect of cracks on the stiffness of the element when the cracking model being discussed is used. The resultant stiffness of the element which contains cracks is in fact an average stiffness obtained by the addition of the particular state at each integration point.

3.6 Conclusion

The model described above is equivalent to introducing a cross anisotropy in the elastic constitutive matrix, making the stiffness in the direction perpendicular to the crack plane zero, while the material is still capable of sustaining stresses in other directions. It becomes increasingly stiffer as the orientation changes from perpendicular to the crack plane to parallel to it.

In comparison with the conventionally used procedure proposed by Zienkiewicz *et al.* in 1968, this method is in general more stable numerically, since as long as the crack is open the stiffness normal to that plane is zero. This avoids the successive attraction and elimination of tension involved in stress release only methods.

In tensile stress release situations, the example used showed both procedures to be equivalent, however, in cases where variation of stresses from tensile to compressive state occurred, the results were very different. When Zienkiewicz's technique was adopted, the stage of the sequential loading imposed in which the magnitude of the external vertical loading was zero did not result in a vertical stress free state, even though only linear elasticity was considered.

When substantial closing of cracks occur, the load increments must be substantially reduced to avoid numerical instability due to excessively high stresses.

This model has physical support in the sense that rocks and cohesive soils indeed have the potential for opening fissures under certain conditions.

This model may be useful in analysing hydraulic fracture potential. Knowledge of the orientation of the cracks may contribute to a better understanding of the mechanisms involved in the problem.

Layer	γ (kn/m^3)	σ_t (kn/m^2)	E (kn/m^2)	μ
Top layer	20	0.0001	50000	0.45
Bottom layer	21	0.0001	150000	0.45

Table 3.1: Material parameters used for the idealized excavation

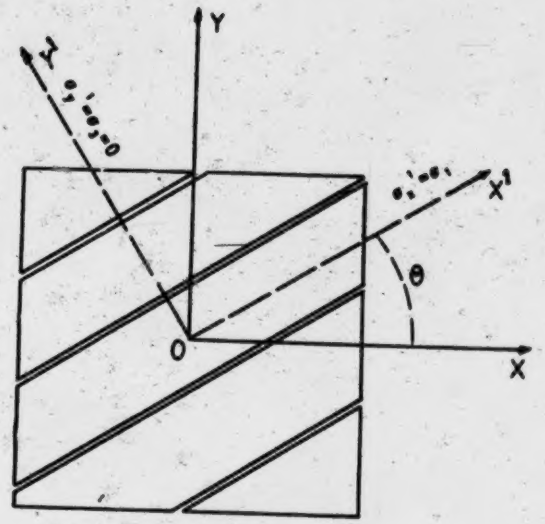
Y
Y'
$e_2'=e_2=0$
$e_1'=e_1$
X^1
θ
O
X

Figure 3.1: Cracks oriented in one direction

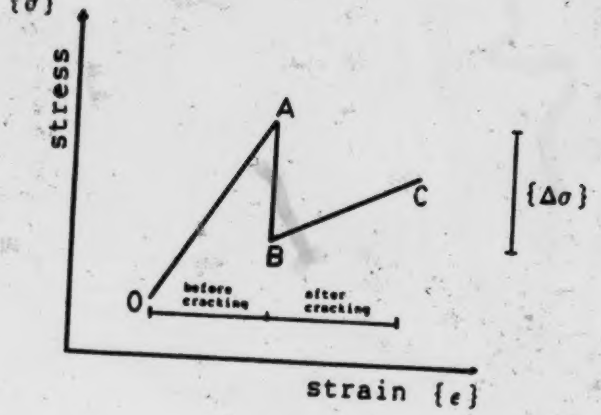
{σ}
stress
A
B
C
O
{Δσ}
before cracking
after cracking
strain {ε}

Figure 3.2: Schematic stress-strain relationship before and after cracking

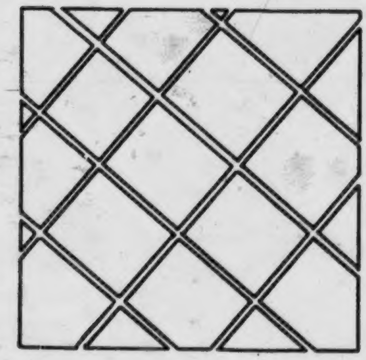

Figure 3.3: Cracks oriented in two directions

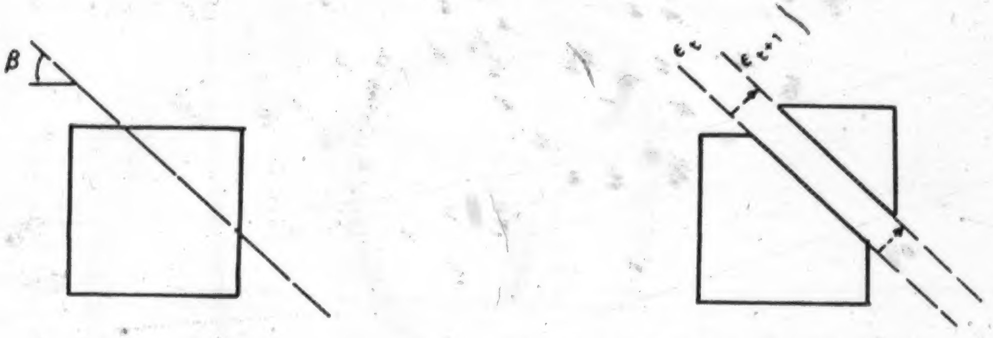

a-no cracks

ε_t-strain level just prior to cracking

b-crack opening

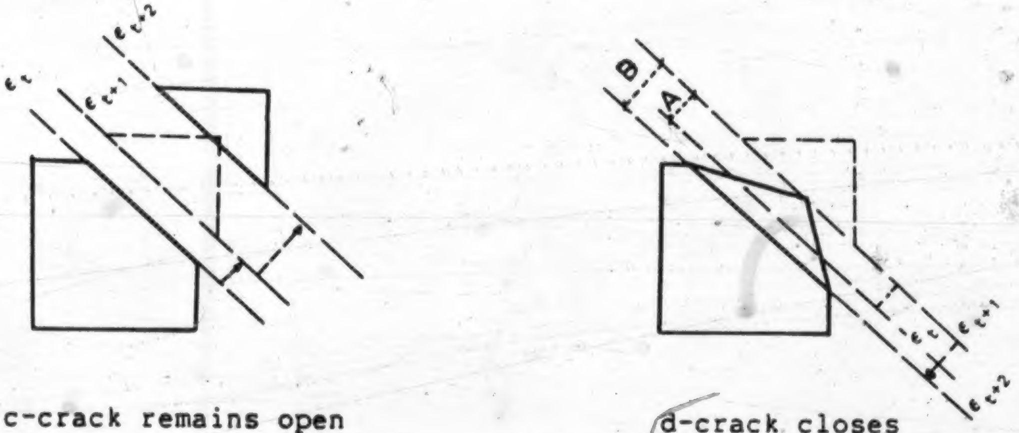
ε t
ε t+1
ε t+2
B
A
ε t
ε t+1
ε t+2

c-crack remains open

d-crack closes

Figure 3.4: Crack opening and closing at an integration point

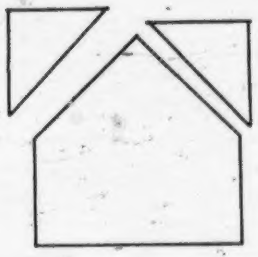

a - stage 1: both cracks open

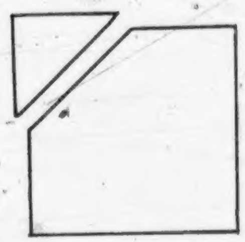

b - stage 2: only one crack remains open

c - stage 3: no crack remains

Figure 3.5: Closure of cracks at an integration point

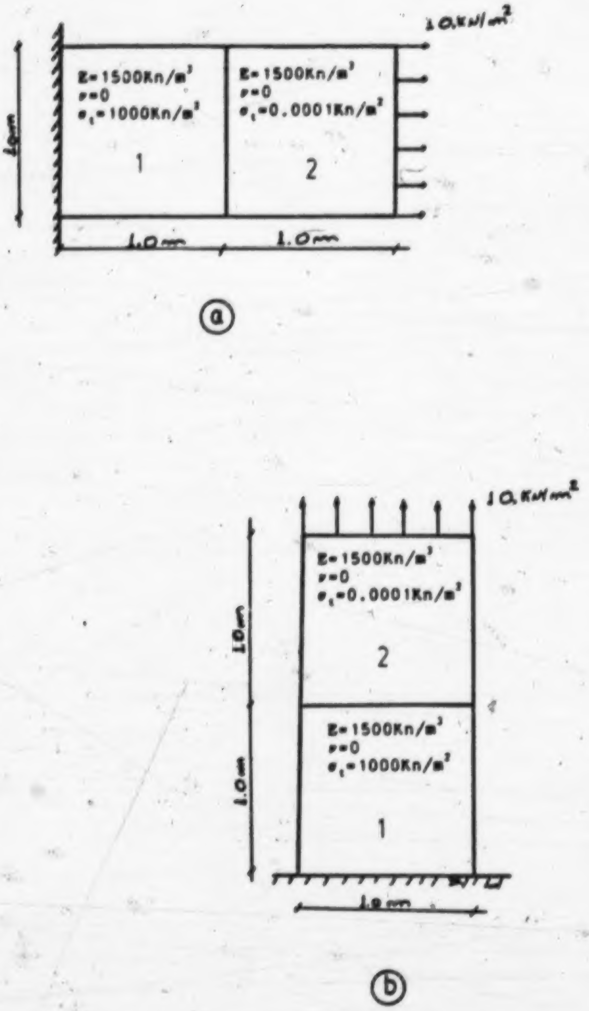
10.KN/m²
E=1500Kn/m²
ν=0
σt=1000Kn/m²
E=1500Kn/m²
ν=0
σt=0.0001Kn/m²
1
2
1.0m
1.0m
1.0m
ⓐ
10.KN/m²
E=1500Kn/m²
ν=0
σt=0.0001Kn/m²
2
E=1500Kn/m²
ν=0
σt=1000Kn/m²
1
1.0m
1.0m
1.0m
ⓑ

Figure 3.6: Uniaxial loading analysis

Zero energy modes

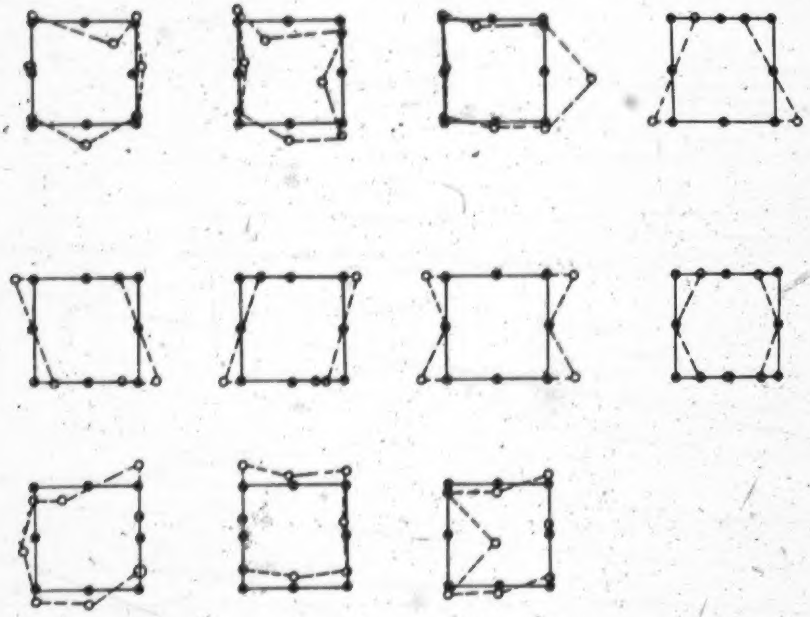

Non-zero energy modes

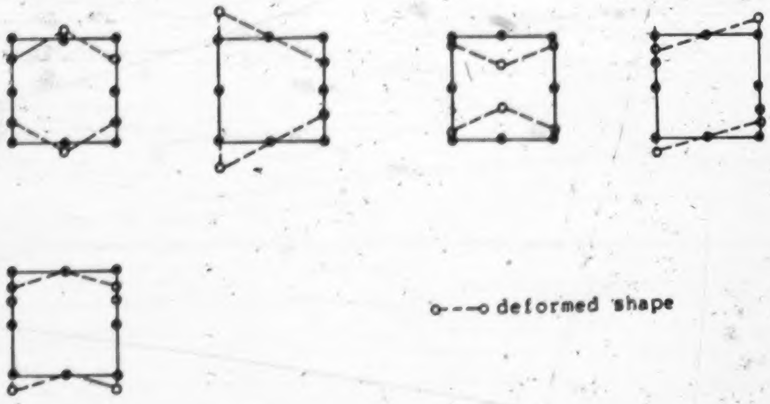
o--o deformed shape

Figure 3.7: Eigenvectors for the vertically cracked element

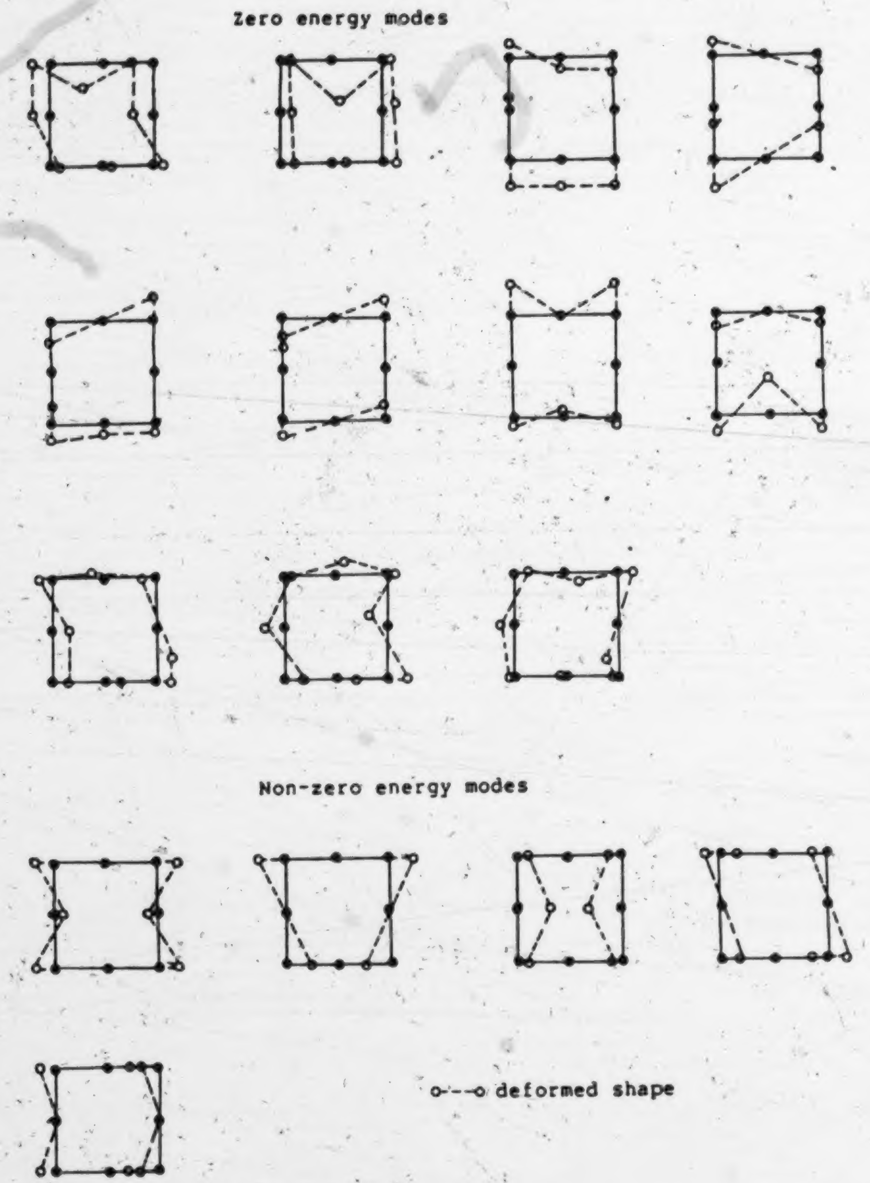
Zero energy modes
Non-zero energy modes
o--o deformed shape

Figure 3.8: Eigenvectors for the horizontally cracked element

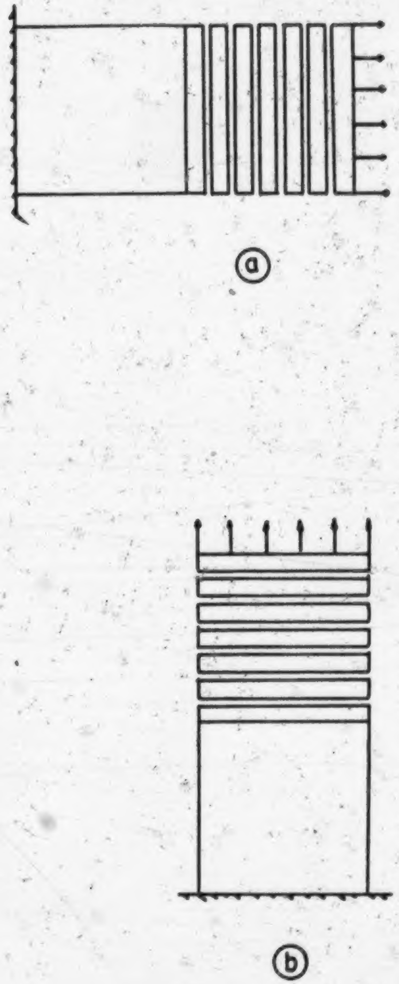

Figure 3.9: Schematic representation of the cracked elements

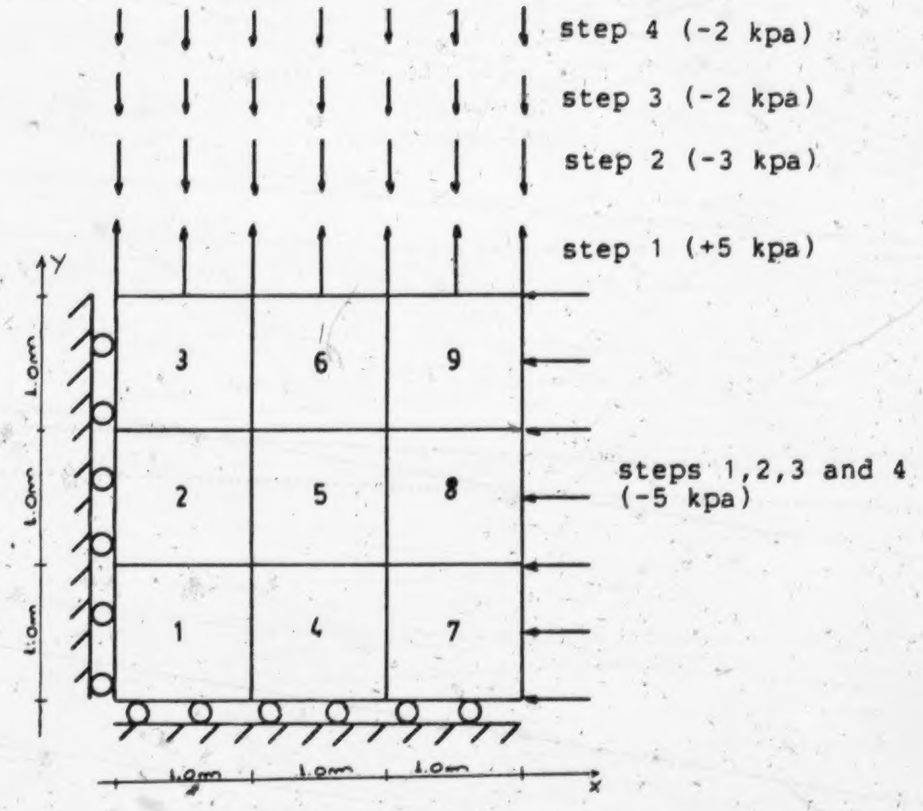
step 4 (-2 kpa)
step 3 (-2 kpa)
step 2 (-3 kpa)
step 1 (+5 kpa)
Y
3
6
9
2
5
8
1
4
7
1.0m
1.0m
1.0m
steps 1,2,3 and 4
(-5 kpa)
1.0m
1.0m
1.0m
x

obs:
$-\sigma_t$ of element 5 = 0.0001 kpa
$-_t$ of other elements = 1000 kpa

Figure 3.10: Problem analized by the use of the cracking model and Zienkiewicz no tension technique

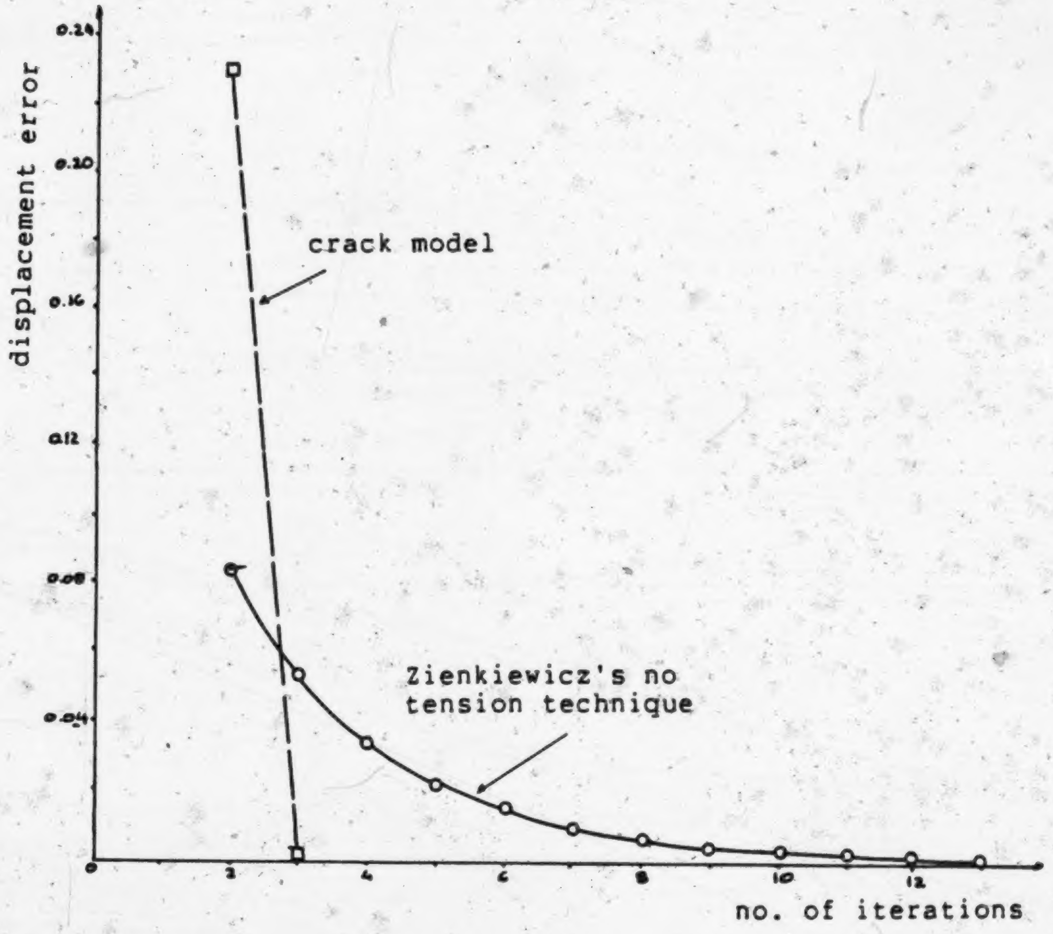

$$ {}^{t+1}E = \sqrt{\frac{\sum_{i=1}^{dof}\left[{}^{t+1}U_i - {}^{t}U_i\right]^2}{\sum_{i=1}^{dof}\left[{}^{t}U_i\right]^2}} $$

${}^{t+1}E$ - disp. error at iteration "t+1"
${}^{t}U_i$ - disp "i" at iteration "t".
dof - total number of degres of freedom

Figure 3.11:Displacement error with the no. of iterations

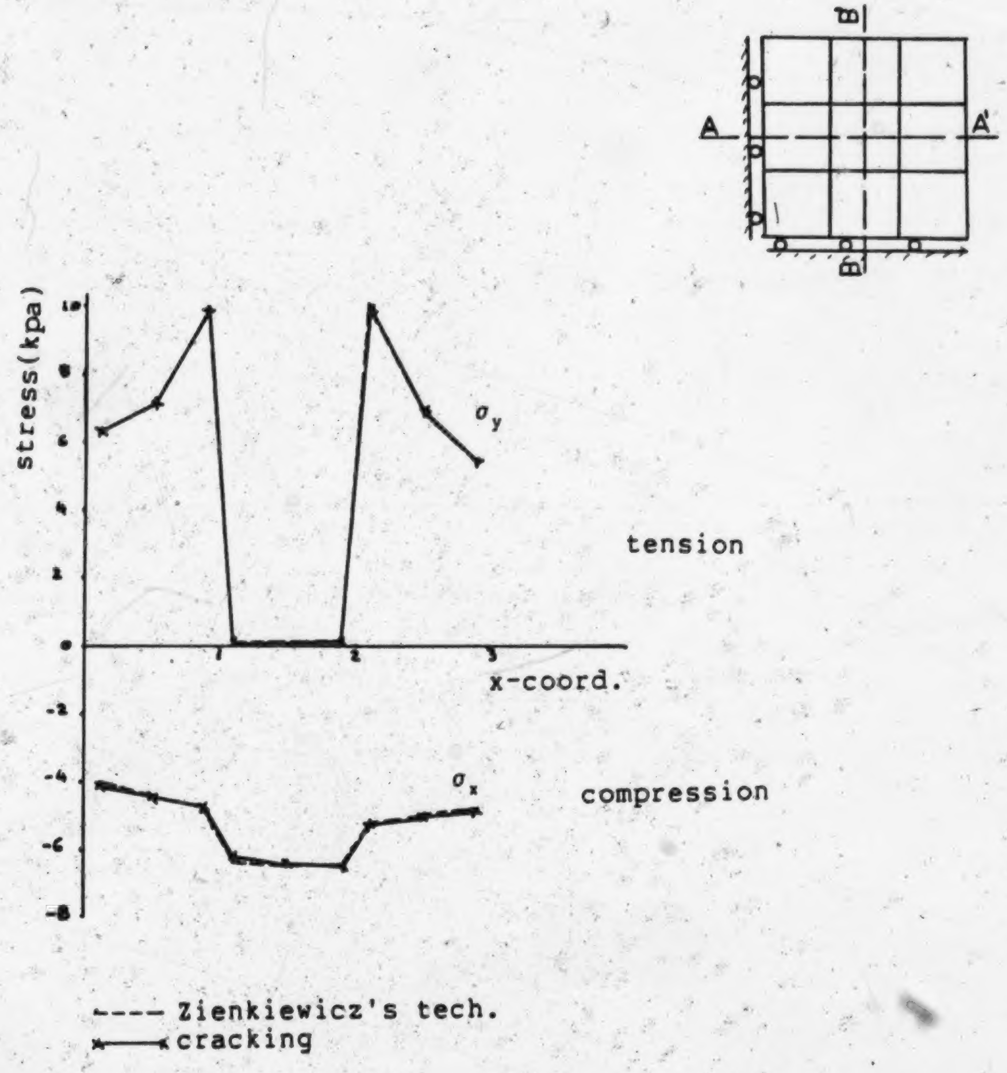

Figure 3.12: Step 1 - vertical and horizontal stresses along section AA'

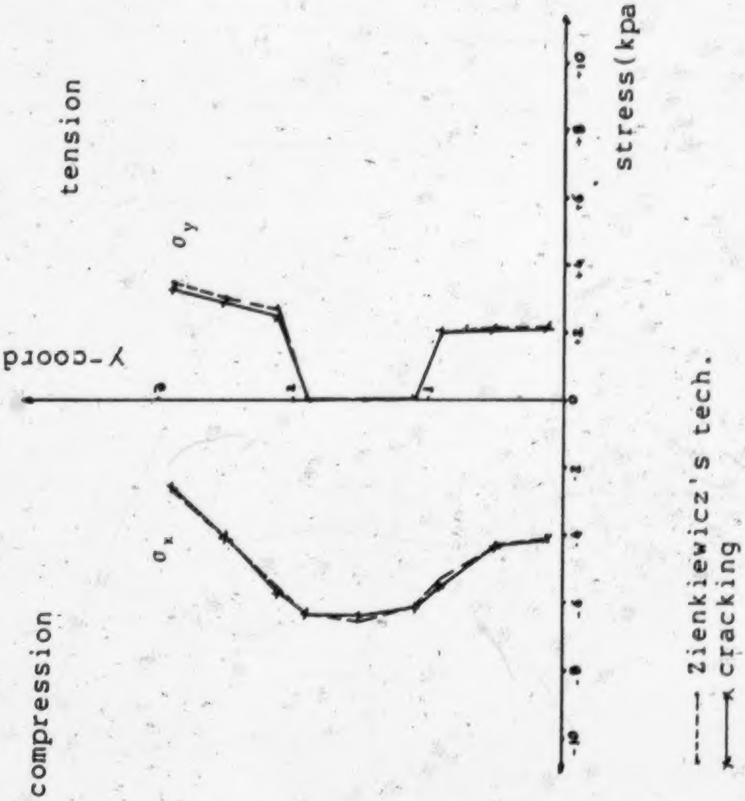

Figure 3.13: Step 1 - vertical and horizontal stresses along section BB'

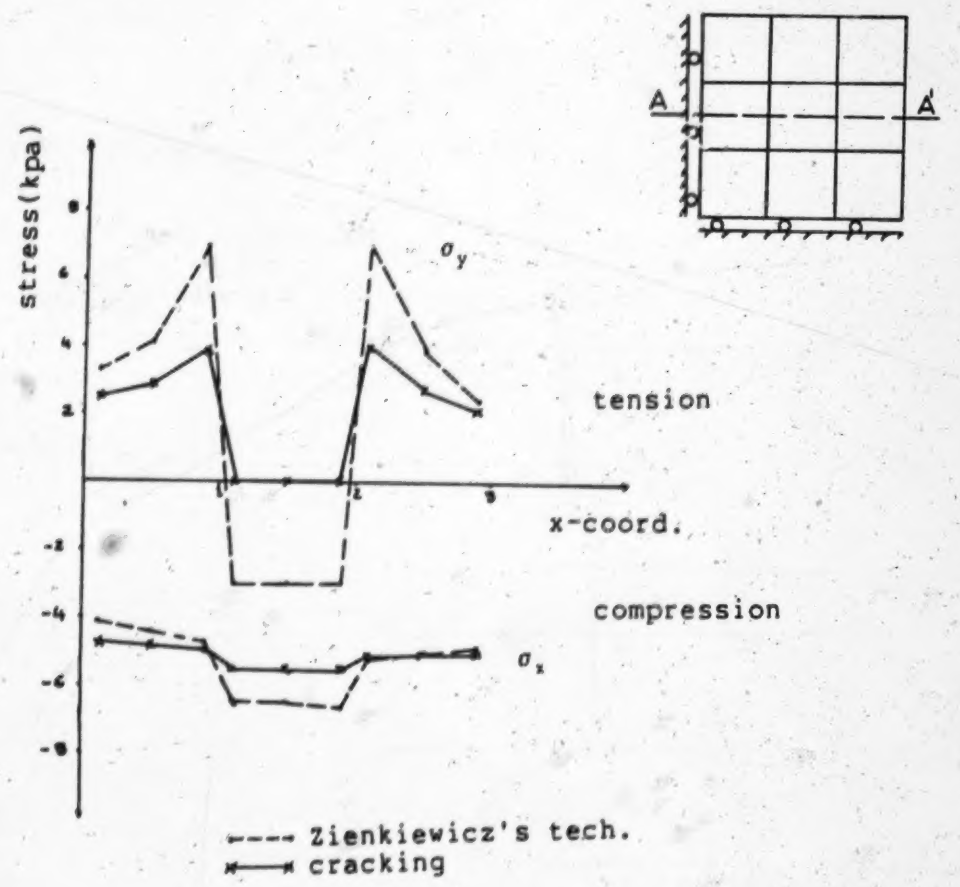

Figure 3.14: Step 2 - vertical and horizontal stresses along section AA'

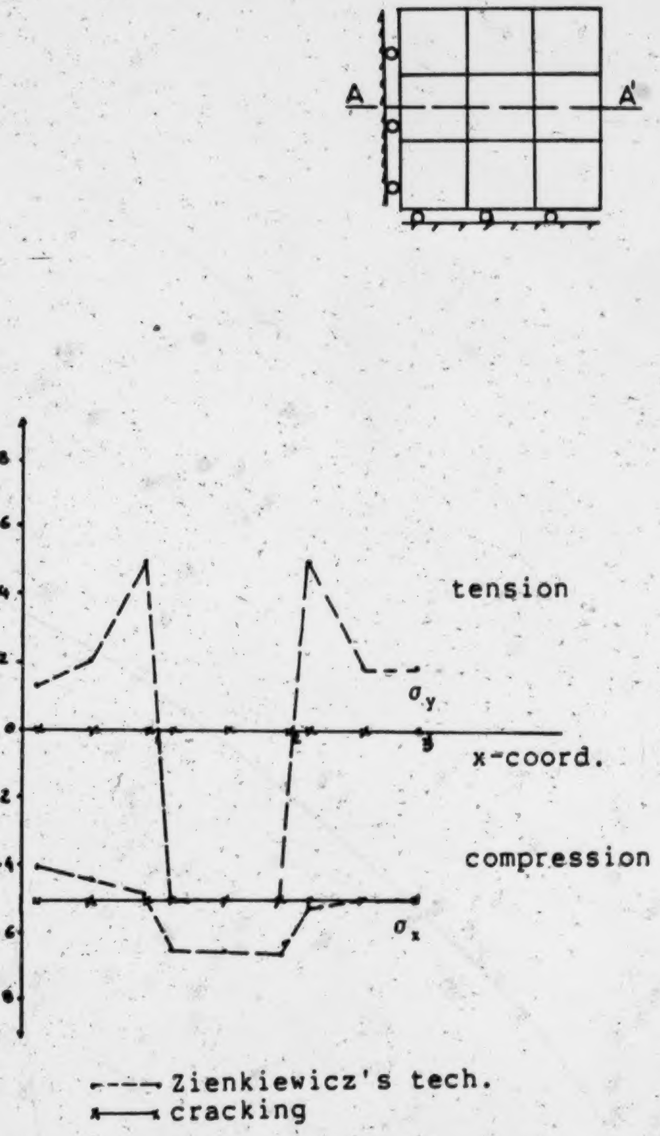

Figure 3.15: Step 3 - vertical and horizontal stresses along section AA'

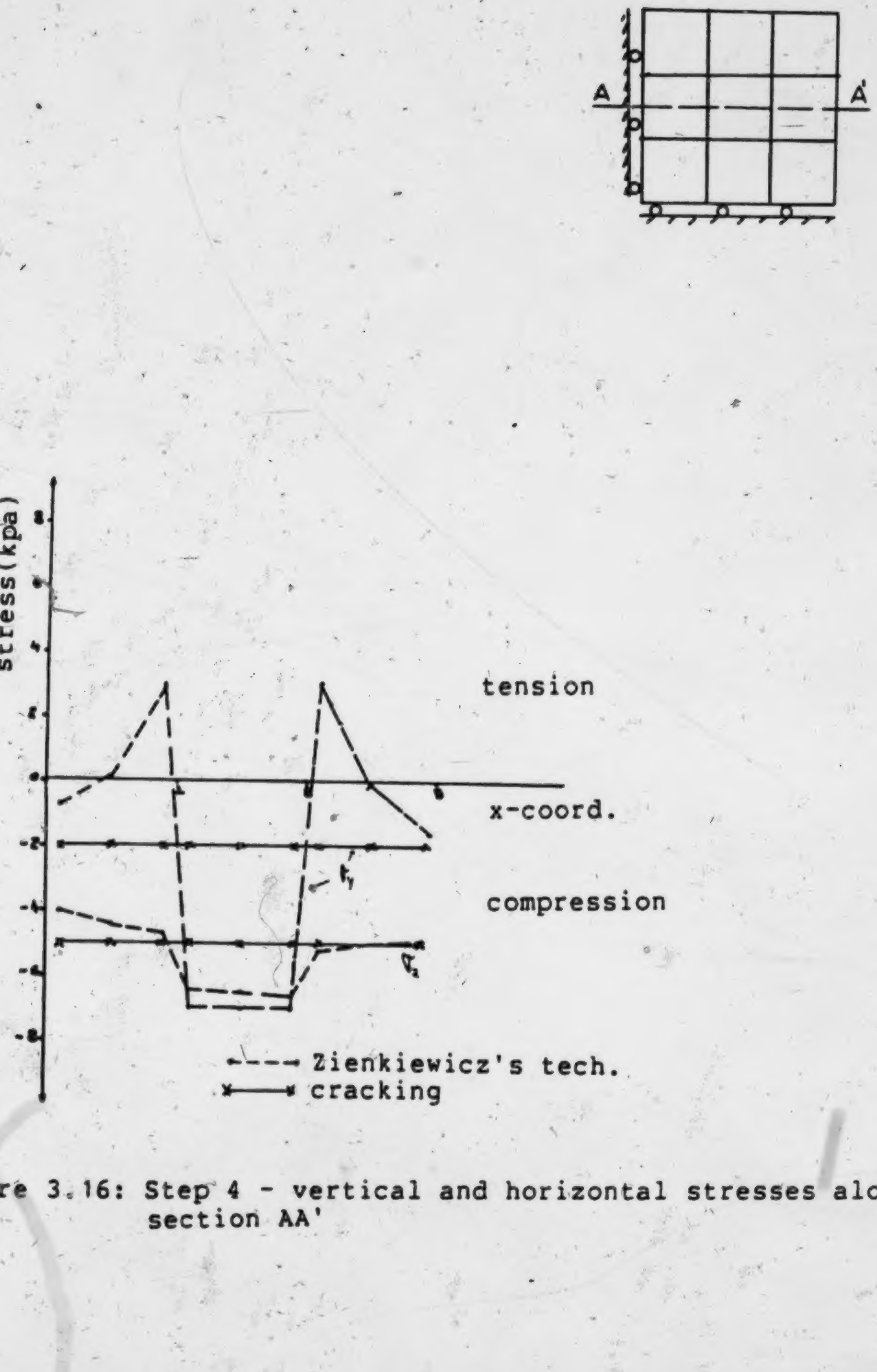

Figure 3.16: Step 4 - vertical and horizontal stresses along section AA'

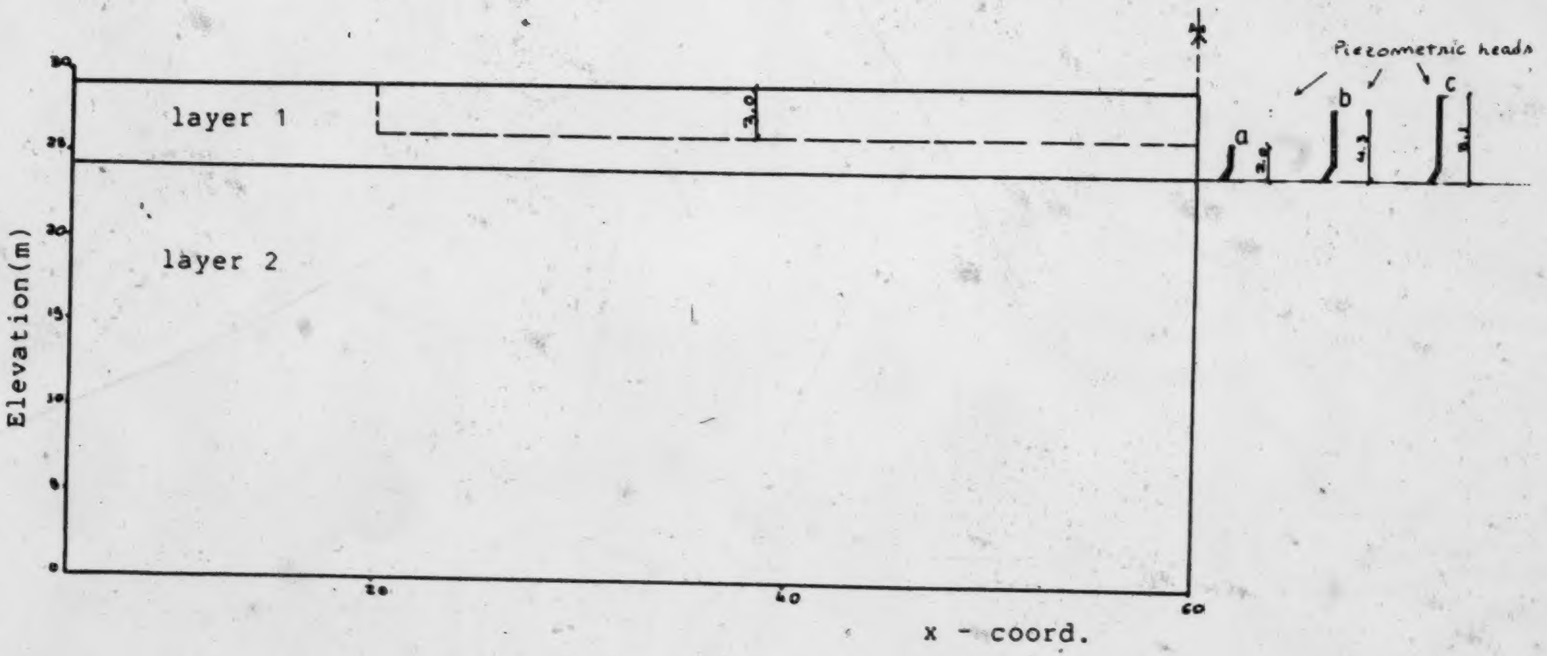
Elevation(m)
30
25
20
15
10
5
0
layer 1
layer 2
3.0
20
40
60
x - coord.
Piezometric heads
a
b
c

Figure 3.17: Excavation analysis - stratigraphy

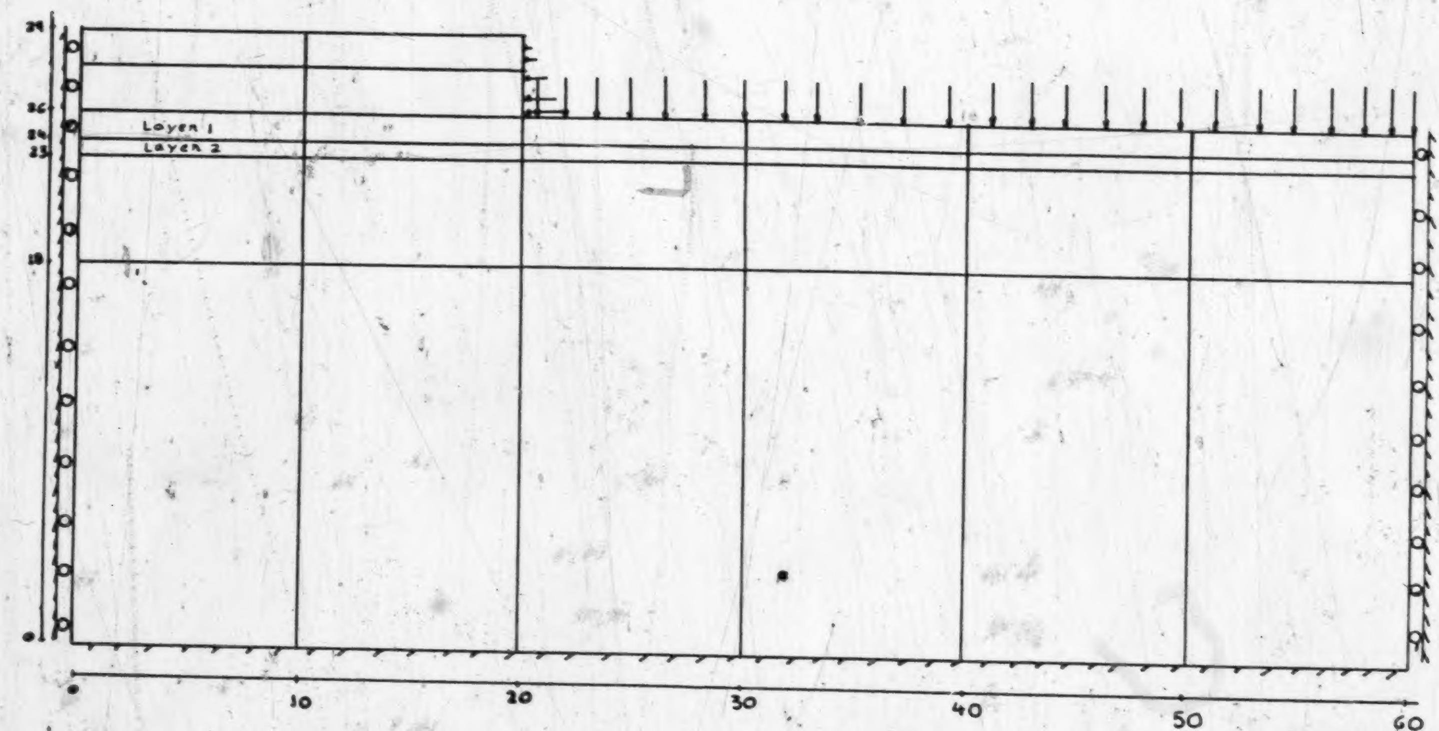
29
26
24
23
18
0
Layer 1
Layer 2
0
10
20
30
40
50
60

Figure 3.18: Finite element mesh

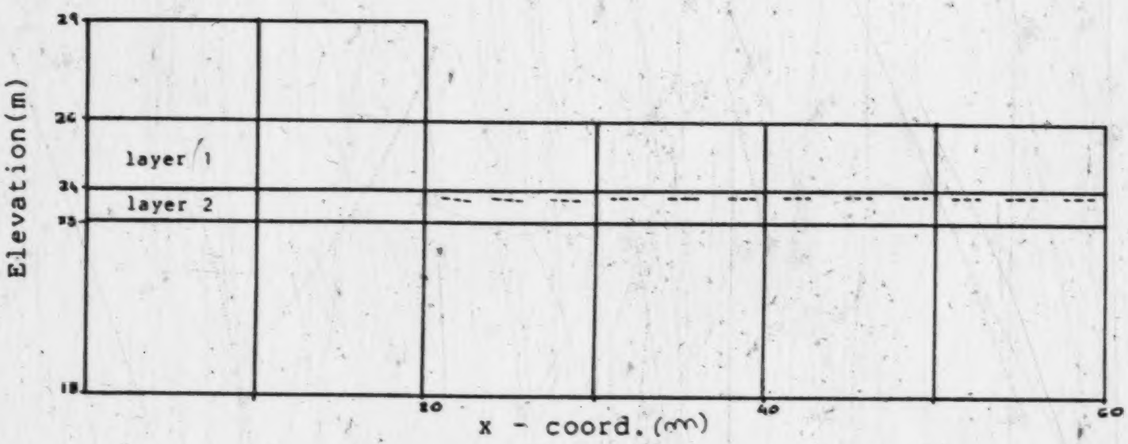
29
26
24
23
18
Elevation(m)
layer 1
layer 2
20
40
60
x - coord.(m)

--- schematic representation of the cracks

Figure 3.19: Schematic representation of cracks formed in case B

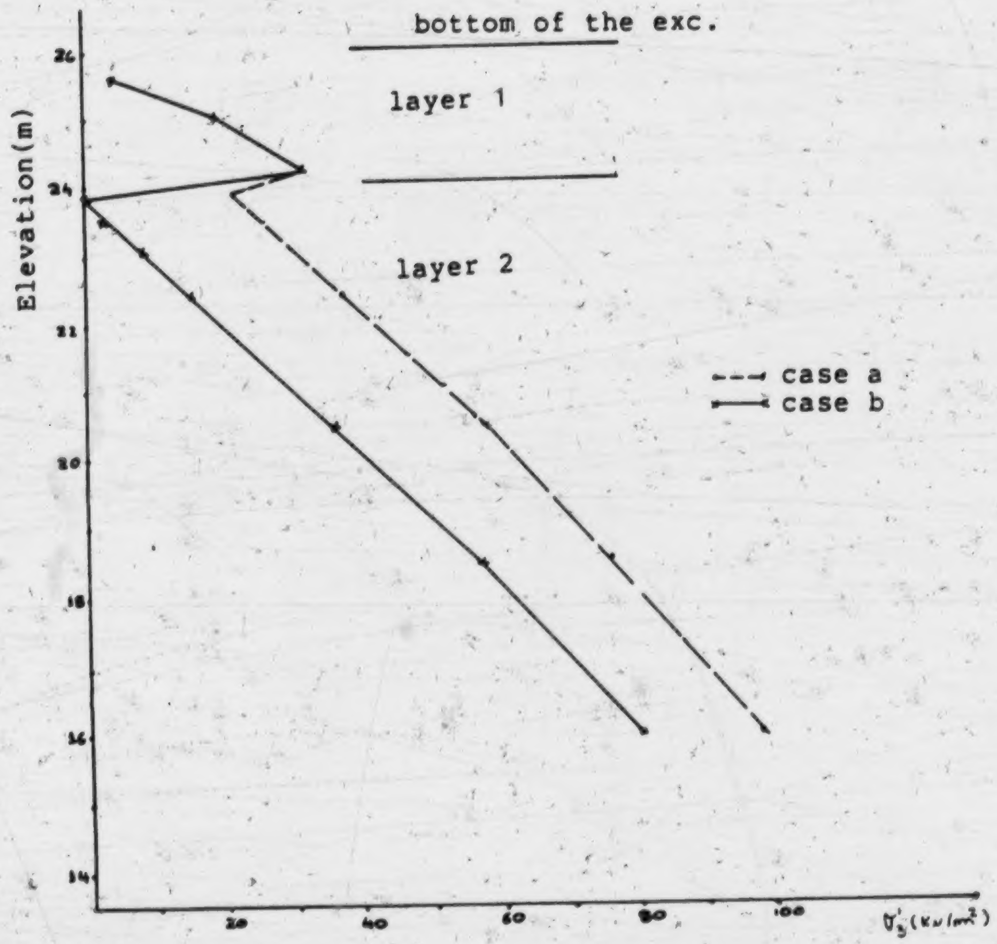

Figure 3.20: Effective minor princ. stress at integ. points closest to the center line of the excavation

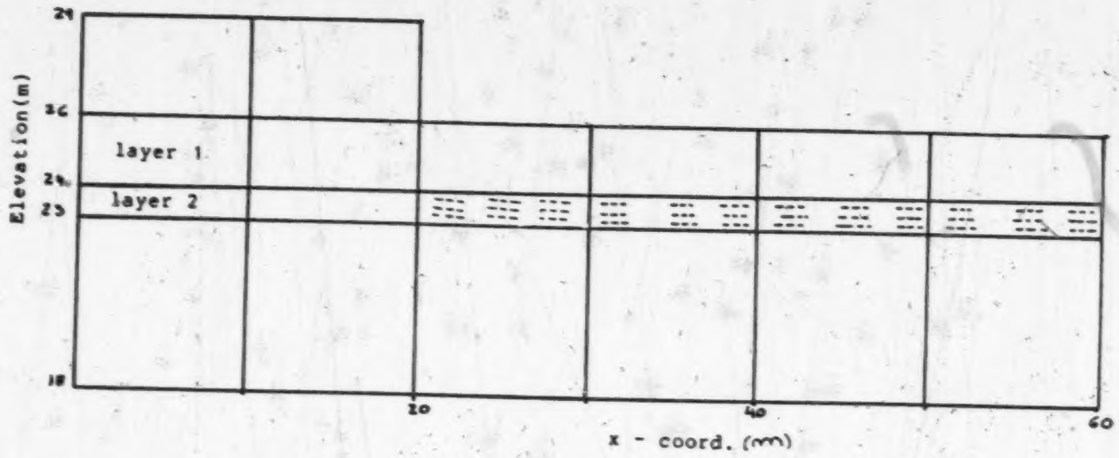
29
26
24
23
18
Elevation(m)
layer 1
layer 2
20
40
60
x - coord. (m)

---schematic representation of the cracks

Figure 3.21: Schematic representation of cracks formed in case C

4. Finite Element Analysis of Syncrude Tailings Dyke

4.1 Introduction

Tailings dams are usually constructed near the location where the wastes are being produced in order to minimize costs relative to waste transportation. Such imposition limits the number of options for the construction site.

This kind of structure, specially for mining operations, involves, in general,very large areas and equally large volume of materials. In many cases the geology of the economically feasible construction sites causes the dam to be built, at least in part, over zones with unfavorable geotechnical characteristics.

Syncrude tailings dyke is located at the Athabasca oil deposit region in northern Alberta and has been used to store oil sand mining wastes. Information about the capacity, dimensions and layout of the dam have been presented by Handford and Fair (1986).

The site investigation for the construction of this dyke indicated in a region of the foundation the existence of a presheared over-consolidated clay shale layer lying practically horizontal at about 20m of depth. Significant horizontal displacements were observed to occur along this layer in a certain area within that region.

In a specific section, the zone of largest lateral displacement level has reached values over 25cm (see Fair and Handford,1986). Piezometers showed substantial increase in pore pressure during the construction period.

Careful monitoring of movements and pore pressure variations, specially over the critical region, associated with the slow rates of dyke construction and filling have facilitated the successful application of the Observation Method(Peck,1969) which form the basis of the design philosophy, and has been discussed by Fair and Handford *op. cit.*.

This Chapter presents the results obtained by the finite element simulation of 8 years of construction of the section of Syncrude's tailings dyke where the largest lateral displacements were observed. The section is identified by Handford and Fair (1986) as section 53+00E at Cell 23.

The purposes of the analysis are to identify the factors which significantly influence the deformation mechanism and to combine parameters, within the acceptable range of values for each material , that would satisfactorily reproduce the field observations.

Previous works related to other dams pursuing similar objectives have been presented in the literature, e.g. Morgenstern and Simmons(1982). The analysis so far have, in general, been performed in terms of total stresses to avoid additional difficulties associated with explicit consideration of pore pressures. Such procedures, on the other hand, when adopted for cases in which pore pressures are significant, implies the compromise of choosing total stress parameters that implicitly account for their effects.

The present analysis may be divided into three distinct stages. Initially, linear elastic analyses were performed. Following that, a series of non-linear total stress analysis was executed. Finally, The problem was modelled in terms of effective stresses.

In this last stage, the pore pressures were introduced in the analysis as known quantities, according to the procedure presented in a previous Chapter. The necessary pore pressure distribution was estimated by interpolation of the values of piezometer measurements taken in field.

4.2 Geology of the Site and Soil Stratigraphy

Studies on the geology of Athabasca oil deposit region have been presented by several authors,e.g. Carrigy (1959), Carrigy and Kramers (1974).

The geology at the site where the tailings dyke is constructed has been described by Fair and Handford(1986). The stratigraphic sequence for the specific section analysed in the present work is shown in fig. 4.1. It consists of an upper layer of fluvial dense sand(denominated by Syncrude as PF material) with an average thickness of 4m underlain by a layer of stiff sandy silt till (PGS material) whose thickness increases from 3m close to the center of the dam to 10m close to the toe. In the region near the center line below the sandy till, there exists an 8m thick layer of stiff clayey till (referred as PGC), which ends at approximately halfway between the center line and the toe. From then on and underneath it, is found the basal units of the Clearwater Formation.

The top unit, referred to as Kca comprises a 5m thick dark slickensided grey clay-silt thinly laminated and with churned bedding. The layer underneath it, referred as Kcw, is a 2m thick grey colored and fissured clay shale, along which the horizontal movement has been observed. The bottom thick layer is the tar-sand, or McMurray Formation, which is the strata of interest in terms of the mining operation. It is a very stiff material and no significant deformation has been observed in it.

4.3 Material properties based on laboratory tests

For simplicity, from now on, the denomination used by Syncrude Canada Ltd for each material, as shown in fig. 4.1, will be adopted.

Handford(1985) presented the results of a testing program conducted by Syncrude on Kca material. Direct shear tests were performed on intact and slickensided samples obtained by the use of Pitcher barrel samplers from various locations in Cell 23.

The tests indicated for the intact samples the following average parameters:

$\phi'_p = 23^\circ$, $\phi_r = 7.5^\circ$............... $c'_p = c'_r = 0$

and for the slickensided samples:

$\phi'_p = 12.5^\circ$, $\phi'_r = 7.3^\circ$............... $c'_p = c'_r = 0$

It is noted that intact samples displayed peak friction angles approximately three times the residual value. This difference, as expected, was reduced for the slickensided samples.

A series of undrained and drained triaxial extension tests were performed on Pgs material samples and undrained triaxial compression tests were performed on Pgc material by Sego and Morgenstern(1986) at the University of Alberta. The samples were obtained from Cell 23, Section 50, by Syncrude Ltd. using pitcher barrel samplers.

The results indicated that the strength parameters could be represented by :

c' = 20 to 30Kpa and ϕ' = 30 to 37° for Pgs

c' = 11Kpa and $\phi' = 32^\circ$ for Pgc

Results of direct shear tests on the tailing sand reported by Handford(1985) indicate the following average strength parameters:

$\phi_p' = 38^\circ$ and $c_p' = 33$kpa

$\phi_r' = 30^\circ$ and $c_r' = 20$Kpa

4.4 Dyke Construction

The dyke's construction began in 1979. The construction technique follows the procedure described by Mittal and Hardy(1977). According to this procedure the tailing stream is sluiced into construction cells oriented parallel to the dyke centerline. During the sluicing operation pad dozers are used to spread and compact the tailings sand placed in the cells, forming a compacted shell. In the winter months when the construction of the cells is not feasible, the tailings stream is discharged upstream of the compacted shell. The coarse sand fraction settles out to form a beach with a 2 to 3 percent slope. The water and sludge fractions of the tailing stream flow into the pond.

The downstream slope was originally 4.1. But localized movements along Kca/Kcw contact were observed with increasing velocity since 1981 and at the end of 1983. It was decided to change the slope to 8.5:1 based on limit equilibrium analyses, which indicated an increase of Factor of Safety at ultimate dam height (elevation 352m) from 1.09 to 1.33 if the new inclination were adopted (Handford,1985). This changed the overall downstream slope to 6.8:1. The construction sequence is shown schematically in fig. 4.2 until the year 1986.

4.5 Monitoring Program and Performace of the Dam

Summary of the field instrumentation installed in Cell 23 has been presented by Fair and Handford(1986). In the present work, it suffices, therefore, to present a brief discription of the measurements related to the particular section being analysed (Section 53).

4.5.1 Slope Indicators

A plan view of the slope indicator locations at section 53 is shown in fig.4.3 and in cross section in fig. 4.4. The first slope indicator installed was SI 81-23-02, in the spring of 1981,at berm 319. It indicated horizontal movement of approximately 3cm that year. Slope indicator SI 81-23-03 was installed at the toe of section 53 in that same year. By the end of 1983 SI 81-23-02 indicated an additional 5cm movement, while at the toe 3cm was registered. In July of 1984 slope indicator SI 84-23-31 was installed approximatelly 55m distant from SI 81-23-02 towards the center of the dam (see fig.4.3 or 4.4).

Each slope indicator has been used until the horizontal displacement over a 2 feet length is about 5cm. At this point another inclinometer is installed close to its location and the additional measurements are then performed on this latest installed instrument. This is why in fig. 4.3 more than one instrument is referred to the same location.

By the end of 1984 a total displacement of 15.5cm was registered at elevation close to Kca/Kcw interface at the location of SI842332. For the same elevation, 4.5cm was recorded at SI842331. At the toe a total of 3.8cm had been recorded.

In April 1985 the slope indicator SI852325 was installed in Section 53. By the end of 1985, at elevation close to the Kca/Kcw interface, the displacement measured at SI842334 position had reached approximately 9.0cm. At SI842332,almost 22cm had been recorded, and at the toe around 8.0cm had been recorded. By the end of 1986 these values had changed to, approximately, 11cm at SI842334 location, 26 cm at berm 319 and 10cm at the toe.

Fig. 4.5 shows the displacements recorded until the end of 1986. It is seen that the movement has happened with little distortion in the Pgs material.

4.5.2 Sliding micrometers

The sliding micrometers are instruments which measure the axial strain distribution along a borehore(see Kovari and Amstad, 1983). Description of the equipment installed at Syncrude tailings dyke as well as the calibration procedure,problems encountered during installation and measurements obtained have been presented by Handford and Fair (1986).

Two inclined units were placed in Section 53. One at the toe and the other at approximately 60m downstream from the toe, at inclinations of 23° and 13° below the horizontal and lengths of 36 and 53 meters, respectively, as shown in fig.4.4. One vertically oriented unit was also installed at the toe, but the application was limited "as the ocurrence of small horizontal slips are impossible to distinguish from extension due to heave"(Handford and Fair,1986).

The initial set of readings were taken before the 1985 loading. The micrometers TSMA3 at the dyke toe and TSMA5, downstream from the toe, presented average axial compressive strains in the Pgs material of 0.2 and 0.44mm/m, respectively. TSMA3 showed practically no axial straining in Pf sand layer.

Both instruments indicated extensional spikes at the region where the horizontal slip was observed.

4.5.3 Piezometers

A plan view of the pneumatic piezometers installed in Section 53 is shown in fig. 4.6 and a cross section is given in fig. 4.7. Table 4.1 contains the position of each piezometer with respect to the toe and to the longitudinal axis and the average piezometric elevation recorded at each year at each piezometer tip. Table 4.2 is similar to 4.1 but it shows pore pressure values. There are relatively few piezometric data until the year of 1983, when, simultaneously with the decision of flattening the downstream slope, additional piezometers were installed.

It can be observed that there is a substantial increase in pore pressures in the region close to the Kca/Kcw interface. This is illustrated in fig. 4.8 where the average phreatic line for each year and the piezometric elevation for points close to Kca/Kcw interface for the year of 1986 are schematically presented. Pore pressures measured at Piezometers PN852307 and PN852311 are shown in fig. 4.9, in which this local increase can be clearly observed.

4.6 Finite Element Analysis

The Dyke construction was simulated using linear and non linear elasticity (hyperbolic) and plasticity models. The finite element mesh used is shown in fig. 4.10. It is composed of 391 triangular and quadrilateral isoparametric elements with 6 and 8 nodes respectively.

It is noted that the crest elevation in the finite element mesh is 352m. This elevation represents the ultimate height that is supposed to be reached by the end of 1990. The present analysis involves the construction period from 1979 to 1986.

Fig. 4.11 indicates the various material layers in the finite element mesh for the region where the largest horizontal movements have been observed (critical region).

Fig.4.2 shows the construction stages from 1979 to 1986.

4.6.1 Linear Elastic Analysis

In order to gain a basic understanding of the behaviour of the dam and foundation, a series of linear elastic analysis was performed. The loading was applied in a multiple stage sequence in order to resemble more approximately the real situation.

The first load stage aimed to simulate the initial gravity stress field,i.e. before the dyke construction. The exact magnitude of these stresses at every point is not known but, for that region, it is believed that the earth pressure coefficient at rest (Ko) is around 0.8 to 1.0, although, as it is well known, Ko values reflect the local stress history and may vary from point to point.

The initial stress field was applied by a " switch-on-gravity" process. The stresses were generated due to the application of gravity forces which are dependent on the unit weight of the material. The vertical stresses are, therefore, close to the total weight of the material above any given point and the horizontal stresses were calculated as a function of the poisson's ratio (μ)of the material. Ko value is equal to $\mu/(1-\mu)$ for homogeneous isotropic linear elastic material under no lateral movement.

Since the actual horizontal *in situ* stresses may not necessarily be related to the elastic parameters of the material, these parameters, for the switch-on-gravity stage, do not have to be the actual material parameters.

Following the switch-on-gravity stage, the dyke was devided into 12 load stages up to its ultimate height. At each stage, a layer of elements was added to the finite element model and the gravity forces due to self weight were applied. The elastic parameters used for each material in each analysis are shown in table 4.3.

4.6.1.1 Analysis LE-1

This analysis was mainly to check the input data. Thirteen stages of construction, including the initial stress stage were used. The displacements calculated until years 1985 and 1990 at the location of slope indicator SI842332 (zone of largest horizontal movements) are shown in fig 4.12. The movements at the interface between Kca and Kcw were found to be around 7.5cm in 1985, while in the field approximately 22cm were recorded. It is also seen that the movements calculated in the Km material(McMurray Formation) were excessively large,wich indicates that the modulus used for that material was too low.

4.6.1.2 Analysis LE-2

In this analysis the dam was constructed in a single stage after the initial stresses were generated. The results were compared with Analysis LE-1 and very little difference was observed in terms of displacements, as illustrated by fig. 4.12. Therefore, two stage analyses were used in subsequent linear analyses.

4.6.1.3 Analysis LE-3

In order to observe the effect of PGS and PGC materials on the movement of the foundation, their elastic moduli were increased and decreased by 50%. The displacement calculated at the ultimate height at the position of SI842332 is shown in fig. 4.13. The results indicated that the movement in the PGS was increased and decreased as the moduli were decreased or increased respectively. The movement in Kca, however,was not increased substantially.

4.6.1.4 Analysis LE-4

In this analysis the elastic modulus of Kca material was increased and decreased by 50%. The elastic modulus of Kcw material was assumed to be the same as in the Km material. It can be observed by fig. 4.14 that the movement increased or decreased as the Kca modulus was decreased or increased respectively. However, the slip near the interface Kca/Kcw was still too small as compared to that observed in field.

4.6.1.5 Analysis LE-5

The results obtained in the previous analysis indicated that in order to model the localized slip along the Kca/Kcw interface variation of moduli of PGS, PGC or Kca materials alone would not lead to the correct mechanism. In this analysis the modulus of Kcw material, which lay continuously underneath the dyke, was reduced to 5000Kpa in order to model a continuous low strength material layer. This does not mean that Kcw is a soft material. It is assumed that there is a continuous plane or number of planes that may be presheared due to some past geological event like unloading caused by erosion of previously existing overburden (see Isaac *et al.*, 1982). These planes do not offer high resistance against horizontal movement. This weak zone may be in the Kca, Kcw or at their interface.

The calculated displacement at SI 842332 location is shown in fig. 4.15. In the same figure is presented the field measurents taken until the end of 1985. It can be observed that, comparatively to the previous analysis the reduction of the modulus of the Kcw material led to a substantial localization of movement along Kcw elevation. It must be remembered that in this analysis the dam was constructed in one step after the initial stress stage, therefore the calculated results refer to the ultimate height.

Although the amount of displacement is much less than that observed in field, the pattern of deformation is in better agreement with the real situation than any of previous analyses.

The linear elastic analysis was used as a relatively inexpensive tool to seek a general understanding of the role of various materials in the global deformation pattern.However, there would not be great additional advantages in trying to match the observed movements by varying elastic parameters.

In a general sense, based on the results presented it can be concluded that decreasing the modulus of Pgs and Kca would result in larger amounts of movement but the localized deformation along the observed slip zone would not be predicted. This localization could be modelled by having a continuous layer of weak material at the Kcw elevation.

4.6.2 Non-linear Finite Element Analysis

The non-linear analysis aims to represent the stress-strain behaviour of each material in a more realistic way. In soil analysis the non-linear elastic and elastic-plastic models are frequently used.

The non-linear models, like the hyberbolic model suggested by Duncan and Chang(1970), have the advantage of relative mathematical and programming simplicity but have some serious disadvantages like the limiting of their validity to specific stress paths. For example, the hyberbolic model, probably the most widely used non-linear elastic model in soil mechanics, was derived based on triaxial compression tests in materials which do not present strain softening behavior,i.e., no decrease in strength after peak. Therefore, if one attempts to use this model for a situation where the stress path is very different from that of triaxial compression tests or in materials presenting strain softening behaviour, the results will very likely be poor. In addition to that if, complete unloading occurs, no permanent deformation remains, which is clearly unrealistic.

Elastic - plastic models have the disadvantage of mathematical and programing complexity but have the advantage of being valid independent of the stress path. This does not imply that the material or the values calculated using plasticity are stress path independent. It is postulated that as long as the stress state satisfies a certain yield criterion the yield surface and all other plasticity concepts are valid independent of the stress path followed to reach that stress state (Hill, 1950), and any changes in the yield surface are uniquely related to the amount of plastic work done. Plasticity fundamentals and implementation are presented with varying degree of detail in several references, e. g. Hill,1950 and Chen and Baladi,1985. Plasticity is also capable of modelling permanent deformations upon unloading.

With respect to some numerical aspects of performing non-linear finite element analysis, it is an iterative process since the stiffness of each point depends on the current stress and sometimes strain level. However, the stresses and strains cannot be calculated without the knowledge of the current stiffness. The final solution, therefore, involves a certain error, which, in the case of the present analysis is measured in terms of displacements. When this error becomes smaller than a specified tolerance the process is stopped. The tolerance must be small not only to ensure the correct results but to minimize numerical instability in subsequent stages.

Divergence or oscillation of the solution, i.e, no convergence, may be due to the accumulation of error in the iterative scheme, an excessively large loading increment, localized or global failures of the structure. Detailed discussion on non-linear finite element techniques can be found in various finite element texts,e.g. Bathe,1982 and Zienkiewicz,1977.

Soils and rocks are very complex materials and their realistic stress- strain modelling at stress levels beyond the very low stages with respect to their strength demands in general the definition of several parameters. In addition to that, a mass of soil or rock envolves, in general, a high degree of heterogeneity. Therefore, the best way for predicting its behaviour is by testing the different materials involved in order to define adequate stress-strain models to be used and develop a feeling for acceptable ranges of values for each of the necessary material parameters. Then, the models are " calibrated " against existing field observations. Pilot projects or reduced scale physical modelling prior to the beginning of the execution of the main project are very suitable for the "calibration" of numerical models.

In the specific case presented here, since field observations were available up to 1986, the initial part could be focussed on matching the history of the movements up to 1986, and, when this matching reached reasonable agreement with the field measurements, the construction of the dyke would then be completed using the finite element model for the purpose of predicting its behaviour.For this thesis only the matching phase is of interest and the one to be discussed further.

Due to the stress path dependence of the material behaviour, a realistic loading sequence is a fundamental requirement for obtaining the correct results. In the analysis to be discussed the loading sequence is composed of an initial linear elastic "switch-on-gravity" step in order to generate a pre-existing stress field with respect to the dyke construction, and subsequent layer by layer construction, each layer corresponding to a one year construction period, as shown in fig.4.2.

4.6.2.1 Material Modelling

4.6.2.1.1. McMurray Formation (Km material):

Insignificant deformation has been observed in this material.It was assumed,therefore, that it behaves as linear elastic.

4.6.2.1.2. Grey Colored and Fissured Over-Consolidated Clay Shale (Kcw material):

The presence of fissures in this material indicates that it has experienced pre-shearing during its geologic history.

The linear elastic analysis results showed that these fissures should be continuous underneath the dam in order to predict the observed deformation mechanism. Therefore, this material was modelled as elastic-perfectly plastic, according to the Mohr-Coulomb yield criterion.

4.6.2.1.3. Dark, Slickensided,Grey Clay Silt thinly laminated and with churned bedding (Kca material):

Due to the presence of slickensides and laminations observed in this material, which, as in the case of kcw material, indicates pre-shearing, it was also modelled as elastic-perfectly plastic according to the Mohr-Coulomb yield criterion.

4.6.2.1.4. Stiff sandy silt till (pgs) and clayey silt till(pgc):

The average level of horizontal strain observed in the pgs material in the field can be estimated as a first approximation by subtracting the displacements measured by two slope indicators and dividing this difference by the distance between them. If this is done for SI842332 and SI842337, the average horizontal engineering strain up to year 1985 is 0.23%.

The stress-strain relationship presented by Sego and Morgenstern(1986), obtained from tests on pgs samples showed that up to an axial strain level of 2% (almost 10 times the estimated average horizontal strain at the critical zone in field) it would be resonable to use the hyperbolic model.

Pgc material was also modelled by the use of the hyperbolic model based on stress -strain curves shown by Sego and Morgenstern *,op. cit.*.

4.6.2.1.5. Fluvial, dense sand(pf) and Tailing sand(Ts):

The hyperbolic model was chosen for both soils based on the characteristic behaviour of medium density sandy materials.

4.6.3 Total Stress Analysis

Several analyses were performed. Some of the material parameters were varied within reasonable ranges, based on the tests discussed before, in order to study the sensitivity of the deformations to each of them and to search for a combination of parameters that would yield results as close to the field measurements as possible.

In all analyses the loading process was modelled by successive placement of layers, each layer corresponding to one year of construction. These layers were initially placed as linear elastic material with a low modulus of deformation. When the overlying layer was placed in the subsequent load step, it would, then, be transformed into hyperbolic material.

This technique was used because the deformation modulus according to the hyperbolic model is a function of the confining stress.When the material was being placed the confining stress would be very low (or zero at surface), what would mean a very low or zero modulus.

The low value for the modulus used for placement had the purpose of minizing the existing shear stresses in the material at the time of its change from linear elastic to hyperbolic.

In the cases where the combinations of material parameters led to numerical instability, or gave results very similar to previous combinations , the analysis was terminated before reaching the height of the dyke corresponding to the year 1985.

All the analyses performed but not completed up to 1985 are summarized in table A1 in the appendix II. Only the analyses which were carried out up to 1985 are discussed below. The parameters used for analysis NLT-1 to NLT-6 are presented in tab.4.4.

4.6.3.1 Analysis NLT-1

This analysis was based on the material parameters available at the time.At that point, no tests had been performed on PGC or PGS materials. Friction angles close to residual was used for Kca and Kcw due to the pre shearing process experienced by both materials.

The values of displacements at locations of SI842334 and SI842332 calculated by this analysis are compared to field measurements in figs.4.16 and 4.17. It can be seen that the analysis underpredicted the movement. It seemed, then, that PGS and PGC were too stiff in the finite element model. Therefore, the modulus of PGC was reduced in the following analysis.

It was observed during this analysis that a small localized failure would occur in the tailings material forming the toe of the dyke. Although this fact did not have any significance in the field, in the numerical model it would destabilize the system and no results could be obtained. As this local instability was relatively far from the area of interest and had no real significance, it was decided that the five elements right at the toe of the dyke would remain as elastic. This was maintained in all subsequent analysis.

4.6.3.2 Analysis NLT-2

The modulus of PGC was reduced by about 65%, and all the other parameters maintained the same values they had in analysis NLT-1. The calculated horizontal displacements are also shown in figs.4.16 and 4.17. No significant difference was observed in comparison with the previous analysis.

Further reduction of the friction angle of kca and kcw materials was attempted, since the linear elastic analysis had shown that the existence of a continuous low stength material was essential in capturing the localized slip.

4.6.3.3 Analysis NLT-3

In this analysis the internal total friction angle of Kcw and Kca was reduced to 4 degrees. Direct shear tests performed in Kca and Kca/Kcw transition had presented an average residual effective stress angle around 8 degrees. The argument for a further decrease of this value to 4 degrees is that in total stress analysis the effect of pore pressures is taken into account in an implicit manner. Therefore, a value of 4 degrees would reflect the reduction of strength due to the pore pressures.

The results are compared to field measurements in figs. 4.16 and 4.17. It is seen that in the SI842332 location the localized slip mechanism was, in this case,observed, although still much underestimated in relation to field values.

In the SI842334 location,although the horizontal movement increased in relation to the previous analysis, no localized slip mechanism was calculated.

4.6.3.4 Analysis NLT-4

The angle of internal friction of Kca material was increased from 4 degrees to 14 degrees. Due to this increase the amount of distortion in Kca was reduced, however,as this material was now able to sustain a higher stress level, the movements in Kcw was a little reduced.

Since there was very little information on the elastic modulus of Kca and Kcw materals, in the subsequent analysis these parameters were reduced in order to increase the movements on Kcw material.

4.6.3.5 Analysis NLT-5

With the reduction in the Kcw and Kca moduli to 20000Kpa the movement was increased only slightly, as shown in figs.4.18 to 4.19, which means that strength and not elastic parameters were dominant in the behaviour of Kca and Kcw at that stage of the loading process , since they were subjected to extensive yielding.

The analysis,so far, suggested that the movement in the foundation was controlled by the properties of Kca,Kcw and Pgs materials and that the weak zone is continuous underneath the dyke with low frictional resistance. The laboratory results presented by Sego and Morgenstern(1986) indicated the angle of internal friction in terms of total stress for Pgs material to be around 17 degrees, and the cohesion intercept varying from 0 to 150Kpa depending on the amount of straining in the soil.

4.6.3.6 Analysis NLT-6

In this analysis the internal friction angle of Pgs was reduced to 16 degrees and a cohesion intercept of 50Kpa was assumed. The computed horizontal movements were increased in Kcw,Kca and Pgs materials, as shown in fig. 4.19, but still underpredicted the measurements on the critical region.

It was then decided to verify the influence of the values of Poisson's ratio of Kcw and Kca.

4.6.3.7 Analysis NLT-7

Values of poisson's ratios close to 0.5 resulted in numerical difficulties due to the incompressible nature of the material. Therefore they had to be lowered to the values shown in tab. 4.5. In can also be observed in this table that a friction angle of 25 degrees and cohesion intercept of 100 Kpa were used for Pgs material in order to obtain a more stable numerical solution when higher values of poisson's ratios were used.

Some results calculated in this analysis are presented in figs.4.18 to 4.19. So far, the total calculated displacements have been compared to measured displacements. In these comparisons it can be observed that besides underestimating the field movements, the shape of elevation versus displacement curves are quite different. The field curves show very little distortion in the Pgs material, specially in berm 319, giving the impression of a rigid block movement, while the calculated ones show larger amount of distortion in Kca and Pgs. However, if it is taken into consideration that the slope indicators were not installed at the beginning of the Dyke construction,i.e., some displacement had already occurred when the instruments were installed, it is necessary, for the correct comparison between calculated and measured data, to subtract from the total calculated displacement the values corresponding to the period of time before the slope indicators installation.

Doing that for analysis NLT-7 it is seen that the shape of the curves from the finite element analysis are in good agreement with the observed ones, as shown in figs.4.20 to 4.21. This means that during the initial loading stages the increment of shear stress in Kca and Kcw materials was not enough to cause substantial movement, but in Pgs material, which is closer to the surface, relatively large distortion was induced in the region being analyzed.

As the loading increased due to additional layer placement,localized yielding was induced in Kca and Kcw materials. As they are more brittle than Pgs and their shear resistance is low, the horizontal displacements along those layers tended to be greater than in Pgs, causing,therefore,a change in the mechanism of deformation . From then on,the resistance to additional horizontal displacement offered by Kca and Kcw materials was significantly reduced, causing the Pgs layer to become the main resisting element. This gave rise to the different shape of the elevation versus displacement curves, measured by the slope indicators.

The comparative figures between measured and calculated data to be presented from this point on will be relative to the period of time posterior to the installation of each slope indicator: for SI842332 and SI842337 locations the displacements calculated up to 1980 will be subtracted from the total displacements and for SI 842334 location displacements up to 1983 will be subtracted.

During NLT-7 analysis it was observed that the higher the Poisson's ratio used for Kcw and Kca, the higher the rotation of principal stresses which occurred during the initial load steps,specially in the region closer to the toe of the dam. This increase in the rotation of principal stresses would generate a higher stress in the horizontal direction, and, consequently, higher horizontal displacements would be calculated.

Fig.4.22 compares the measured and calculated displacements at the elevation correspondent to Kca/Kcw interface at the location of Si842332 at each year. It is seen that up to 1982 the displacements were overestimated but from 1984 to 1986 the opposite happened.

4.6.3.8 Total Stress Analysis - Conclusion

At this point it was concluded that no additional fundamental understanding of the significance of the factors involved in the problem would be obtained by further variations of total stress parameters. It is evident that if the friction angle of Kcw is further reduced greater horizontal displacements would be calculated, although, numerical stability would tend to deteriorate even more.

The non-linear total stress analysis demonstrated that the movements are very much dependent on the strength and deformability parameters of Kca,Kcw and Pgs materials.

During the initial load steps the deformation process is controlled by the elastic parameters, and at this stage, higher values of Poisson's ratios cause higher rotation of principal stresses which generates higher horizontal displacements. The effect of the rotation of principal stresses is felt even after substantial yielding has occurred since the major principal stress direction is closer to the horizontal direction and higher horizontal normal stresses exist.

The analysis promoted a better understanding of the changes in the deformation mechanisms that probably happened during construction and may explain the shape of the elevation versus displacement curves measured by the slope indicators, in which little distortion was observed in the pgs material up to 1986. The calculated elevation versus displacement curves, although underestimating the field values, are in reasonable agreement with the observed shapes.

The implicit consideration of the effect of pore pressures by the total stress strength parameters adds a great degree of difficulty to the analysis, since,in this case, they should change depending on the pore pressure level, which varies from point to point within the soil. Under these circumstances laboratory tests have little significance, since the pore pressures generated in the tests are generally very different from the ones generated in field.

It was,then, decided that a more fundamental approach to the problem should be undertaken by performing an effective stress analysis.

4.6.4 Effective Stress Analysis

This kind of analysis requires the pore pressures to be considered in an explicit way. This may be undertaken by calculating them through coupled or uncoupled formulations or by introducing the pore pressures in the analysis as known quantities in the way presented in a previous Chapter.

In the specific case of Syncrude's tailing Dyke, the pore pressures have been monitored at Section 53 of Cell 23 specially after 1983, when the horizontal movements were substantially increased. Therefore, it seemed more appropriate to treat these pressures as known quantities, and avoid the difficulties and increase in costs involved in attempting to predict them.

As in the total stress analysis, the material parameters were varied within a certain range in order to observe the sensitivity of the results to these variations and search for an optimum combination of parameters. For economy, when at a certain load step prior to 1986 it was observed that the calculated displacements were too small, the analysis would be stopped and the parameter combination would be changed. The parameters used in the various effective stress analyses are presented in tab.4.6.

4.6.4.1 Pore Pressures

Pore pressure measurements in field are made at specific locations corresponding with the piezometers' tips. For the numerical analysis it is necessary to define, or estimate, pore pressure values at any point within the region being studied. This requires interpolation of the local measured values to form a "surface" over the entire area of interest.

Such interpolation was performed by the use of the scheme presented in a previous Chapter. The use of that technique requires an initial assumption about the pore pressure distribution. This assumption is then corrected as a function of the measured pore pressure values.

The initial assumptions made with respect to the pore pressures in this case were that before the dyke construction the pore pressure condition was hydrostatic and the water level was at elevation 300m. After each lift the phreatic surface would be raised as presented in fig. 4.8, but at any point below the phreatic surface the pore pressures were assumed as hydrostatic, i.e., their values were calculated as the vertical distance between the point being considered and the phreatic line multiplied by the unit weight of the water. Obviously, this is not in accordance with the measured values in which a substantial localized increase was observed close to the Kca/kcw interface elevation.

The initial assumption for each year was then corrected as a function of the average field pore pressure measurement at that year. The inital and corrected values are compared to the field mesurements along piezometers PN852307 and PN852311 in figs. 4.23 and 4.24, respectively. The results were considered very good.

It is well known that one should not judge the quality of any analysis by observing the values calculated at only one point of the structure. This was not done when analysing the numerical model response.But as an illustrative measure of the difference between the finite element model and the field measurement the calculated horizontal displacement at SI842332 location at elevation correspondent to Kca/Kcw interface will sometimes be compared with the field observation at the same point.

4.6.4.2 Analysis NLE-1

At the time of this analysis the tests performed by Sego and Morgenstern(1986) were already available and the strength parameters calculated by these tests were used for Pgs and Pgc materials as shown in tab.4.6. The friction angle for Kcw was set equal to the average residual value and the friction angle for Kca was set approximately equal to the peak value for the slickensided samples on direct shear tests. The initial water level was considered to be at elevation 300m.

The calculated displacements were found to be too small in the critical region and the analysis was terminated in 1982. At that stage, at SI842332 location,the calculated horizontal displacement at Kca/Kcw interface was 1.9cm, while the observed measurement was approximately 3cm, and experience in this specific case history suggested that in these cases this difference would tend to increase at later stages.

4.6.4.3 Analysis NLE-2

The cohesion intercept of Pgs material was reduced to zero and the friction angle increased to 38°. All other material parameters were kept the same as in analysis NLE-1. There was no significant change in the displacements along Kca/Kcw interface relatively to the values previously calculated, and the analysis was terminated after 1981 load step.

4.6.4.4 Analysis NLE-3

In this analysis the friction angle of Kca was reduced to 11 degrees and the friction angle of Kcw to 7.5degrees. The displacements increased with respect to the previous analysis but were still too small. At the SI842332 location, at interface Kca/Kcw,the calculated horizontal displacement was 2.1cm in 1982, while the measured displacement reached 3.00cm. In 1983 the difference between calculated and measured values at this point increased to 4.2cm and the analysis was stopped.

4.6.4.5 Analysis NLE-4

The initial water level was set to elevation 305m, at the top of Pgs and the material parameters kept the same as in the previous analysis.

In this case the calculated displacements at Kca/Kcw interface at SI842332 position were very close to the measured values up to 1982, but the difference between them increased significantly in 1983 and even more in 1984. The analysis was then stopped.

The effect of increasing the elevation of the initial water level was that a lower confining effective stress level would exist at the early loading stages. This would allow greater movements and greater rotation of principal stresses, therefore, increasing the normal stresses in the horizontal direction.

4.6.4.6 Analysis NLE-5

The initial water level was raised to the ground surface. The friction angle of Kcw and Kca had to be raised to 8 and 14 degrees respectively in order to reduce the movements in the initial load stages, which, in the case of 7.5 and 11 degree friction angles, were excessive. It must be recalled that 8 deg. corresponds approximately to the residual value for Kcw material, while 14 deg corresponds to the peak value for the slickensided samples of Kca according to the direct shear tests.

The results of this analysis were in much better agreement than any of the previous analysis up to the 1983 load stage. When the 1984 load step was applied, tension started developing in some kcw elements close to the toe of the dam due to the progressive upwards inclined movement in that region.

The program initially handled tension by a stress transfer technique (Zienkiewickz *et al.*, 1968). By this procedure the elastically calculated tensile stresses in excess of the tensile strength are eliminated and no anisotropy is introduced in the stiffness of the region in tension (i.e. in the stiffness of the element where tension occurred).In general the material in this region remains with its original isotropic elastic parameters. The equilibrium configuration is then searched iteratively,even in case of the linear elastic model, by successive application of the work equivalent unbalanced load vector. This is not a very stable procedure, since that same point, at each iteration, would attract and release tension continuously loading the surrounding elements. And,in fact,in this case, no convergence was obtained after 1983 using this technique.

It was decided that a more appropriate scheme would be the method proposed by Chen and Suzuki(1980) in which a crack is assumed to occur in a plane normal to the direction of the minimum principal stress whenever it reaches the tensile resistance of the material.

The principal stress across the crack as well as the stiffness in that direction drop to zero. However, in the direction parallel to the crack the material is still capable of carrying stresses according to a biaxial stress condition.

The elasto-plastic material stiffness matrix is replaced by a linear elastic one which reflects the sudden change of the stiffness from the current state to an orthotropic elastic state.

In the case of closure of the crack the material switches back to its original condition and in the case of opening of two perpendicular cracks the point becomes incapable of sustaining any load. More detailed discussion on this model and its implementation has been presented in a previous Chapter.

The use of the cracking model proved to be numerically more stable and allowed the analysis to be continued. The results for the years of 1985 and 1986 are compared to the field measurements on figs. 4.25 to 4.27. It is observed that the shapes of the curves as well as the values of displacements are in better agreement with the field values than any of the ones obtained using the total stress analysis.

A very important point to be noticed is that in the effective stress analysis the value of the friction angle for the Kcw material is much more realistic than in the case of the total stress analysis.

It is seen in fig.4.25 that the shape of the calculated displacement versus elevation curves at SI842334 are in reasonable agreement with the measured ones at that position. In 1985, the field values were underestimated by about 35%, but in 1986 this percentage dropped to less than 10%.

In Berm 319, see fig. 4.26, very good agreement is seen between measured and calculated displacement versus elevation curve shapes. The calculated displacements in 1985 and 1986 represent, approximately, 75% and 90% of the measured values,respectively. This approximation is actually very good, specially considering that this represents more that 10% of shear strains in the Kcw material and the absolute values of the displacements involved are quite high.

At the toe, the calculated values of displacements are very close to the measured data, as shown in fig. 4.27. In 1986 an almost perfect match was obtained.

Comparison between calculated and measured displacement values at the Kca/Kcw interface elevation in Berm 319 and toe locations at different time intervals is shown in fig. 4.28. It is observed that in both locations the calculated values present the same tendency as the field data. At berm 319 a slight overestimation of the movements before 1983 and underestimation after that is found. In the case of the displacements at the toe the difference between calculated and measured displacements is much smaller.

The horizontal displacements along an approximately horizontal plane corresponding to the Kca/Kcw elevation is shown in fig. 4.29. The locations of three slope indicators are present for a clearer interpretation of the figure, but no comparison between measured and calculated values is shown since, in this case, the total displacement values are plotted, i.e.,they were not subtracted from the amount of displacement calculated for the period of time before the installation of the slope indicators.

Fig. 4.29 shows,in accordance with what has been observed in the field, that the higher displacements occur at the berm 319 region, rapidly decreasing towards the toe and the center of the dam.

It is noticed by figs. 4.25 to 4.27 that the displacements until 1985 at the SI842334 location are significantly underestimated , while at the berm 319 and at the toe the calculated results are progressively closer to the measured values. This may be indicating that Pgc material might be weaker than expressed in the finite element model and/or the center line in the finite element model should be shifted to the left, causing less restraint to the horizontal movement in that region.

These changes were not tried since the quality of the results seemed already to be enough to validate the analysis and show that the effective stress analysis, using average values of pore pressures as known quantities presented much better and more realistic results as well as a better understanding of the problem than the total stress analysis.

Contours of maximum shear strains are shown in fig. 4.30 for the year of 1986. It is noted that the zone of higher distortion values are concentrated in a limited region around the Kca/Kcw contact. Very little distortion is observed in Pgs material, which is in agreement with the movement pattern shown by the slope indicators the in field.

With respect to extensional strains, the cracking model indicated in the 1984 load step the formation of practically vertical superficial cracks close to the position of SI842334 and 2 cracks with orientations of approximatelly 30° clockwise relative to the horizontal in Kcw material in the toe region. These cracks express a movement pattern involving a descending and horizontal sliding at the region close to SI842334 and upwards inclined movement close to the dam toe.

In 1985 the vertical cracks were deepened and some more cracks appeared at Kcw material at the toe region. These results may be considered to agree with the micrometer measurements at the toe, which presented an overall compressive state, except at the Kca/Kcw interface region. Although, as has been mentioned, it is not possible to decide whether the measured extensional strains were real or due to the horizontal sliding. The orientation of the cracks at the end of 1986 are schematically presented in fig. 4.31

4.6.4.7 Effective stress analysis - conclusion

The effective stress analysis presented results in better agreement with field measurements than the total stress analysis.

The parameter combination to reach a good history match in this case are within an acceptable range of variability with respect to the laboratory results.

The pore pressure interpolation technique as well as the method of introducing these pressures into the analysis as known quantities were shown to form a relatively simple and efficient way of explicitly considering field pore pressures.

The finite element technique and the material models used seem to be adequate tools for analysing the problem if the critical aspects involved are adequately accounted for.

It must also be noted that relatively to the dimensions, degree of heterogeneity, high level of displacements, stresses and strains involved in this specific case studied, the results obtained were, in fact, very good, specially if it is considered that the problem was approached using a time independent, small strain, small displacement formulation and relatively simple material models as isotropic and anisotropic linear elastic, hyperbolic (non-linear elastic) and elastic perfectly plastic with the Mohr-Coulomb yield criterion.

Piezometer tip location and total head (m)								
Piezometer	Tip elev.	1980	1981	1982	1983	1984	1985	1986
PN802303	291.44	302.30	301.98	303.17	303.31	305.48	306.01	305.90
PN802304	300.56	308.64	308.46	309.60	309.28	311.46	311.85	311.80
PN802305	293.00	309.12	309.18	320.50	318.84	318.49	318.14	309.12
"	302.42	313.28	326.46	318.52	319.30	319.28	319.29	319.20
PN802310	291.00	301.82	309.75	312.80	312.47	313.42	312.32	312.70
"	292.65	302.98	309.09	312.18	312.00	314.04	312.37	312.50
"	301.79	308.55	307.40	307.34	307.60	308.04	307.90	307.90
PN832305	290.91	-	-	-	-	291.30	291.25	291.30
PN842302	292.60	-	-	-	-	303.12	303.40	303.30
PN842318	291.35	-	-	-	-	297.50	297.60	297.60
"	293.33	-	-	-	-	303.04	303.25	303.24
"	298.06	-	-	-	-	304.60	304.50	304.50
"	300.34	-	-	-	-	304.90	304.70	304.70
"	304.31	-	-	-	-	306.03	305.90	305.90
PN842319	290.53	-	-	-	-	343.36	349.11	351.50
"	294.19	-	-	-	-	319.20	319.30	320.3
"	297.54	-	-	-	-	313.14	312.0	312.0
"	299.68	-	-	-	-	312.60	312.80	312.80
"	303.64	-	-	-	-	312.40	312.60	312.60
"	307.60	-	-	-	-	313.60	313.90	313.70
PN852304	285.89	-	-	-	-	-	309.03	308.20
"	288.08	-	-	-	-	-	327.40	327.70
"	291.43	-	-	-	-	-	350.40	356.70
"	294.12	-	-	-	-	-	319.42	319.90
PN852305	289.20	-	-	-	-	-	319.39	319.80
"	291.49	-	-	-	-	-	345.77	360.00
"	296.82	-	-	-	-	-	318.97	318.70
"	300.63	-	-	-	-	-	319.12	319.15

Table 4.1:Piezometer tip elevations and total head

Piezometer tip elevation and total head (continue)								
Piezometer	Tip elev.	1980	1981	1982	1983	1984	1985	1986
PN852306	287.67	-	-	-	-	-	332.13	334.03
"	289.65	-	-	-	-	-	343.69	359.60
"	291.63	-	-	-	-	-	345.78	360.70
"	296.20	-	-	-	-	-	314.98	315.00
"	302.91	-	-	-	-	-	317.80	317.60
PN852307	288.30	-	-	-	-	-	307.10	306.70
"	290.30	-	-	-	-	-	318.04	317.60
"	291.40	-	-	-	-	-	332.47	340.06
"	292.90	-	-	-	-	-	335.43	343.03
"	294.40	-	-	-	-	-	328.41	331.80
"	296.00	-	-	-	-	-	315.00	313.92
"	304.60	-	-	-	-	-	311.10	311.10
"	309.70	-	-	-	-	-	311.50	311.40
PN852311	290.20	-	-	-	-	-	309.50	309.20
"	291.00	-	-	-	-	-	318.27	320.40
"	292.50	-	-	-	-	-	316.03	318.30
"	294.80	-	-	-	-	-	315.82	321.40
"	297.80	-	-	-	-	-	309.50	309.10
"	306.80	-	-	-	-	-	308.80	308.70
"	310.60	-	-	-	-	-	310.80	311.00
PN852312	288.50	-	-	-	-	-	305.80	306.50
"	289.50	-	-	-	-	-	305.70	306.40
"	290.80	-	-	-	-	-	305.20	306.50
"	295.22	-	-	-	-	-	305.90	305.90
PN852316	290.74	-	-	-	-	-	305.50	305.50
"	295.31	-	-	-	-	-	305.4	305.6
"	301.40	-	-	-	-	-	305.50	305.50
"	304.45	-	-	-	-	-	305.50	305.50

Table 4.1:Piezometer tip elevations and total head (continue)

Piezometer tip elevation and pore pressure (kpa)								
Piezometer	Tip elev.	1980	1981	1982	1983	1984	1985	1986
PN802303	291.44	106.54	103.40	115.10	116.50	137.70	142.90	141.80
PN802304	300.56	79.30	77.50	88.70	85.50	106.90	110.80	110.90
PN802305	293.00	158.40	158.70	270.00	253.50	250.10	239.20	158.14
"	302.42	106.50	235.80	157.90	165.60	165.40	165.50	164.60
PN802310	291.00	106.10	184.00	213.90	210.60	220.00	209.10	212.90
"	292.65	101.30	161.30	191.60	190.00	210.13	193.50	194.70
"	301.79	66.30	55.04	54.50	57.00	61.30	60.00	59.94
PN832305	290.91	-	-	-	-	3.80	3.40	3.83
PN842302	292.60	-	-	-	-	103.20	106.00	104.90
PN842318	291.35	-	-	-	-	60.30	61.30	61.30
"	293.33	-	-	-	-	99.80	97.320	97.20
"	298.06	-	-	-	-	64.20	63.20	63.20
"	300.34	-	-	-	-	44.70	42.80	42.80
"	304.31	-	-	-	-	16.90	15.60	15.60
PN842319	290.53	-	-	-	-	518.30	575.30	598.10
"	294.19	-	-	-	-	245.40	246.30	256.10
"	297.54	-	-	-	-	153.04	143.80	141.80
"	299.68	-	-	-	-	126.70	128.70	128.70
"	303.64	-	-	-	-	86.00	88.00	87.80
"	307.60	-	-	-	-	59.00	62.00	59.80
PN852304	285.89	-	-	-	-	-	227.00	218.8
"	288.08	-	-	-	-	-	386.00	388.6
"	291.43	-	-	-	-	-	578.00	640.2
"	294.12	-	-	-	-	-	319.42	252.9

Table 4.2: Piezometer tip elevation and pore pressure

Piezometer tip elevation and pore pressure (continue)								
Piezometer	Tip elev.	1980	1981	1982	1983	1984	1985	1986
PN852305	289.20	-	-	-	-	-	296.20	300.1
"	291.49	-	-	-	-	-	532.50	672.0
"	296.82	-	-	-	-	-	217.30	214.6
"	300.63	-	-	-	-	-	181.40	181.6
PN852306	287.67	-	-	-	-	-	436.20	457.7
"	289.65	-	-	-	-	-	527.20	686.2
"	291.63	-	-	-	-	-	531.20	677.5
"	296.20	-	-	-	-	-	184.20	184.4
"	302.91	-	-	-	-	-	146.10	144.1
PN852307	288.30	-	-	-	-	-	184.40	180.5
"	290.30	-	-	-	-	-	272.10	267.8
"	291.40	-	-	-	-	-	403.00	477.3
"	292.90	-	-	-	-	-	417.20	491.7
"	294.40	-	-	-	-	-	333.70	366.8
"	296.60	-	-	-	-	-	180.50	175.7
"	304.60	-	-	-	-	-	63.80	63.7
"	309.70	-	-	-	-	-	17.70	16.6
PN852311	290.20	-	-	-	-	-	189.00	186.3
"	291.00	-	-	-	-	-	267.50	288.4
"	292.50	-	-	-	-	-	231.00	253.09
"	294.80	-	-	-	-	-	206.20	260.9
"	297.80	-	-	-	-	-	115.00	110.8
"	306.80	-	-	-	-	-	19.62	18.6
"	310.60	-	-	-	-	-	2.40	3.9
PN852312	288.50	-	-	-	-	-	168.00	176.5
"	289.50	-	-	-	-	-	158.24	165.7
"	290.80	-	-	-	-	-	141.30	154.01
"	295.22	-	-	-	-	-	105.00	104.70
PN852316	290.74	-	-	-	-	-	144.7	144.7
"	295.31	-	-	-	-	-	100.0	100.0
"	301.40	-	-	-	-	-	40.22	40.20
"	304.45	-	-	-	-	-	10.30	10.30

Table 4.2:Piezometer tip elevations and pore pressures (continue)

	MATERIAL															
MAT.	km		kcw		kca		pgs		pgc		pf		ho		ts	
Weight	21.5		20.0		20.0		21.5		21.5		20.0		20.0		20.0	
LE#	E	u	E	u	E	u	E	u	E	u	E	u	E	u	E	u
1	200000	0.45	70	0.30	50	0.45	100	0.40	100	0.40	70	0.30	70	0.30	70	0.30
2	200000	0.45	70	0.30	50	0.45	100	0.40	100	0.40	70	0.30	70	0.30	70	0.30
3A	200000	0.45	70	0.30	50	0.45	50	0.40	50	0.40	70	0.30	70	0.30	70	0.30
3B	200000	0.45	70	0.30	50	0.45	150	0.40	150	0.40	70	0.30	70	0.30	70	0.30
4A	200000	0.45	70	0.30	25	0.45	100	0.40	100	0.40	70	0.30	70	0.30	70	0.30
4B	200000	0.45	70	0.30	75	0.45	100	0.40	100	0.40	70	0.30	70	0.30	70	0.30
5	200000	0.45	5	0.30	50	0.45	100	0.40	100	0.40	70	0.30	70	0.30	70	0.30

notes/

E - Elastic modulus (MPa)
u - Poisson's ratio
Weight - Unit Weight (kN/m3)

ts - Tailing sand

Table 4.3: Summary of material parameters in the linear elastic analyses

		MATERIAL									
NO.#	PAR.	hm	kcw	kca	pgc	pgs	pf	no	ts1	ts2	ts3
NO.1	E	3000	45	45						5	
	u	0.35	0.48	0.48	0.40	0.40	0.30	0.30	0.30	0.30	
	ϕ		8.00	8.00	38.7	37.0	38.0	38.0	38.0		
	C		0.00	0.00	35.0	0.00	35.0	35.0	35.0		
	k				750.0	410.0	280.0	380.0	750.0		
	n				0.34	0.68	0.68	0.66	0.34		
	Rf				0.87	0.90	0.83	0.83	0.87		
NO.2	E	3000	45	45						5	
	u	0.35	0.48	0.48	0.40	0.40	0.30	0.30	0.30	0.30	
	ϕ		8.00	8.00	38.7	37.0	38.0	38.0	38.0		
	C		0.00	0.00	5.0	0.00	35.0	35.0	35.0		
	k				280.0	410.0	280.0	380.0	750.0		
	n				0.24	0.68	0.68	0.68	0.24		
	Rf				0.87	0.90	0.83	0.83	0.87		
NO.3	E	3000	45	45						5	
	u	0.35	0.48	0.48	0.42	0.30	0.30	0.30	0.30	0.30	
	ϕ		4.00	4.00	30.0	38.0	[illegible]	30.0	38.0		
	C		0.00	0.00	5.0	0.00	5.0	5.0	35.0		
	k				150.0	400.0	280.0	280.0	750.0		
	n				0.24	0.90	0.50	0.50	0.24		
	Rf				0.87	0.90	0.83	0.83	0.87		
NO.4	E	3000	45	45						5	10
	u	0.35	0.48	0.48	0.42	0.30	0.30	0.30	0.30	0.30	0.30
	ϕ		4.00	14.00	30.0	37.0	30.0	30.0	38.0		
	C		0.00	0.00	5.0	0.00	5.0	5.0	35.0		
	k				150.0	400.0	280.0	280.0	750.0		
	n				0.24	0.90	0.50	0.50	0.34		
	Rf				0.87	0.90	0.83	0.83	0.87		
NO.5	E	3000	30	30						5	10
	u	0.35	0.48	0.40	0.42	0.30	0.30	0.30	0.30	0.30	0.30
	ϕ		4.00	14.0	30.0	37.0	30.0	30.0	38.0		
	C		0.00	0.00	5.0	0.00	5.0	5.0	35.0		
	k				150.0	400.0	280.0	380.0	750.0		
	n				0.24	0.90	0.90	0.50	0.24		
	Rf				0.87	0.90	0.83	0.83	0.87		
NO.6	E	3000	20	20						5	10
	u	0.35	0.45	0.45	0.42	0.30	0.30	0.30	0.30	0.30	0.30
	ϕ		4.00	14.0	30.0	18.0	30.0	30.0	38.0		
	C		0.00	0.00	5.0	80.0	5.0	5.0	35.0		
	k				150.0	400.0	280.0	280.0	750.0		
	n				0.24	0.90	0.90	0.80	0.24		
	Rf				0.87	0.90	0.83	0.83	0.87		

Notes/

E - Elastic Modulus (MPa)
u - Poisson's Ratio
ϕ - Friction angle (Degree)
C - Cohesion (kPa)
k - Modulus in hyperbolic elastic model
n - Exponent in hyperbolic elastic model
Rf - Rf factor in hyperbolic elastic model
Unit weights same as Table 1

ts1 - Tailing sand using hyperbolic elastic model
ts2 - Tailing sand using linear elastic model when layer is added
ts3 - Tailing sand using linear elastic model to minimize converge problem

Table 4.4: Summary of material parameters used in the non-linear total stress analyses

		MATERIAL									
NL#	PAR	km	kcw	kca	pgc	pgs	pf	ho	ts1	ts2	ts3
NL7	E	2000000	20000	20000						5000	10000
	u	0.35	0.47	0.47	0.45	0.40	0.40	0.40	0.30	0.30	0.30
	ϕ		4.00	14.00	30.0	25.0	30.0	30.0	38.0		
	c		0.00	0.00	5.0	100.0	5.0	5.0	35.0		
	k				150.0	400.0	280.0	280.0	750.0		
	n				0.24	0.50	0.25	0.25	0.24		
	Rf				0.87	0.90	0.93	0.93	0.87		

Notes/

E - Elastic Modulus (kPa)
u - Poisson's Ratio
ϕ - Friction angle (degree)
c - Cohesion (kPa)
k - Modulus in hyperbolic elastic model
n - Exponent in hyperbolic elastic model
Rf - Rf factor in hyperbolic elastic model
Unit Weights same as Table 1

ts1 - Tailing sand using hyperbolic elastic model
ts2 - Tailing sand using linear elastic model when layer is added
ts3 - Tailing sand using linear elastic model to mininize convergce problem

Table 4.5: Summary of material parameters used in the non-linear finite element analysis NL7 in terms of total stresses

Parameters used in the effective stress analysis

Anl.	Par.	Km	Kcw	Kca	Pgc	Pgs	Pf	Ts1	Ts2
1	E	2×10	45000	45000	-	-	-	5000	-
	μ	0.35	0.45	0.45	0.40	0.40	0.30	0.30	0.30
	ø		8.00	14.00	11.00	25.00	35.00		35.00
	c				32.00	33.00	38.00		38.00
	K				300.00	235.00	280.00		750.00
	n				0.54	1.1	0.65		0.24
	Rf				0.80	0.9	0.93		0.87
2	E	2×10	45000	45000				5000	
	μ	0.35	0.45	0.45	0.40	0.40	0.30	0.30	0.30
	ø		8.00	14.00	11.00	38.00	35.00		35.00
	c				32.00	0.00	38.00		38.00
	K				300.00	235.00	280.00		750.00
	n				0.54	1.10	0.65		0.24
	Rf				0.80	0.90	0.93		0.87
3	E	2×10	45000	45000				5000	
	μ	0.35	0.45	0.40	0.40	0.40	0.30	0.30	0.30
	ø		7.50	11.00	11.00	38.00	35.00		35.00
	c				32.00	0.00	38.00		38.00
	K				300.00	400.00	280.00		750.00
	n				0.54	0.50	0.65		0.24
	Rf				0.80	0.90	0.93		0.87
4	E	2×10	45000	45000				5000	
	μ	0.35	0.45	0.40	0.40	0.40	0.30	0.30	0.30
	ø		7.50	11.00	11.00	38.00	35.00		35.00
	c				32.00	0.00	38.00		38.00
	K				300.00	400.00	280.00		750.00
	n				0.54	0.50	0.65		0.24
	Rf				0.80	0.90	0.93		0.87
5	E	2×10	45000	45000				5000	
	μ	0.35	0.45	0.40	0.40	0.40	0.30	0.30	0.30
	ø		8.00	14.00	38.00	37.00	35.00		35.00
	c				32.00	0.00	38.00		38.00
	K				750.00	400.00	280.00		750.00
	n				*0.24	0.24	0.65		0.24
	Rf				0.80	0.90	0.93		0.87

Notes/

E - Elastic Modulus (MPa)
μ - Poisson's Ratio
ø - Friction angle (degree)
c - Cohesion (kPa)
k - Modulus in hyperbolic elastic model
n - Exponent in hyperbolic elastic model
Rf - Rf factor in hyperbolic elastic model
Unit Weights same as Table 1

ts1 - Tailing sand using hyperbolic elastic model
ts2 - Tailing sand using linear elastic model when layer is added
ts3 - Tailing sand using linear elastic model to minimize converge problem

Table 4.6: Summary of material parameters used in the non-linear effective stress analyses

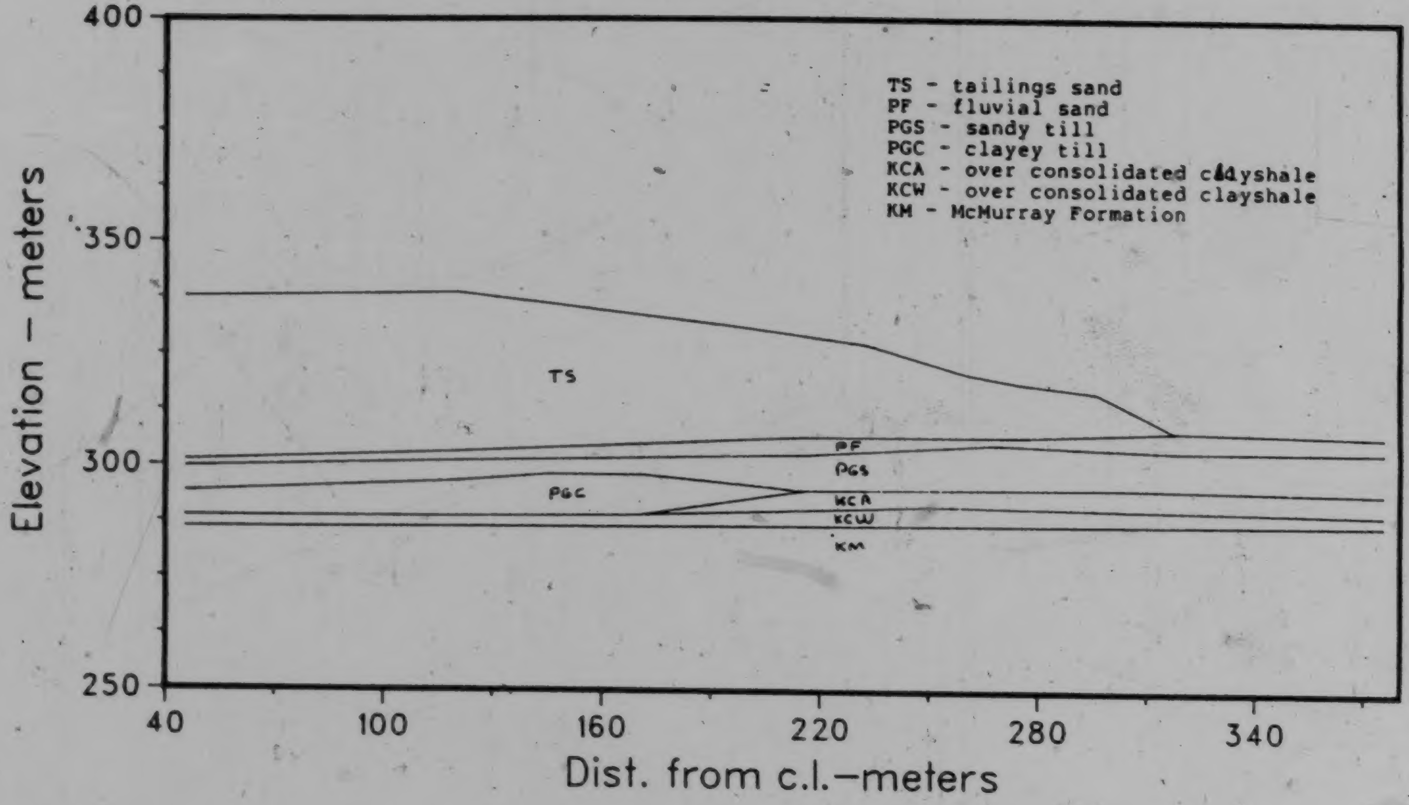

Figure 4.1: Stratigraphy of Cell 23, Section 53

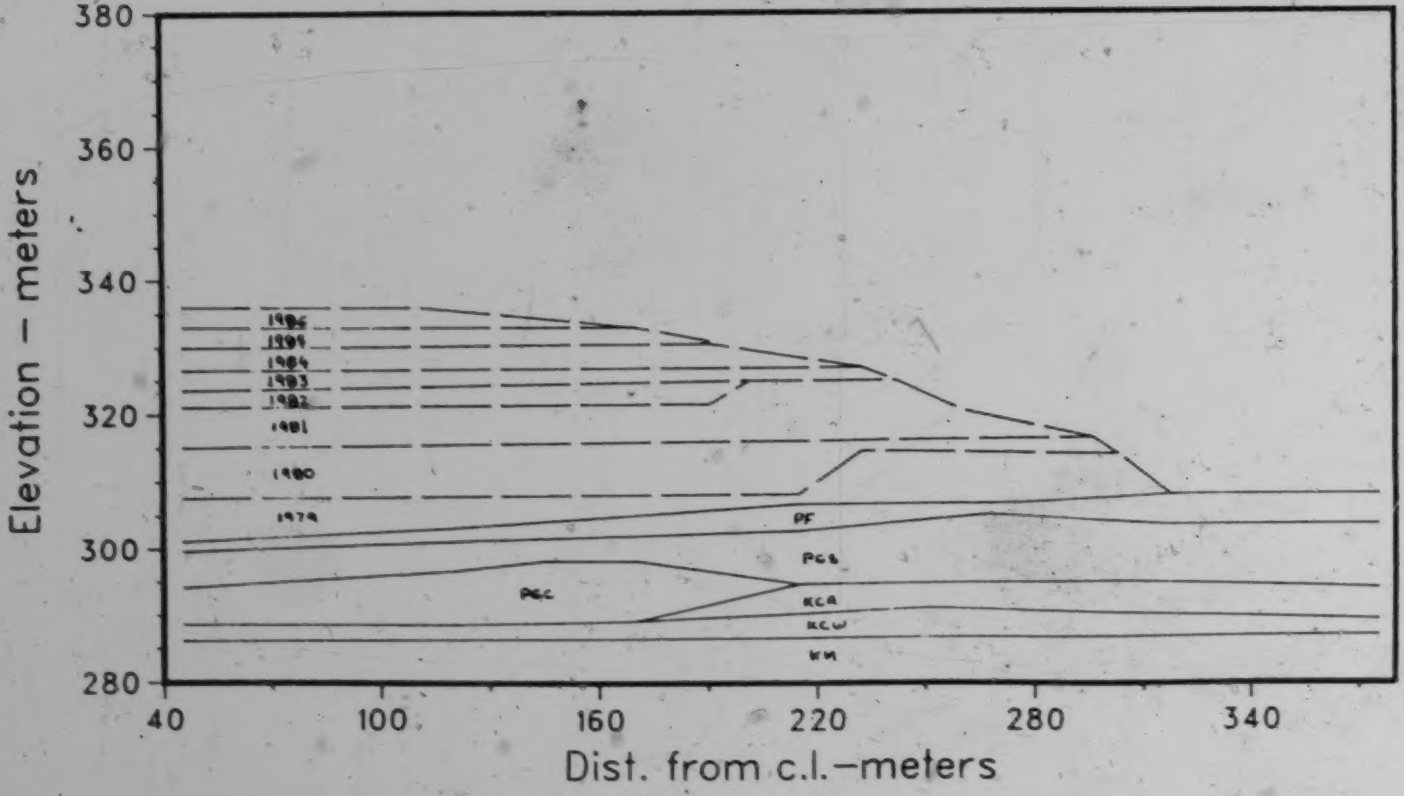

Figure 4.2: Construction stages from 1979 to 1986

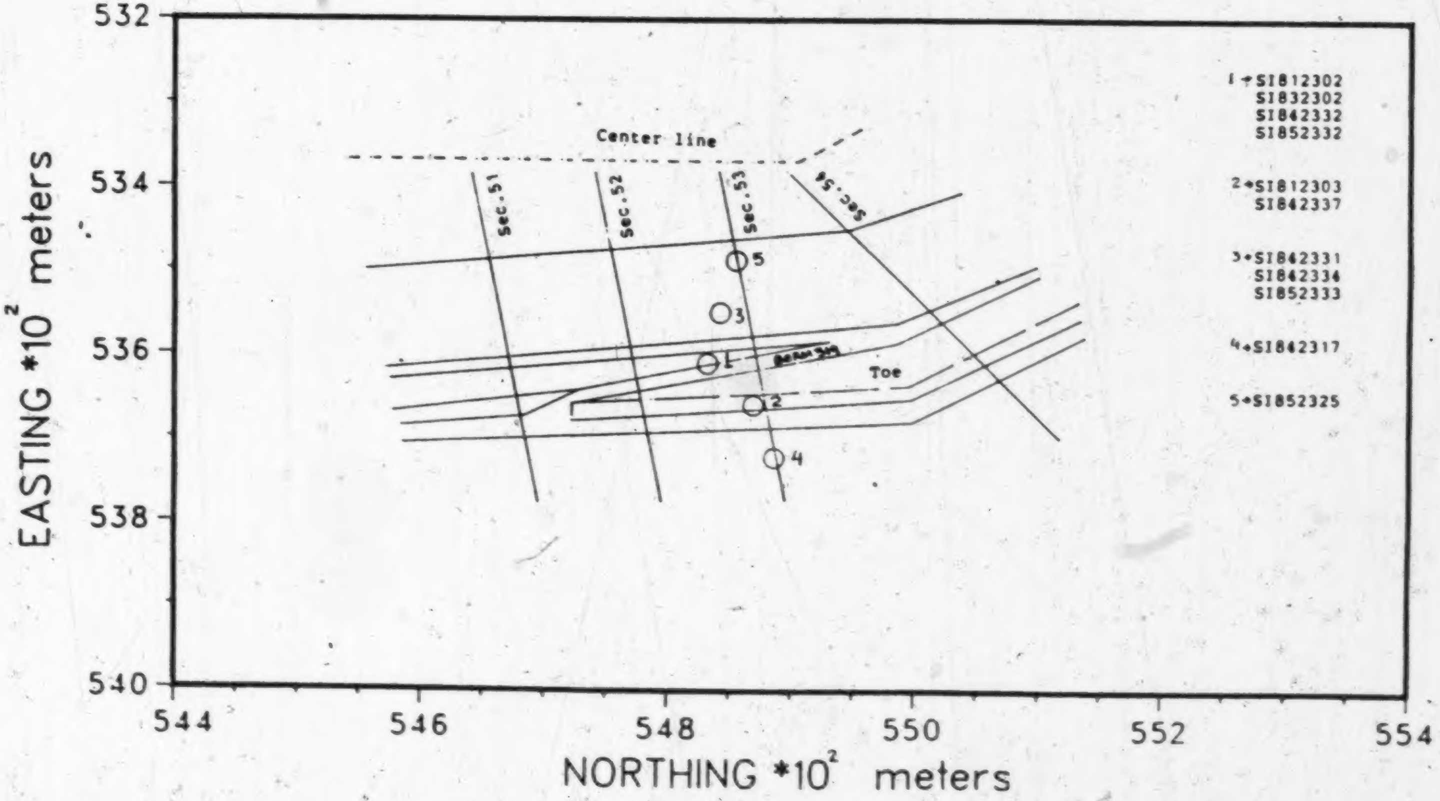
1→SI812302
SI832302
SI842332
SI852332
2→SI812303
SI842337
3→SI842331
SI842334
SI852333
4→SI842317
5→SI852325
Center line
Sec.51
Sec.52
Sec.53
Sec.54
Toe
1
2
3
4
5
532
534
536
538
540
EASTING *10² meters
544
546
548
550
552
554
NORTHING *10² meters

Figure 4.3: Plan view of slope indicators locations

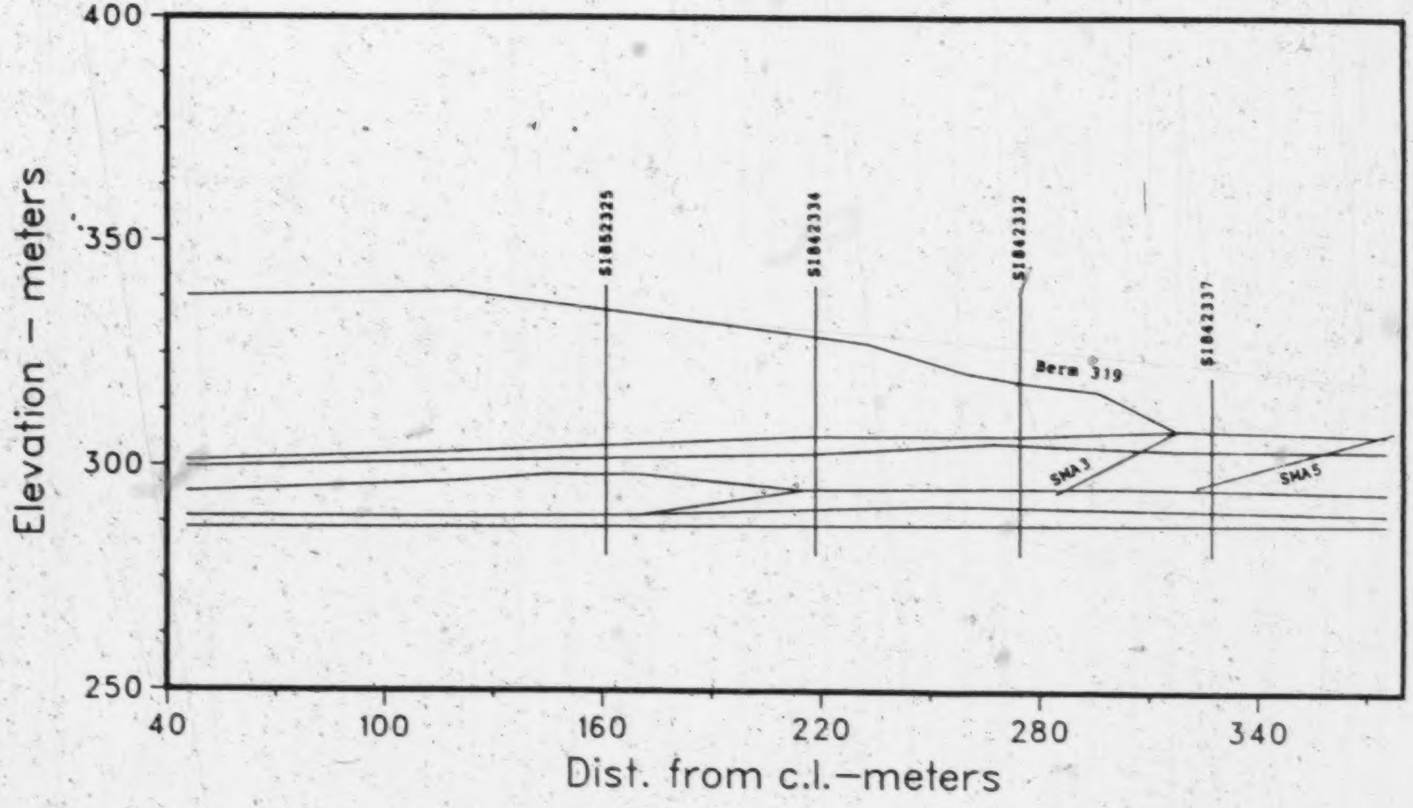

Figure 4.4: Slope indicators positions - cross section

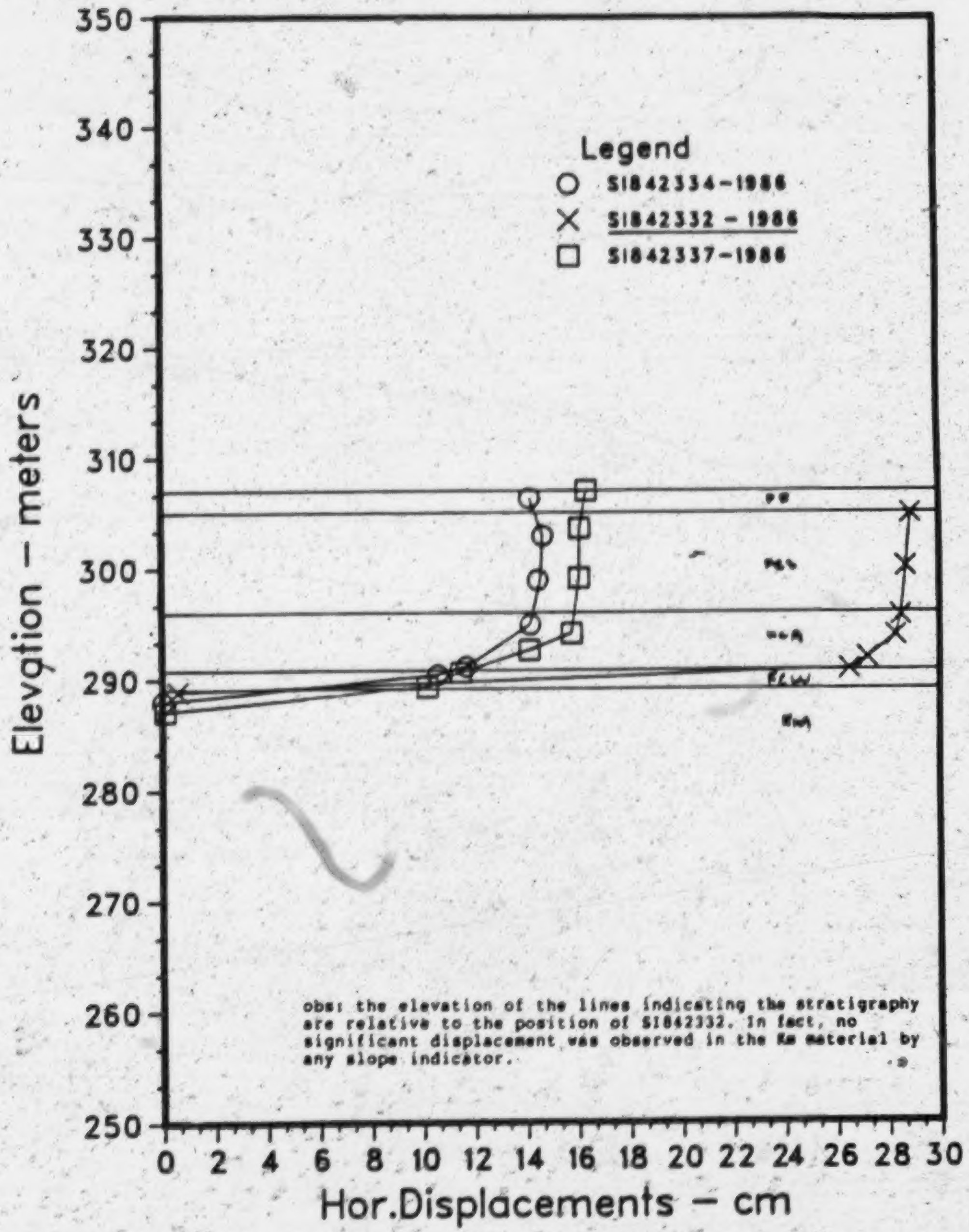

obs: the elevation of the lines indicating the stratigraphy are relative to the position of SI842332. In fact, no significant displacement was observed in the Km material by any slope indicator.

Figure 4.5: Measured horizontal displacements until 1986

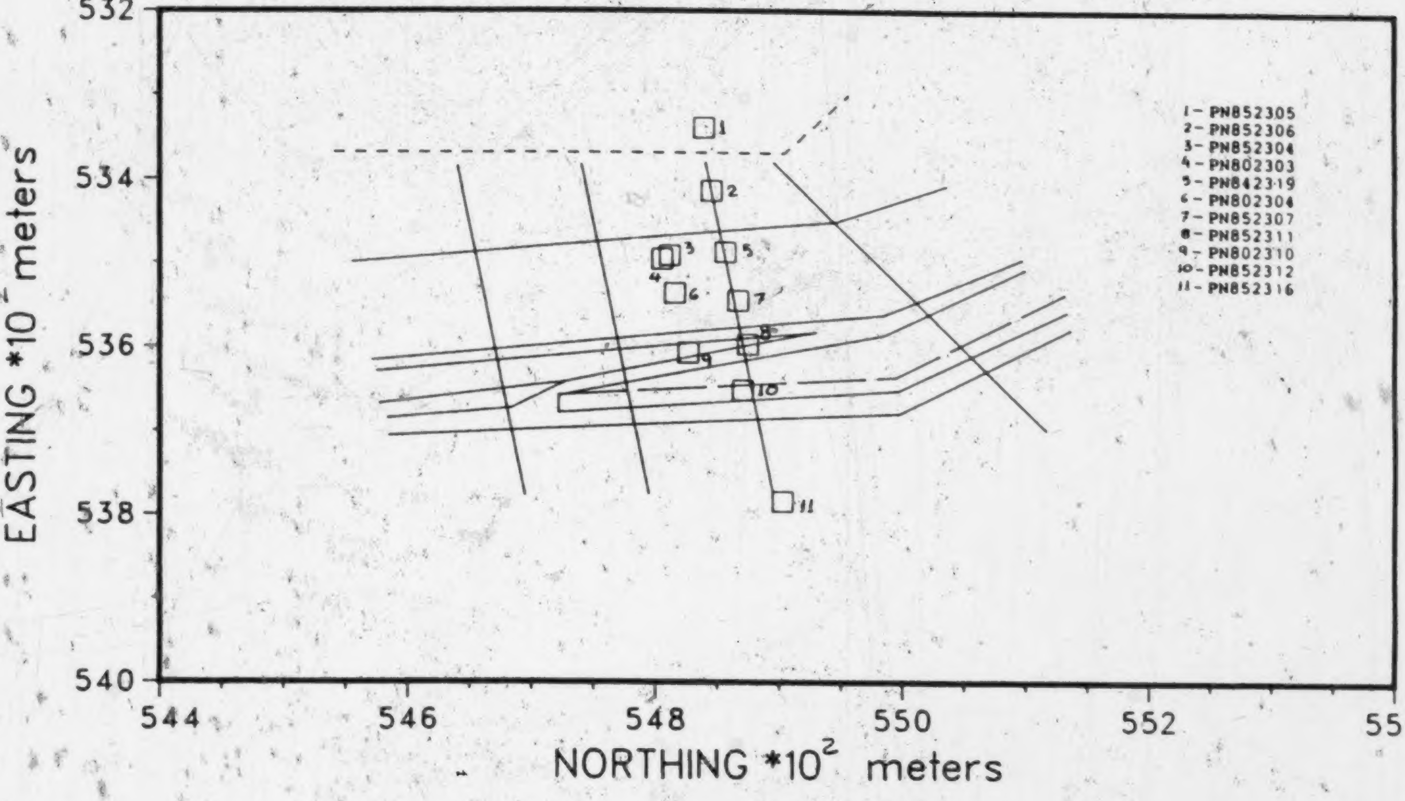
1 - PN852305
2 - PN852306
3 - PN852304
4 - PN802303
5 - PN842319
6 - PN802304
7 - PN852307
8 - PN852311
9 - PN802310
10 - PN852312
11 - PN852316
1
2
3
4
5
6
7
8
9
10
11
532
534
536
538
540
544
546
548
550
552
554
EASTING *10² meters
NORTHING *10² meters

Figure 4.6: Plan view of piezometers positions

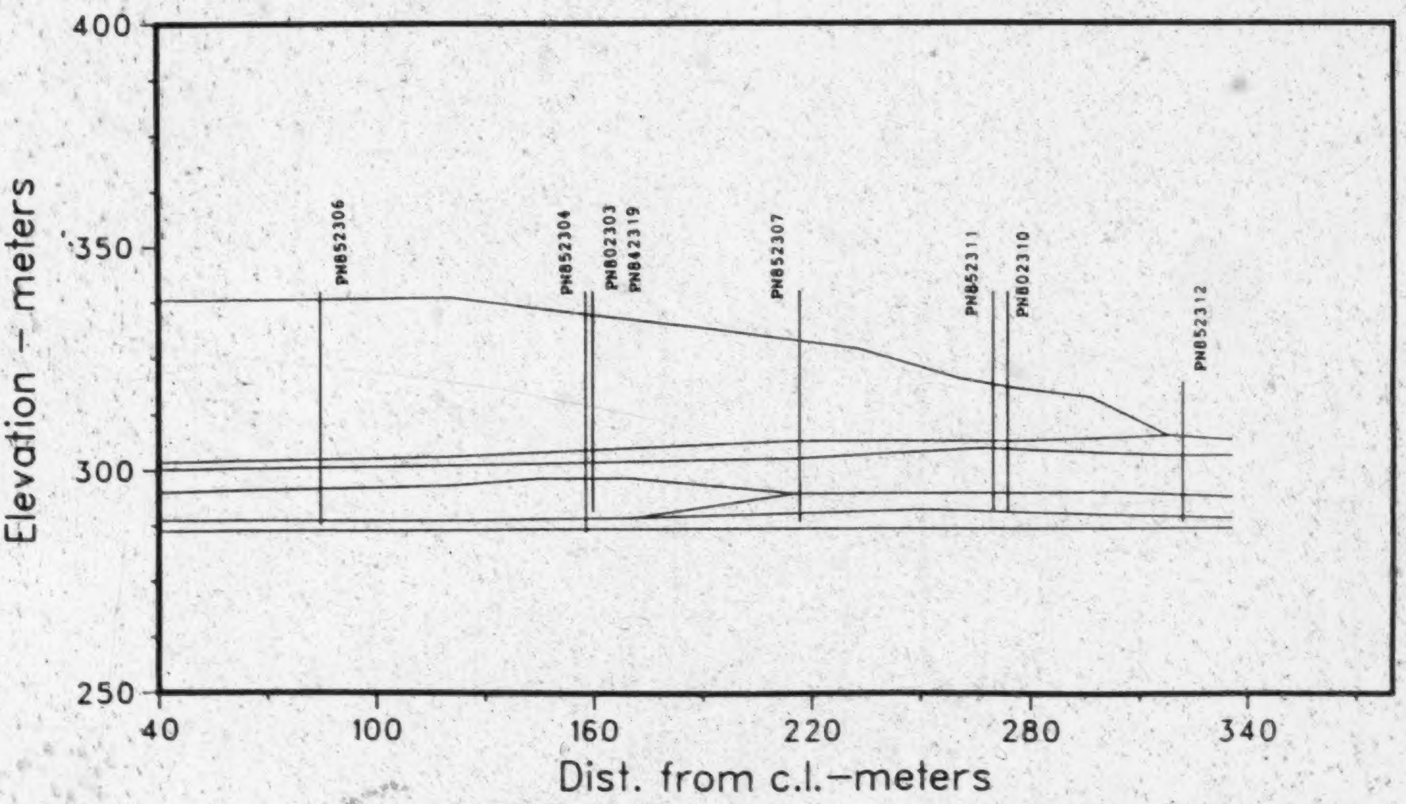

Figure 4.7: Piezometers positions - cross section

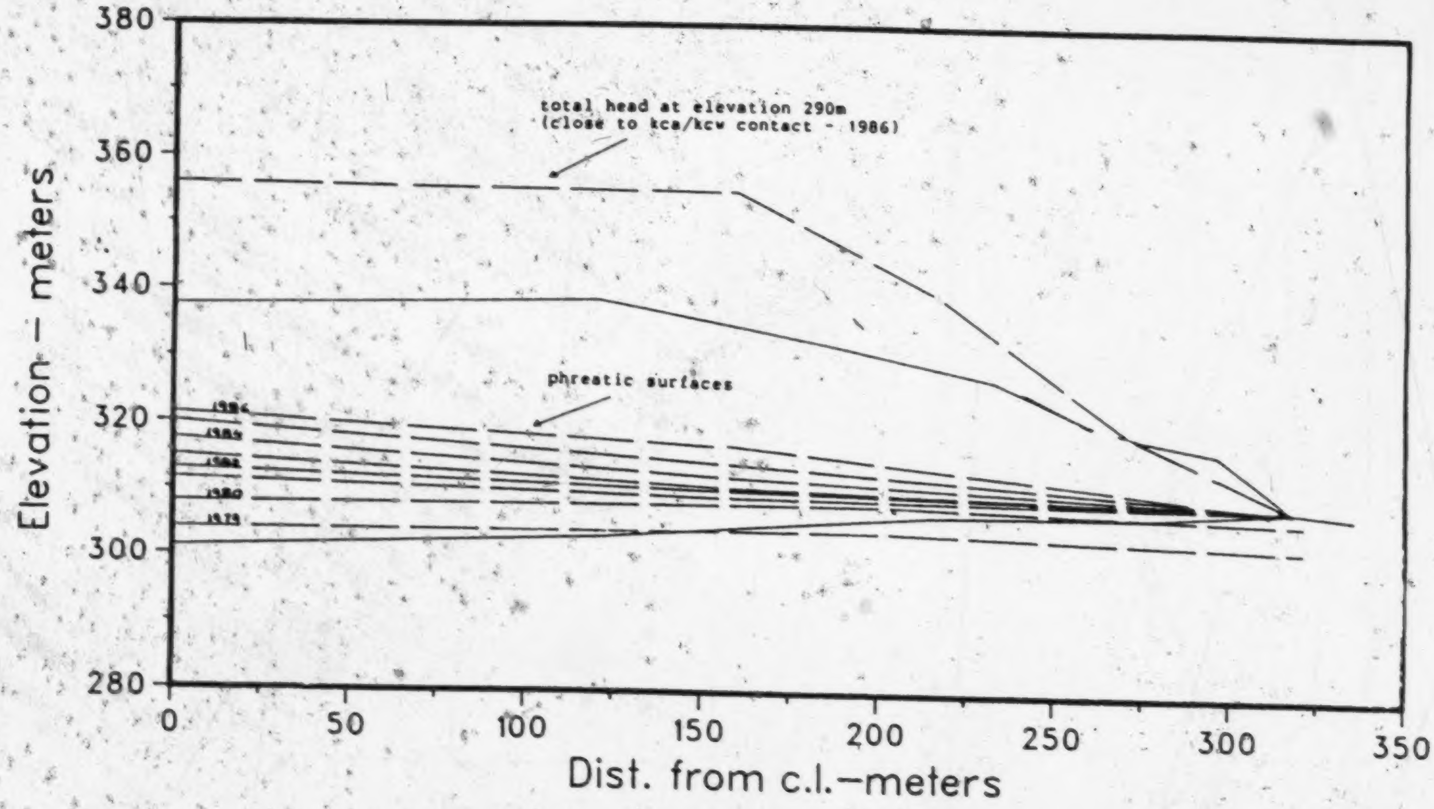

Figure 4.8: Phreatic surfaces at each year of construction and average total head at elevation 290m measured in 1986

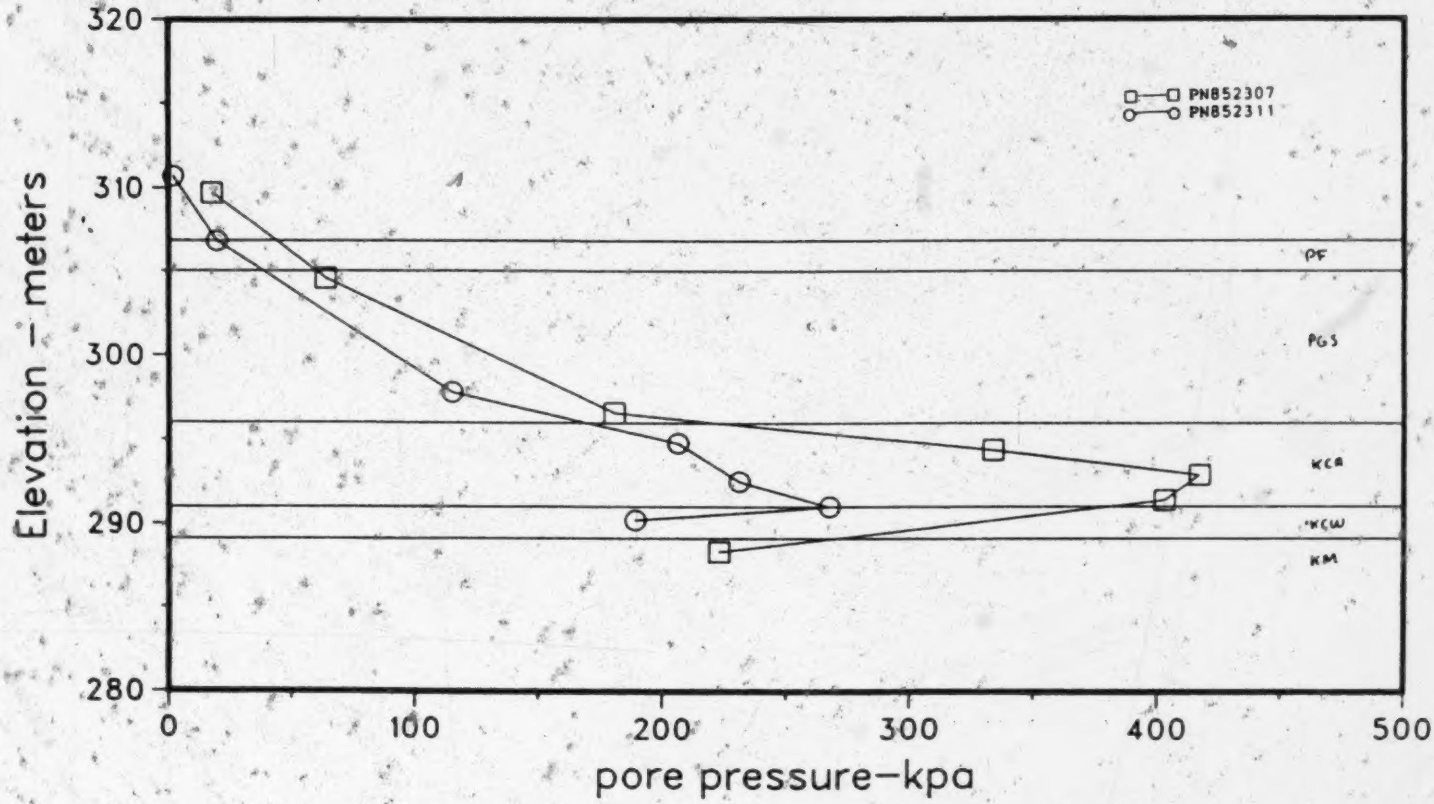

Figure 4.9: Average pore pressures measured by PN852307 and PN852311 in 1985

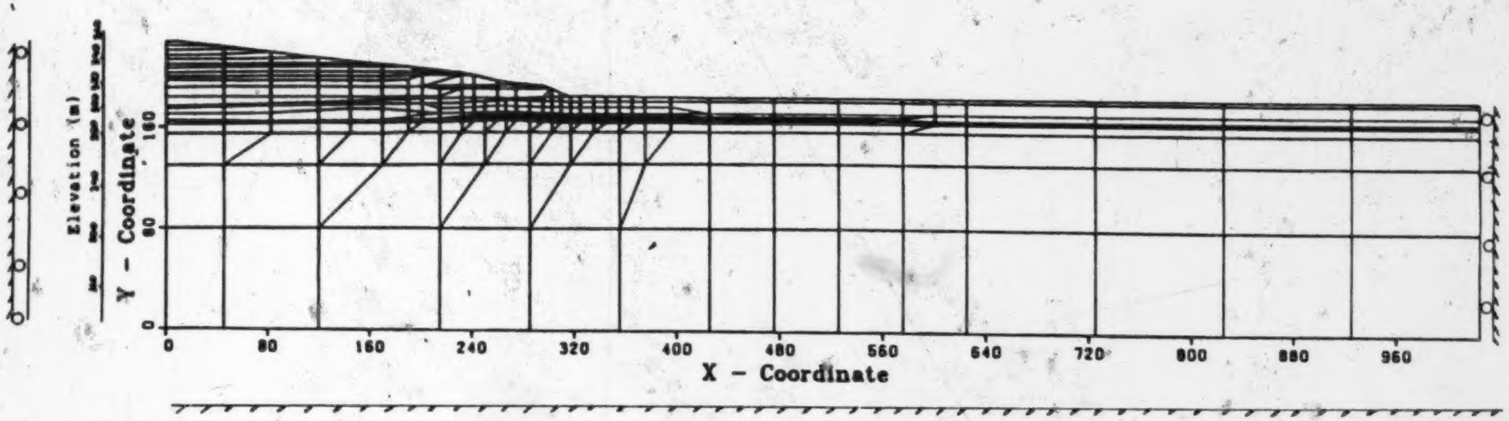
Elevation (m)
Y - Coordinate
0
80
160
X - Coordinate
0
80
160
240
320
400
480
560
640
720
800
880
960

Figure 4.10: Finite element idealization of the Dyke and Foundation

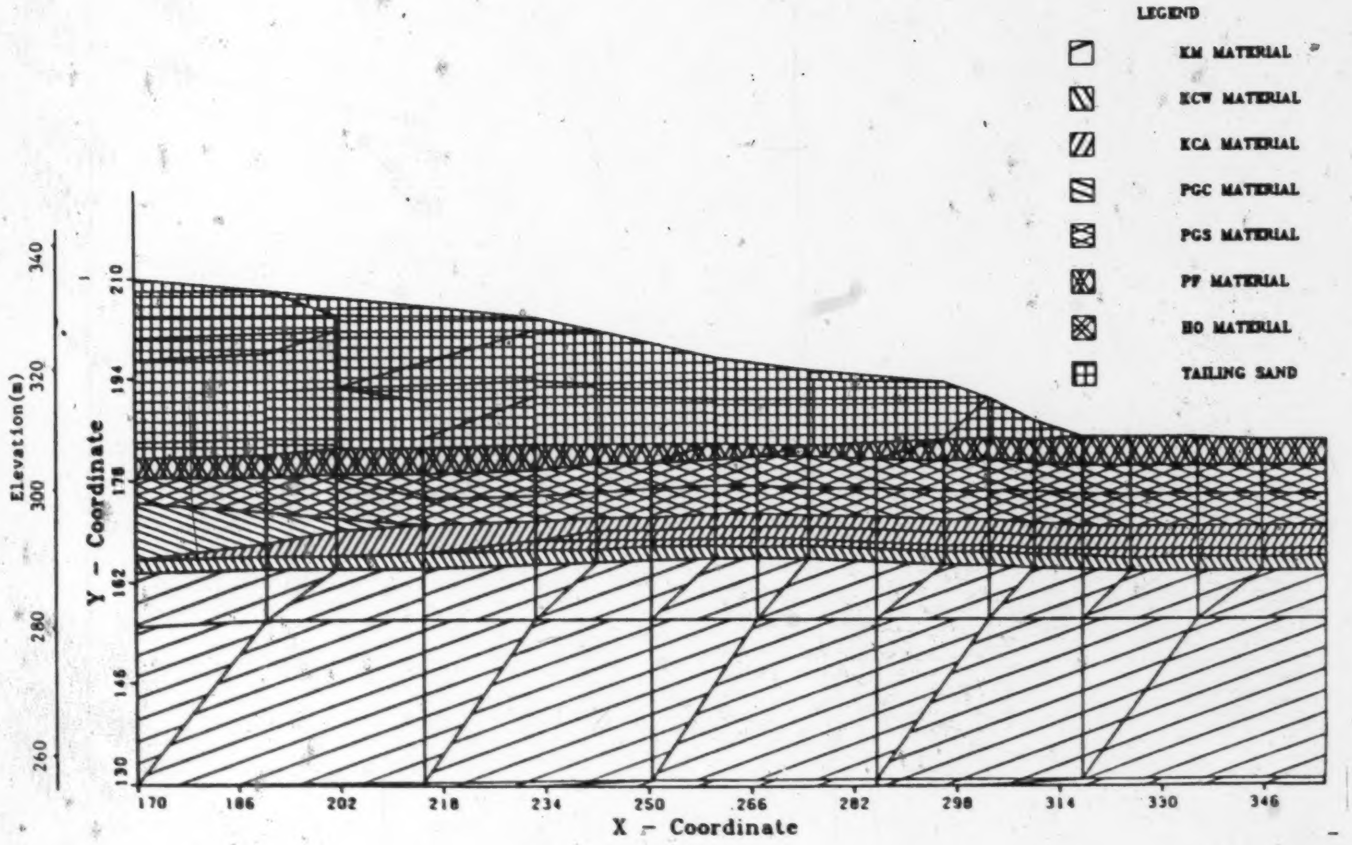
LEGEND
KM MATERIAL
KCW MATERIAL
KCA MATERIAL
PGC MATERIAL
PGS MATERIAL
PF MATERIAL
HO MATERIAL
TAILING SAND
Elevation(m)
340
320
300
280
260
Y - Coordinate
210
194
178
162
146
130
170
186
202
218
234
250
266
282
298
314
330
346
X - Coordinate

Figure 4.11: Soil stratigraphy used in the finite element analyses

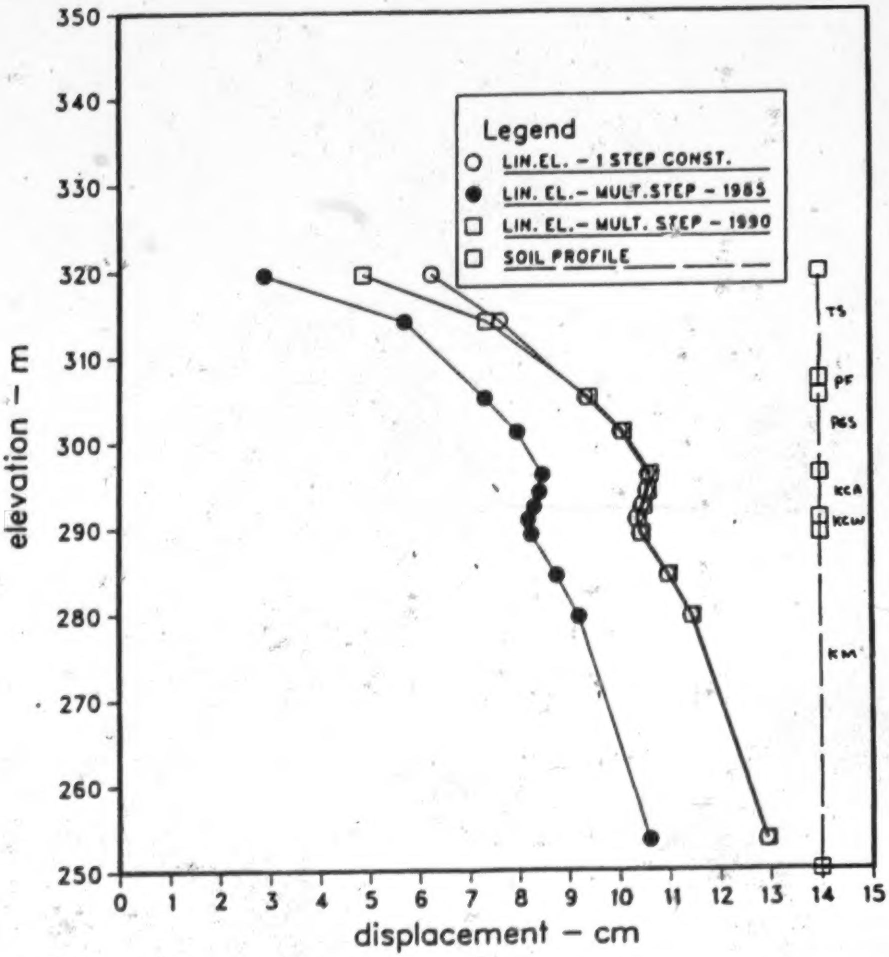

Figure 4.12: Horizontal displacements at SI842332(Berm 319) position for single and multiple steps - linear elastic analysis

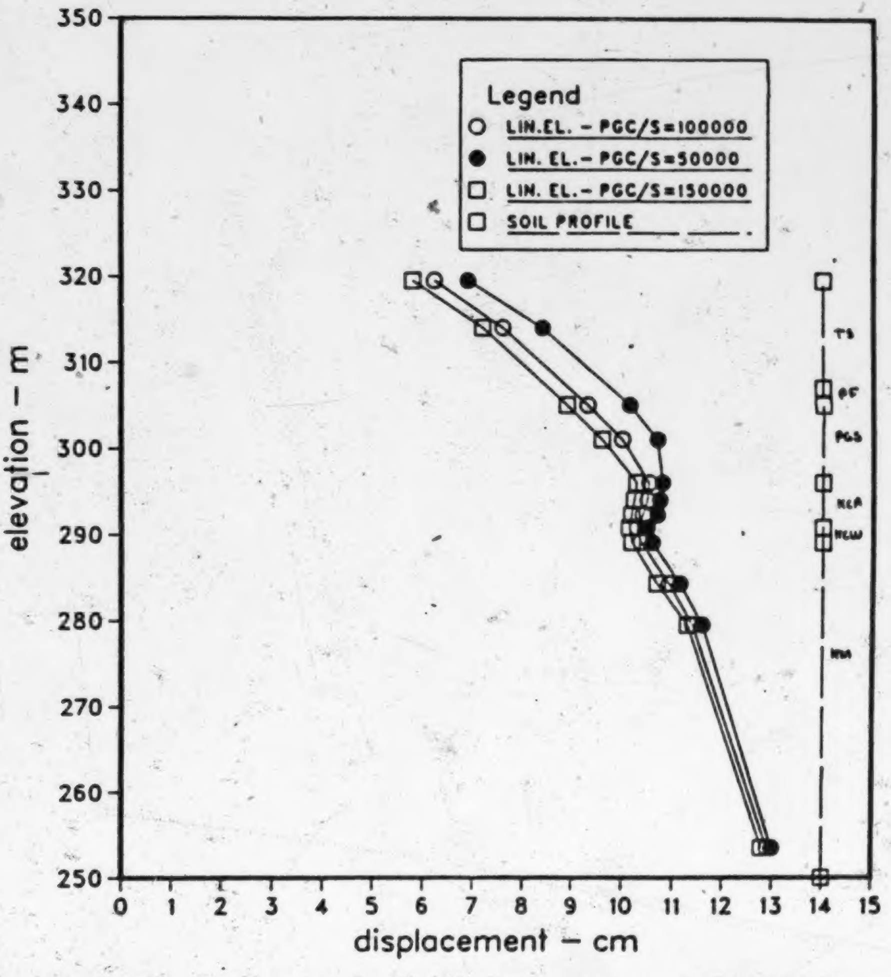

Figure 4.13: Horizontal displacements at SI842332(Berm 319) position for different elastic modulus for PGS and PGC materials

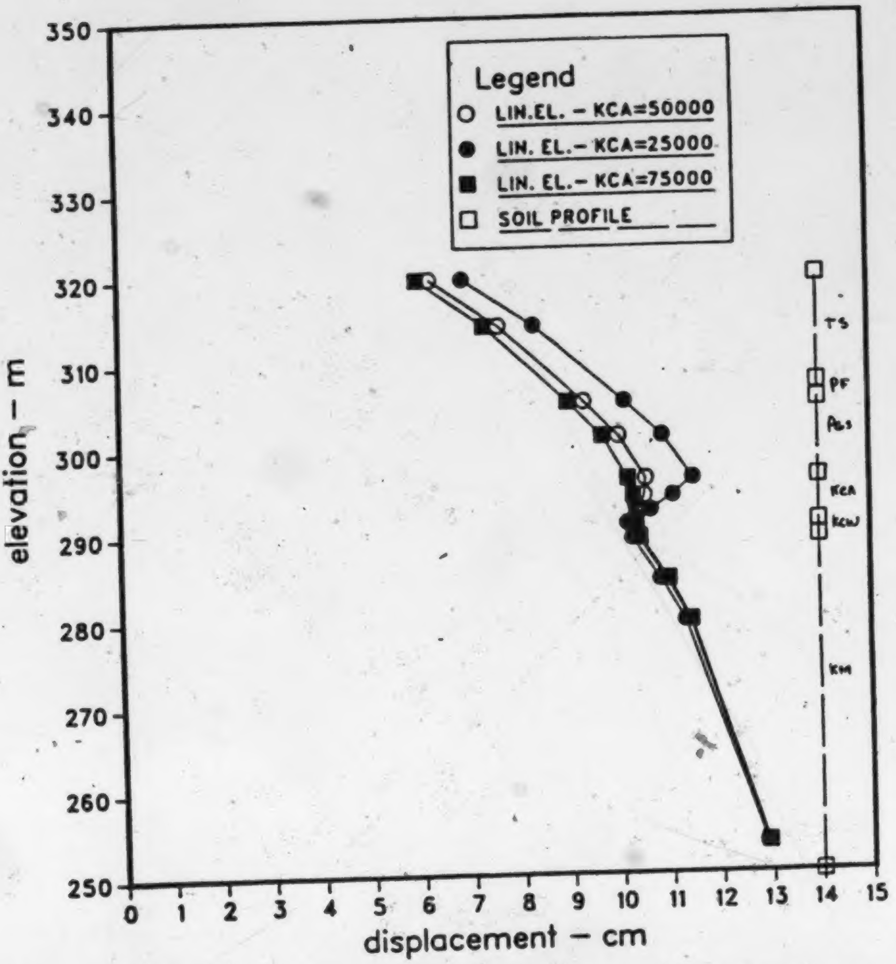

Figure 4.14: Horizontal displacements at SI842332(Berm 319) position for different elastic modulus for KCA material

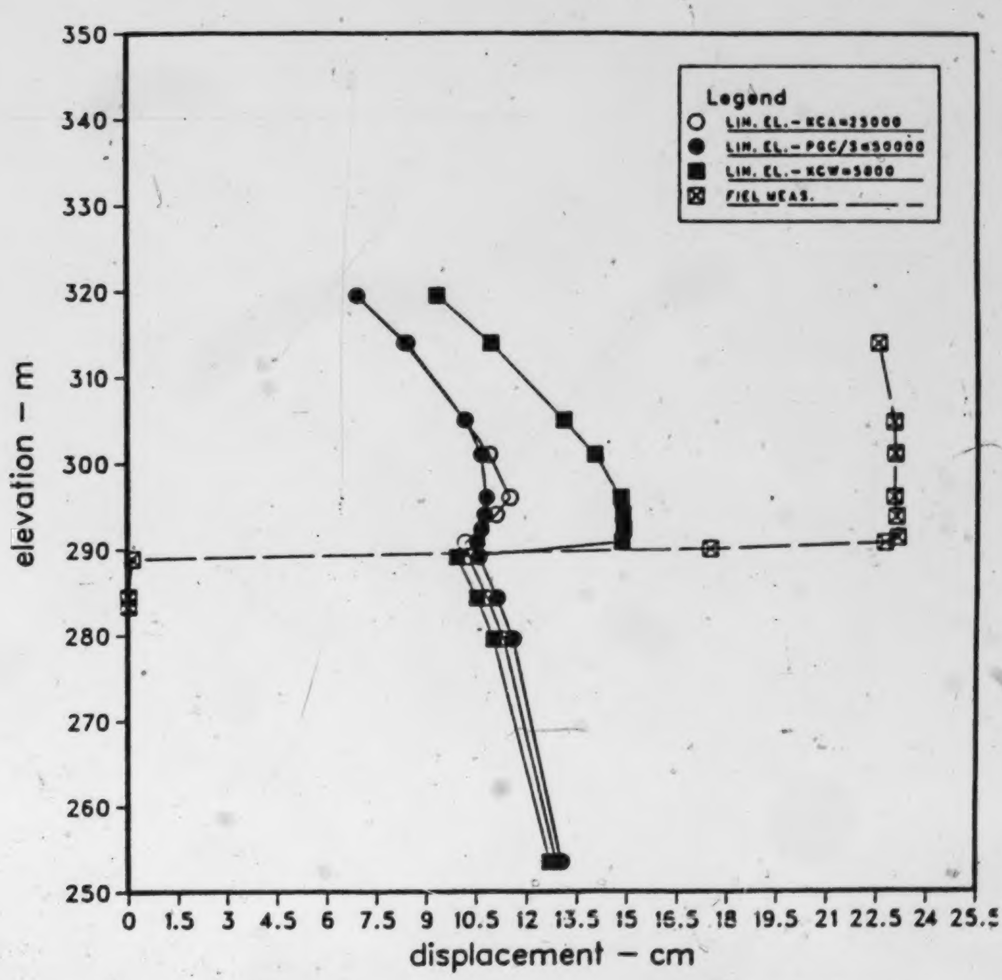

Figure 4.15: Comparison between measured and calculated Horizontal displacements at SI842332(Berm 319) position for reduced modulus for KCW material - linear elastic analysis

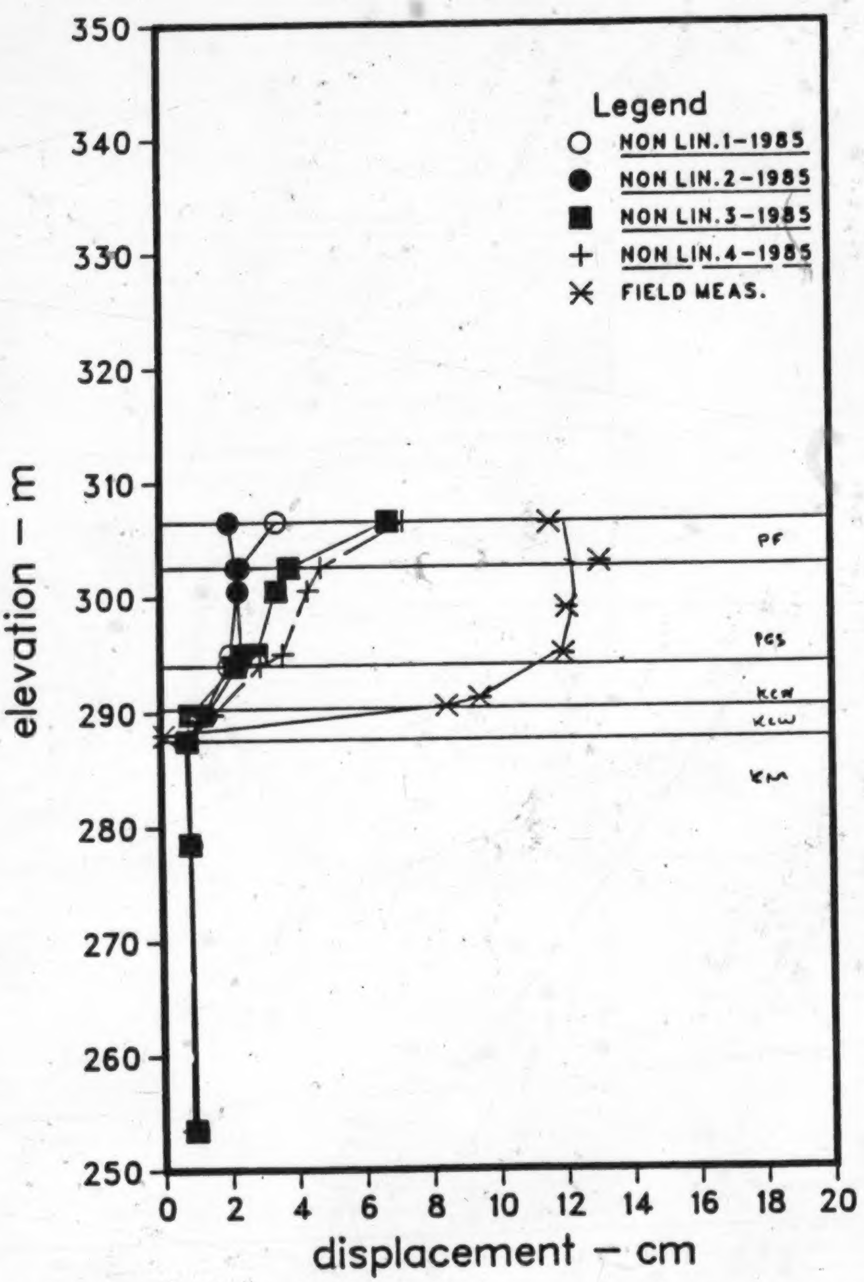

Figure 4.16: Comparison between measured and calculated Horizontal displacements at SI842334(Crest) position - non-linear total stress analysis

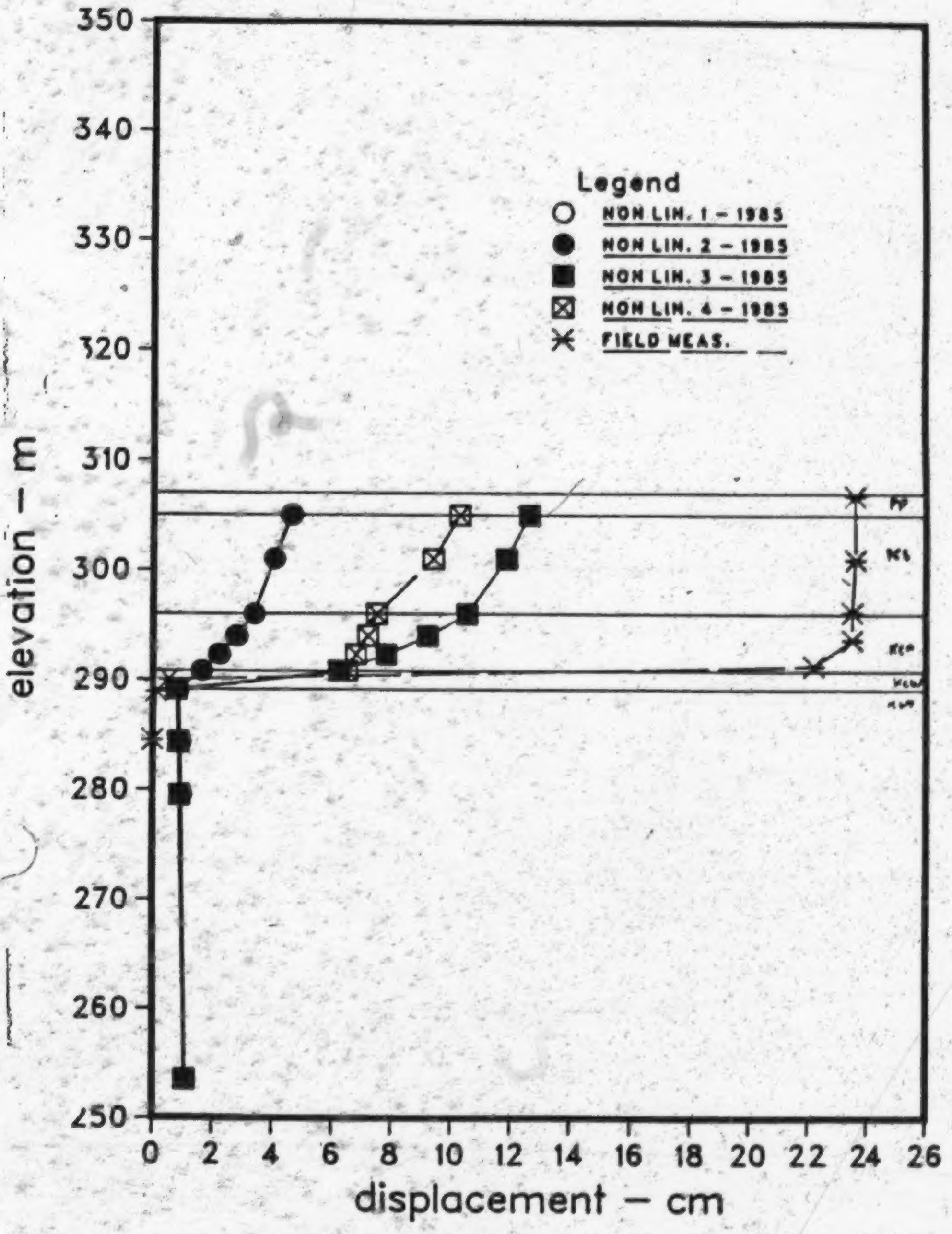

Figure 4.17: Comparison between measured and calculated Horizontal displacements at SI842332(Berm 319) position - non-linear total stress analysis

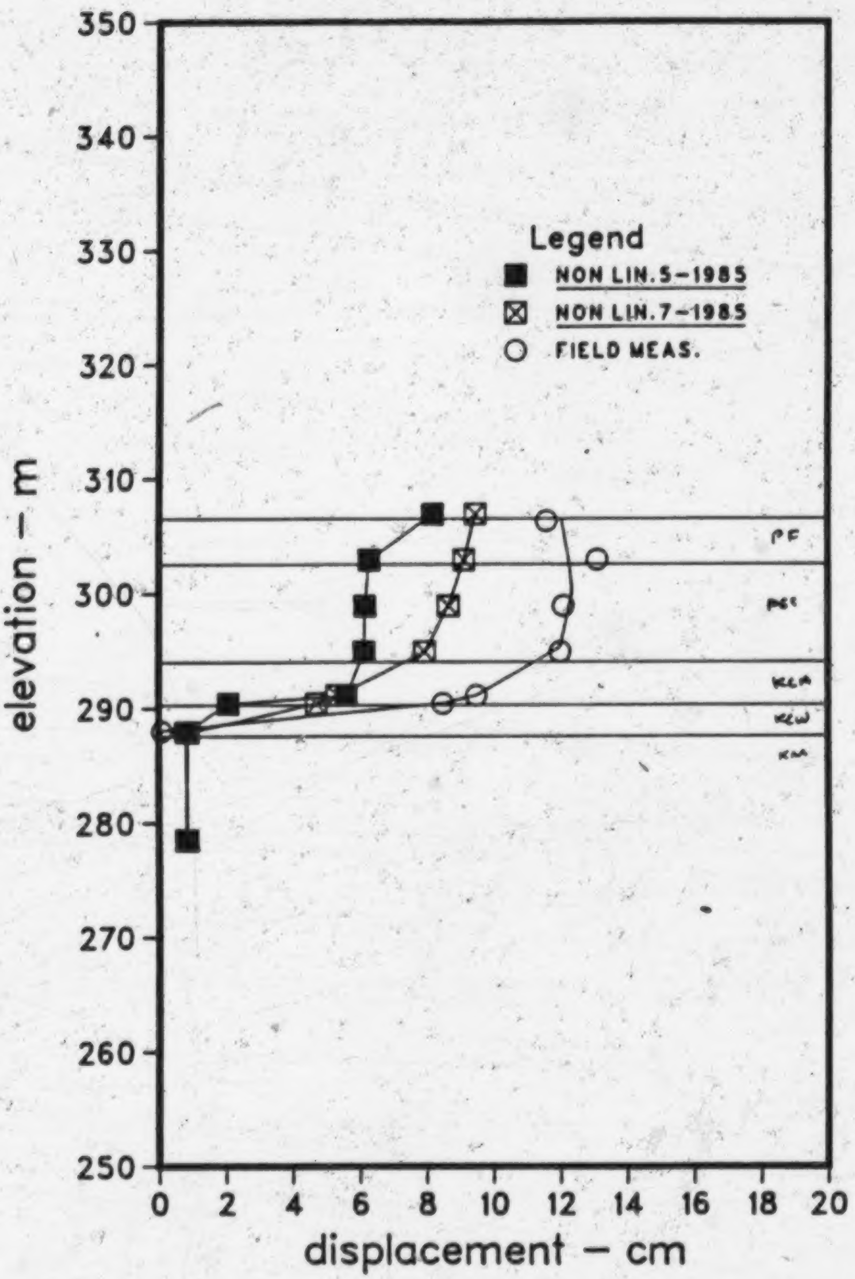

Figure 4.18: Comparison between measured and calculated Horizontal displacements at SI842334(Crest) position - non-linear total stress analysis

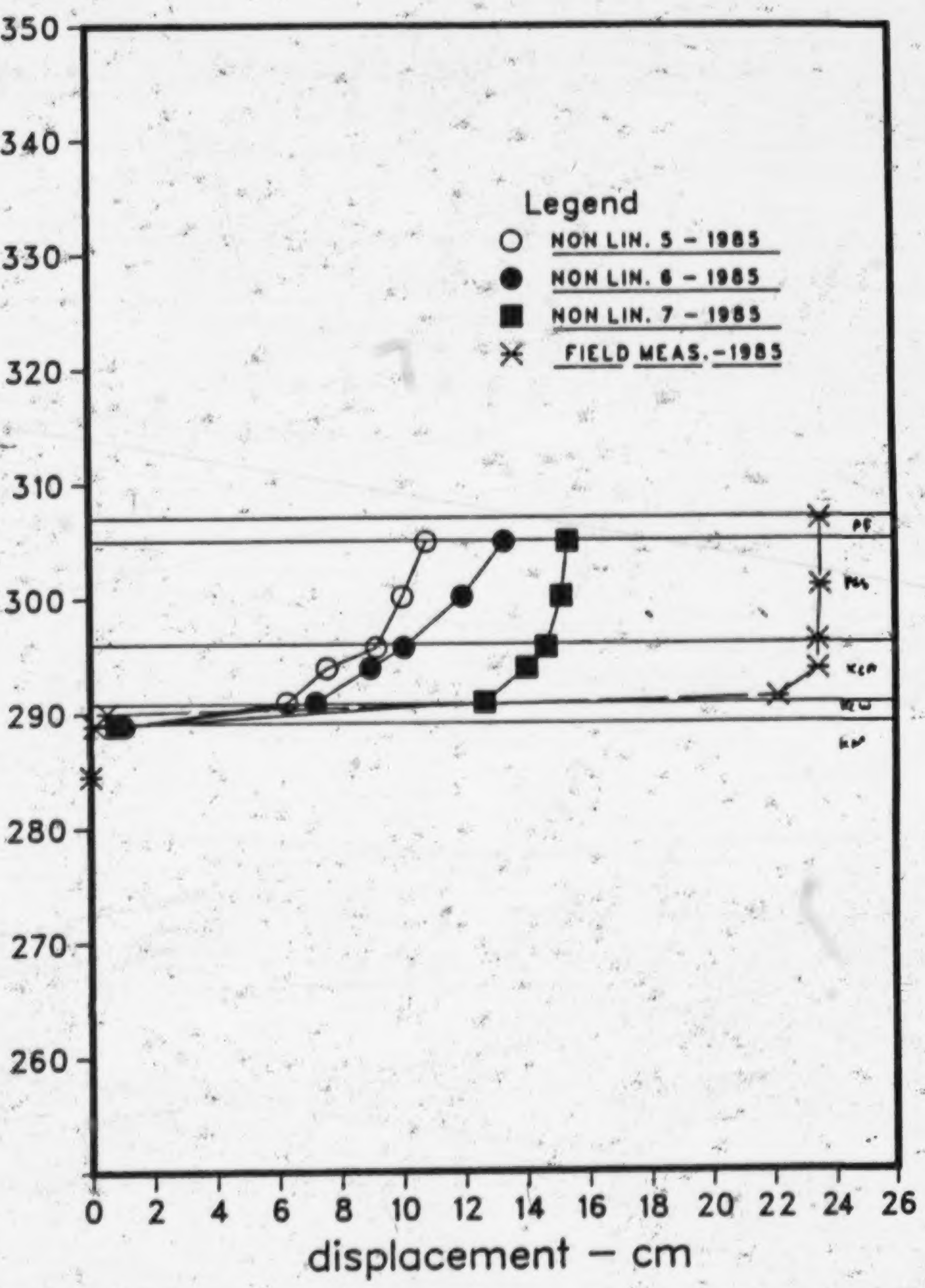

Figure 4.19: Comparison between measured and calculated Horizontal displacements at SI842332(Berm 319) position - non-linear total stress analysis

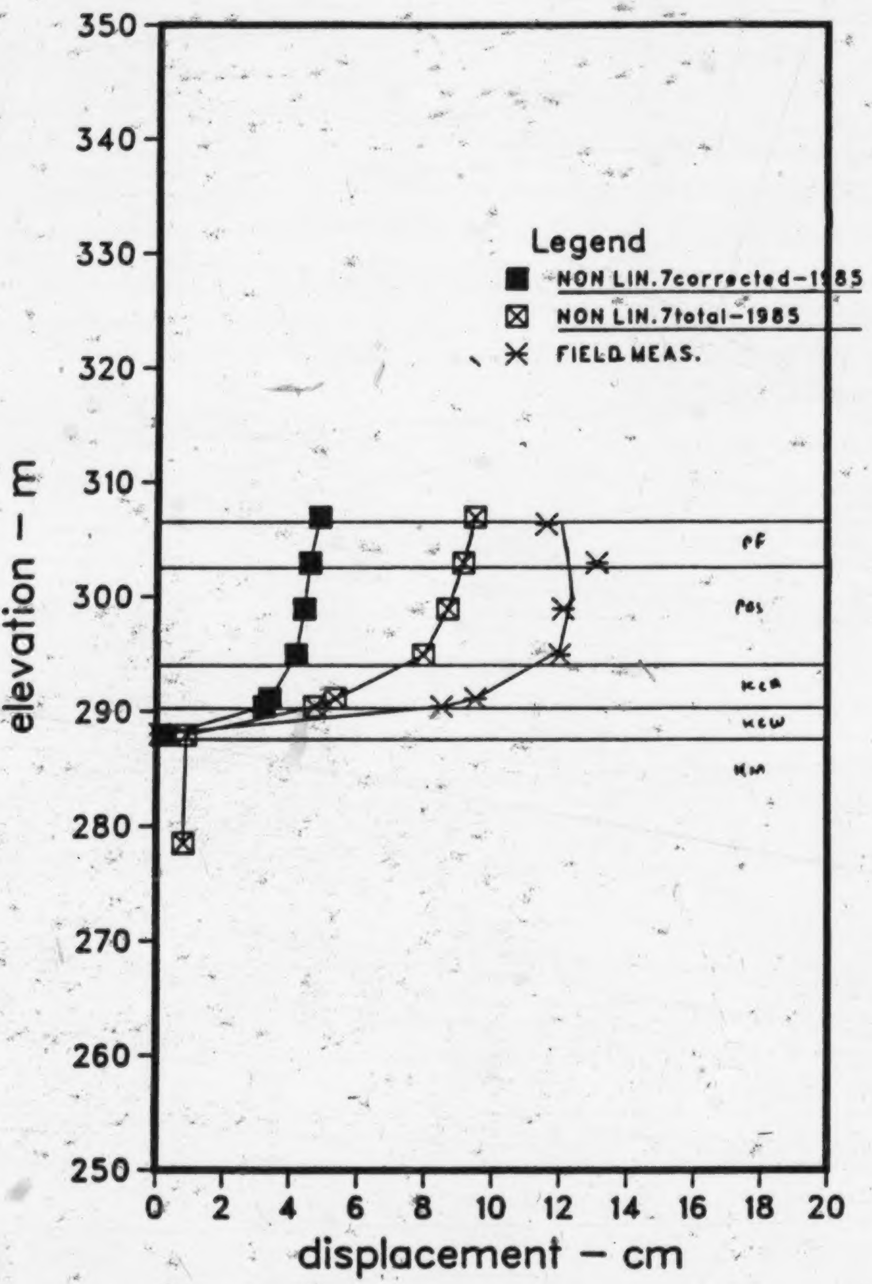

Figure 4.20: Comparison between measured and calculated Horizontal displacements at SI842334(Crest) position - non-linear total stress analysis

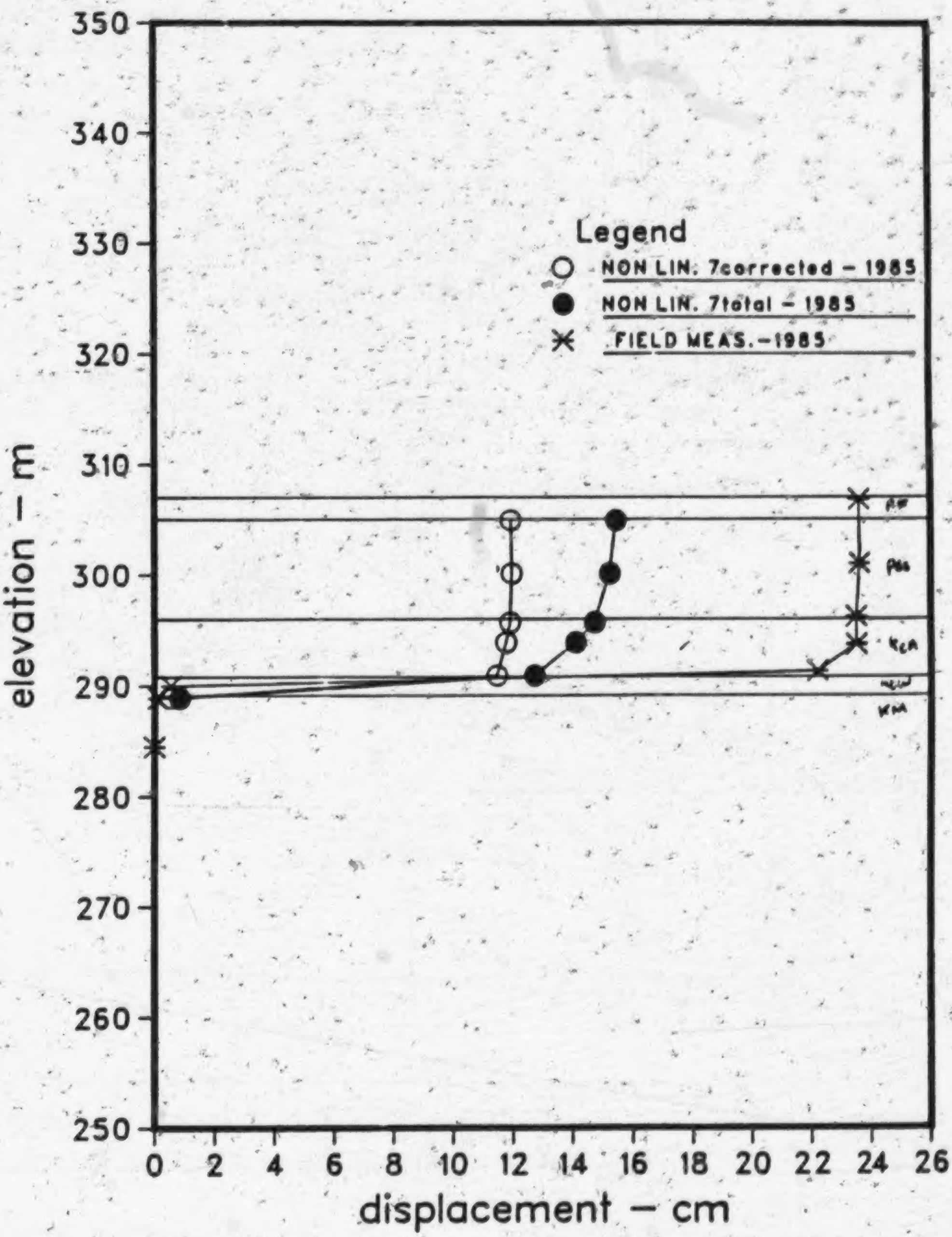

Figure 4.21: Comparison between measured and calculated Horizontal displacements at SI842332(Berm 319) position - non-linear total stress analysis

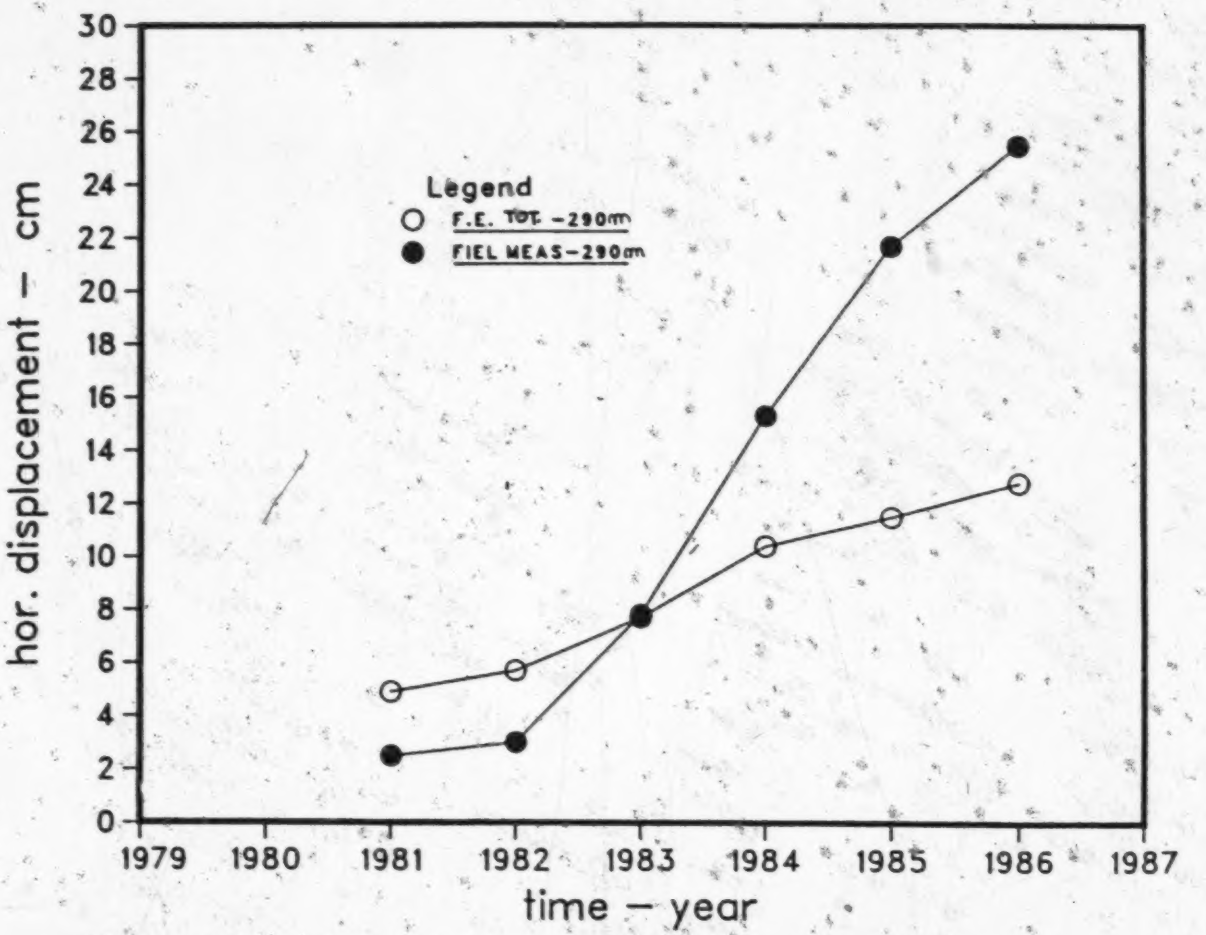

Figure 4.22: Comparison between measured and calculated horizontal displacements with time at SI842332(Berm 319) position(elevation 290m) - non-linear total stress analysis

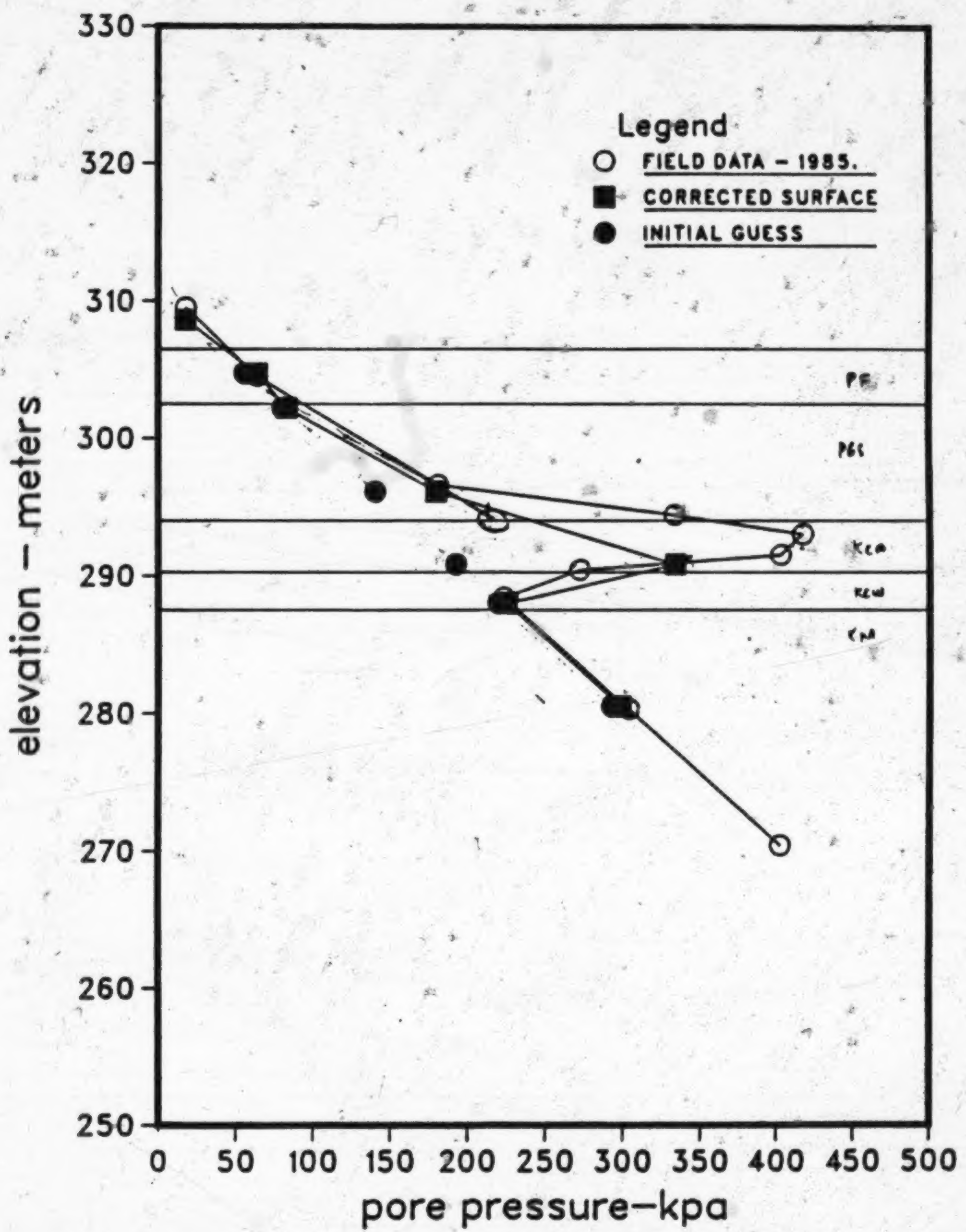

Figure 4.23: Comparison between measured and interpolated pore pressures at PN852307 position

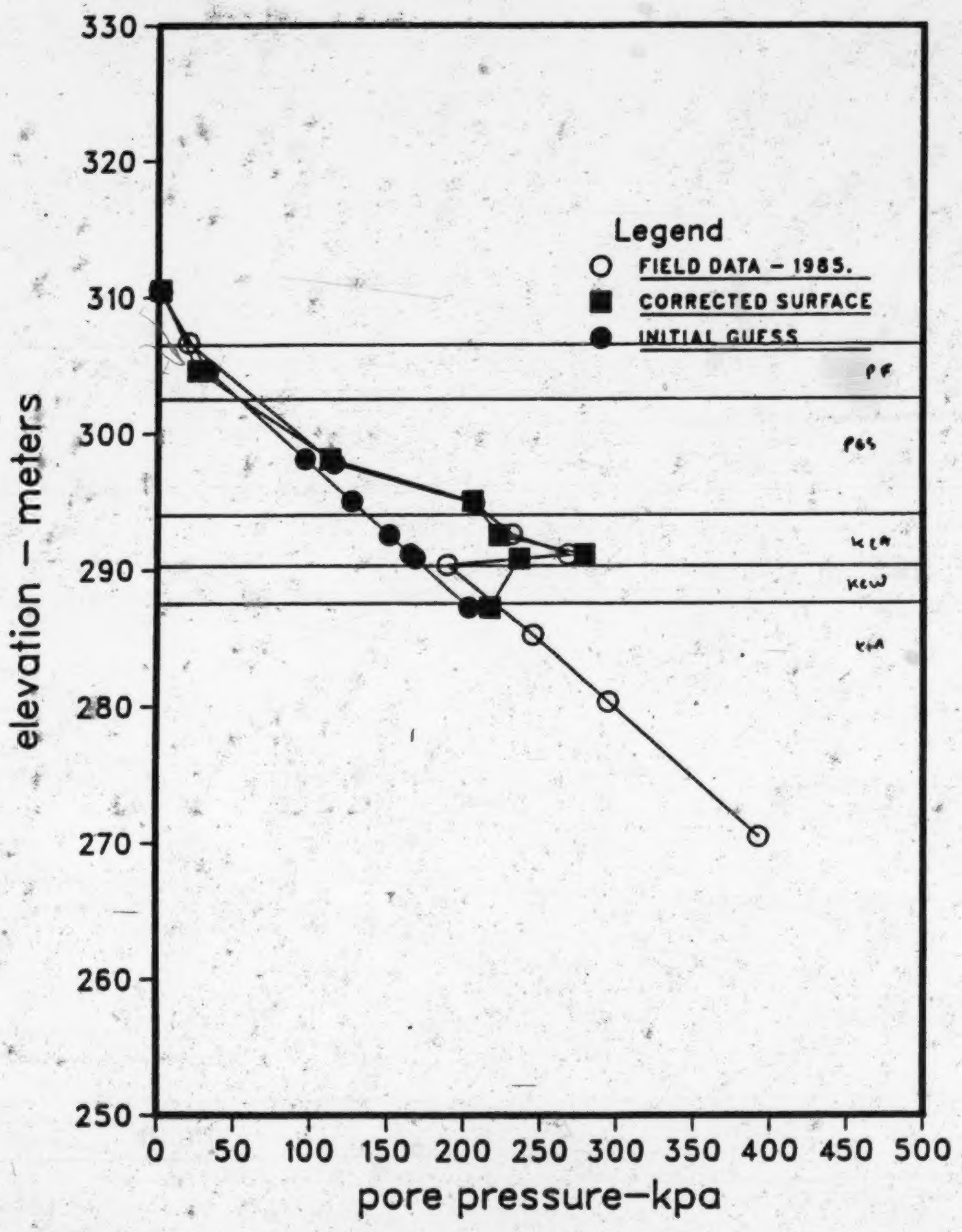

Figure 4.24: Comparison between measured and interpolated pore pressures at PN852311 position

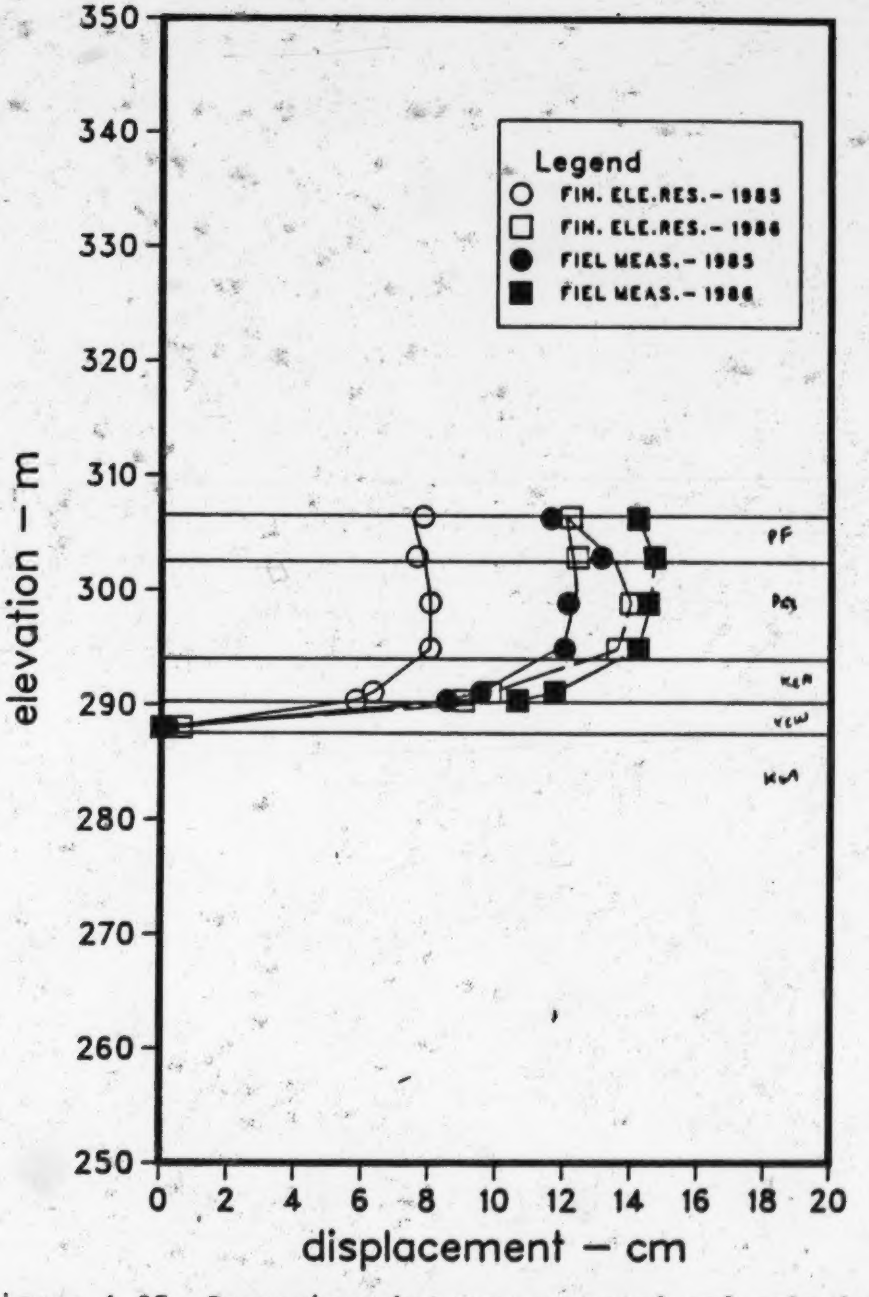

Figure 4.25: Comparison between measured and calculated Horizontal displacements at SI842334(Crest) position - non-linear effective stress analysis

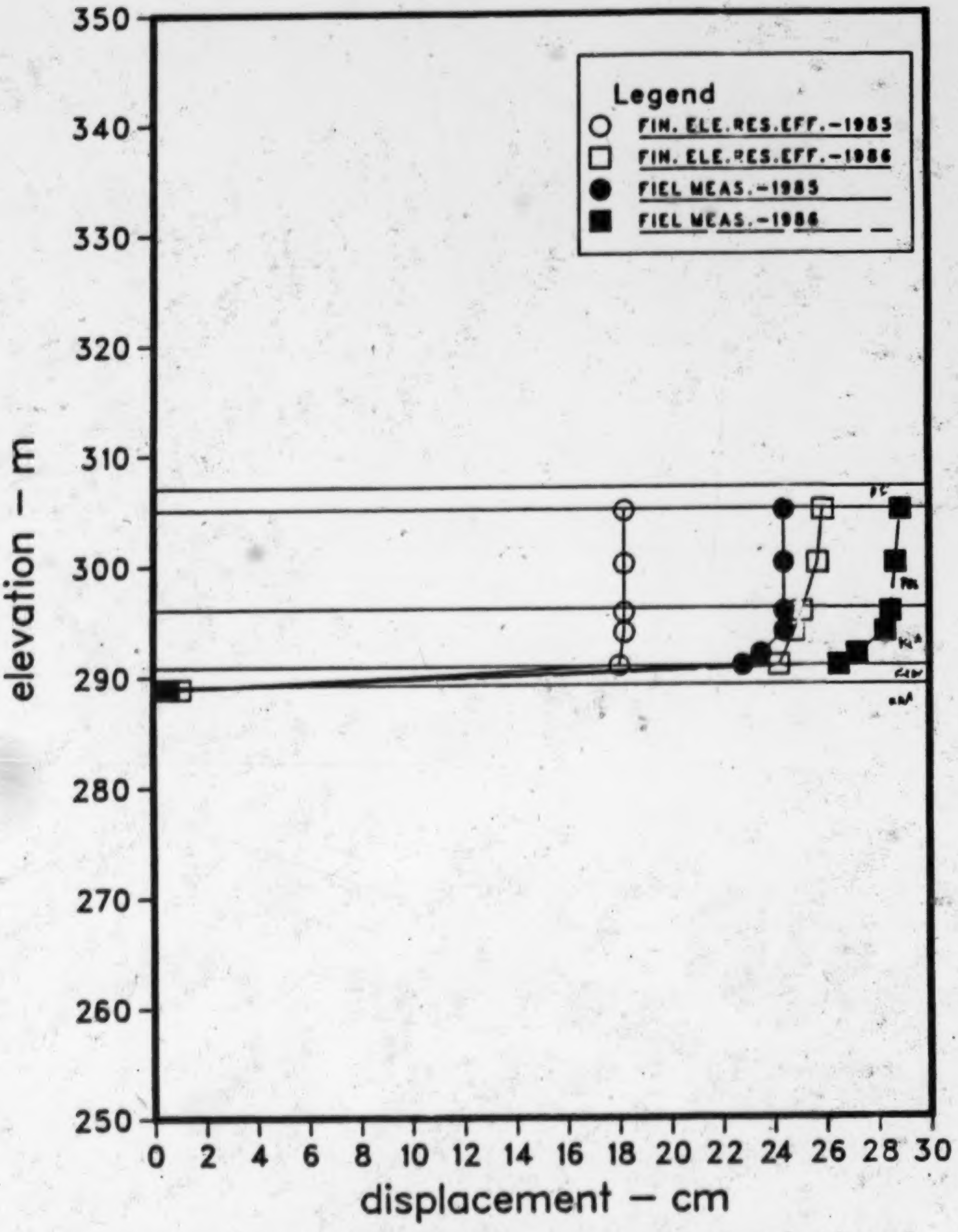

Figure 4.26: Comparison between measured and calculated Horizontal displacements at SI842332(Berm 319) position - non-linear effective stress analysis

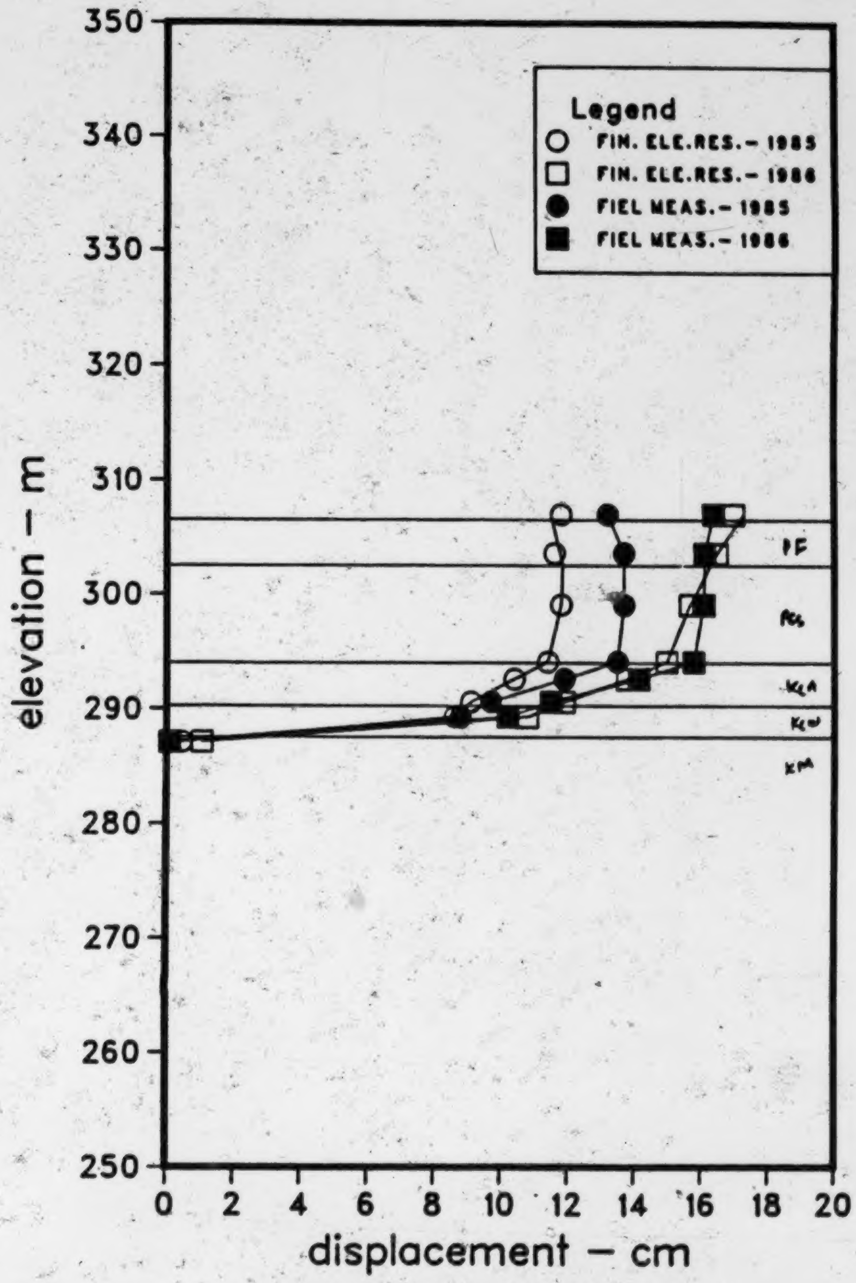

Figure 4.27: Comparison between measured and calculated Horizontal displacements at SI842337(Toe) position - non-linear effective stress analysis

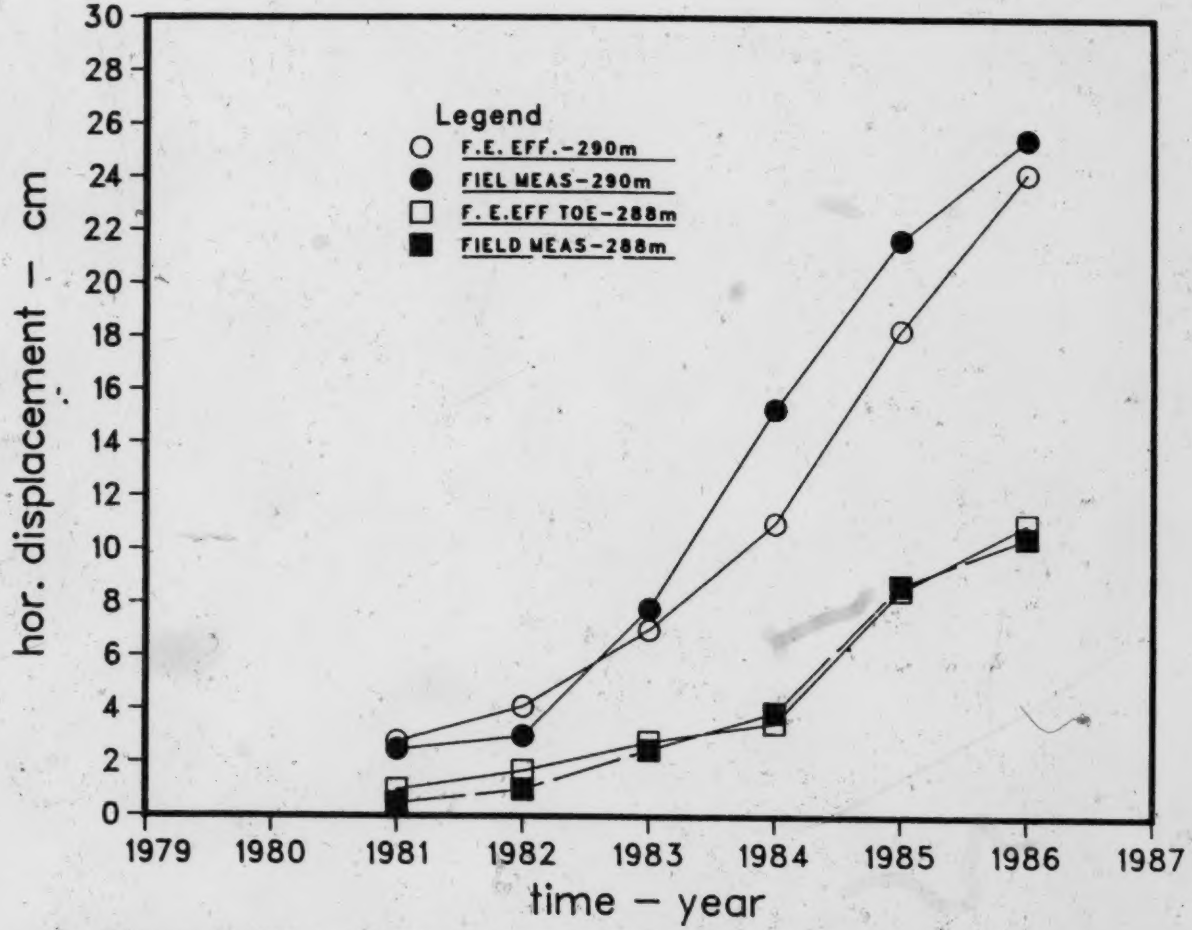

Figure 4.28:Comparison between measured and calculated horizontal displacements with time at SI842332(berm 319) and SI842337(toe) positions at elevation of Kca/Kcw contact - non-linear effective stress analysis

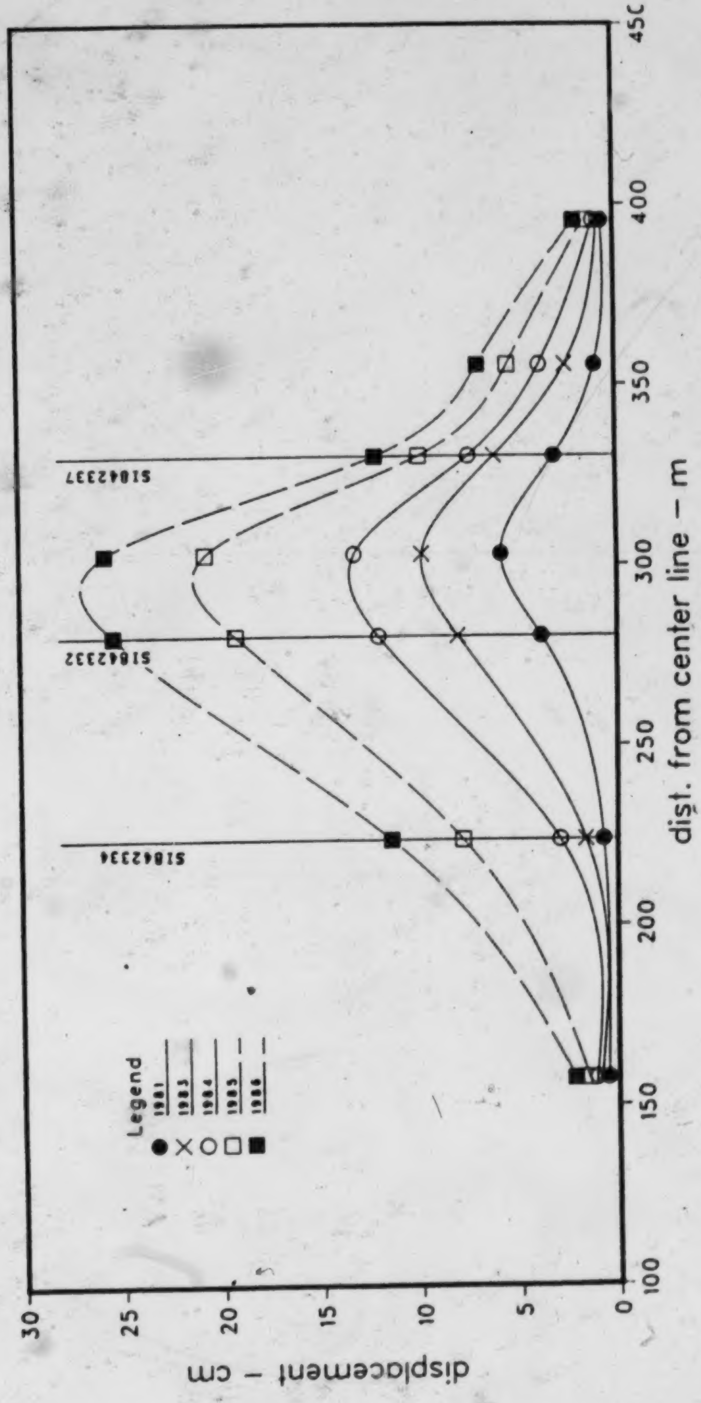

Figure 4.29: Calculated horizontal displacements along KCA/KCW contact non-linear effective stress analysis

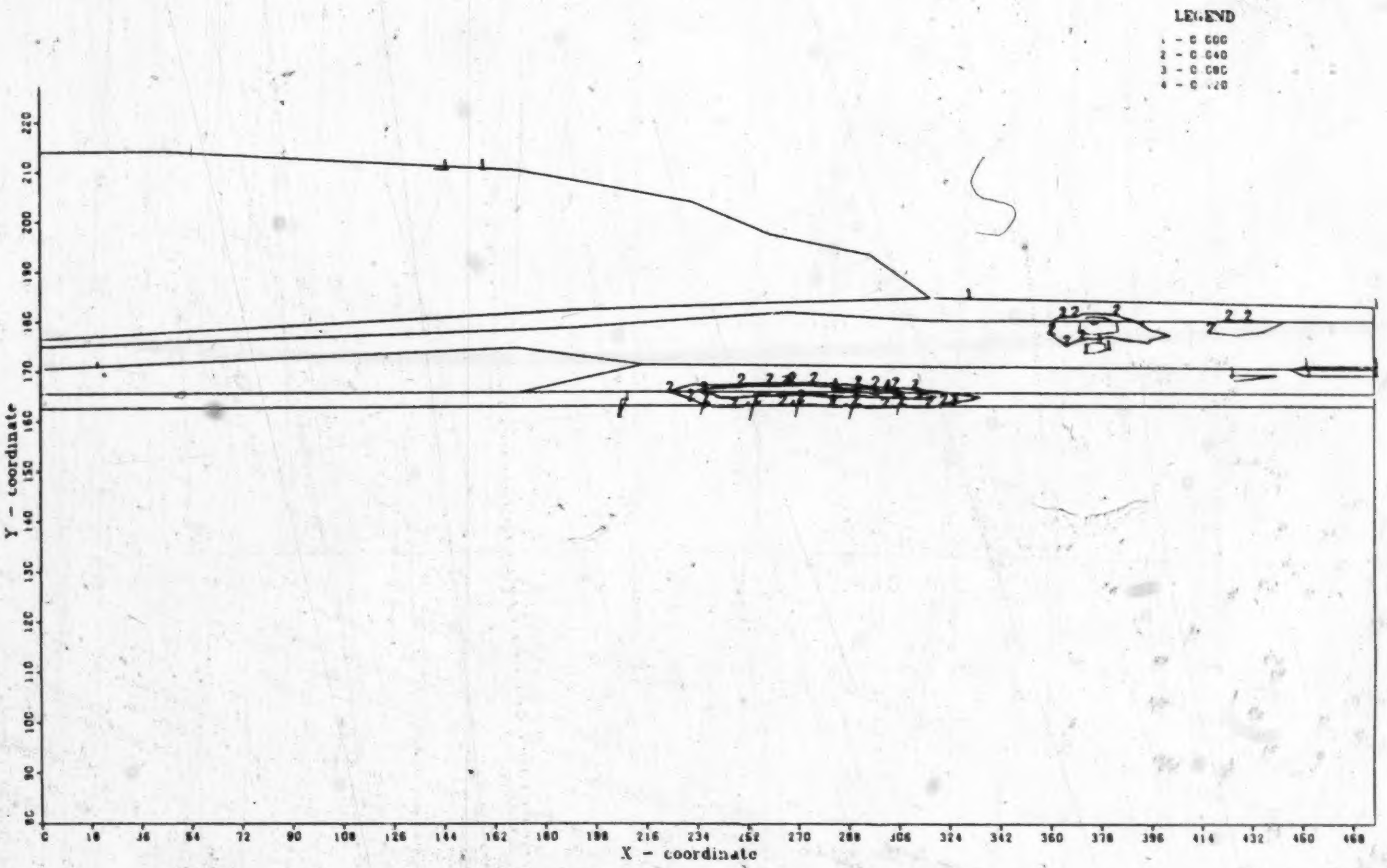

Figure 4.30: Contours of maximum shear strain - 1986

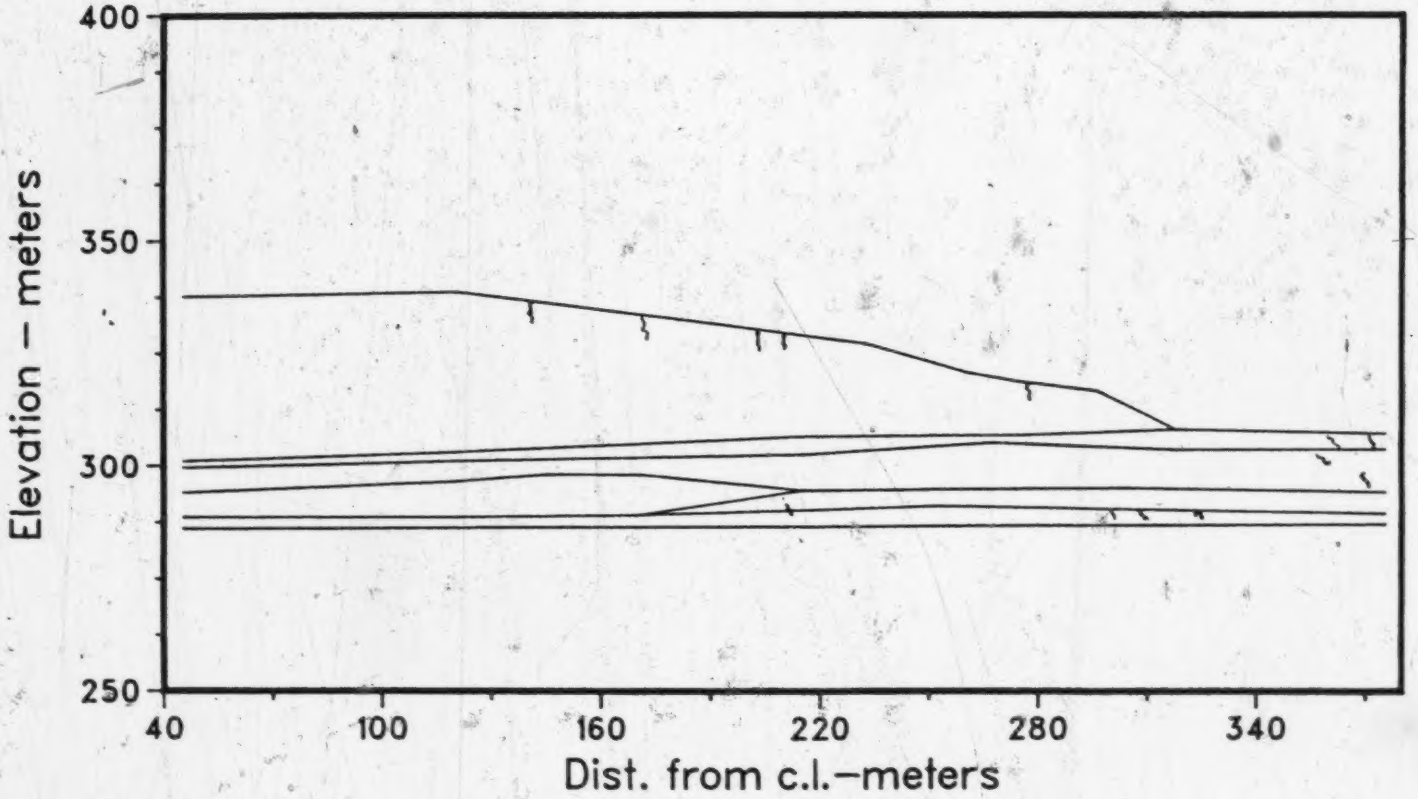

Figure 4.31: Schematic representation of the cracks - 1986

5. Parametric Analysis

5.1 Introduction

The occurrence of weak seams in the foundation of dams is fairly frequent.The term may refer to a thin layer of softer or weaker material existing within a relatively stronger material profile, or a discontinuity zone formed by a single or various presheared planes.

Stability evaluations using limit equilibrium methods often indicate the critical potential failure surface passing, at least in part, along these seams. In addition to the stability against failure, it is also important to evaluate and control the level of lateral deformation expected to occur in the foundation material, since,excessive movements in the foundation may have serious implications on the working conditions or even on the structural integrity of the facility.

In design practice, lateral deformations are often controlled in a completely empirical way, by the establishment of a minimum acceptable limit equilibrium analysis Factor of Safety, assuming that the higher the Factor of Safety the lower the deformation level. Since in many cases the Factor of Safety is controlled by the strength characteristics of the weak seam, such an assumption implicitly means that the deformations are also controlled by the same parameters.

In reality,however, the effect of the presence of seams on the deformability levels is a function not only of its strength characteristics, but depends very much on the geometry of the specific problem being analysed. An illustration of this is shown in figs.5.1 and 5.2.

In the case shown in fig.5.1 the lateral displacement along the weak seam cannot occur without sufficient straining of material 1. The same is not true in the case shown in fig.5.2, where the weak seam "daylights" downstream of the dam. In this situation, the lateral movements along the seam are not necessarily dependent on the deformation of the upper foundation layer.

The mechanisms involved in the two cases are different, as a consequence of this, the controlling factors are different. An alternative, then, to systematically study the problem of presence of seams in foundation materials is to identify the potential mechanisms of deformation and study them separately.

Previous published numerical analyses involving the existence of seams on dam foundations are performed in terms of total stresses and most of them are related to concrete dams. In general they focus on a specific case, in which the geometry and material parameters values are fixed, e.g. Mueller et. al.(1977), Souza Lima et. al.(1980), or the geometry is fixed but the parameters are varied in search for a combination that best reproduces field measurements, e.g. Morgenstern and Simmons(1982). In some cases geometry has been varied while values of the parameters are maintained constant, e.g. Sharma et. al.(1986).

A very limited amount of work has been published attempting to correlate limit equilibrium analyses Factors of Safety with deformation levels during earth dam contruction, and those which have been presented do not involve the foundation material, e.g., Rezendiz and Romo(1972), Walter and Duncan(1984).

The present work studies the mechanism of deformability of the foundation material in cases where an earth dam is constructed on a site containing a horizontal weak seam overlaid by a relatively stronger material, as shown in fig.5.1. It evaluates the relative significance of the position of the weak seam and the stiffness of the upper foundation material. Tentative correlations between Factors of Safety as calculated by a limit equilibrium method and lateral displacement levels in the foundation are indicated.

The analyses are carried out in terms of effective stresses, explicitly considering pore pressure as known quantities, which are introduced in the calculation using the procedure described in a previous Chapter.

5.2 Geometry

The geometry studied is shown in fig 5.3. Due to symmetry, only half of the dam was considered. Depth ratios (h_1/H) of 0.25, 0.5 and 0.75 were tested. A 45 meters high dam with slope of 3:1 was considered.

The crest was made wide enough so that the critical failure surfaces calculated based on limit equilibrium analyses did not cross the center line of the dam.

5.3 Embankment and Foundation Materials

In order to make the analysis more generic, it was decided to identify the materials involved and select strength and deformability parameter values which are within acceptable ranges for each material.

The materials composing this hypothetical stratigraphy, in fact, are often encountered on the deposits of western Canada. The material combination shown in fig.5.3 consists of:

a. Foundation material:

- Layer 1: Till
- Layer 2: Slickensided clay or clay shale
- Layer 3: Relatively stiffer bedrock (e.g. hard clay shale or sandstone)

b. Embankment material: compacted till.

The stratigraphy described resembles the ones found at the sites where Syncrude's Dyke (see Fair and Handford,1986) and Nipawin dam (see Matheson *et al.*,1987) are constructed.

5.3.1 Numerical modelling,deformability and strength parameters

5.3.1.1 Layer 1: Till

Till is a material of engineering significance in most of North America, Northern Europe and Asia. A large number of studies has been published about the geological formation of this kind of material(e.g. Boulton , 1972; Shaw,1977; Dreimanis,1976) and its geotechnical characteristics(e.g. Wittebolle,1983; Milligan,1976).

Terzaghi and Peck(1948) defined till as: "an unstratified glacial deposit of clay, silt, sand, gravel and boulders". This definition shows that a wide range of variability should be expected in the geotechnical characteristics of such material, which depend on the relative proportion of each component.

The selection of the stress-strain model and range of parameters will be based mainly on some of the data available involving tills existing in the Canadian west.

Results of laboratory tests on till, like those presented by Wittebolle(1983) and Sego and

Morgenstern(1986), indicate that the hyperbolic model as proposed by Duncan and Chang(1970) is a very reasonable way of modelling this material.

Such choice requires the definition of values for the following parameters:

-Strength parameters in terms of effective stress:

Table 5.1 summarizes some of the strength values presented in the literature. Based on the values shown, it seemed reasonable to assume c'_p=10Kpa and $\phi'_p=37^\circ$. The failure ratio R_f was assumed as 0.9.

-Deformability parameters

According to the hyperbolic model the initial modulus is expressed by:

$$E_i = K\,pa\,\left(\frac{\sigma'_3}{pa}\right)^n \qquad [5.1]$$

in which:

E_i = initial modulus

pa = atmospheric pressure

σ'_3 = minor effective principal stress

K = modulus number

n = modulus exponent

and the tangent modulus:

$$E_t = \left[1 - \frac{R_f(1 - \sin\phi')(\sigma'_1 - \sigma'_3)}{2c'\cos\phi' + 2\sigma'_3\sin\phi'} \right]^2 E_i \qquad [5.2]$$

in which

E_t = tangent modulus

R_f = failure ratio

ϕ' = friction angle of the material in terms of effective stress

σ'_1, σ'_3 = major and minor principal effective stresses, respectively

c' = effective cohesion intercept

It can be seen that the constant n indicates a degree of dependence of the initial modulus relatively to the confining stress. This parameter was assumed to be 0.2.

Table 5.2 presents some values of deformability modulus collected from various published works. The values were obtained under undrained conditions. On the table is indicated the equivalent drained modulus based on:

$$G_d = G_u \qquad [5.3]$$

in which

G_d = drained shear modulus

G_u = undrained shear modulus

The equation above may be rewritten as:

$$\frac{E_d}{2(1 + \mu_d)} = \frac{E_u}{2(1 + \mu_u)} \qquad [5.4]$$

that is

$$E_d = \frac{(1 + \mu_d)}{(1 + \mu_u)} E_u \qquad [5.5]$$

in which

E_d = drained elastic modulus

μ_d = drained poisson's ratio

E_u = undrained elastic modulus

μ_u = undrained poisson's ratio

The poisson's ratio under drained conditions was considered constant and equal to 0.4.The undrained value was assumed to be 0.50.

Table 5.2 shows a wide range of values. E_i=70,350 and 700Mpa seem a resonable selection, since they cover the range where most of the test results concentrates.

Values of total unit weight ranging from 21 to 24Kn/m^3 have been reported in the literature. A total unit weight of 22Kn/m^3 was assumed. The values of parameter K selected were 700, 3500, 7000.

Considering the values chosen for n, K and total unit weight , and an initial hydrostatic pore pressure condition, the initial modulus can be calculated as a function of the effective confining stress . The values shown in table 5.3 correspond to the initial modulus at the center of the upper foundation layer for each weak seam position. It can be observed that they approximate the values of 70, 350 and 700Mpa mentioned above.

The stress-strain curves using the parameters selected are shown in fig.5.4, for a confining effective stress level correspondent to a depth of 15 meters. The variation of the initial modulus with depth is shown in fig.5.5.

5.3.1.2 Layer 2: Slickensided clay seam

In the present work, the term slickensided clay seam must be understood as a thin layer consisting of clay or clay shale material, or a transition zone around the contact between the till and the clay shale, which has been pre-sheared due to some past deformational process like glacial shove, landsliding or valley rebound. The slickensides are assumed to form a continuous plane or number of planes along the entire seam length. This kind of occurrence is fairly common.

A linear elastic-perfectly plastic stress-strain model using the Mohr-Coulomb yield criterion and residual strength parameters were used for this material, since it has been observed (see Matheson-1972) that in these situations relatively small displacements longitudinally to the seam orientation are sufficient to reduce the strength parameters to residual level.

Table 5.4 presents some values of deformability and residual strength parameters reported in the literature. Based on the ranges presented, values of E_d=50Mpa, c'_r=0 and ϕ'_r= 10° were assumed as representative of this material. Poisson's ratio under drained conditions equal to 0.4 and total unit weight of 21Kn/m^3 were considered.

5.3.1.3 Layer 3: Bedrock

In the present work, this material is considered to be significantly stiffer than the other materials. It was represented as linear elastic. Values of E=2000Mpa and μ=0.3 were assumed. These values are within the acceptable range for sandstones and hard clayshales.

5.3.1.4 Embankment material: compacted till

Various references can be found in the geotechnical literature reporting the use of compacted till as embankment material. In this work it was assumed to behave according to the hyperbolic stress-strain model. Table 5 shows some of the published data on compacted till. The values indicate that c'=10Kpa and ϕ'=37° are representative parameters for this material. For the other constants required, the values used were: K=800; n=0.20; R_f=0.87

5.4 Pore pressures

The initial pore pressure condition and subsequent induced variations are very much dependent on the local geology as well as on the stress history and certain material characteristics like permeability and compressibility of the strata involved.

In the present analysis the initial pore pressure condition was considered as hydrostatic with the water level at the ground surface. The increase of pore pressure due to the dam construction was introduced by the use of the pore pressure ratio ru, defined as:

$$ru = \frac{\Delta u}{\gamma \ \Delta h} \qquad [5.6]$$

Where Δu is the increase in pore pressure , γ is the unit weight of the dam material and Δh is the increase in height of the dam above the point being considered.

The value of ru for the foundation materials was considered 0.2 and for the dam material 0.3.The piezometric level for the foundation material after the completion of the dam is shown in fig.5.6.

No pore pressures were considered to exist within the dam, close to the face of the slope, as indicated in fig.5.6, simulating the effect of horizontal drains in that region.

The parametric analysis is composed of 9 cases. A summary of the values of material parameters used is presented in table 5.6.

5.5 Limit equilibrium analysis

Stability analysis considering only the embankment was performed using simplified Bishop's method. The minimum Factor of Safety was found to be 1.81.

Morgenstern and Price's method was used for the stability analysis involving the embankment and foundation materials. The variation of the minimum Factor of Safety with the depth of the weak layer is almost linear, as shown in fig.5.7. The deeper the weak layer, the higher the critical Factor of Safety.

The critical failure surfaces calculated are shown in figs. 5.8 to 5.10. In each of these figures two surfaces are presented. One refers to the analysis of the embankment only and the other to the analysis of the embankment and foundation. It is seen that as the weak seam gets deeper the critical surface plane which intersects the dam crest gets closer to the center line of the dam and the plane which intersects the original ground surface gets farther from the toe.

5.6 Finite element analysis

The meshes used in the analyses are shown in fig. 5.11 to 5.13. They are formed by quadrilateral and triangular isoparametric elements of 8 and 6 nodes respectively. The number of elements varies from 305 in the smallest mesh to 381 in the largest, and the number of nodes from 962 to 1192. The element stiffness was integrated using a 3x3 Gaussian integration scheme for the 8 node elements and 2x2 for the 6 node elements.

The analyses were performed in terms of effective stresses. The material models selected have already been discussed and the parameters used are shown in table 5.6.

The load was applied incrementally. The initial state of stress (before the dam construction) was imposed by the use of linear elastic "switch-on-gravity" technique, in order to generate a stress field correspondent to a soil profile with K_o=0.82 and hydrostatic pore pressure distribution with the water level at the ground surface. The linear elastic modulus for the till at this stage has approximately the same value as the initial modulus calculated according to the hyperbolic model considering the effective confining stress level at the center of the layer.

The dam construction was divided into 10 load steps, each step being divided in 5 load subincrements. The total load was, therefore, imposed in fifty load increments. At each load step, the pore pressures were introduced as known quantities using the procedure previously described.

Each embankment layer was initially placed as a linear elastic material, with a low deformation modulus. When the overlying layer was placed in the subsequent load step, it was, then, transformed into hyperbolic material. The low value for the modulus during placement was used for reducing the shear stress level at the time of the change from linear elastic to hyperbolic.

For the foundation materials, the eventual tensile stresses were handled by the use of the cracking model described in a previous Chapter. In the embankment material, tensile stresses were expected to occur in the regions close to the upper part free boundaries of the dam. Although this fact would not interfere significantly in the interpretation of the results, numerical convergence might be upset by the formation of cracks in such regions.Therefore, for the embankment material a high tensile resistance was considered as shown in table 5.6.

5.7 Presentation and Interpretation of the results

5.7.1 Lateral displacements

5.7.1.1 Foundation displacements

The horizontal displacements of the foundation and embankment along four distinct vertical sections are shown in figs 5.14 to 5.16 for the depth ratios (h_1/H) 0.75,0.50 and 0.25, respectively.

Considering the same depth of the weak seam, see for example fig. 5.14, the softer the foundation till the larger the lateral displacement occurring in the foundation , even though the Factor of Safety based on limit equilibrim methods is the same independent of the foundation stiffness. This shows that the foundation displacements are not controlled mainly by the strength parameters along the weak seam, but by the stiffness of the till above it.

This fact means that the assessment of displacement levels through limit equilibrium analysis for this kind of mechanism must involve the stiffness of the foundation layer above the weak layer or plane.

The understanding of such a mechanism is very important in practice, since it indicates, contrary to what is generally thought, that a high value of limit equilibrium Factor of Safety does not ensure small displacement levels. This can be observed by comparing, for example, the foundation displacements for the case where the depth of the weak seam is 22.50m, i.e. $(h_l/H)=0.5$ and $K_{till}=7000$, to the one where the depth is 33.75m, i.e. $(h_l/H)=0.75$ and $K_{till}=700$. In the first case the Factor of Safety based on limit equilibrium analysis is 1.51 and in the second 1.82. These numbers alone might suggest that the displacements associated with the lower Factor of Safety should be expected to be higher than those associated to the higher Factor of Safety. In this case, the opposite occurs, as shown in fig.5.17. As the stiffness of the foundation till in the case of the lower Factor of Safety is much higher than in the other, the foundation lateral displacements are smaller.

Results presented by the analysis in which the weak seam is 11.25m deep(depth ratio=0.25) and $K_{till}=700$ were disregarded because a large number of cracks appeared in the zone of the clay shale layer where the displacements were higher (between a vertical section through the middle of the slope and the toe). The cracks were oriented approximately 30° clockwise from the horizontal and started when the fourth layer was placed ,increasing significantly during subsequent stages.

According to the cracking model used, when the minor principal stress becomes tensile, a crack is formed perpendicular to the direction of that principal stress and the stiffness in that orientation is set to zero. The material is still capable of sustaining stresses in other orientations according to an orthotropic linear elastic stress-strain relationship. Linear elasticity was used in such circumstances because it was not expected for the cases studied in the present work that the mechanism being analysed at some point would become controlled by tensile regions.

In the case of $(h_1/H)=0.25$ with $K_{till}=700$ this seems to have happened.The large number of cracks in the clay shale controlled the deformation mechanism of the foundation material, causing an unrealistic reduction of the displacements. This can be observed in fig.5.16, where the lateral displacements in the region where the cracks appeared, mentioned above, are reduced to values even lower that those obtained with $K_{till}=3500$, which is contrary to the results obtained in all other cases. The model used is not appropriate for this specific case ,and therefore, the results obtained will not be used in the present interpretation.

With respect to the other cases, considering the same stiffness for the foundation till, the shallower the weak seam, the larger the displacement along the contact till/clay shale, as shown in fig.5.18 and fig.5.19 for $K_{till}=7000$ and 3500, respectively. It is noted in these figures that the location of the region of largest displacements is not significantly affected by the depth of the weak layer.

In order to verify if the stiffness of the dam within a relatively wide range would significantly influence the foundation displacements a case was analysed in which the weak seam was 33.75m deep , i.e. $(h_1/H)=0.75$, $K_{till}=700$ and $K_{dam}=4000$, that is, five times the original dam stiffness. The results shown in fig. 5.20 indicate that the foundation displacements were reduced, but not very significantly (around 10%).

5.7.1.2 Correlation between Factor of Safety and Foundation displacement

The limit equilibrium analysis Factor of Safety is a measure of strength mobilization along a certain surface.It reflects, therefore, a stress level. If it is wanted to relate stress level to displacements it is necessary to take into consideration the deformability characteristics of the material controlling the deformation mechanism, which, in the cases being analysed is the upper foundation till.

It has been shown in fig.5.7 that the Factor of Safety is a function of the depth of the weak seam, considering all other conditions are maintained constants,i.e,dam height and slope, pore pressure and strength parameters.

It has also been observed that for a certain depth of the weak seam, considering the same geometry, pore pressure distribution and strength parameters, the horizontal foundation displacements are a function of the stiffness of the foundation till layer.

Plotting the depth ratio (h_1/H) against the following dimensionless factor :

$$\Pi = \frac{U\ E}{H^2\ \gamma} \qquad [5.7]$$

in which,

U = largest lateral displacement along the till/clay shale contact

E = average initial modulus for the till

H = height of the dam

γ = total unit weight of the embankment material

fig.5.21 is obtained. It shows that considering the same stiffness and dam geometry, as the depth ratio(h_1/H) increases the lateral displacement level in the foundation decreases. It seems that for large values of the ratio depth ratio the factor Π tends to a constant value, indicating that after a certain value the depth ratio does not influence significantly the lateral displacements in the foundation. It is noted that for a specific depth ratio there is a certain range of values depending on the stiffness of the till. Fig. 5.21 and fig. 5.7 show that the Factor of Safety may be indirectly correlated with the foundation horizontal displacements through the depth ratio and by the use of the dimensionless factor Π, which involves information about the stiffness of the upper foundation material(E) and about the load level imposed on that material ($H\gamma$).

The major purpose of this analysis is to determine the key factor controlling the lateral deformation mechanism in the kind of problem studied, which has been found to be the stiffness of the foundation layer above the horizontal weak seam, and show how the Factor of Safety as calculated by limit equilibrium methods may be correlated with the lateral displacements in the foundation.

It is not intended to produce design charts, although such charts could be produced by performing similar analysis for different conditions. The usefulness of such charts would be limited since recent advances in computer sciences have been rapidly reducing computer processing time and costs. Therefore, the numerical analysis of specific cases has become increasingly faster and less expensive.

5.7.1.3 Horizontal displacement within the embankment

The displacement levels calculated in the embankment material overestimate the expected level in a real case with the same material parameters ,geometry and average ru value. This overestimation is due to the fact that a constant ru value of 0.3 was used for all the embankment material, except for the narrow area close to the edge of the slope, where drains were assumed to be placed.

In reality, the pore pressure ratio ru would not be uniform throughout the embankment. The material in the shoulder of the dam would have, in fact, a lower ru level than the material under the crest and far from the drains.

To show the effect of the pore pressure level within the shoulder region in the displacement level, an analysis was performed for the case of depth ratio $(h_1/H)=0.75$ and $K_{till}=7000$ in which the ru for the shoulder material was reduced to 0.1 and ru for the material under the crest maintained as 0.3. The results are presented in fig.5.22. It can be observed that the reduction in the displacements whithin the dam is quite significant, even though,in the foundation, neglegible difference is noticed compared to the case where an uniform ru value was used for the entire dam.

The displacements within the dam are reasonably sensitive to the stiffness of the embankment material.

Fig 5.20 shows that an increase of five times in the stiffness parameter K of soil composing the dam caused significant reduction in the displacement level within the embankment.

Although, as discussed previously, the stiffness of the dam did not have a very significant effect on the foundation displacements, the reverse is not true. The foundation stiffness significantly influenced the level of displacements within the embankment, as is shown,for example, in fig.5.14. Considering the same depth ratio (h_1/H), the larger the foundation displacements, i.e. the softer the foundation till, the larger the embankment displacements. Considering the same foundation stiffness, the shallower the weak seam position, the larger is the foundation displacement level and consequently the larger are the embankment displacements.

It must be noticed that neither the variation of the embankment material stiffness nor the foundation stiffness or foundation geometry would cause any variation of the Factor of Safety calculated for the embankment alone using limit equilibrium analysis. However, it has been shown that they affected in a significant way the level of displacement within the embankment. Therefore, any attempt to correlate the Factor of Safety calculated for the embankment material with displacements needs to take into consideration not only the stiffness of that material but also the foundation characteristics.

5.7.2 Shear strains

The contours of maximum shear strains are plotted in figs. 5.23 to 5.25 for the case of $(h_1/H)=0.75$, in figs.5.26 to 5.28 for $(h_1/H)=0.50$ and in figs.5.29 to 5.30 for $(h_1/H)=0.25$. Also shown in each figure is the position of the critical failure surfaces calculated by the limit equilibrium analyses as discussed previously.

The contours show quite evidently two different deformation mechanisms occurring. One corresponds to the deformation within the dam, which forms a relatively narrow band of higher distortion with the highest values approximately at one fifth of the dam height and close to the middle section of the slope, spreading towards the toe on one side and towards the crest on the other, as tending to form a slip surface.

The other mechanism indicated by the contours corresponds to the deformation of the foundation material. In this case the higher distortion band is concentrated in a certain zone of the weak seam beneath the dam slope and extends a little beyond the toe. Very little distortion level is observed in the foundation till material. This level increases as the stiffness of this material decreases for the same depth ratio, or as the weak seam gets shallower for the same stiffness.

5.7.3 Mobilization of shear strength

The analysis showed that in all cases the yielding process within the weak layer started approximately at the same region, indicated in fig.5.31. The shallower the weak layer, considering the same till stiffness, or the smaller the stiffness of the till, considering the same depth of the weak layer, the earlier the yielding process started during dam construction.

Contours of mobilized shear strength together with the position of the critical limit equilibrium failure surfaces are presented in figs.5.32 to 5.34 for the analysis in which $(h_1/H)=0.75$ and in figs.5.35 to 5.37 for those in which $(h_1/H)=0.50$. Figs.5.38 and 5.39 are relative to the case of depth ratio=0.25.

Note that for this last case, the mobilized contours plotted are only 99%,90% and 80%, instead of the wider range plotted in the other cases. The reason is that for the shallowest seam position there is a much higher mobilization of shear strength in the foundation compared to the others, and the contour values selected for each case were the ones that most clearly expressed the mechanism being studied.

Considering the same stiffness for the foundation till, for example K_{till}=7000, it can be observed by comparing figs.5.32 with fig.5.35 and fig.5.38 that as the weak seam is deeper the lower is the strength mobilization level both in the dam and in the foundation. This should be expected since, as discussed before, the deformation level decreases as the depth ratio (h_1/H) increases, for the same stiffness.

For a certain depth of the weak layer, it is shown by figs.5.35, 5.36 and 5.37 that the stiffer the foundation till, the higher is the mobilization of shear strength in the foundation material, even though the deformation level is smaller(see fig.5.13 to 5.15). This can be understood by observing the stress-strain relationship of the foundation till as a function of the stiffness parameters K, shown in fig.5.4. The difference in deformation level between the stiffest and softest cases for the same degree of shear strength mobilization varies according to its proximity to failure. A softer foundation may present a higher level of deformation, but it is not necessarily high enough to mobilize the same or greater amount of shear strength as a stiffer foundation, even though the later develops lower deformation levels.

The two distinct deformation mechanisms discussed based on the maximum shear strain contours can also be observed by the strength mobilization contours. The highest mobilization zone occuring within the dam forms a band indicating a potential failure mechanism in that material. The band of highest mobilization in the foundation is concentrated in the weak seam, also indicating a potential failure surface being formed through that layer.

For the cases with depth ratio of 0.5 and 0.75 the band of highest strength mobilization within the embankment is positioned between the critical potential failure surface calculated for the dam material alone and the critical failure surface passing through the foundation. As the displacement level increases it spreads towards the surface passing through the foundation , as can be observed by comparing figs.5.35, 5.36 and 5.37.

The critical potential failure surfaces calculated by limit equilibrium analysis are in good agreement with the strength mobilization calculated by the numerical analysis. It can be noticed, for example in fig.5.32 or fig.5.36, that the failure surface passes through the zones of highest strength mobilization both in the weak seam and in the till.

In the case of the smallest weak seam depth, with Factor of Safety of 1.18, that is,close to failure according to the limit equilibrium analysis , figs 5.38 and 5.39 show that the zone of highest strength mobilization has spread through the foundation till and forms a contiunous, relatively wide band from the embankment material to the weak seam. The foundation till at the toe region, however, has not yet been stressed to failure conditions, which indicates that this region is supporting the whole system from a total collapse at that stage. This observations emphasize that the upper foundation material at the toe region must be considered as an element of major importance in the stability of structures involving similar deformation mechanisms.

In this case also, good agreement is observed between the position of the critical potential failure surface passing through the foundation and the strength mobilization contours calculated numerically.

It can be noticed that as the foundation is softer for the same depth ratio(see for example figs.5.32 to 5.34) , or as the depth ratio decreases for the same stiffness (see for examples figs.5.32,5.35 and 5.38), the tensile zone in the upper part of the dam increases. Such spreading is due to the increase of the lateral displacements, which causes a simultaneous reduction of the minor principal stress level.

5.8 Case Histories presenting similar deformation mechanism

The deformation mechanism observed in the foundation of two dams during their construction phase will be briefly discussed with the purpose of supporting the applicability of the results obtained from the parametric analysis. The dams were constructed on sites in which the stratigraphy resembles the one studied in the parametric analysis, that is, a relatively weak layer with approximately horizontal orientation existing between stronger layers.

5.8.1 Syncrude Tailings Dyke

The geology of the site and detailed analysis of the movements observed in one section of this tailings dam during construction has been presented in a previous Chapter. The stratigraphic sequence is shown in fig.4.1 (Chapter 4). The maximum horizontal displacement observed in the foundation sandy till was approximately 29cm until the end of 1986, and little distortion was observed in that material, as shown in fig. 4.5 (Chapter 4).

Based on the material parameters assumed for the numerical analysis that best reproduced the movements observed(see tab.4.6 of Chapter 4), and which are within an acceptable range of values expected for those materials, the initial modulus of the foundation sandy till is around 40Mpa. The Factor of Safety calculated by limit equilibrium analysis was approximately 1.6(see Morgenstern,1987).

5.8.2 Nipawin dam

Nipawin dam is a 42 meters high structure constructed of compacted till for hydroelectric power purposes. Detailed description of geological and geotecnical characteristics of the site, construction sequence and materials, as well as field monitoring made during and after construction can be found on Matheson *et al.*, 1987.

The foundation stratigraphy at the section of the main dam referenced as "MC" by the authors *op. cit.* is schematically shown in fig.5.40.It consists of approximately 30 meters of stiff silty till, underlain by 12 meters of montmorillonitic clay shale containing random slickensides and fractures. This pre sheared material overlies a stiffer silty shale layer.

The average elastic modulus of the foundation till layer based on field pressuremeter tests is approximately 700Mpa. The end of construction Factor of Safety was around 1.6.The zone of largest observed lateral displacement level on the clayshale indicated values around 4 cm.

5.8.3 Comparisson of some aspects of Syncrude and Nipawin dams

Both dams are constructed on sites where a till layer overlies a weak pre sheared clay shale layer, underneath which there exists a relatively stiffer material.

The critical Factor of Safety based on limit equilibrium analysis involving the foundation materials were at approximately the same level. However, the maximum lateral displacements observed in the foundation were almost one order of magnitude different.

In both cases the movement occurred along the pre-sheared clay shale layers which have approximately the same strength parameters. In both cases relatively high levels of pore pressure were observed during construction.These factors,therefore, are not sufficient to explain the difference in displacements.

Such difference in displacements can only be explained by the very large difference observed between the stiffness of the upper foundation till layer existing an both sites, which was shown by the parametric analysis discussed above to be the controlling factor for this kind of deformation mechanism.

A simplified uniaxial compression analysis was performed for each case using the displacements measured along two slope indicators in field. It was tried to back calculate the stiffness of foundation till and compare it with the range of values expected for that material.

5.8.4 Simplified uniaxial compression analysis

A schematic representation of the problem is shown in fig.5.41a. It can be said that:
-The horizontal stresses in the till are not uniform with depth
-The higher confinement underneath the dam tends to increase the stiffness in the till and the shear strength of the clay material below(see fig.5.41b and 5.41c). On the other hand, the concentration of shear stresses in the foundation material, close to the toe of the dam, tends to reduce the

stiffness and concentrate the displacements in that region (see figs. 5.41b and 5.41d).

Assuming that it is a uniaxial compression problem, that the resistance to the movement offered by the pre sheared weak layer is not significant and that the horizontal stresses are uniformly distributed with depth in the till layer, the problem was reduced to:

$$\frac{\Delta U}{L} = \frac{\Delta\sigma'_h}{E} \qquad [5.8]$$

in which

ΔU = difference in displacement between the slope indicators

L = distance between the slope indicators

$\Delta\sigma'_h$ = average increment of effective horizontal stress along the section where the slope indicator closer to the centerline of the dam is positioned

E = average stiffness of the region between the slope indicators

In Syncrude Dyke's case, the average horizontal displacements observed in the foundation till, along slope indicators SI842332 and SI842337 (see fig. 4.4 - chapter 4) were approximatelly 29 and 17 cm, respectively, until

1986(see fig. 4.5 - chapter 4). The distance between them is 52m.

The height of the dam at the section where SI842332 is located is approximately 12m. Considering the total unit weight to be 20Kn/m^3, the increment of total vertical stress is 240Kpa. From the finite element results discussed in previous chapter the average value for the increment of horizontal effective stress at that section was 98Kpa, that is $0.41\Delta\sigma_v$

Using these values, the back calculated average deformability modulus for the till in the region between the slope indicators considered,according to the equation above, is 42.5Mpa. Such result is within the range of values believed to represent that material, at that particular site.

In the case of Nipawin dam , the average horizontal displacements observed in the foundation till along the inclinometers IC-3 and IC-6, showed in fig.5.30, were approximately 4 and 2.5 cm, respectively. The distance between them is 50m.

The height of the dam at the section where IC-3 is located is approximatelly 20m and the total unit weight of the compacted material is close to 21Kn/m^3. The increment of horizontal effective stress was assumed to be $0.41\Delta\sigma_v$.

The deformability modulus calculated based on the equation above, for the region between IC-3 and IC-6 is 574Mpa. In this case, also, the value obtained is within the range of values for the till material based on the field test results presented by Matheson *et al.*, 1987.

5.9 Conclusion

The parametric analysis promoted a better understanding of the lateral deformation mechanism of the foundation of dams constructed on sites whose stratigraphy presents a weak layer with horizontal orientation overlain by a stronger material.

It showed that the lateral displacement level in the foundation is mainly controlled by the stiffness of the upper foundation material, and that the relationship between Factor of Safety as calculated based on limit equilibrium methods and the lateral displacements in the foundation has to take into consideration the stiffness of this material.

The results of the analysis of the case with depth ratio of 0.25 (lowest Factor of Safety), showed that the characteristics of the foundation material above the weak layer, at the toe region, are of major importance for the stability of the structure.

The stiffness of the embankment within a relatively wide range did not affect the foundation displacements in a very extensive way, even though it caused significant variations in the dispacements within the dam. On the other hand, the stiffness of the upper foundation layer was found to significantly influence the displacements within the embankment. Such displacements were also shown to be very much affected by the pore pressure level in the shoulder of the dam.

The mobilization of shear strength was in good agreement with the critical failure surface calculated by the use of Morgenstern and Price stability analysis method.

It was shown that the smaller the stiffness of the upper foundation layer or the shallower the position of the weak layer, the lower the height of dam construction at which the yielding process started at the weak layer.

A relatively small shear strain level was observed in the upper foundation material even for the smallest stiffness cases. Two narrow bands of high shear strains were observed, one within the embankment and the other in the weak layer which indicated two major distinct deformation mechanisms occurring.

The tensile region observed in the upper part of the embankment was sensitive to the displacement level within the embankment. Such region increased as the displacements increased.

Two case histories presenting similar foundation stratigraphy were compared. The very large difference observed in the foundation displacement levels of these cases were explained by the difference in the stiffness of the upper foundation layer. A simplified uniaxial compression analysis, using measured lateral displacements at two distinct vertical sections of each case, was performed with the purpose of back-analysing the stiffness of the upper foundation material. The results obtained were within the range expected for both cases, which, again, indicates that the major cause of the difference in displacements was indeed the difference in stiffness of the upper foundation layer.

Ref	material	area	test	sample	c'_p(kpa)	ϕ'_p
1	very dense sandy till	Wesleyville (Ont.)	CU triaxial comp.	block	47	35
2	dense sandy silt till	Nipawin(Sask.)	CU triaxial comp.	block	0	38
2	sandy silt till	Nipawin(Sask.)	CU triaxial comp.	block	0	35
2	very dense sandy silt till	Nipawin(Sask.)	CU triaxial comp.	block	0	42
3	clayey till	Fort McMurray (Alta.)	CU triaxial comp.	core barrel	11	32
3	sandy silt till	Fort McMurray (Alta.)	CU and CD triaxial ext.	core barrel	20	37
4	sandy silt till	Nipawin(Sask.)	CU and CD triaxial comp.	block	38	39
4	sandy silt till	Edmonton(Alta.)	CU and CD triaxial comp.	block	47	43

References:

1 - Radhakrishna and Klyn (1974)

2 - Matheson,*et al.* (1987)

3 - Sego,D. and Morgenstern,N.R.(1986)

4 - Witebolle,R.(1983)

Table 5.1: Strength parameters for till

Ref.	material	area	test	E_u(Mpa)	E_e(Mpa>
1	very dense sandy till	Nipawin(Sask.)	pressuremeter	563-1387	525-1300
1	dense sandy silt till	Nipawin(Sask.)	pressuremeter	100-503	93-460
2	dense snady till	Wesleyville (Ont.)	plate load	780	730
2	dense sandy silt till	Wesleyville (Ont.)	plate load	340	320
3	sandy silt till	Edmonton (Alta.)	pressuremeter	200	185
4	very dense sandy	Squaw rapids (Sask.)	plate load	500-1500	450-1400

References:

1 - Matheson, *et al*. (1987)

2 - Radhakrishna and Klin (1974)

3 - Eizenstein and Morrisson (1973)

4 - Klohn (1968)

Table 5.2: Deformability parameters for the till

h_1/H	K	σ'_3(Kpa)	E_i(Mpa)
0.25	700	56.2	62.9
	3500	56.2	314.4
	7000	56.2	628.9
0.50	700	112.5	72.2
	3500	112.5	361.2
	7000	112.5	722.4
0.75	700	168.7	78.3
	3500	168.7	391.7
	7000	168.7	783.4

Table 5.3: Initial modulus at the center of the foundation till

Ref.	material	area	test	sample	E_u(Mpa)	E_d(Mpa)	c'_r(Kpa)	ϕ'_r
1	bentonite	Edmonton	CU triaxial comp.			35-49	0	8-10
2	clayey bedding seam in general						0	10-15
3	clayshale	Fort McMurray	CU triaxial comp.	core barrel	12-35	11-32		
3	clayshale	Fort McMurray	direct shear	core barrel				6-9
4	clayshale	Nipawin	pressuremeter		107-209	100-250		
4	clayshale	Nipawin	direct shear					7-11
5	alternating clay and sand seams	Edmonton	pressuremeter comp.		200	185		

References:

1 - Chan,D.(1985)

2 - Cassinader (1980)

3 - Handford,H. (1985)

4 - Matheson, *et al.* (1987)

5 - Eizenstein and Morrisson (1973)

Table 5.4: Clayey seams characteristics

Ref.	area	W_{opt}(%)	γ_d(kn/m^3)	c'$_p$(kpa)	ϕ'_p
1	Arrow lakes(B.C.)	8	21.6	0	37.5
2	Otter Rap.(Ont.)	10	22.5	7	38.0
2	Cornwall(Ont.)	9	22.7	15	38.0
3	Vanc. Isl.(B.C.)	10	21.6	54	35.0
4	Nipawin(Sask.)	7.6	20.8	0	37.5

References:

1 - Milligan,V. (1976)

2 - Adams,J.I. (1961)

3 - MacDonald, *et al*. (1961)

4 - Matheson, *et al*. (1987)

Table 5.5: Compacted till characteristics

Analysis	Material	σ_t (kpa>	γ (kn/m^3)	E (mpa)	μ	K	n	c' (kpa)	ϕ'	R_f
switch-on-gravity (linear elastic)	Found. till(1)	0.0001	22	65,325,650* 75,375,750 80,400,800	0.45					
	Clayshale(2)	0.0001	20	50	0.45					
	Bedrock(3)	0.0001	22	2000	0.45					
	Comp. till(4)	1000	20	15	0.40					
non-linear	Found. till(1)	0.0001	22		0.40	700 3500 7000	0.2	10	37	0.9
	Clayshale(2)	0.0001	20	50	0.40			0	10	
	Bedrock(3)	0.0001	22	2000	0.30					
	Comp. till(4)	1000	20		0.40	800	0.2	10	37	0.87

* each value refers to one analysis

Table 5.6: Material parameters used in the parametric analysis

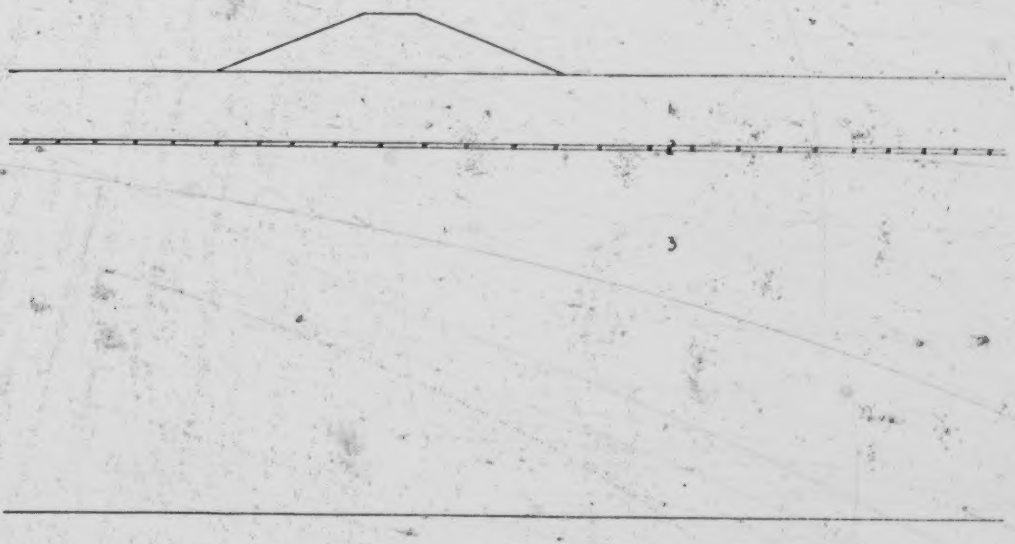

Figure 5.1: Foundation containing horizontal weak seam

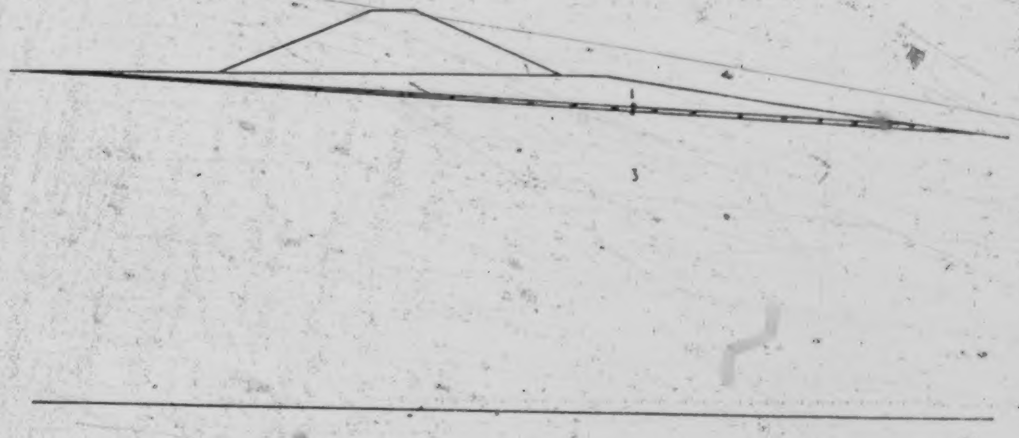

Figure 5.2: Weak seam "daylights" downstream of the dam

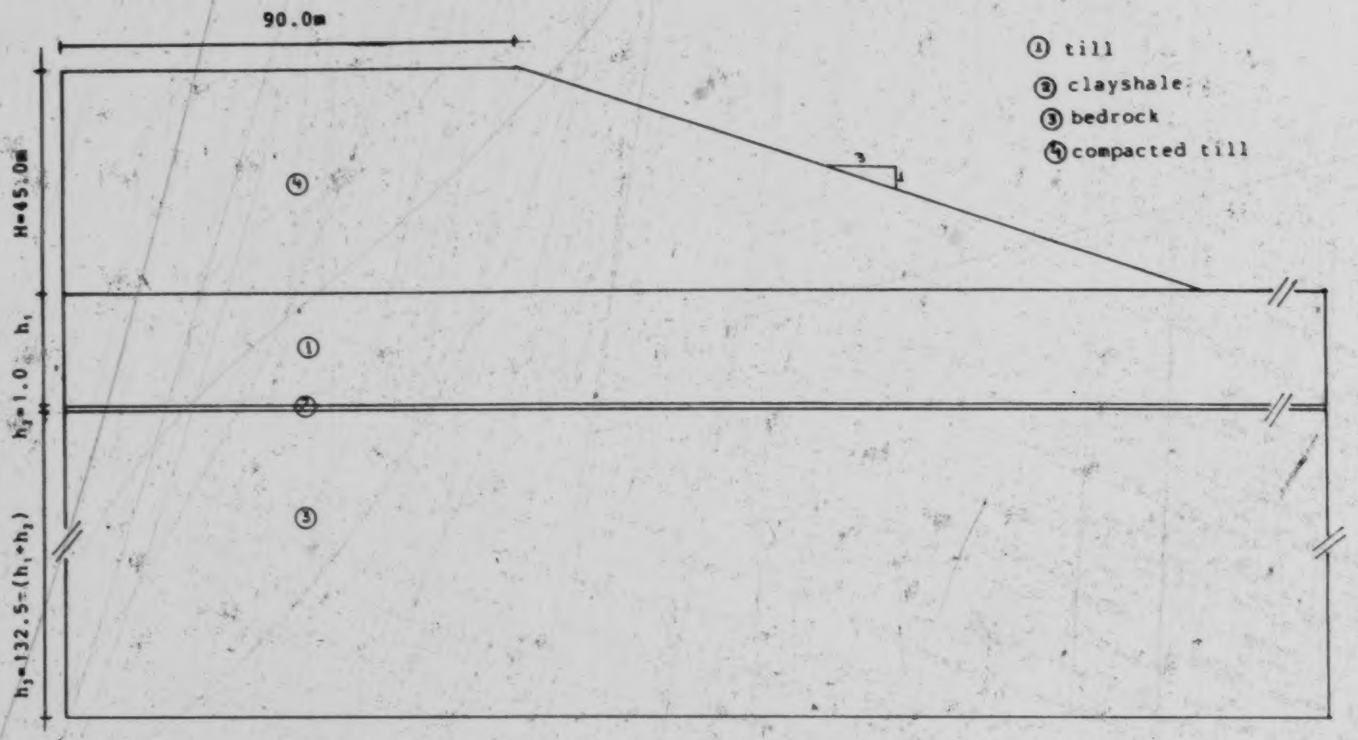
90.0m
① till
② clayshale
③ bedrock
④ compacted till
3
1
④
①
②
③
H=45.0m
h₁
h₂=1.0
h₃=132.5-(h₁+h₂)

Figure 5.3: Stratigraphy used in the parametric analysis

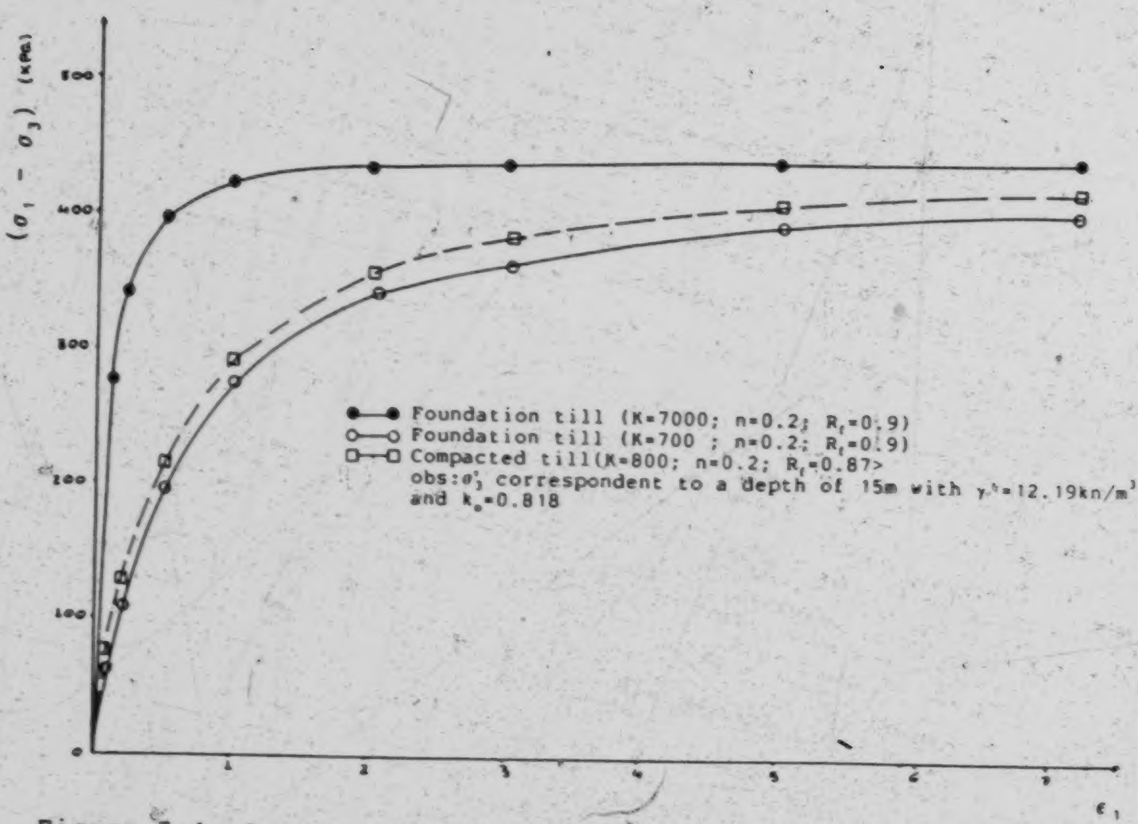

Figure 5.4: Stress - strain curves for the till with various stiffnesses

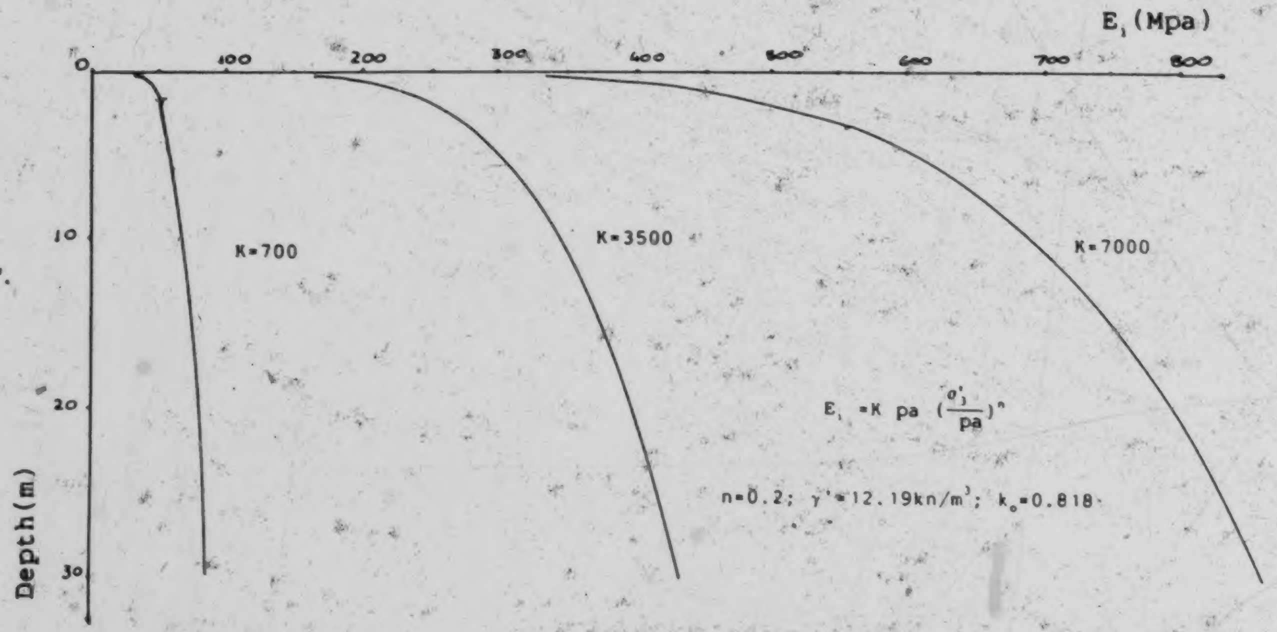

Figure 5.5: variation of the initial modulus of the foundation till with depth

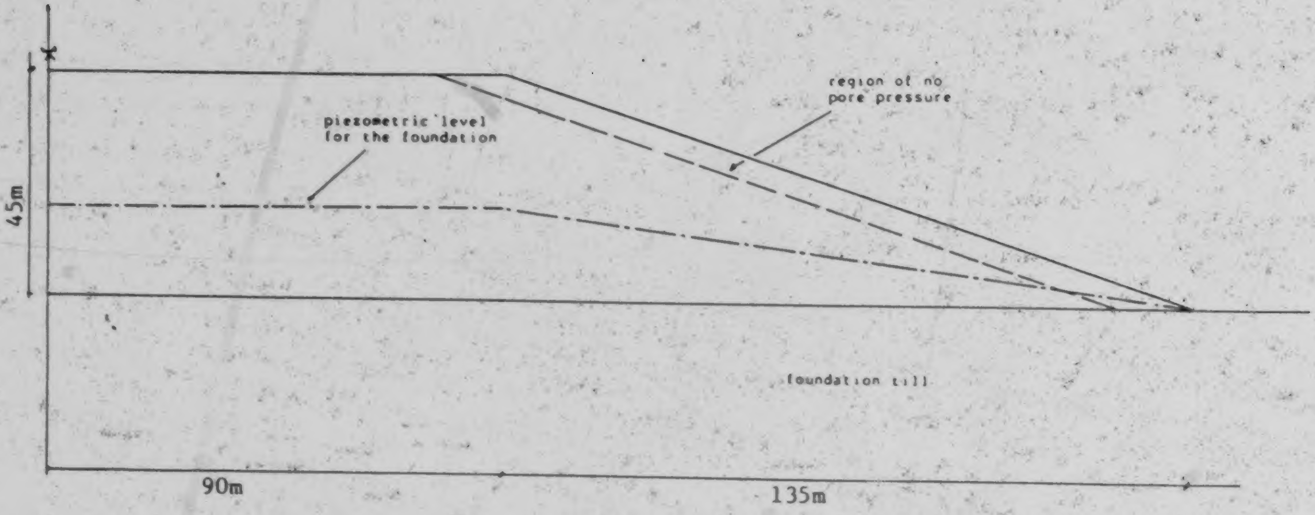
45m
piezometric level
for the foundation
region of no
pore pressure
foundation till
90m
135m

Figure 5.6: Piezometric level for the foundation after the completion of the dam

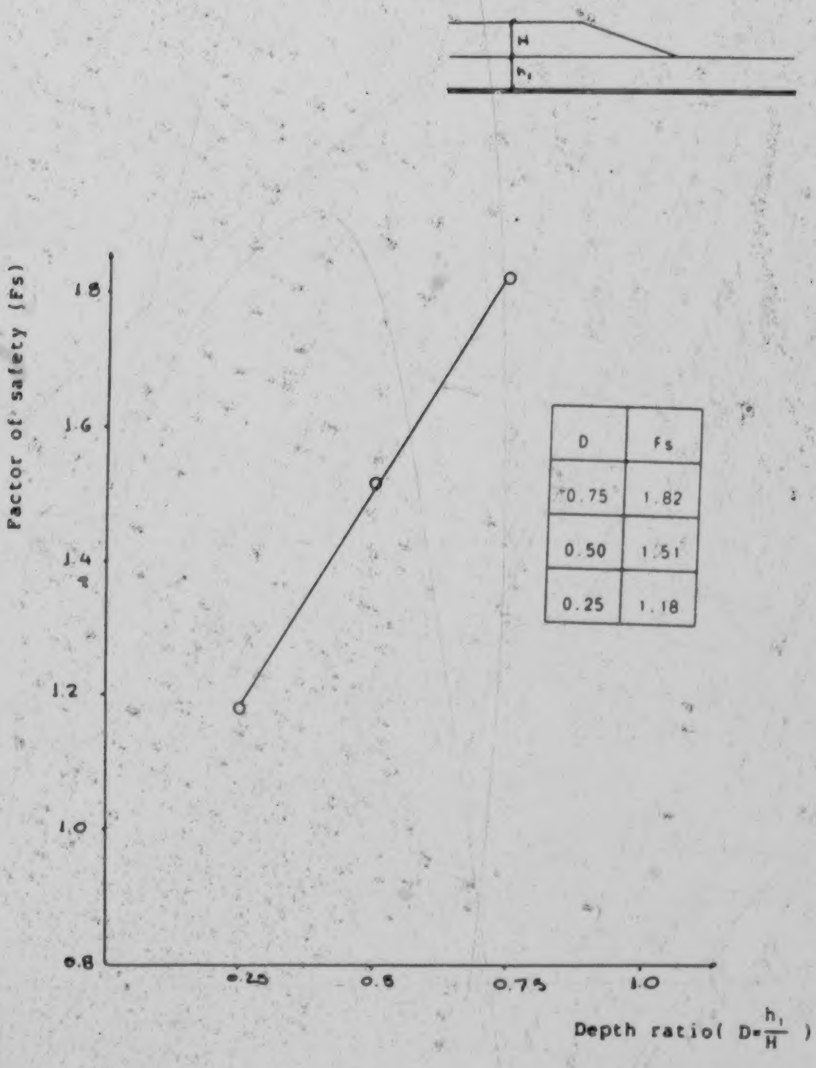

D	Fs
0.75	1.82
0.50	1.51
0.25	1.18

Figure 5.7: Variation of factor of safety with the position of the weak seam

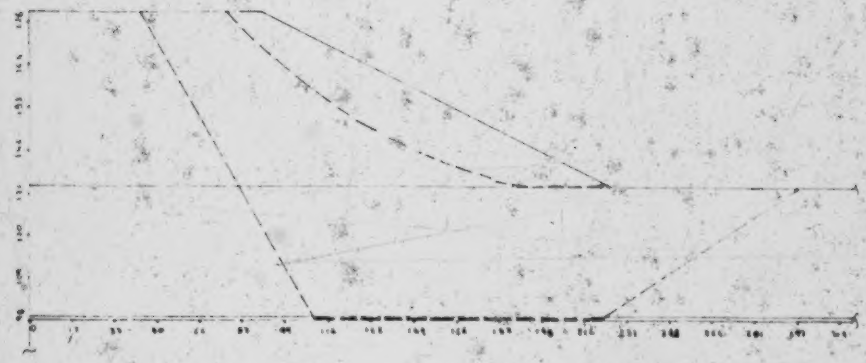

Figure 5.8: Critical failure surfaces - $\frac{h_1}{H}=0.75$

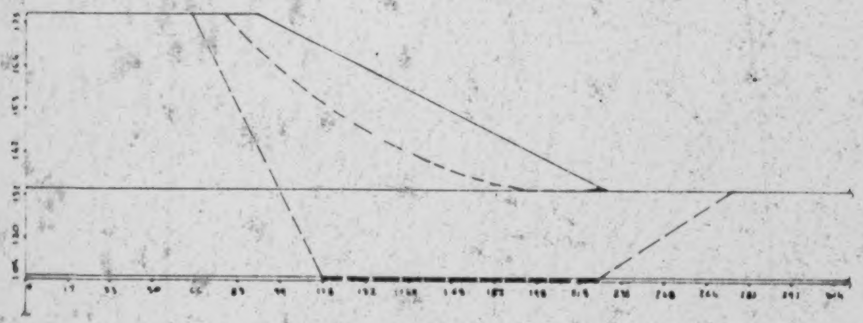

Figure 5.9: Critical failure surfaces - $\frac{h_1}{H}=0.50$

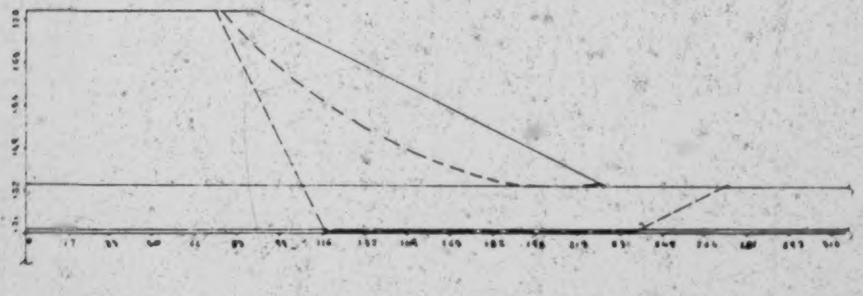

Figure 5.10: Critical failure surfaces - $\frac{h_1}{H}=0.25$

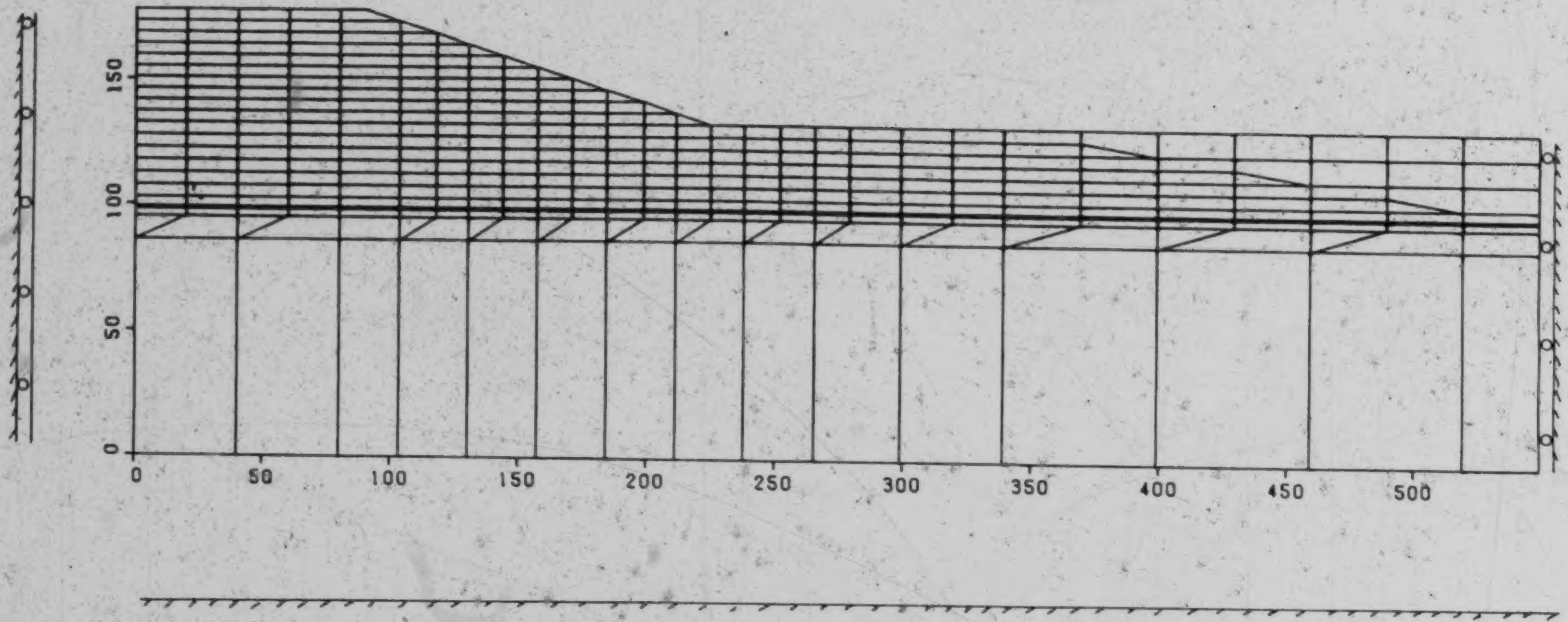
0
50
100
150
0
50
100
150
200
250
300
350
400
450
500

Figure 5.11: Finite element mesh - $\frac{h_1}{H}=0.75$

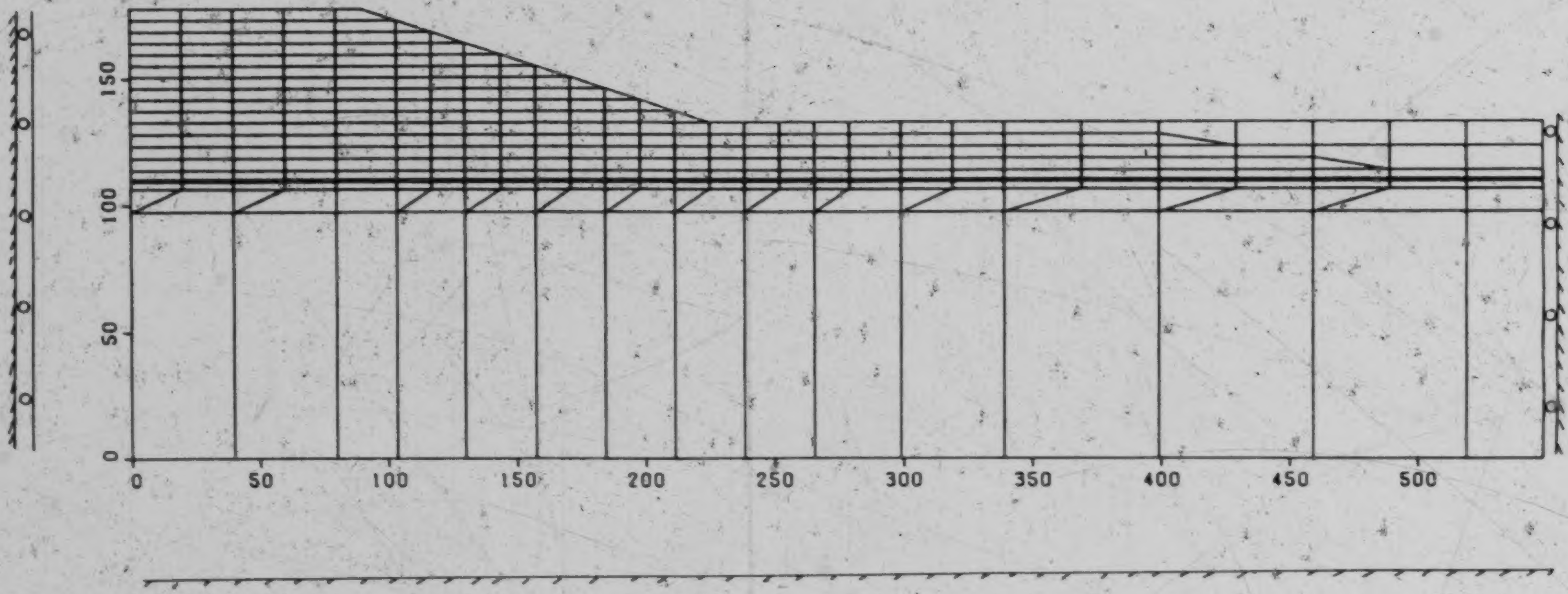
0
50
100
150
0
50
100
150
200
250
300
350
400
450
500

Figure 5.12: Finite element mesh - $\frac{h_1}{H}$=0.50

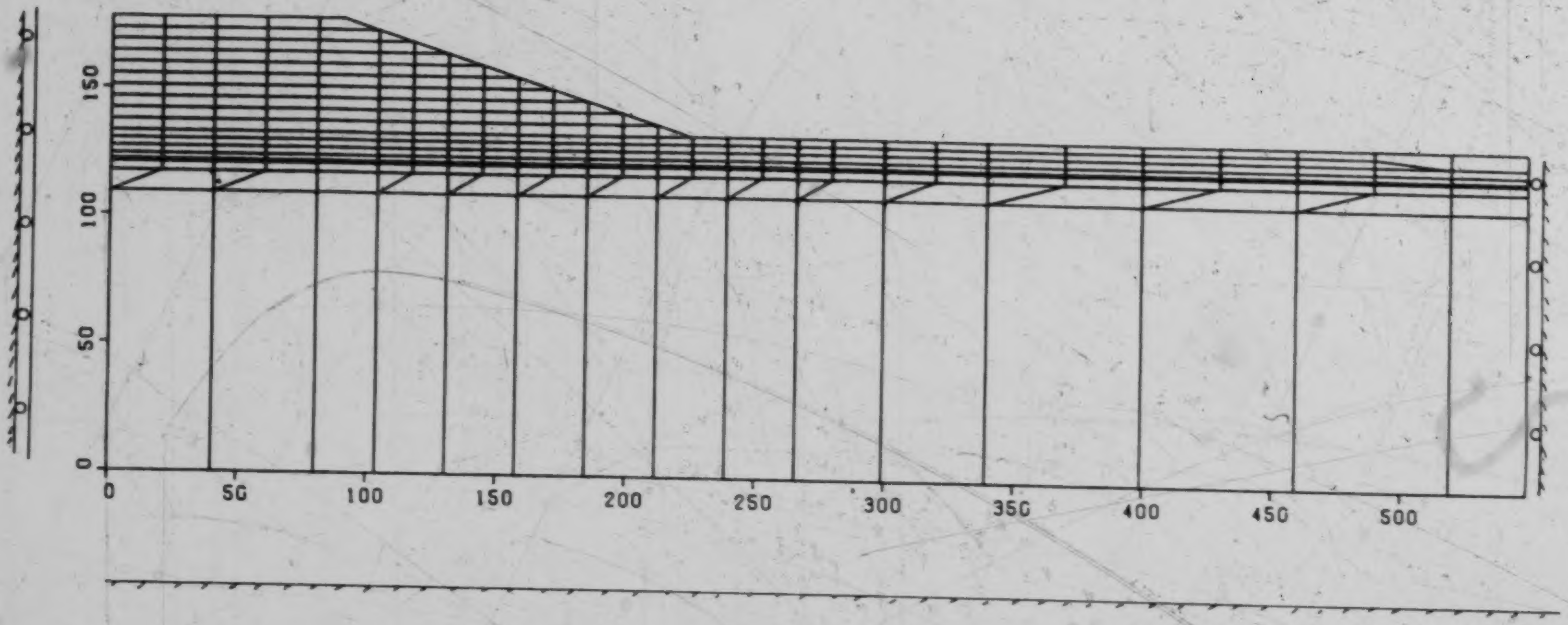
0
50
100
150
0
50
100
150
200
250
300
350
400
450
500

Figure 5.13: Finite element mesh - $\frac{h_1}{H}=0.25$

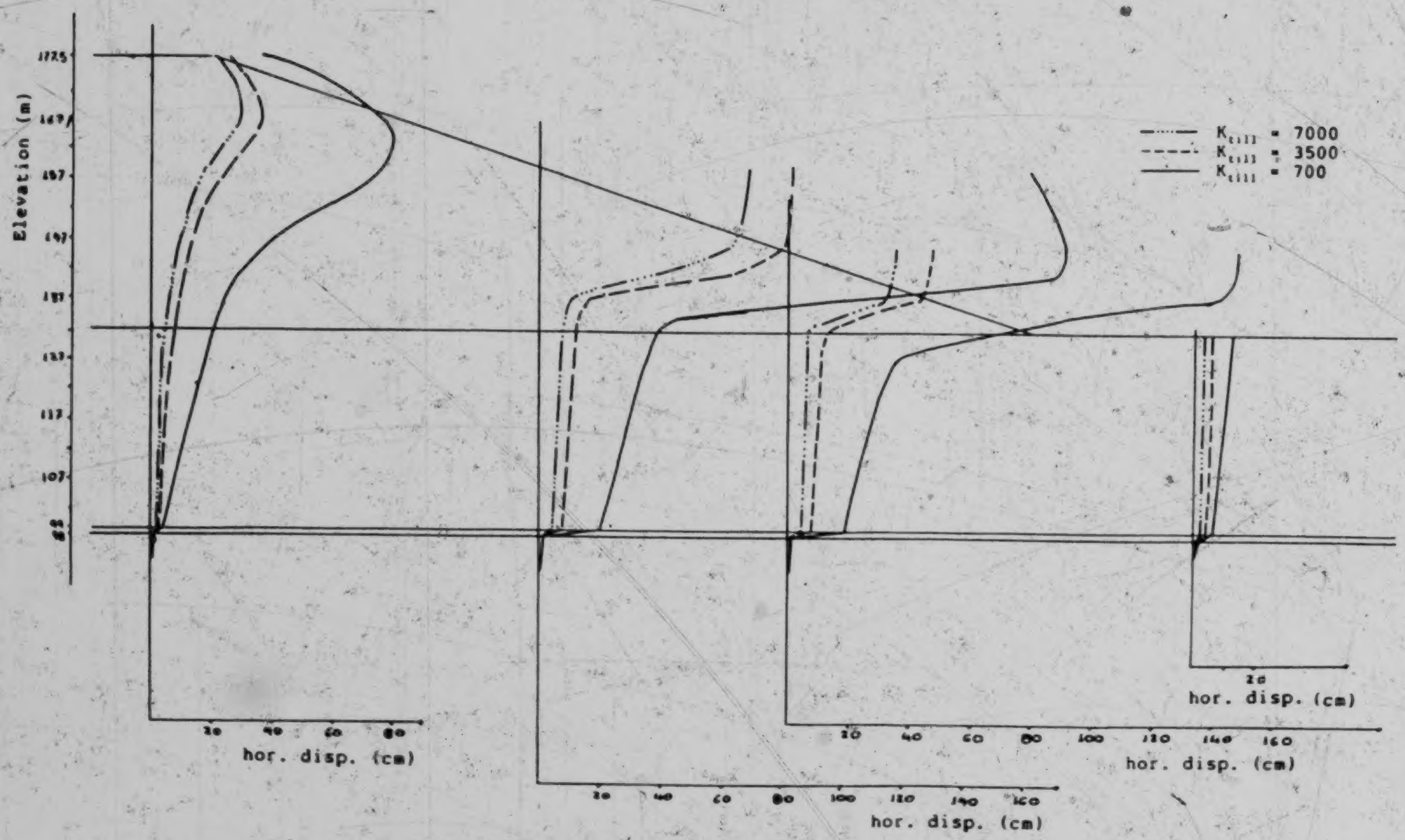

Figure 5.14: Variation of horizontal displacements with the foundation stiffness - $(h_1/H)=0.75$

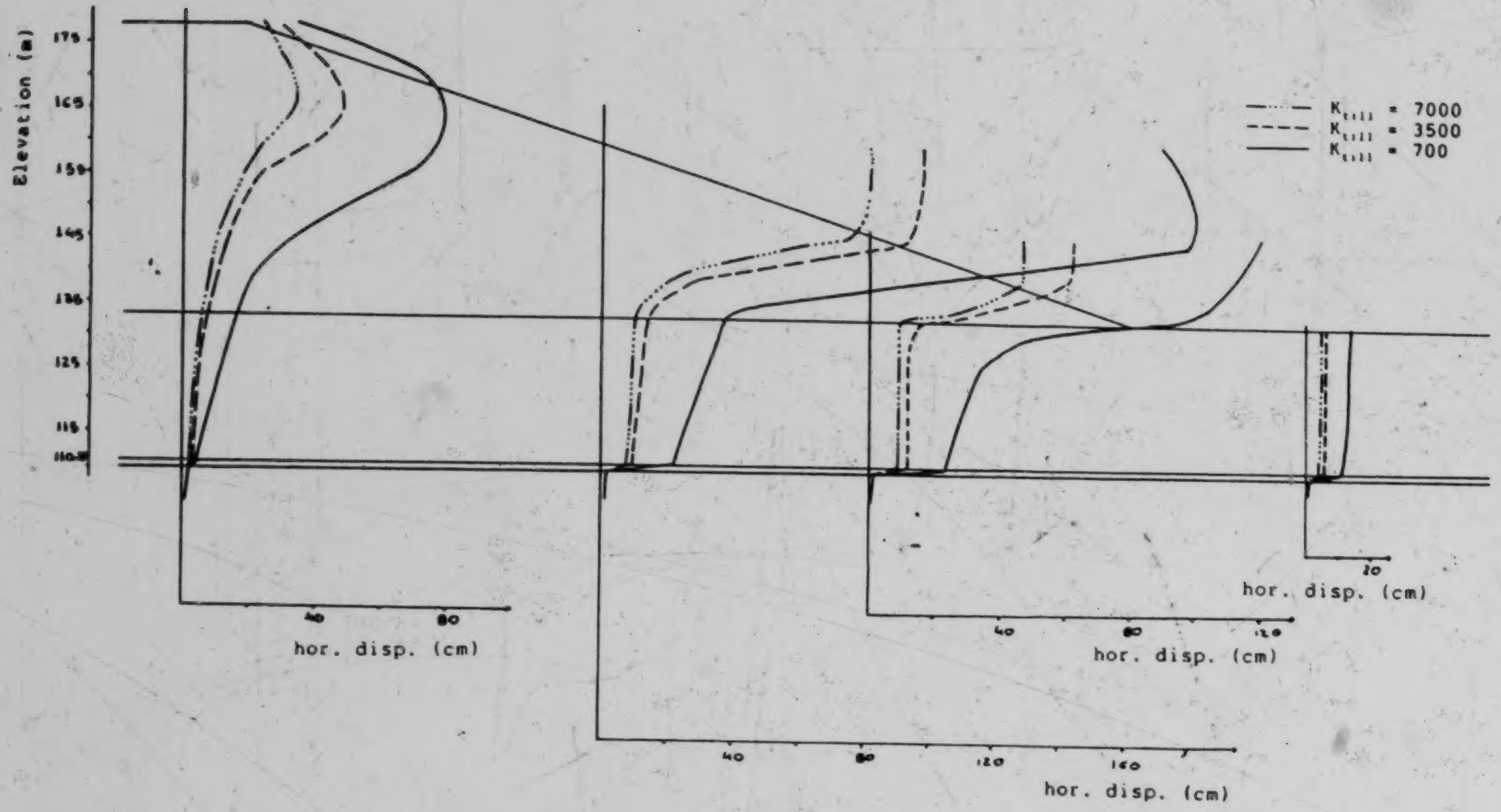

Figure 5.15: Variation of horizontal displacements with the foundation stiffness - $(h_1/H)=0.50$

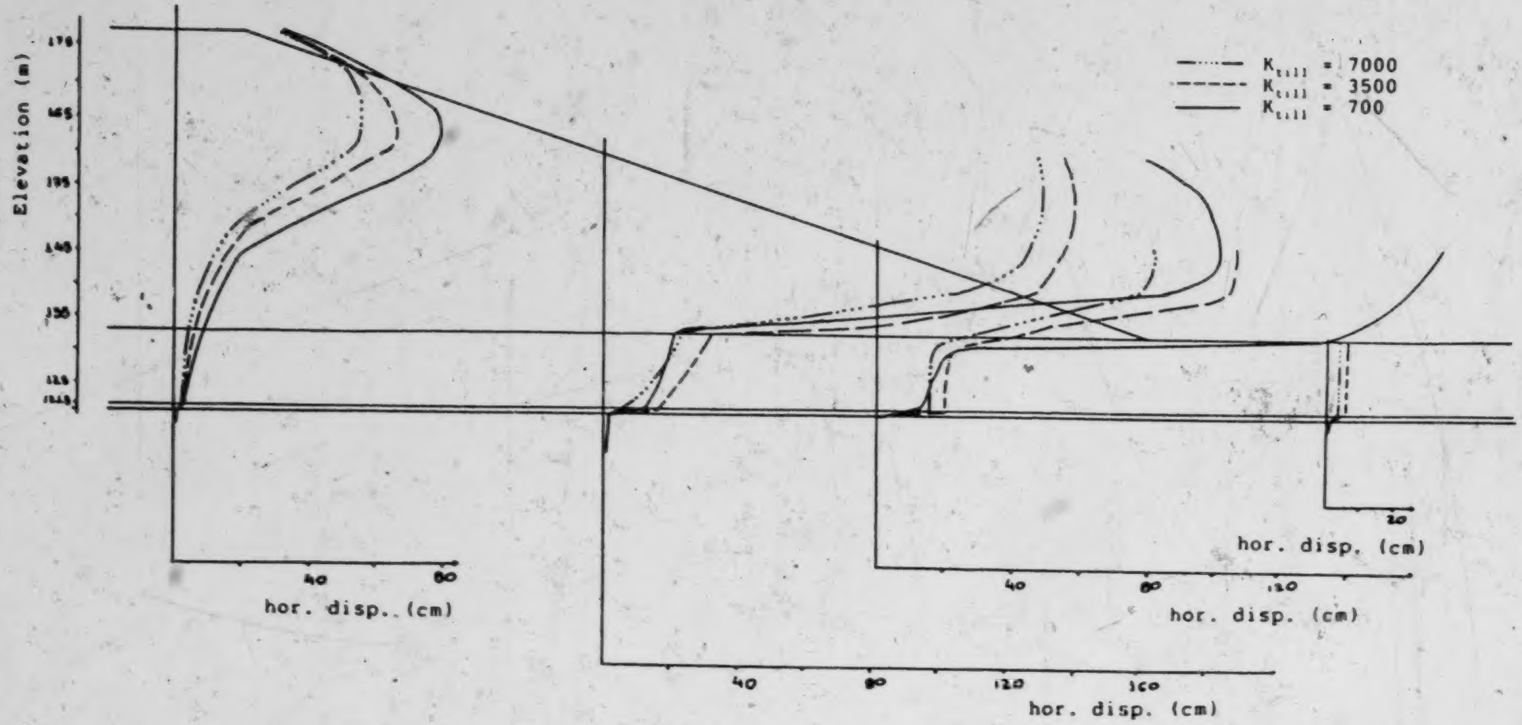

Figure 5.16: Variation of horizontal displacements with the foundation stiffness - $(h_1/H)=0.25$

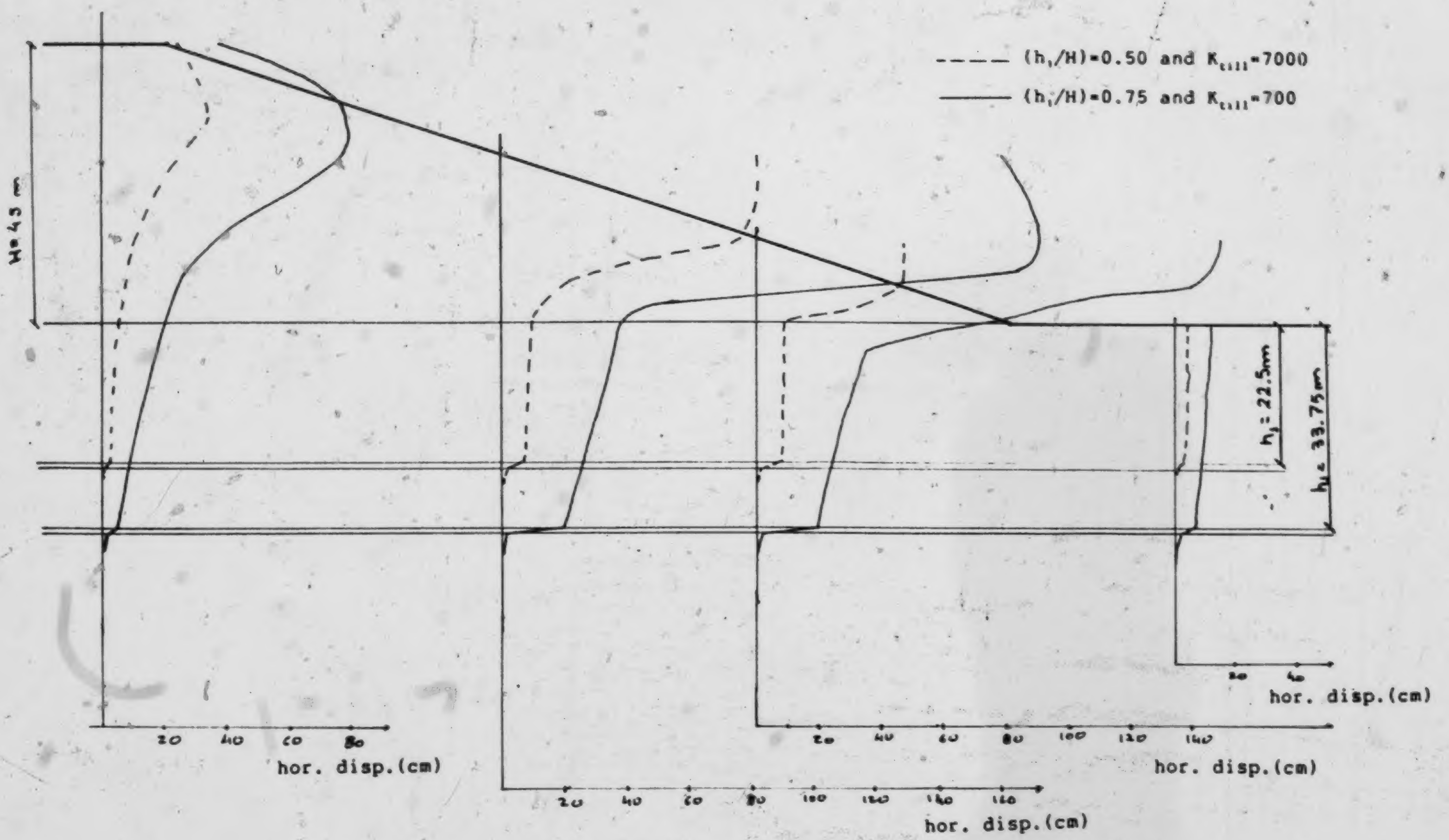

Figure 5.17: Comparison between horizontal displacements in cases with different depth ratios and different foundation stiffnesses

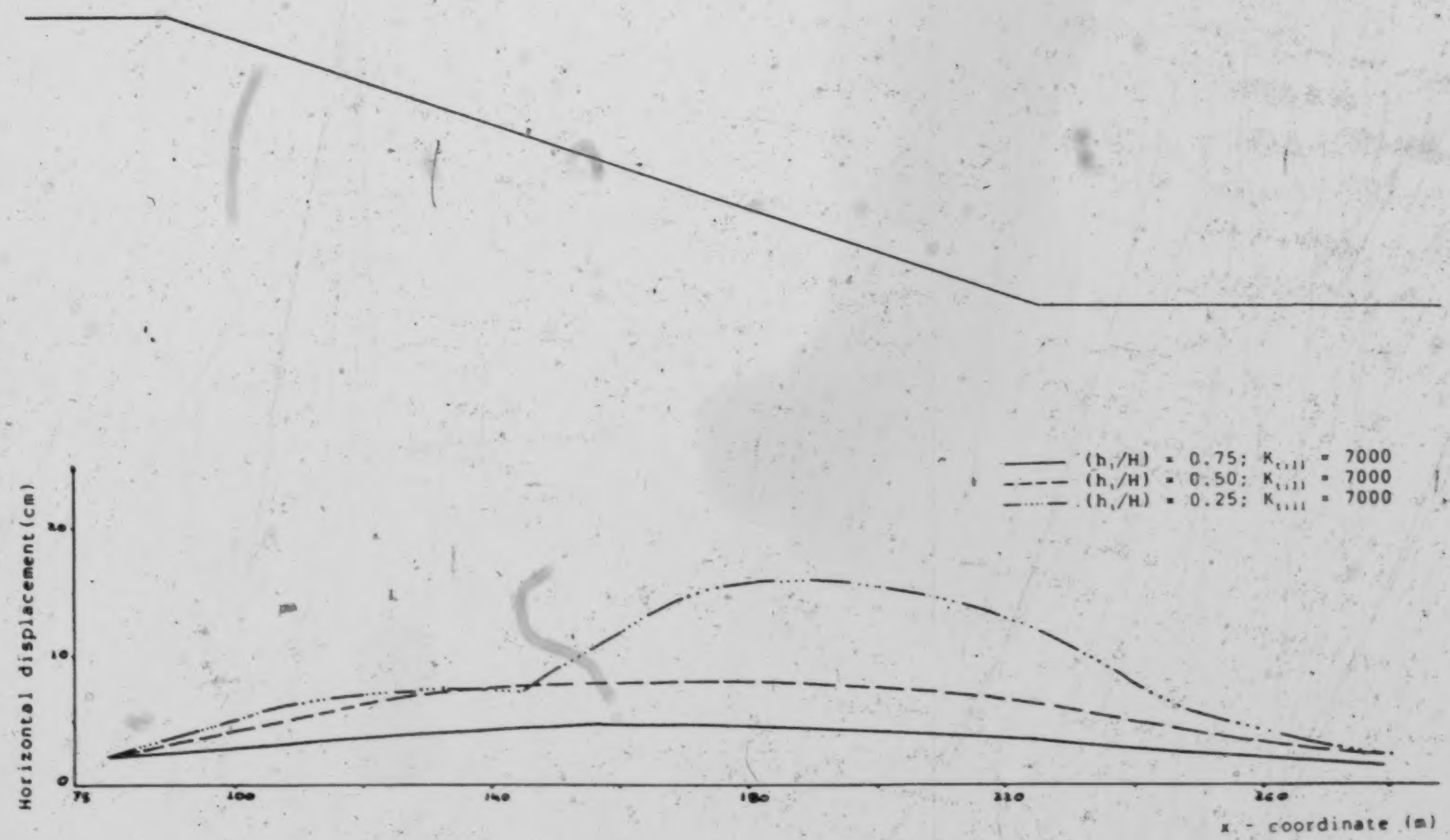

Figure 5.18: Variation of the horizontal displacements along clayshale/till contact with the depth ratio

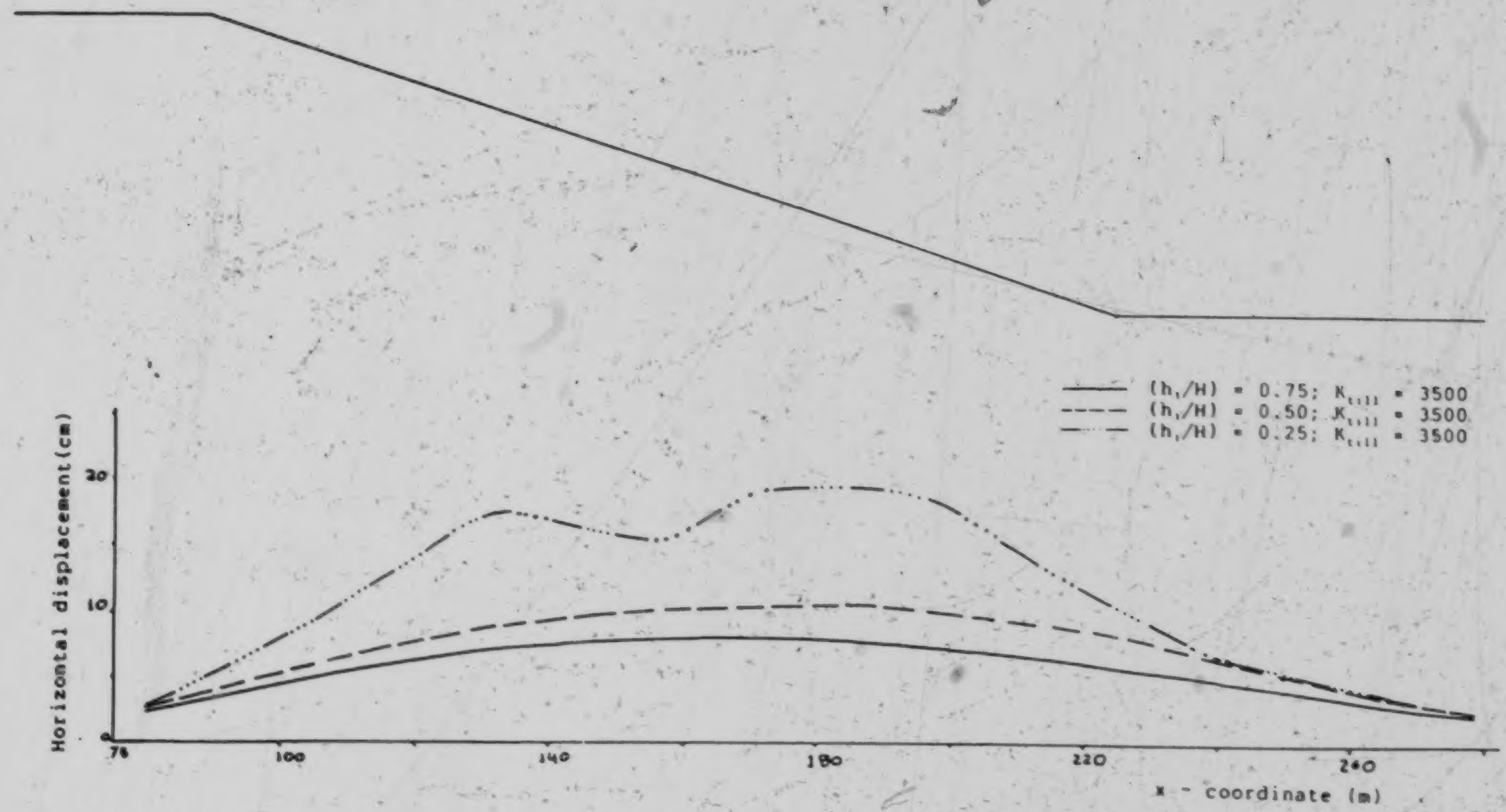

Figure 5.19: Variation of the horizontal displacements along clayshale/till contact with the depth ratio

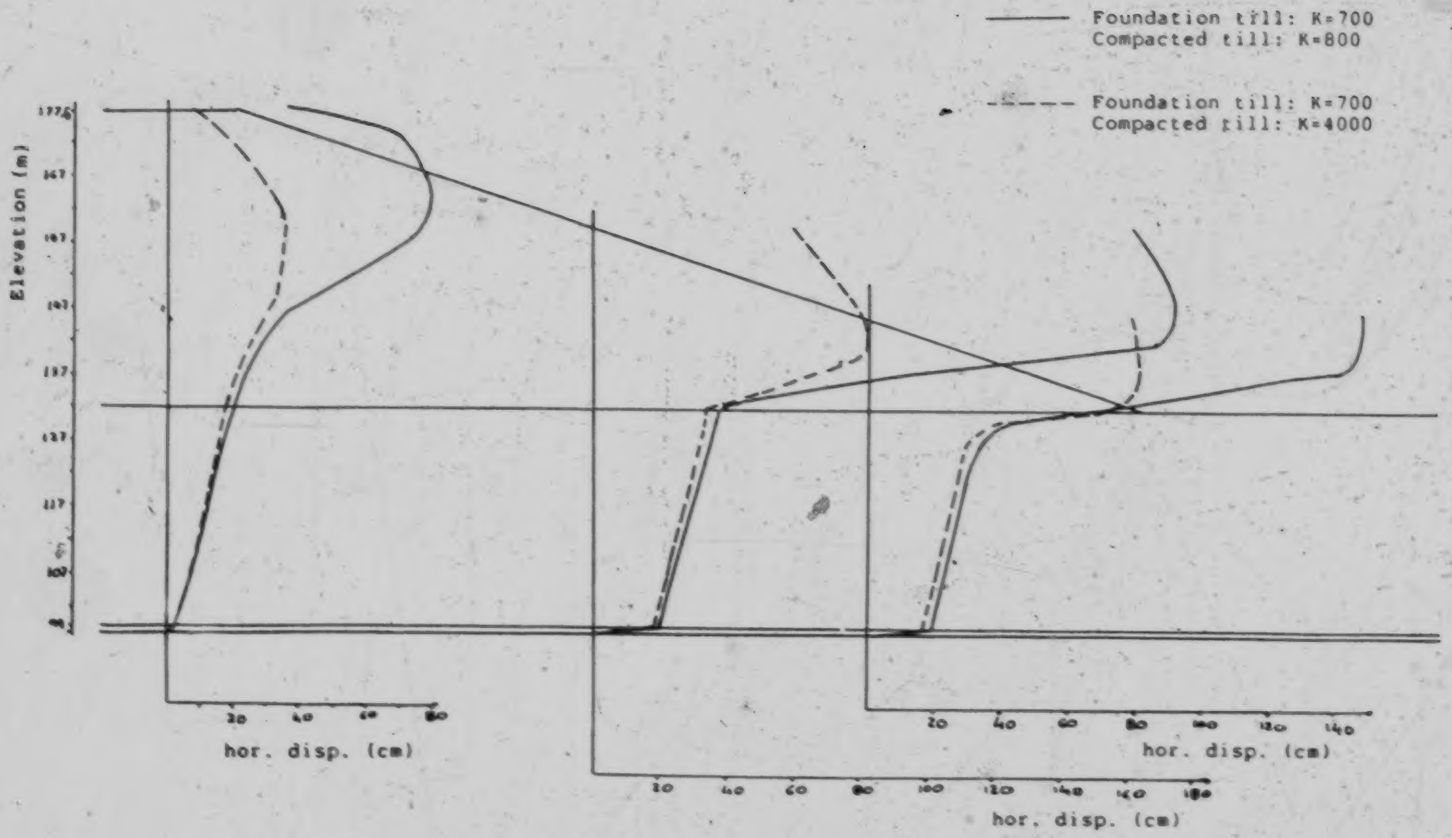

Figure 5.20: Influence of the embankment stiffness on the horizontal displacements

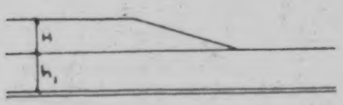

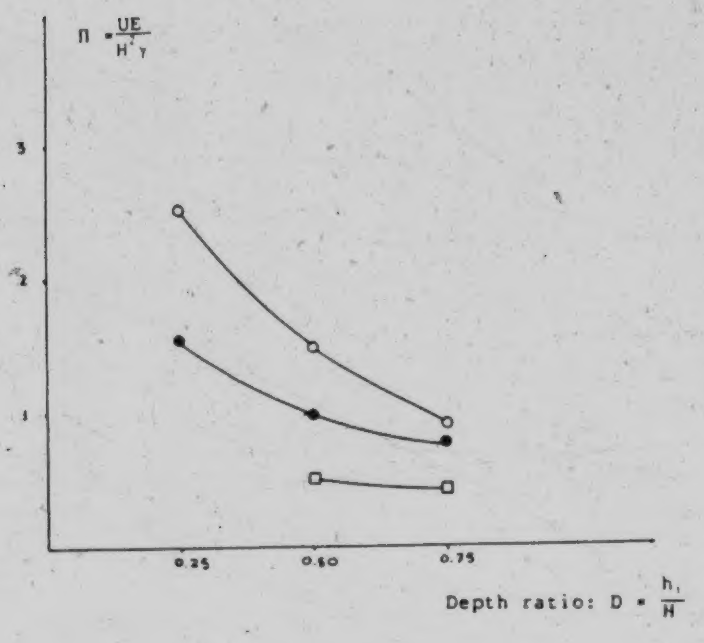

Figure 5.21: Dimensionless factor Π versus Depth ratio

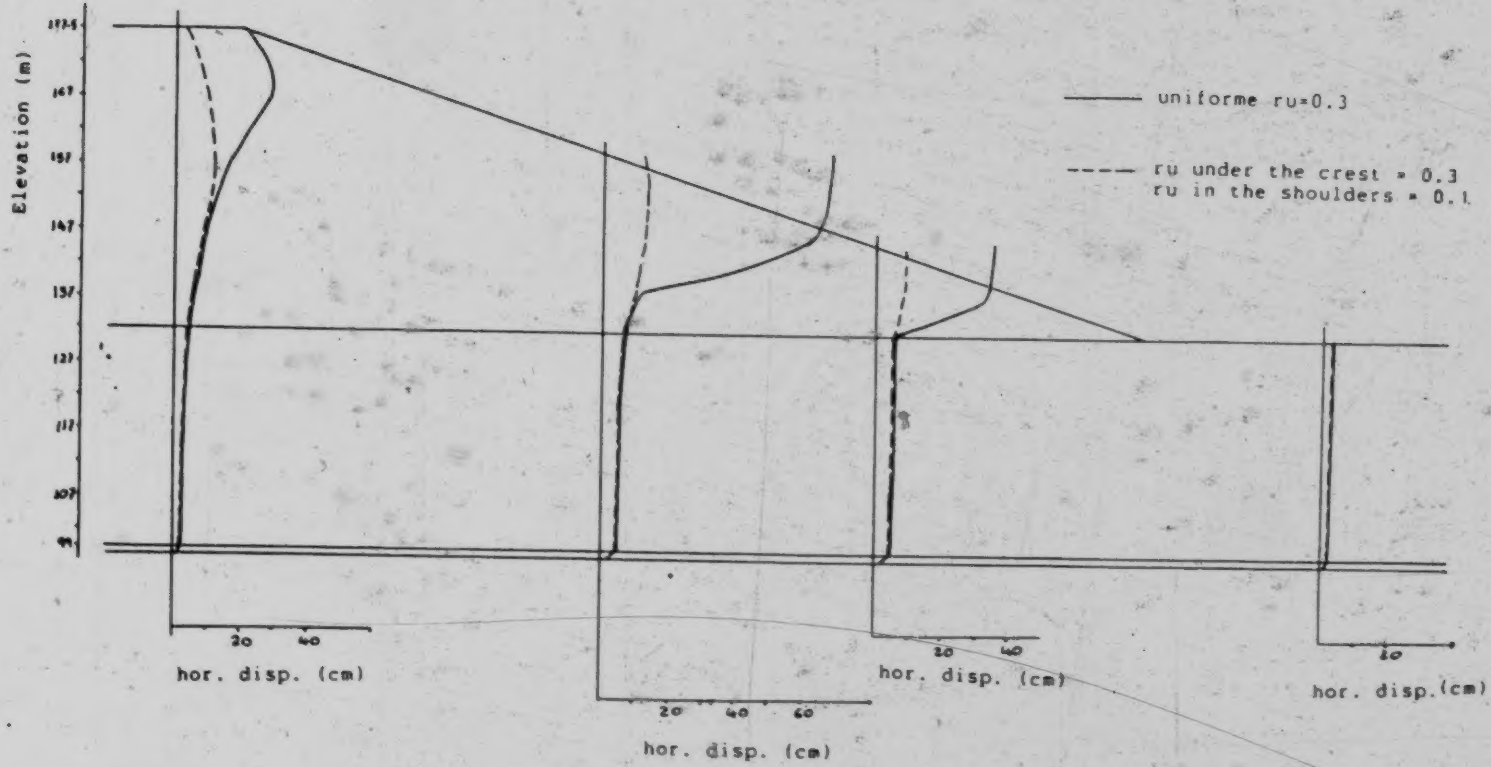

Figure 5.22: Effect of the ratio ru of the embankment on the horizontal displacements ($(h_1/H)=0.75$ - $K_{till}=7000$)

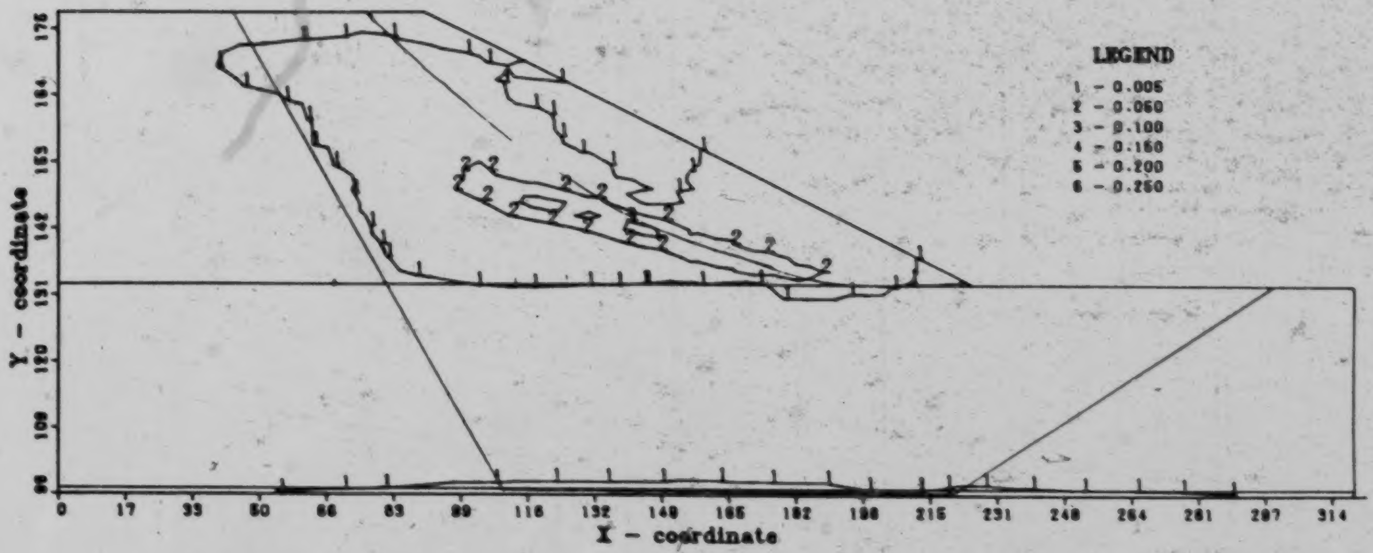

Figure 5.23: Maximum shear strain ($\frac{h_1}{H}$=0.75 - K_{till}=7000)

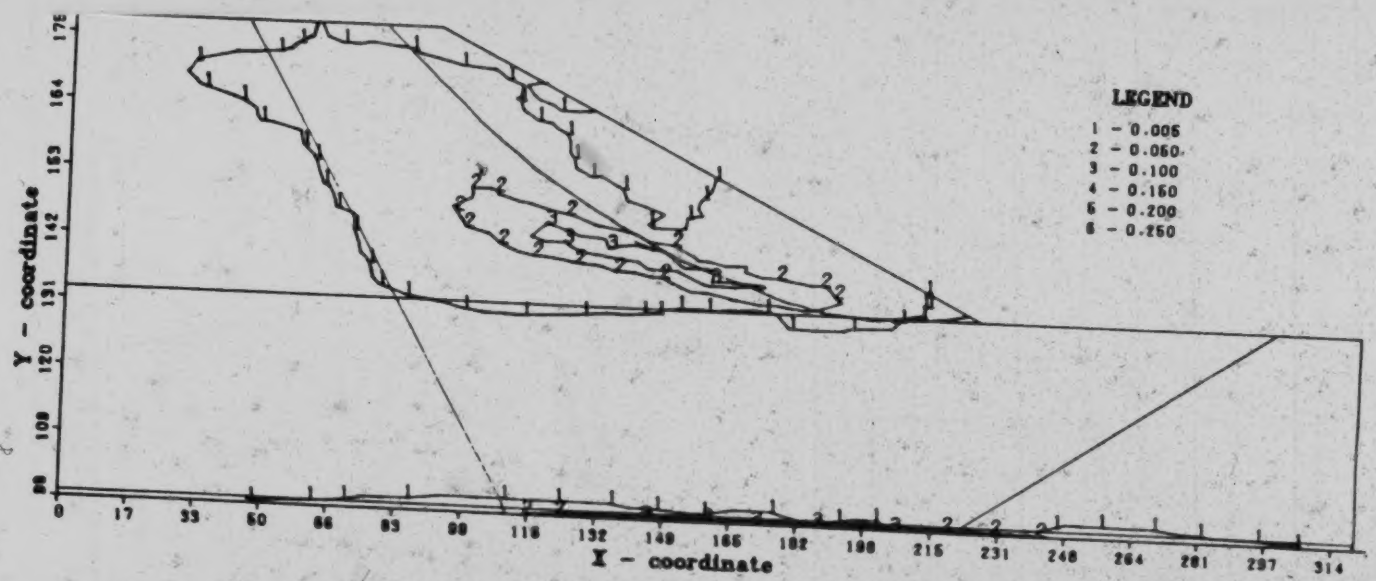

Figure 5.24: Maximum shear strain ($\frac{h_1}{H}$=0.75 - K_{till}=3500)

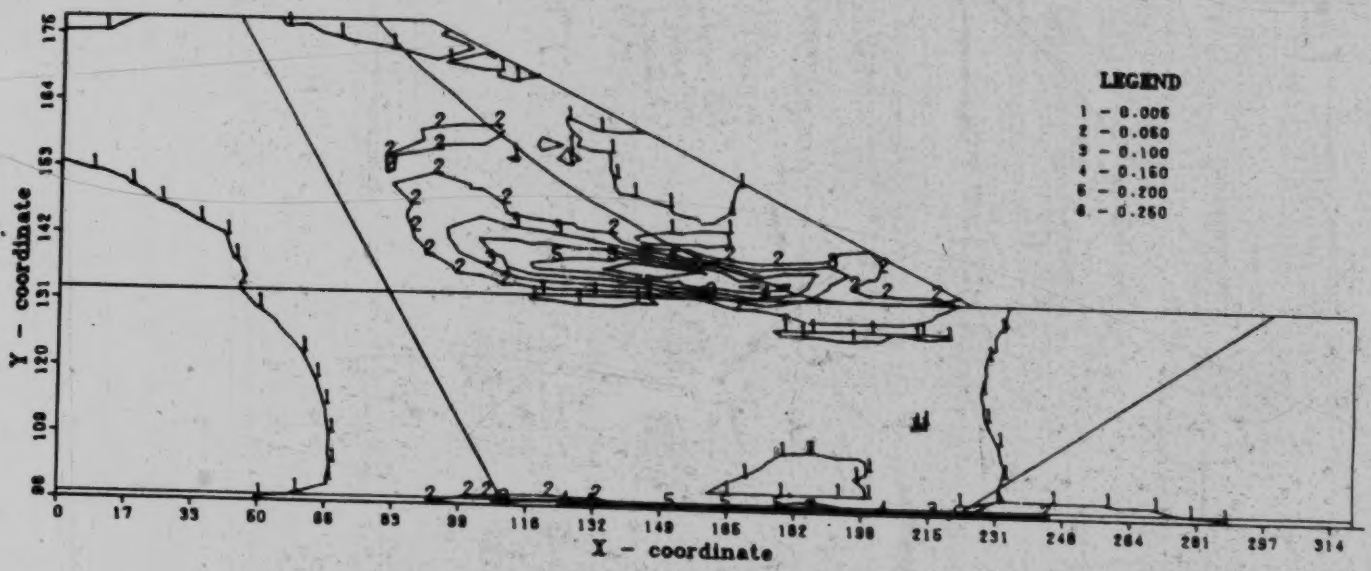

Figure 5.25: Maximum shear strain ($\frac{h_1}{H}$=0.75 - K_{till}=700)

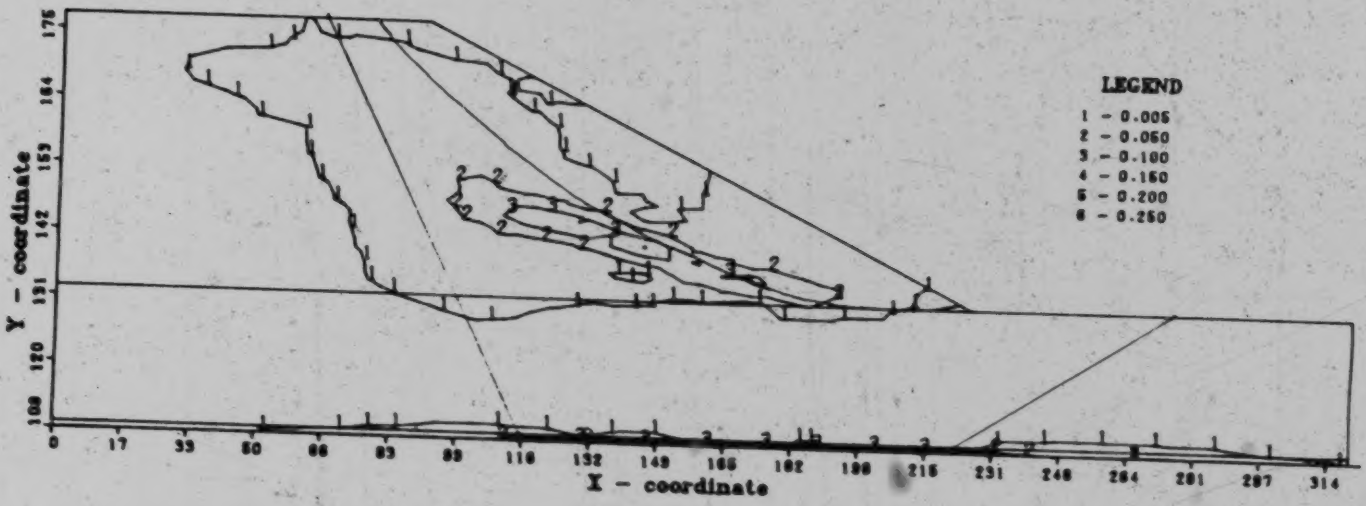

Figure 5.26: Maximum shear strain ($\frac{h_1}{H}$=0.50 - K_{till}=7000)

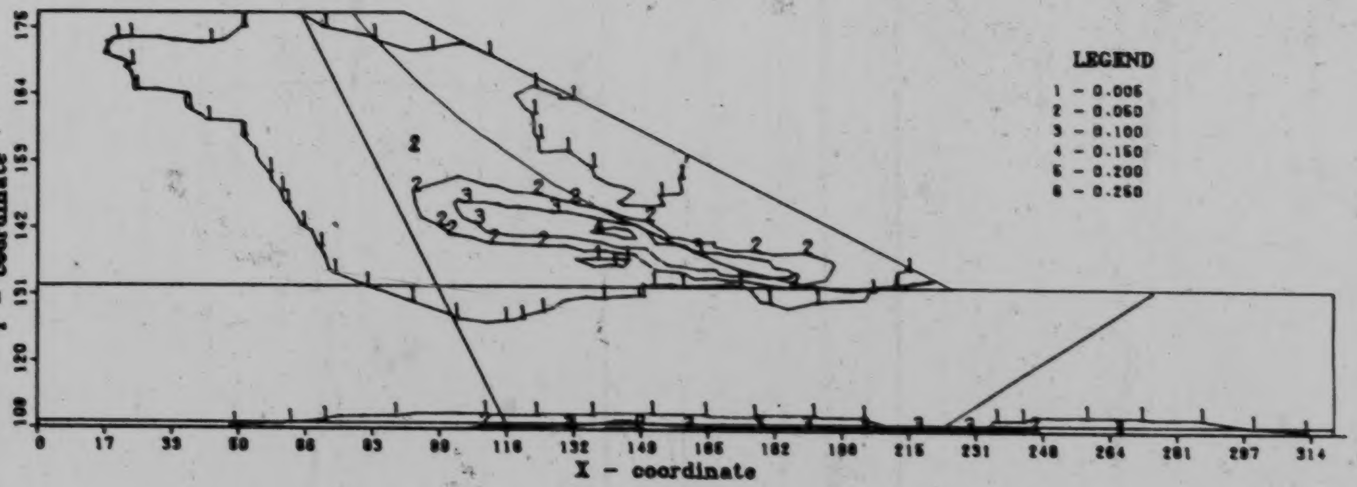

Figure 5.27: Maximum shear strain ($\frac{h_1}{H}$=0.50 - K_{till}=3500)

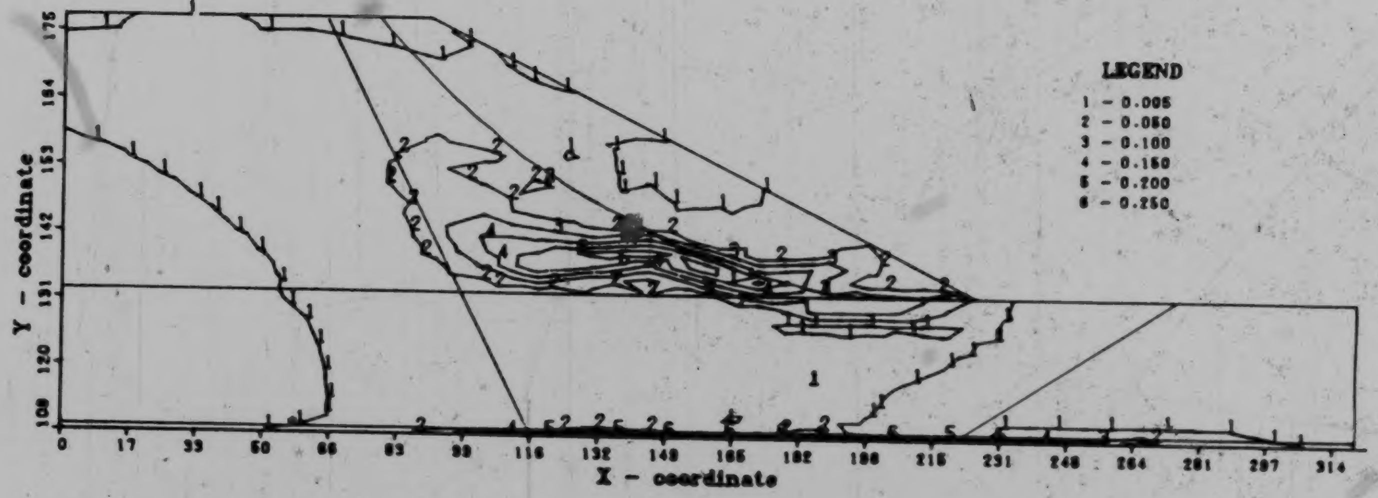

Figure 5.28: Maximum shear strain ($\frac{h_1}{H}$=0.50 - K_{till}=700)

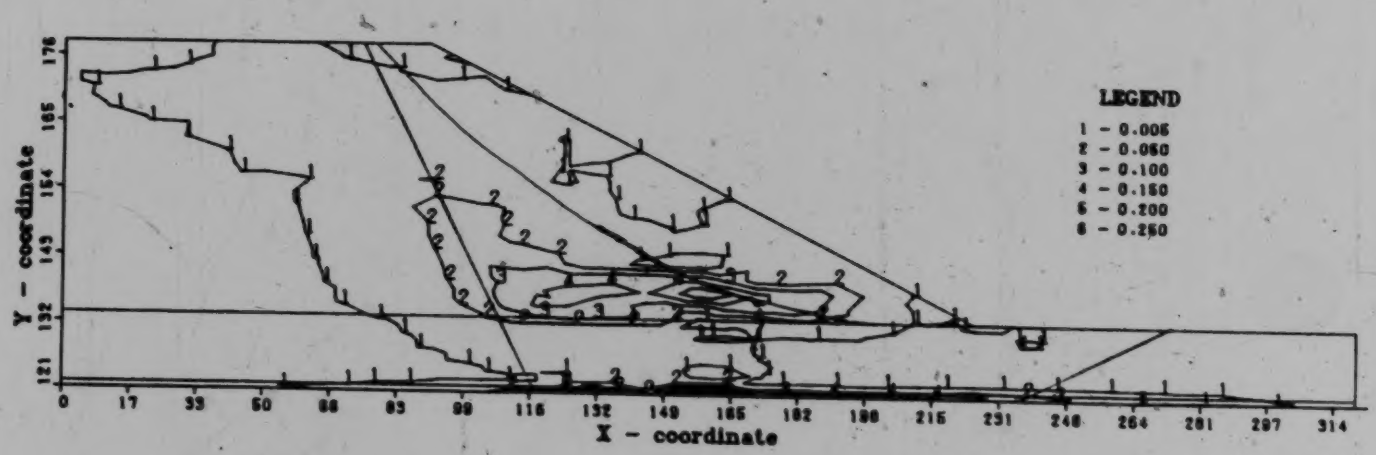

Figure 5.29: Maximum shear strain ($\frac{h_1}{H}=0.25$ - $K_{till}=7000$)

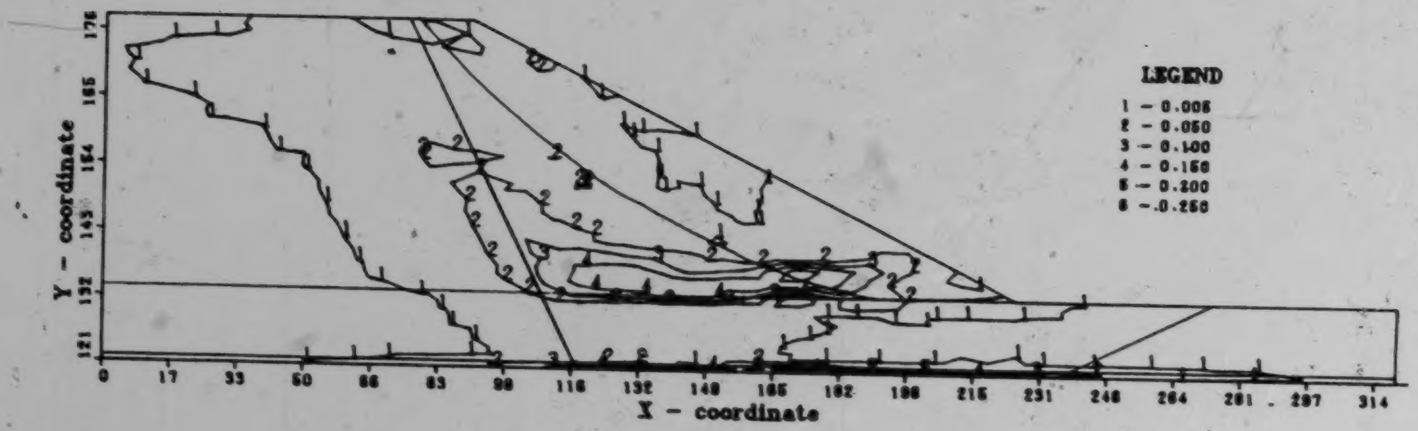

Figure 5.30: Maximum shear strain ($\frac{h_1}{H}$=0.25 - K_{till}=3500)

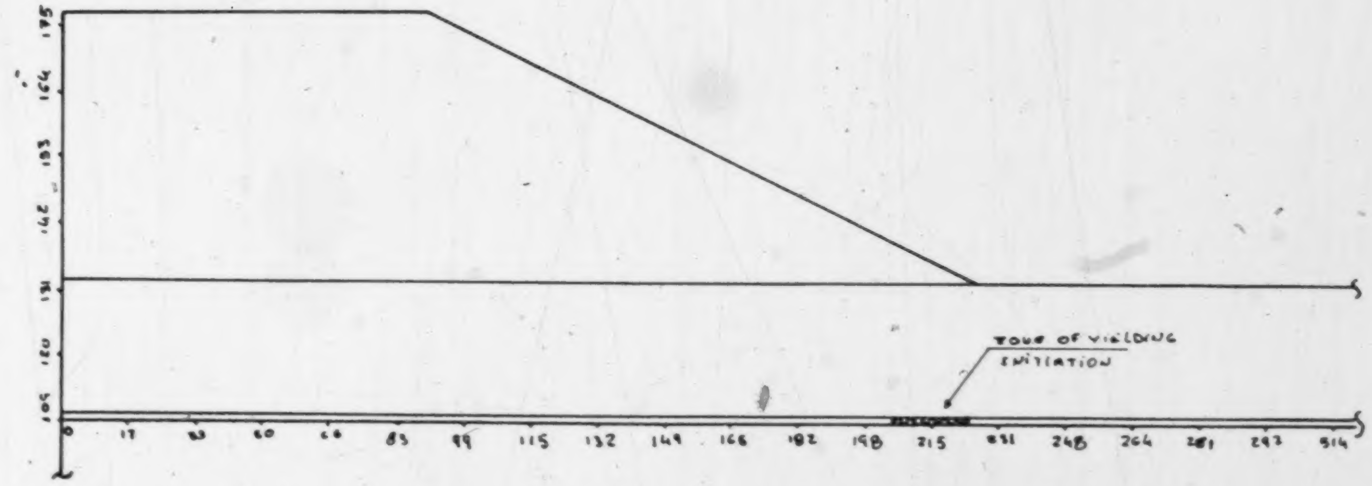
175
164
153
142
131
120
105
0
17
33
50
66
83
99
115
132
149
166
182
198
215
231
248
264
281
297
314
ZONE OF YIELDING
INITIATION

Figure 5.31: Zone of yielding initiation

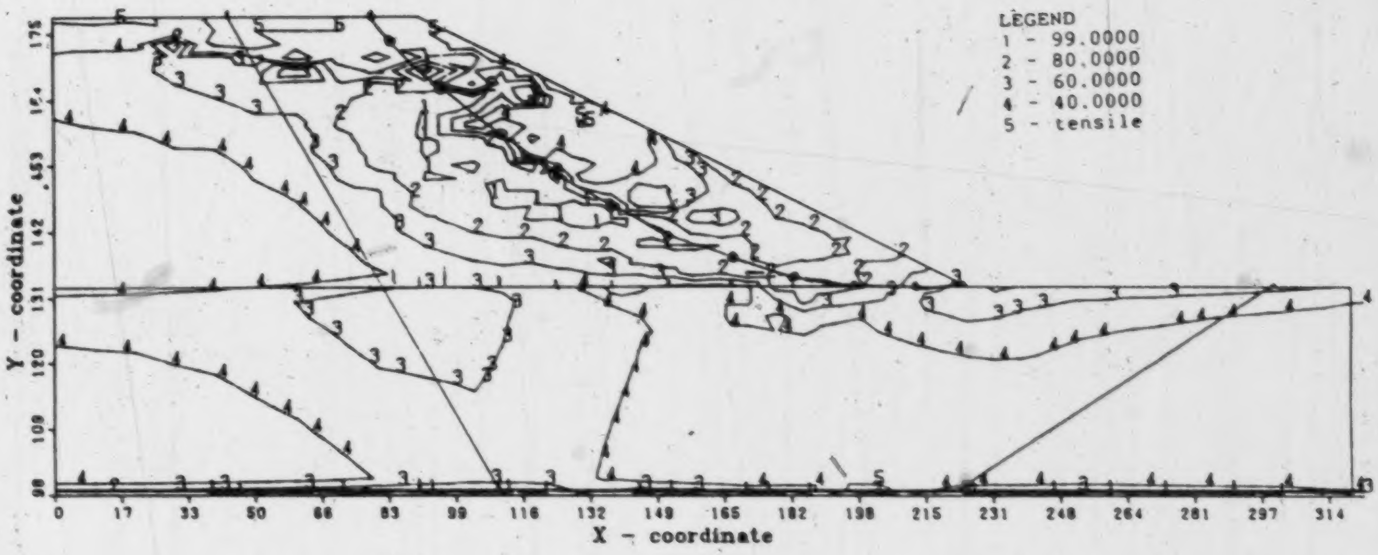

Figure 5.32: Mobilized shear strength ($\frac{h_1}{H}$=0.75 - K_{till}=7000)

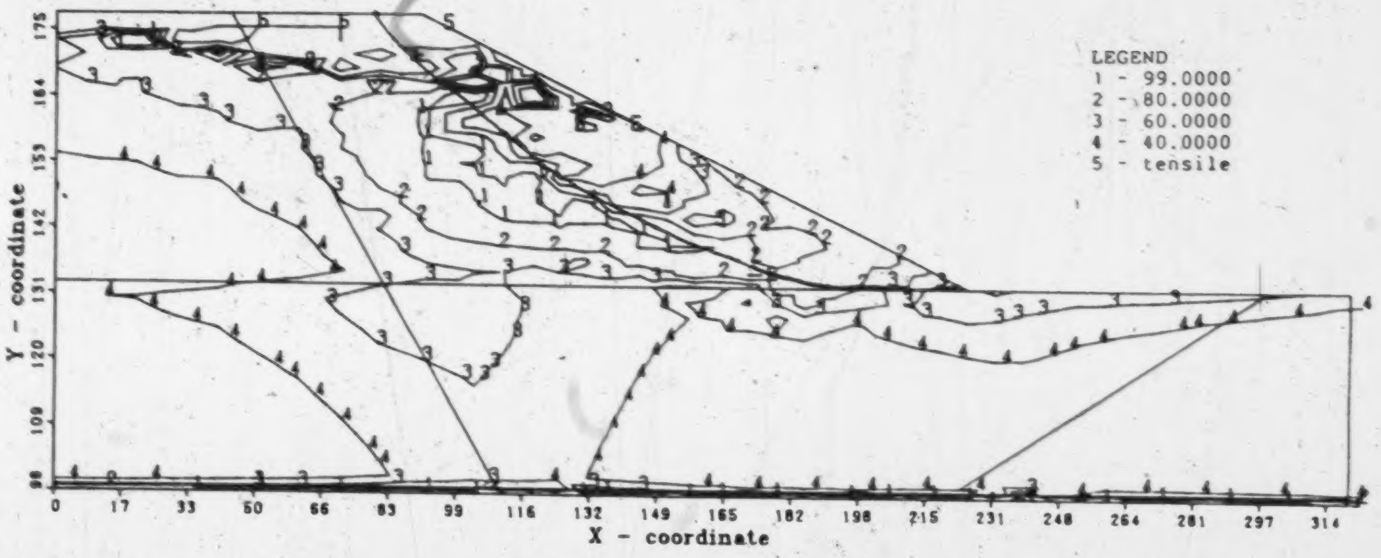

Figure 5.33: Mobilized shear strength ($\frac{h_1}{H}$=0.75 - K_{t11}=3500)

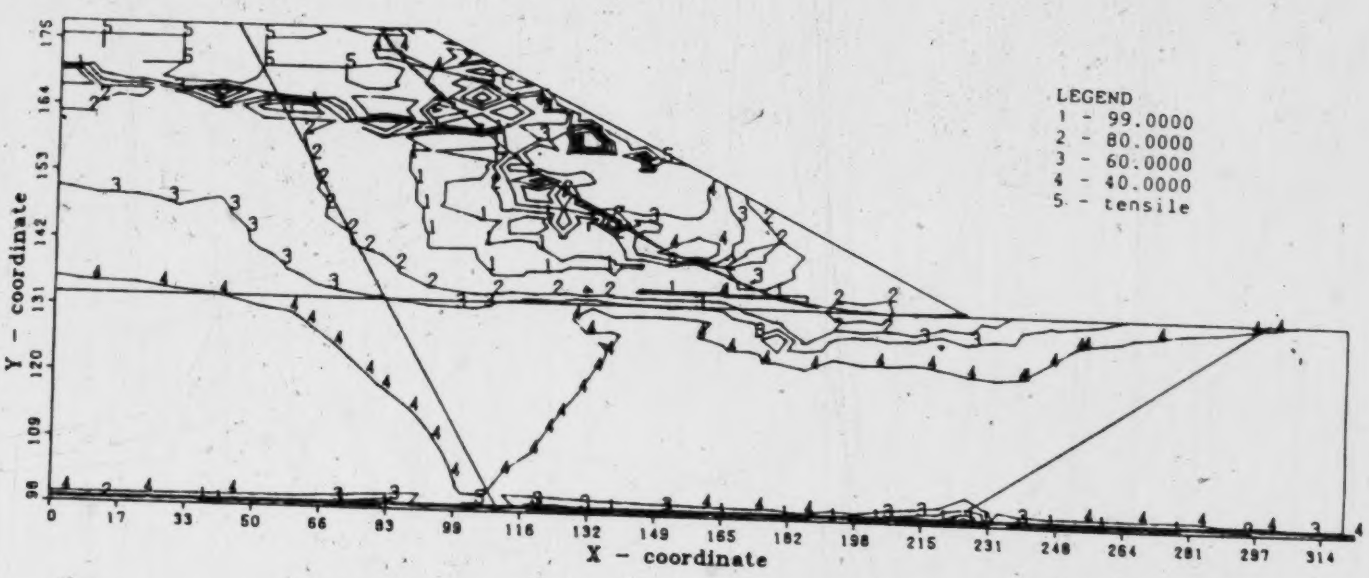

Figure 5.34: Mobilized shear strength ($\frac{h_1}{H}$=0.75 - K_{till}=700)

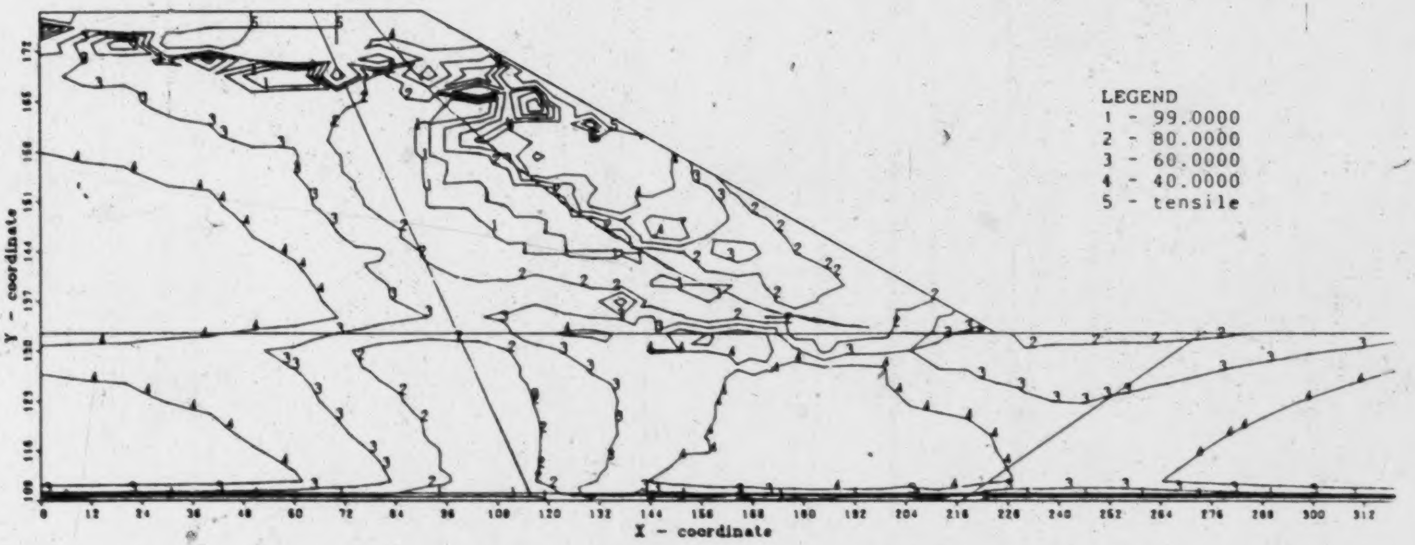

Figure 5.35: Mobilized shear strength ($\frac{h_1}{H}$=0.50 - K_{fill}=7000)

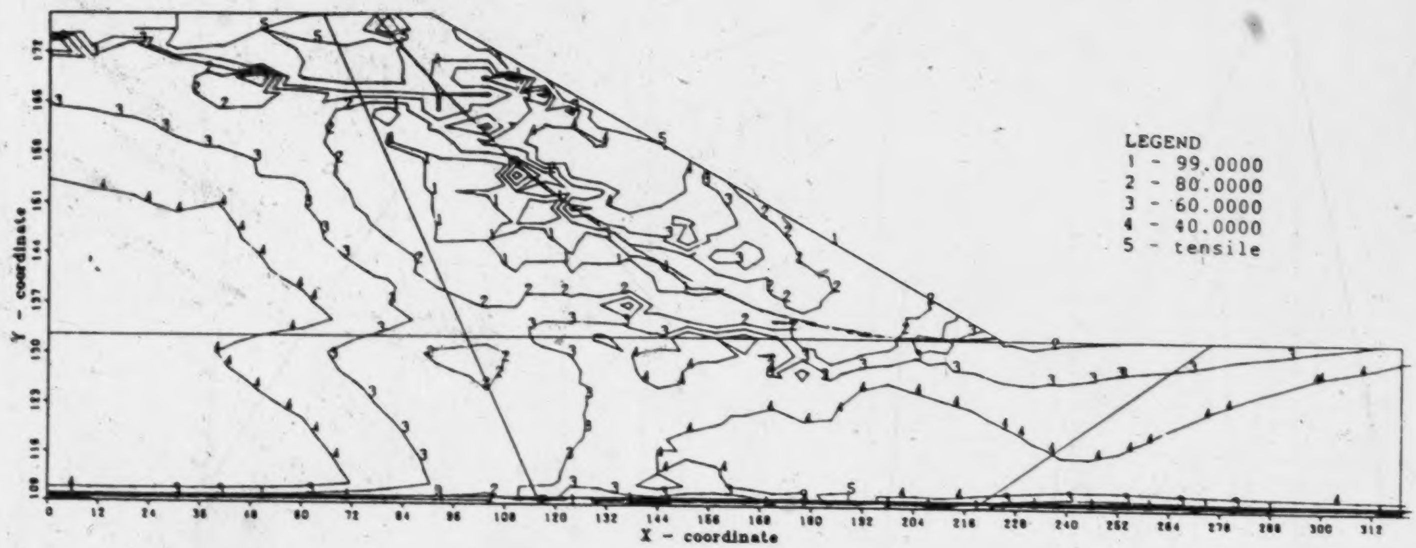

Figure 5.36: Mobilized shear strength ($\frac{h_1}{H}$=0.50 - K_{till}=3500)

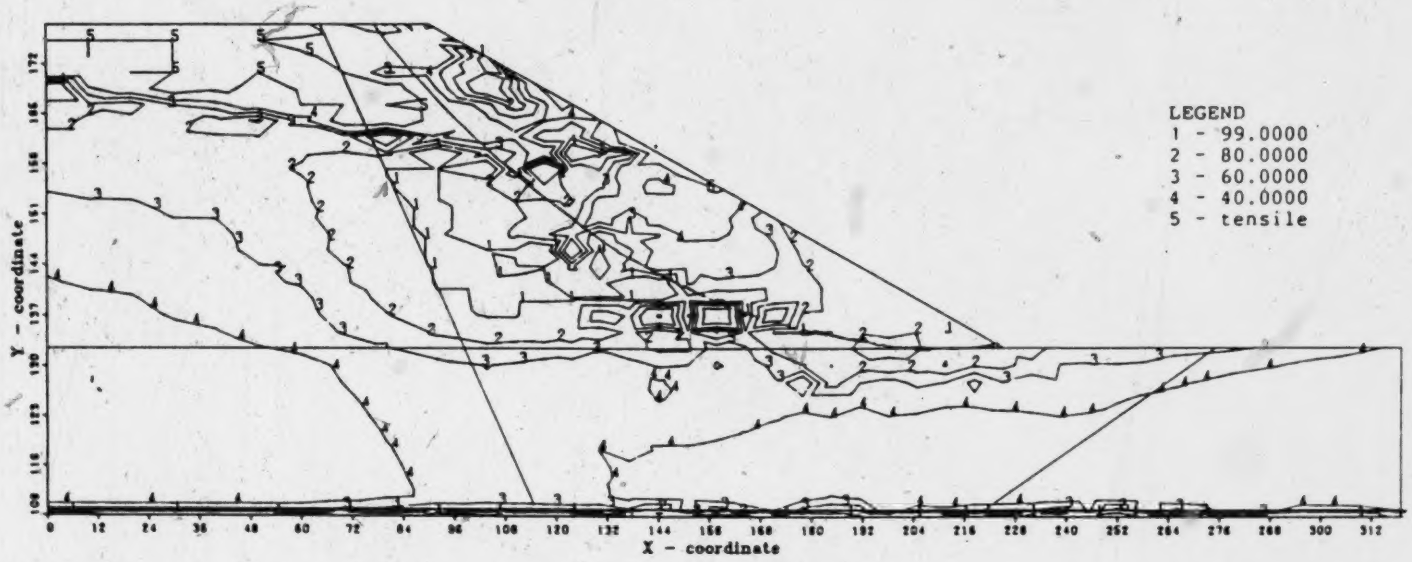

Figure 5.37: Mobilized shear strength ($\frac{h_1}{H}$=0.50 - K'_{till}=700)

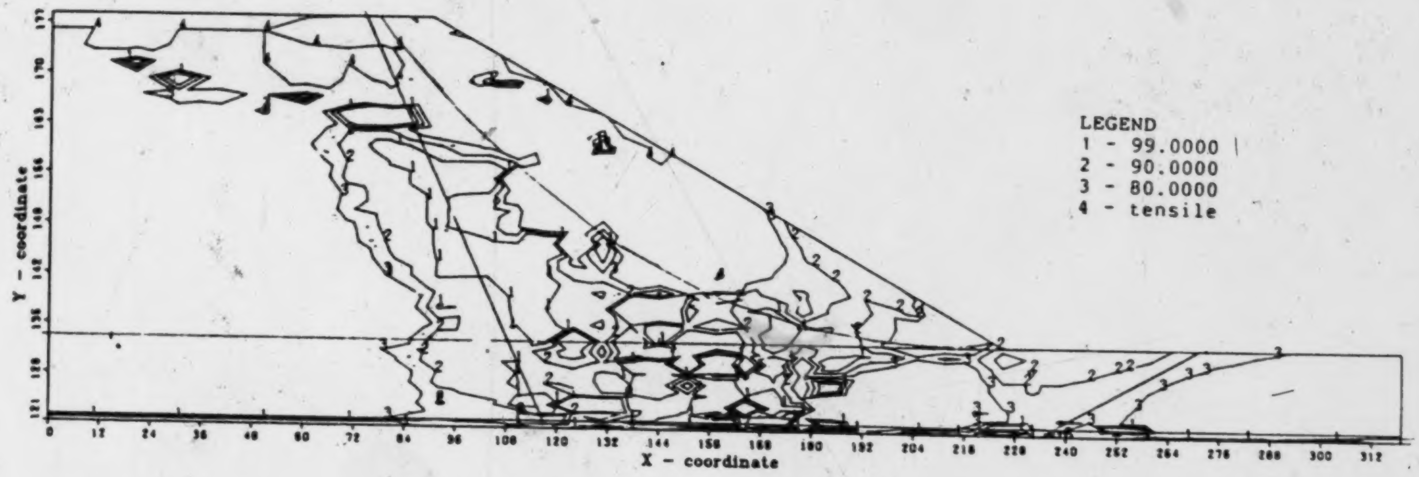

Figure 5.38: Mobilized shear strength ($\frac{h_1}{H}$=0.25 - K_{till}=7000)

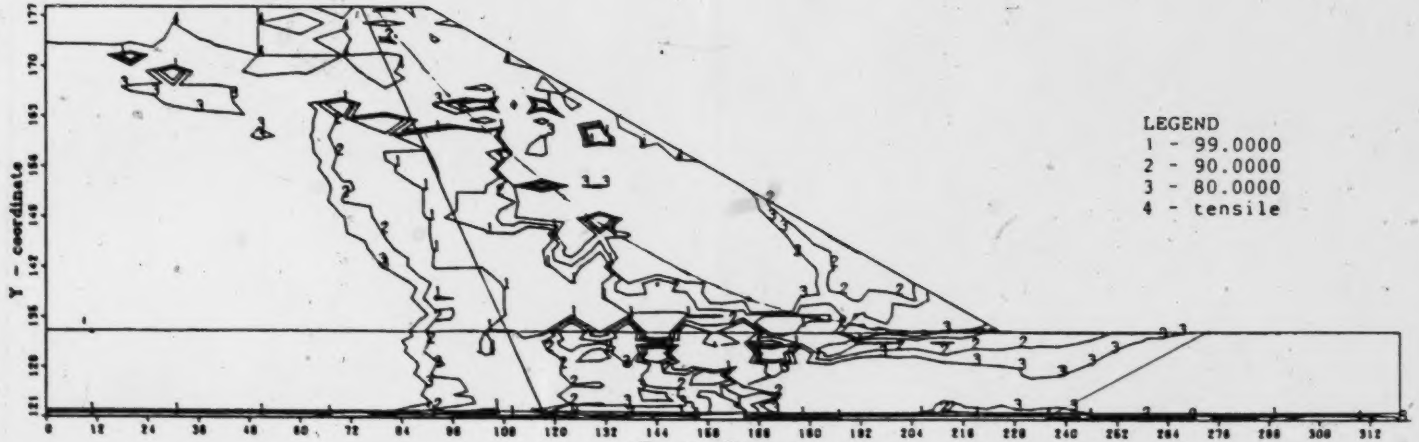

Figure 5.39: Mobilized shear strength ($\frac{h_1}{H}$=0.25 - K_{till}=3500)

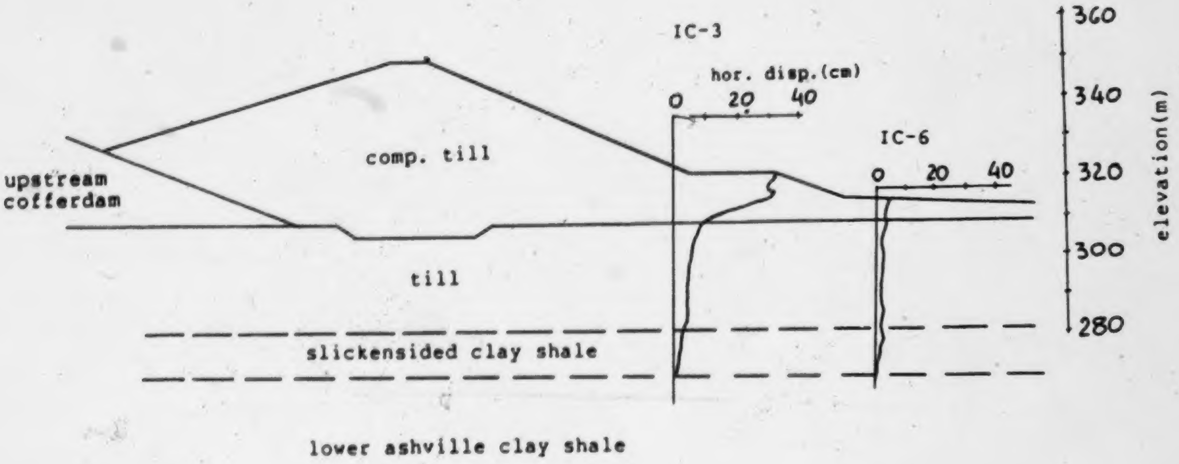
IC-3
hor. disp.(cm)
0
20
40
IC-6
0
20
40
360
340
320
300
280
elevation(m)
comp. till
upstream cofferdam
till
slickensided clay shale
lower ashville clay shale

Figure 5.40: Schematic stratigraphy and horizontal displacements - Nipawin dam

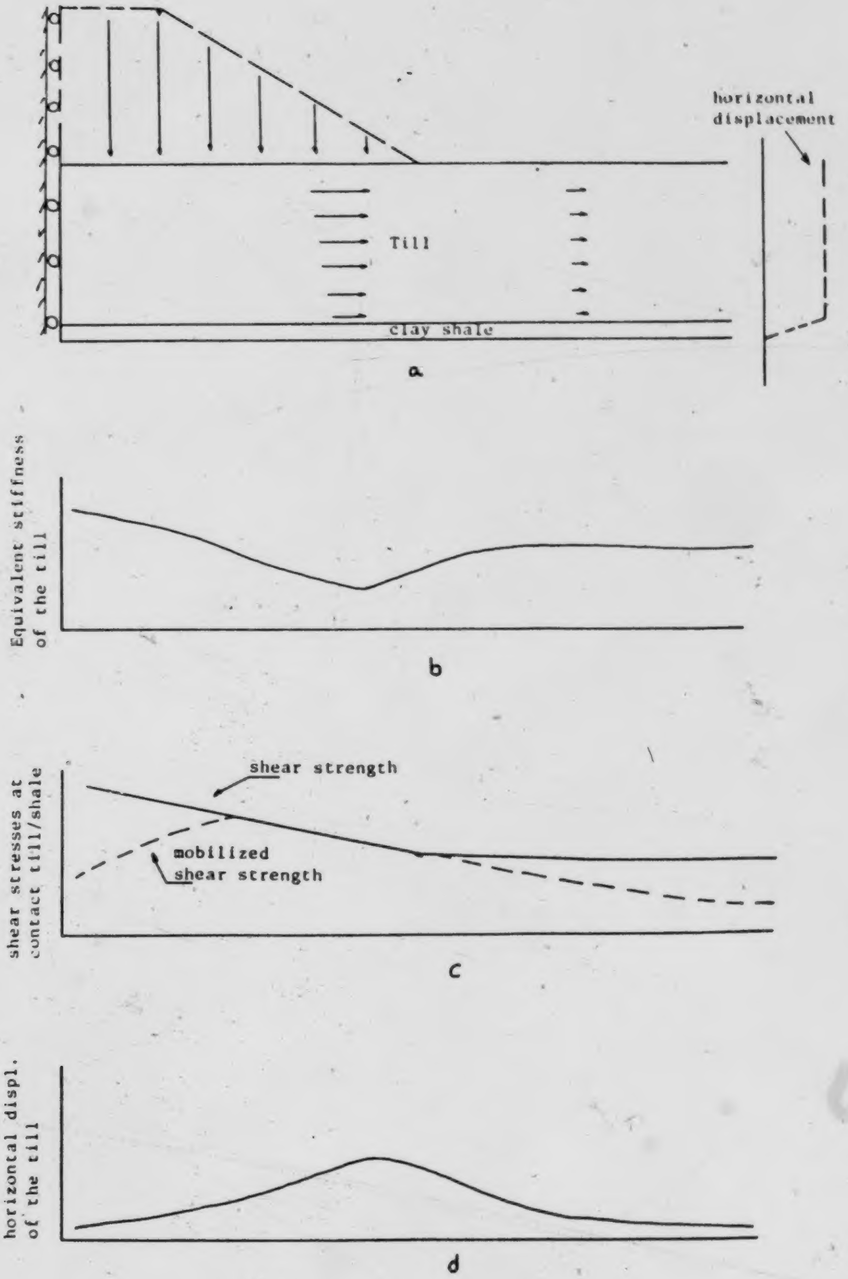
horizontal displacement
Till
clay shale
a
Equivalent stiffness of the till
b
shear stresses at contact till/shale
shear strength
mobilized shear strength
c
horizontal displ. of the till
d

Figure 5.41: Schematic representation of the problem in an unidimensional situation

6. Conclusions

6.1 Conclusions

The evaluation of the deformability of dam foundations has been the subject of various finite element analyses. However, in the case of earth dams constructed on sites where geologically defined weak seams exist there is still a lack of studies which approach the problem in a generic way. Besides the fact that the works presented so far are most of the times related to a specific case, the analyses are in general performed in terms of total stresses, as discussed in Chapter 1.

Pore pressure measurements in the field have become relatively commom practice during the construction of dams, specially on large projects. Total stress analyses in these cases, disregards these valuable information and hence significantly limits the potential usefulness of the numerical analysis. In Chapter 2 a technique is presented for using the measured pore pressures in the finite element analysis in terms of effective stresses. It involves the interpolation of the measured pore pressure values at the integration point (or node) positions and introduction of these values into the analysis as known quantities at each stage of construction and analysis.

This technique was used in the back analysis of the construction of a tailings dam over the period of eight years, which is described in Chapter 4. The displacements calculated were in much better agreement with field measurements than the values calculated by performing the analysis in terms of total stresses. Besides that, the material parameters used in the analysis in terms of effective stresses were within the range of values expected for each material, while in the case of the total stress analysis some of these parameters had to be lowered to imagined values so that the lateral displacements of the foundation could be increased. These results showed that the effective stress analysis performed according to the procedure described is efficient and able to avoid the complexities and increase in cost generally involved in attempting to predict the pore pressures based on theoretical models alone.

Difficulties in numerical convergence due to tensile stresses during the back analysis mentioned above led to the comparative analyses between two techniques for dealing with this problem, as presented in Chapter 3. The cracking model proposed by Chen and Suzuki(1980) was found to be numerically more stable than the stress transfer method presented by Zienkiewicz *et al.*(1968) in the cases studied, as discussed also in Chapter 4.

Chapter 5 presents a generic study of the deformability of the foundations of dams constructed on sites possessing a horizontal weak seam overlain by a stronger material. This was developed by performing a non-linear parametric analysis in terms of effective stresses and introducing the pore pressures as known quantities.The position of the weak seam and the stiffness of the upper foundation layer were varied. The analyses yielded a clearer understanding of the deformation mchanisms involved in the problem. They indicated that the stiffness of the upper foundation layer is the element controlling the lateral displacements of the foundation prior to collapse. This is supported by the comparative analysis of two cases histories presenting similar foundation stratigraphy and approximately the same Factor of Safety as calculated by limit equilibrium methods. The stiffness of the material above the horizontal weak layer in one case was much higher than in the other. Much larger horizontal displacements were observed in the latter.

These analyses also indicated that the empirical assessment of lateral deformations by the establishment of a minimum acceptable value for the Factor of Safety assuming that the higher the Factor of Safety the lower the displacement level is not appropriate for the cases studied. Correlations between Factor of Safety and displacements must involve the stiffness of the foundation layer above the weak layer as well as a measure of the stress level imposed on that material. Such a correlation was indicated based on the results obtained.

This thesis shows that the finite element method combined with relatively simple material models may be a very efficient and powerful instrument of analysis once the relevant factors influencing the deformation mechanisms occurring in the problem are taken into consideration, even in quite complex cases like the tailings dam analysed, in which high pore pressure and displacement levels were involved.

There is no question about the necessity of developing and using in many cases more sophisticated material models that best reproduce real materials behaviour. However, it is noted that the higher degree of sophistication of the analyses in general involves increases in cost despite accelerating processing speeds of modern computers. These costs in addition to the quality of the material parameters available most of the time have limited the application of these models in practice. In many cases, the wise and efficient use of less sophisticated stress-strain relationships which are widely known and usually available in various finite element codes used in geotechnical engineering, like the ones used in this work(linear elastic, hyperbolic and elastic-perfectly plastic using the Mohr-Coulomb yield criterion) may yield very good results.

In this thesis only the case of foundations possessing one horizontal weak layer has been analysed, and of course the subject of deformability of foundations of dams possessing weak seams demands a much larger amount of work to be performed. In this respect a few suggestions for further research are briefly stated in the following.

6.2 Suggestions for further research

The technique described for the use of pore pressure measurements in the finite element analyses in terms of effective stresses should be further investigated through the back analysis of case histories in which pore pressures have been measured. This could contribute to accumulated experience with the method and optimize the interpolation procedure for this purpose.

Generic studies of the kind performed in this thesis should be extended to include the existence of more than one weak seam in the foundation, various seam orientations, other dam geometries and pore pressure levels. This would deepen the understanding of the deformation mechanisms involved in each case and possibly identify the elements controlling these mechanisms. These systematic studies could also be used for attempting the development of a sounder basis for correlations between limit equilibrium analyses Factors of Safety and displacements in the foundation and in the embankment by taking into consideration the stiffness of the materials controlling the deformation mechanisms. Detailed study of the stress distribution in the foundation and in the embankment could also be performed. Such a body of information would constitute an invaluable basis for design decisions in practice.

Bibliography

Adams,J.I., 1961. "Tests on glacial till". Proceedings, 14th Canadian Soil Mechanics Conference, Ottawa, pp. 37-48.

Bathe,K.J., 1982. "Finite element procedures in engineering analysis". Prentice Hall Inc.

Bulton,G.S., 1976. "The development of geotechnical properties in glacial tills". In "Glacial Till", The Royal Society of Canada Special Publications, No. 12, ed. by R.F. Legget, pp. 292-303.

Byrne,P.M., 1976. "Effective stress finite element slope analysis". Proceedings, 29th Canadian Geotechnical Conference, Vancouver, Session 8, pp. 35-55.

Carrigy,M.A., 1959. "Geology of the McMurray Formation". General Geology of McMurray area. Research Council of Alberta. Memoir 1, 130 p.

Carrigy,M.A. and Kramers,J.W., 1974. "Geology of Alberta oil sands ". Proceedings, Conference on Athabasca Oil Sands. Engineering Institute of Canada, Western Region, pp. 13 - 24.

Cassinader,R., 1980 "Systematic weak seams in dam foundations". Proceedings, Symposium on Problems and Practice of Dam Engineering, Bangkok, pp. 253-264.

Chan,D.H.K., 1986. "Finite element analysis of strain softening material". Ph.D. Thesis, University of Alberta.

Chen,W.F. and Baladi,G.Y., 1985. "Soil plasticity - theory and implementation". Elvesier Science Pub.

Chen,W.F. and Suzuki,H., 1980. "Constitutive models for concrete". Computers and Structures, Vol. 12, pp. 23-32.

Christian,J.T., 1968. "Undrained stress distribution by numerical methods". Journal of the Soil Mechanics and Foundations Division, A.S.C.E., Vol. 94, SM 6, pp. 1333-1345.

Deere,D.V., 1973. "The foliation shear zone - an adverse engineering geologic feature of metamorphic rocks". Journal, Boston Society pf Civil Engineers, Vol. 60, pp. 163-176.

Desdemukh,M.D., Ratnapakhi,T.G., Kulkarni,R.G. and Dodihal,A.R., 1982. "Dudhganga dam on quartizitic rock formation interspersed with shale partings and bands". Proceedings, 14th International Congress on Large Dams, Vol. 2, Rio de Janeiro, pp. 663-642.

Dreimanis,A., 1976. "Tills: Their origin and properties". In "Glacial Till", The Royal Society of Canada Special Publications, No. 12, ed. by R.F. Legget, pp. 11-49.

Duncan,J.M. and Chang,C.Y., 1970. "Nonlinear analysis of stress and strain in soils". Journal of the Soil Mechanics and Foundations Division, ASCE, Vol. 96, SM 5, pp. 1629-1653.

Eisenstein,Z. and Morrisson,N.A., 1973. "Prediction of foundation deformation in Edmonton using an in situ pressure probe". Canadian Geotechnical Journal, Vol. 10, pp. 193-210.

Fair,A.E. and Handford,G.T., 1986. "Overview of tailings dyke intrumentation program at Syncrude Canada Ltd.". Proceedings International Symposium on Geotechnical Stability in Surface Mining, Calgary, pp. 245-253.

Handford,G.T., 1985. "Review of Cell 23 slope design". Syncrude Canada Ltd. internal report.

Handford,G.T. and Fair,A.E., 1986. "In situ strain measurements using the sliding micrometer at Syncrude's tailings dyke". Proceedings 39th Canadian Geotechnical Conference, Ottawa, pp. 277-282.

Hill,R., 1950. "The mathematical theory of plasticity". Oxford University Press.

Isaac,B.A., Dusseault,M.B., Lobb,G.D. and Root,J.D., 1982. "Characterization of the lower cretaceous overburden for oil sands surface mining within Syncrude Ltd. leases northeast Alberta, Canada". Proceedings, 4th Congress International Association of Engineering Geology,New Dellhi, Vol. 2, pp. 371-384.

Klohn,E.J., 1968: " The elastic properties of a dense glacial till deposit". Canadian Geotechnical Journal, Vol.2, pp. 116-128.

Kovari,K. and Amstad,C., 1983. "Fundamental of deformation measurements". Proceedings, International Symposium on Field Measurèments in Geomechanics, Zurich, Vol. 1, pp.219-239.

MacDonald,D., De Ruiter,J. and Kenney,T.C., 1961. "The geotechnical properties of impervious fill materials in some Canadian dams". Proceedings, 5th International Conference of Soil Mechanics and Foundation Engineering, Paris, Vol. 2, pp. 657-662.

Matheson,D.S., 1972. "Geotechnical implications of valley rebound". Ph.D. Thesis, University of Alberta.

Matheson,D.S., Morgenstern,N.R. and Nussbaum,H., 1987. "Design, performance and construction of the Nipawin dams". Proceedings, 40th Canadian Geotechnical Conference, Regina, pp. 139-171.

Milligan,V.,1976. "Geotechnical aspects of glacial till". In "Glacial Till", The Royal Society of Canada Special Publications, No. 12, ed. by R.F. Legget, pp. 269-291.

Mittal,H. and Hardy,R., 1977. "Geotechnical aspects of a tar sand tailings dyke". Proceedings, Conference on Geotechnical Practice for Disposal of Solid Waste Materials, A.S.C.E., University of Michigan, pp. 327-347.

Morgenstern,N.R., 1987. "Geological control of stability on large projects". Proceedings, 8th Pan American Conference on Soil Mechanics and Foundation Engineering, Cartagena, Vol. 1, pp. 293-316.

Morgenstern,N.R., Blight,G.E., Jambu,N. and Resendiz,D., 1977. "Slopes and excavations - state of the art report". Proceedings, 9th International Conference in Soil Mechanics and Foundation Engineering, Tokio, Vol. 2, pp. 547-604.

Morgenstern,N.R. and Simmons,J.V., 1982. "Analysis of the movements of Gardiner Dam". Proceedings 4th International Conference on Numerical Methods in Geomechanics, Vol. 3, pp. 1003-1027.

Mueller,L., Muehlhaus,H.B., Reik,G. and Sharma,B., 1977. "Stability of foundations in complex rock formations". Proceedings, International Symposium on the Geotechnics of Structurally Complex Formations, Vol. 2, pp. 127-139.

Peck,R.B., 1969. "Advantages and limitations of the observational method in applied soil mechanics". Geotechnique, Vol. 19, pp. 171-187.

Radhakrishna,A.S. and Klyn,T.W., 1974. "Geotechnical properties of a very dense glacial till". Canadian Geotechnical Journal, Vol. 11, pp. 396-408.

Resendiz,D. and Romo,M.P., 1972. "Analysis of embankment deformations". Proceedings, International Conference on Performance of Earth and Earth Supported Structures, A.S.C.E., Vol. 1, pp. 817-836.

Sampson,R.J., 1978. "Surface II Graphics System", revision one. Pub. by Kansas Geological Survey, Lawrence, Kansas, p. 95.

Sego,D.C. and Morgenstern,N.R., 1986. "Strength behavior of foundation material, Syncrude Tailings Dyke". A report submitted to Syncrude Canada Ltd.

Sharma,K.G., Varadarajan,A. and Chimmaswamy,C., 1986. "Finite element analysis of dam foundations with seams". Proceedings, 2nd International Symposium on Numerical Models in Geomechanics, Ghent, pp. 473-480.

Shaw, J., 1977. "Till body morphology and structure related to glacier flow". Boreas, Vol. 6, pp.189-201.

Skempton,A.W., 1954. "The pore pressure coefficients A and B". Geotechnique,Vol. 4, pp. 143-147.

Souza Lima,V.M., Abrahao,R.A., Pinheiro,R. Degaspare,J.C., 1982. "Rock foundations with marked discontinuities, criteria and assumptions for stability analysis". Proceedings, 14th International Congress on Large Dams, Vol. 2, Rio de Janeiro, pp. 1155-1181.

Taylor,R.G. and James,P.M., 1967. "Geotechnical aspects of the Muda irrigation project". Proceedings, 1st Southeast Asian Regional Conference on Soil Engineering, Bangkok, pp. 33-42.

Terzaghi,K. and Peck,R.B., 1948. "Soil mechanics in engineering practice". John Wiley and Sons Inc.

Walker,L.W. and Duncan,M.J., 1984. "Lateral bulging of earth dams". Journal of Geotechnical Engineering,A.S.C.E., Vol. 110, pp. 923-937.

Wittebolle,R.J., 1983. "The influence of microfabric on the engineering properties of glacial tills". M. Sc. Thesis, University of Alberta.

Zienkiewicz,O.C., 1977. "The finite element method". McGraw Hill Book Company.

Zienkiewicz,O.C. and Humpheson,C., 1977. "Viscoplasticity: A generalized model for description of soil behavior". In "Numerical Methods in Geotechnical Engineering", ed. by S. Desai and J.T. Christian, McGraw-Hill Book Company, Chapter 3, pp. 116-147.

Zienkiewicz,O.C., Villiappan,S. and King,A.P, 1968. "Stress analysis of rock as a 'no tension' material". Geotechnique, Vol. 18, pp. 56-66.

Appendix I - Extension of the cracking model to allow for shear stress on the plane of the crack

The discussion in Chapter 3 concerns to materials which cannot sustain tensile stresses.Soils and most rocks are considered to fall into this category. In this case the minimum value the minor principal stress can reach is zero,what implies that the plane of crack is a plane of principal stress,i.e., the shear stress on that plane is zero(i.e. the crack is "smooth"). This stress condition remains as long as the crack is open.

For materials which can take some tension, like some hard rocks, that is not necessarily true.If a "rough" crack is formed(see fig. A.1), despite the normal stiffness being reduced to zero, there may still remain some shear stiffness on the crack plane. This means that subsequent loading may induce shear stresses along the crack, causing a rotation of principal stresses,as shown in fig. A.2. Under these conditions the plane of crack is no longer a principal stress plane. The derivation below concerns to the incremental stiffness relative to the situation when some shear stiffness may remain on the plane of crack. The "smooth" crack condition is therefore a particular case of this relation.

A.1. Incremental contitutive relationship for cracked material in plane strain - "rough" crack.

The incremental stress vector for a cracked material is(see fig. A.1):

$$\begin{Bmatrix} d\sigma_x' \\ 0 \\ d\tau_{xy}' \end{Bmatrix} = \left[C_{cr} \right] \begin{Bmatrix} d\varepsilon_x' \\ d\varepsilon_y' \\ d\gamma_{xy}' \end{Bmatrix}$$

Assuming linear elasticity and plane strain:

$$\begin{Bmatrix} d\sigma_x' \\ 0 \\ d\tau_{xy}' \end{Bmatrix} = \begin{bmatrix} \frac{E}{1-\mu^2} & 0 & 0 \\ 0 & 0 & 0 \\ 0 & 0 & G_{cr} \end{bmatrix} \begin{Bmatrix} d\varepsilon_x' \\ d\varepsilon_y' \\ d\gamma_{xy}' \end{Bmatrix}$$

G_{cr} is the shear stiffness at the plane of the crack.

$$G_{cr} = \eta G$$

η is a reduction factor with values between zero and one. and G is the shear modulus of the material in its non-cracked condition

It can be shown that:

$$d\varepsilon_x' = \langle \cos^2\theta \quad \sin^2\theta \quad \cos\theta\sin\theta \rangle \begin{Bmatrix} d\varepsilon_x \\ d\varepsilon_y \\ d\gamma_{xy} \end{Bmatrix}$$

$$d\gamma_{xy}' = 2 \langle -\cos\theta\sin\theta \quad \cos\theta\sin\theta \quad \tfrac{1}{2}(\cos^2\theta - \sin^2\theta) \rangle \begin{Bmatrix} d\varepsilon_x \\ d\varepsilon_y \\ d\gamma_{xy} \end{Bmatrix}$$

Therefore:

$$\begin{Bmatrix} d\sigma'_x \\ d\tau'_{xy} \end{Bmatrix} = \begin{bmatrix} \frac{E}{1-\mu^2} & 0 \\ 0 & \eta G \end{bmatrix} \begin{bmatrix} \cos^2\theta & \sin^2\theta & \cos\theta\sin\theta \\ -2\cos\theta\sin\theta & 2\cos\theta\sin\theta & (\cos^2\theta-\sin^2\theta) \end{bmatrix} \begin{Bmatrix} d\varepsilon_x \\ d\varepsilon_y \\ d\gamma_{xy} \end{Bmatrix}$$

or

$$\begin{Bmatrix} d\sigma'_x \\ d\tau'_{xy} \end{Bmatrix} = \begin{bmatrix} C_e \end{bmatrix} \begin{bmatrix} BB \end{bmatrix}^T \begin{Bmatrix} d\varepsilon_x \\ d\varepsilon_y \\ d\gamma_{xy} \end{Bmatrix}$$

Multiplying both sides by [BB]

$$\begin{bmatrix} BB \end{bmatrix} \begin{Bmatrix} d\sigma'_x \\ d\tau'_{xy} \end{Bmatrix} = \begin{bmatrix} BB \end{bmatrix} \begin{bmatrix} C_e \end{bmatrix} \begin{bmatrix} BB \end{bmatrix}^T \begin{Bmatrix} d\varepsilon_x \\ d\varepsilon_y \\ d\gamma_{xy} \end{Bmatrix}$$

but, by tranformation of coordinates it can be shown that:

$$\begin{Bmatrix} d\sigma_x \\ d\sigma_y \\ d\tau_{xy} \end{Bmatrix} = \begin{bmatrix} \cos^2\theta & -2\cos\theta\sin\theta \\ \sin^2\theta & 2\cos\theta\sin\theta \\ \cos\theta\sin\theta & (\cos^2\theta-\sin^2\theta) \end{bmatrix} \begin{Bmatrix} d\sigma'_x \\ d\tau'_{xy} \end{Bmatrix}$$

That is,

$$\begin{Bmatrix} d\sigma_x \\ d\sigma_y \\ d\tau_{xy} \end{Bmatrix} = \begin{bmatrix} BB \end{bmatrix} \begin{Bmatrix} d\sigma'_x \\ d\tau'_{xy} \end{Bmatrix}$$

therefore,

$$\begin{Bmatrix} d\sigma_x \\ d\sigma_y \\ d\tau_{xy} \end{Bmatrix} = \begin{bmatrix} BB \end{bmatrix} \begin{bmatrix} C_e \end{bmatrix} \begin{bmatrix} BB \end{bmatrix}^T \begin{Bmatrix} d\varepsilon_x \\ d\varepsilon_y \\ d\gamma_{xy} \end{Bmatrix}$$

If η=0 the constitutive matrix reduces to the one presented by Chen and Suzuki(1980)

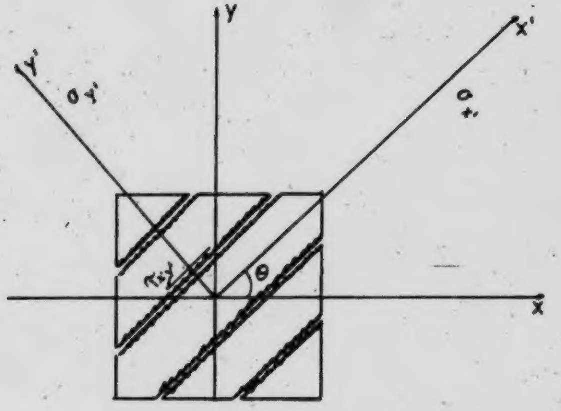
y
y'
x'
$\sigma_{y'}$
$\sigma_{x'}$
$\tau_{x'y'}$
θ
x

Figure A.1: Rough cracks oriented in one direction

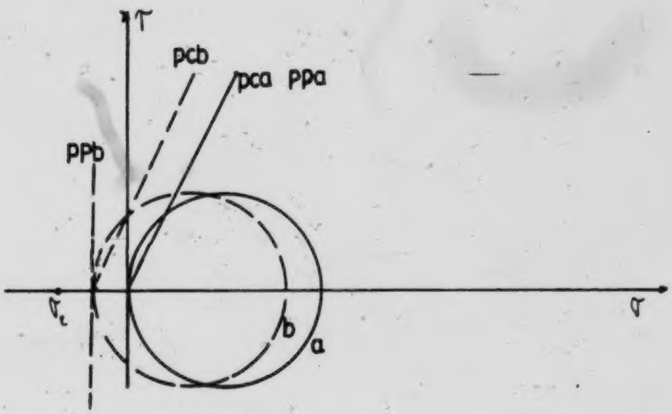
τ
pcb
pca ppa
ppb
σ_t
σ
b
a

- circle "a": state of stress just after cracking
- circle "b": state of stress after increment of shear stress on the plane of the crack
- pca: plane of crack at stage "a"
- ppa: plane of the minor principal stress at stage "a"
- pcb: plane of crack at stage "b"
- ppb: plane of the minor principal stress at stage "b"

Figure A.2: Mohr circle for cracked material

Appendix II - Analyses terminated before reaching 1985 in the finite element analyses of Syncrudes tailings dyke, presented in chapter 4

NL	Para	MATERIAL										Remarks
		km	kcw	kca	pgc	pgs	pf	ho	ts1	ts2	ts3	
NL8	E	2000	45	45						5		Displacement at kcw/kca Boundary similliar to Analysis NL1 Stopped at 1983
	u	0.35	0.45	0.45	0.40	0.40	0.30	0.30	0.30	0.30		
	φ		8.00	8.00	30.0	30.0	30.0	30.0	38.0			
	c		0.00	0.00	5.0	0.0	5.0	5.0	5.0			
	k				250.0	200.0	280.0	280.0	750.0			
	n				0.24	0.69	0.65	0.65	0.24			
	Rf				0.87	0.90	0.93	0.93	0.87			
NL9	E	2000	45	45						5		Displacement at kcw/kca Boundary similliar to Analysis NL1 Stopped at 1981
	u	0.35	0.45	0.45	0.40	0.40	0.30	0.30	0.30	0.30		
	φ		8.00	8.00	15.0	30.0	30.0	30.0	38.0			
	c		0.00	0.00	5.0	0.0	5.0	5.0	5.0			
	k				100.0	150.0	150.0	150.0	750.0			
	n				0.24	0.69	0.65	0.65	0.24			
	Rf				0.87	0.90	0.93	0.93	0.87			
NL10	E	2000	7.5	7.5						5		Displacement at kcw/kca still too small Analysis stopped at 1981
	u	0.35	0.45	0.45	0.42	0.30	0.30	0.30	0.30	0.30		
	φ		8.00	8.00	30.0	38.0	38.0	30.0	38.0			
	c		0.00	0.00	5.0	0.0	0.0	5.0	35.0			
	k				150.0	410.0	410.0	280.0	750.0			
	n				0.24	0.50	0.50	0.50	0.24			
	Rf				0.87	0.90	0.93	0.93	0.87			
NL11	E	2000	7.5	7.5						5		Displacement at kcw/kca still too small Analysis stopped at 1981
	u	0.35	0.35	0.45	0.42	0.30	0.30	0.30	0.30	0.30		
	φ		8.00	8.00	30.0	30.0	30.0	30.0	38.0			
	c		0.00	0.00	5.0	0.0	5.0	5.0	35.0			
	k				150.0	150.0	150.0	150.0	750.0			
	n				0.24	0.25	0.25	0.25	0.24			
	Rf				0.87	0.90	0.93	0.93	0.87			
NL12	E	2000	2000	7.5						5		Displacement at kcw/kca still too small Analysis stopped at 1981
	u	0.35	0.35	0.45	0.42	0.30	0.30	0.30	0.30	0.30		
	φ		8.00	8.00	30.0	30.0	30.0	30.0	38.0			
	c		0.00	0.00	5.0	0.0	5.0	5.0	35.0			
	k				150.0	150.0	150.0	150.0	750.0			
	n				0.24	0.25	0.25	0.25	0.24			
	Rf				0.87	0.90	0.93	0.93	0.87			

Table A1: Summary of material parameters used in the non-linear finite element analysis in terms of total stresses terminated prior to 1985

NL	Para	MATERIAL										
		km	kcw	kca	pgc	pgs	pf	no	ts1	ts2	ts3	Remarks
NL 13	E	2000	35	35.						5		Displacement at kcw/kca simillar to anlaysis NL3. Analysis stopped at 1983
	u	0.35	0.45	0.45	0.42	0.30	0.30	0.30	0.30	0.30		
	φ		4.00	4.00	30.0	38.0	30.0	30.0	38.0			
	c		0.00	0.00	5.0	0.0	5.0	5.0	35.0			
	k				150.0	400.0	280.0	280.0	750.0			
	n				0.24	0.50	0.50	0.50	0.24			
	Rf				0.87	0.90	0.93	0.93	0.87			
NL 14	E	2000	20.	20						5	10	Solution diverge at 1981 Analysis stopped at 1981.
	u	0.35	0.49	0.49	0.49	0.49	0.49	0.49	0.30	0.30	0.30	
	φ		3.00	8.00	30.0	16.0	30.0	30.0	38.0			
	c		0.00	0.00	5.0	50.0	5.0	5.0	35.0			
	k				150.0	400.0	280.0	280.0	750.0			
	n				0.24	0.50	0.50	0.50	0.24			
	Rf				0.87	0.90	0.93	0.93	0.87			
NL 15	E	2000	20.	20.						5	10	Solution diverge at 1980. Analysis stopped at 1980.
	u	0.35	0.49	0.49	0.49	0.49	0.49	0.49	0.30	0.30	0.30	
	φ		3.00	8.00	30.0	16.0	30.0	30.0	38.0			
	c		0.00	0.00	5.0	100.0	5.0	5.0	35.0			
	k				150.0	400.0	280.0	280.0	750.0			
	n				0.24	0.50	0.50	0.50	0.24			
	Rf				0.87	0.90	0.93	0.93	0.87			
NL 16	E	2000	20	20.						5	10	Solution diverge at 1980. Analysis stopped at 1980.
	u	0.35	0.45	0.45	0.49	0.49	0.49	0.49	0.30	0.30	0.30	
	φ		3.00	8.00	30.0	16.0	30.0	30.0	38.0			
	c		0.00	0.00	5.0	100.0	5.0	5.0	35.0			
	k				150.0	400.0	280.0	280.0	750.0			
	n				0.24	0.50	0.50	0.50	0.24			
	Rf				0.87	0.90	0.93	0.93	0.87			
NL 17	E	2000	20	20.						5	10	Solution diverge at 1980. Analysis stopped at 1980.
	u	0.35	0.45	0.45	0.49	0.49	0.49	0.49	0.30	0.30	0.30	
	φ		4.00	8.00	30.0	30.0	30.0	30.0	38.0			
	c		0.00	0.00	5.0	100.0	5.0	5.0	35.0			
	k				150.0	400.0	280.0	280.0	750.0			
	n				0.24	0.50	0.50	0.50	0.24			
	Rf				0.87	0.90	0.93	0.93	0.87			

Table A1: Summary of material parameters used in the non-linear finite element analysis in terms of total stresses terminated prior to 1985 (continue)

NL.	Para	MATERIAL										Remarks
		km	kcw	kca	pgc	pgs	pf	ho	ts1	ts2	ts3	
NL 18	E	2000	20.	20.						5	10	Solution diverge at 1980. Analysis stopped at 1980.
	u	0.35	0.45	0.45	0.45	0.45	0.45	0.45	0.30	0.30	0.30	
	ϕ		4.00	8.00	30.0	25.0	30.0	30.0	38.0			
	c		0.00	0.00	5.0	100.0	5.0	5.0	35.0			
	k				150.0	400.0	280.0	280.0	750.0			
	n				0.24	0.50	0.50	0.50	0.24			
	Rf				0.87	0.90	0.93	0.93	0.87			
NL 19	E	2000	20.	20						5	10	Solution diverge 1980. Analysis stoppeu 1980.
	u	0.35	0.45	0.45	0.45	0.45	0.45	0.45	0.30	0.30	0.30	
	ϕ		4.00	8.00	30.0	25.0	30.0	30.0	38.0			
	c		0.00	0.00	5.0	100.0	5.0	5.0	35.0			
	k				150.0	400.0	280.0	280.0	750.0			
	n				0.24	0.50	0.50	0.50	0.24			
	Rf				0.87	0.90	0.93	0.93	0.87			
NL 20	E	2000	20	20						5	10	Solution diverge at 1980. Analysis stopped at 1980.
	u	0.35	0.49	0.49	0.45	0.45	0.45	0.45	0.30	0.30	0.30	
	ϕ		4.00	8.00	30.0	25.0	30.0	30.0	38.0			
	c		0.00	0.00	5.0	100.0	5.0	5.0	35.0			
	k				150.0	400.0	280.0	280.0	750.0			
	n				0.24	0.50	0.50	0.50	0.24			
	Rf				0.87	0.90	0.93	0.93	0.87			

Notes/

E - Elastic Modulus (MPa)
u - Poisson's Ratio
ϕ - Friction angle (degree)
c - Cohesion (kPa)
k - Modulus in hyperbolic elastic model
n - Exponent in hyperbolic elastic model
Rf - Rf factor in hyperbolic elastic model
Unit weights same as Table 1

ts1 - Tailing sand using hyperbolic elastic model
ts2 - Tailing sand using linear elastic model when layer is added
ts3 - Tailing sand using linear elastic model to minimize converge problem

Table A1: Summary of material parameters used in the non-linear finite element analysis in terms of total stresses terminated prior to 1985 (continue)